School of Medicine and Population Health
Division of Clinical Medicine, Faculty of Health

The Development of a Novel Strategy to Target Dormant Myeloma Cells by Standard of Care Therapy

Thesis Submitted for the Degree of Doctor of Philosophy

Dr Hawazen Algifry

Supervised by
Dr Michelle Lawson
Dr Munitta Muthana

September 2024

Acknowledgement

I would like to thank Dr Michelle Lawson and Dr Munitta Muthana for their guidance and supervision, and the University of Sheffield for allowing me to do this study. I am really thankful to my country, the Royal Embassy of Saudi Arabia and Umm Al-Qura University for granting this scholarship. Thank you to all members of the Sheffield Myeloma Research Team (SMaRT) for making the PhD years a pleasant experience despite the circumstances of the COVID-19 pandemic. A special thanks to Jenny Down, Darren Lath, Dr Georgia Stewart, and Alex Sprules for helping me understand the work and research experience throughout the four years of my study. I would like to thank Dr Oyajobi at the University of Texas for providing us with the murine 5TGM1 myeloma cell line. I will not forget to thank the Flow Cytometry core facility, especially Susan Clark, for the support and assistance.

I wish to thank my lovable husband (Abdulhady) for being with me in the UK to support and encourage me throughout my journey. His presence and constant support have been invaluable to me. I am also eternally grateful to my Mom, Dad, my daughter (Hiba), and family for their unwavering belief in me and their continuous encouragement throughout my PhD journey.

I would also like to express my sincere gratitude to my friends both in Saudi Arabia and the UK. The friendships I have forged during my time abroad have enriched my life with wonderful memories and shared experiences through both good and challenging times. A special mention to my close friends Dr Reham Filfilan and Dr Nadiya Qurban for the time we spent together as we progressed in our journey towards our PhD degrees.

Declaration

The work presented in this thesis was carried out by the candidate with the following exceptions;

Processing of tissue sample for histology was done by Ms Orla Gallagher Research Technicians, Mellanby Centre for Bone Research, Sheffield.

Computerised Image Analysis technique for osteolytic lesion detection was designed by Mr Holly Evans, Research Technician, Mellanby Centre for Bone Research, Sheffield.

Fluorescent activated cell sorting was done by Mrs Sue Clark and Mrs Kay Hopkinson, Core Facilities, University of Sheffield.

Abstract

Introduction: Multiple myeloma is an incurable disease caused by the abnormal growth of plasma cells in the bone marrow and characterised by hypercalcaemia, renal insufficiency, anaemia, and lytic bone disease. Despite current treatments debulking the majority of tumour burden, disease relapse often occurs due to minimal residual disease (MRD), including dormant myeloma cells (DMCs). DMCs can remain inactive for years before being reactivated by the bone microenvironment (BMME). Previous studies have revealed a crosstalk between DMCs in the BMME, and several biomarkers have been discovered (e.g., AXL, TRIM44). However, currently, there is limited knowledge of the effects of myeloma standard of care (SoC) therapies on DMCs. We **hypothesised** that DMCs would be targeted more effectively by combined SoC therapies than monotherapy. To test this hypothesis, both *in vitro* and *in vivo* model systems were used. **Methodology:** *In vitro* studies were performed using myeloma cell lines (5TGM1, JJN3, OPM2, and U266) transduced previously with GFP and/or Luc. Cells were also labelled with a vybrant membrane dye (DID) to measure and identify DMCs. Flow cytometry and fluorescent imaging were used to determine optimum time points for drug evaluation on DMCs. Drug assays were then performed by treating myeloma cells over time with SoC therapies with different mechanisms of action: Bortezomib (Btz) is a reversible proteosome inhibitor (PI), Pomalidomide (Pom) is an immunomodulatory (IMiD), Melphalan (Mel) is a bifunctional alkylating agent, and Panobinostat (Pan) is a histone deacetylase inhibitor (HDACi). Drug IC_{50} values were determined and then used to assess the most effective drug combination to target DMCs *in vitro* and *in vivo*. **Results:** Fluorescent imaging and flow cytometry showed the presence of DID^{high} cells (potential DMCs) over 21 days in the *in vitro* culture of all four myeloma cell lines. JJN3-DID^{high} cells were sensitive to single treatments and the combination of Btz and Pan compared to single Btz, and OPM2-DID^{high} were sensitive to single drugs and to the combination of Btz /Mel compared to Btz, Btz/ Pan compared to Btz, and Mel/ Pan compared to Mel. NSG mice injected with JJN3-GFP-Luc-DID cells and treated with Btz and/or Pan showed that Btz reduced tumour burden and increased osteoblasts (OB), thus increasing DMCs. **Conclusion:** DMCs were present in all myeloma cell cultures, combined treatment was more effective than monotherapy *in vitro*. The *in vivo* showed some

combinations reduced the tumour burden but resulted an increase in DMCs. These unexpected results remain inconclusive and require further investigation.

Table of Contents

Summary of tables

Summary of figures

Summary of abbreviations

(miR)-126	Micro-RNA-126
µCT	Micro computed tomography
3D	Three-dimensional
AHCT	Autologous hematopoietic cell transplantation
AID	Activation induced deaminase
anti-CD38	Daratumumab
APC	Antigen presenting cell
ASCT	Allogeneic stem cell transplantation
AXL	AXL receptor tyrosine kinase
BLI	Bioluminescence imaging
BLIMP1	B lymphocyte induced maturation protein
BMME	Bone marrow microenvironment
BMPC	Bone marrow plasma cells
BMSCs	Bone marrow stromal cells
BTK	Bruton's tyrosine kinase
Btz	Bortezomib
BV/TV	Trabecular bone volume
Carf	Carfilzomib
CAR-T	Chimeric antigen receptor T cell
CAT scan	Computerised axial tomography
CCND1	Cylclin D1 gene
CFSE	Carboxyfluorescein succinimidyl ester
Cis	Cisplatin
CML	Chronic myeloid leukaemia
CSCs	Cancer stem cells
CSR	Class switch recombination
CT	Low-dose whole-body computed tomography
Ct.V	Cortical bone volume
Cyc	Cyclophosphamide
DAC	Deacetylase
Dex	Dexamethasone
DID	1,1'-dioctadecyl-3,3,3',3'-tetramethylindodicarbocyanine
DMSO	Dimethyl sulfoxide
Dox	Doxorubicin
DSB	Double strand DNA breaks
DW	Distilled water
EDTA	Ethylenediaminetetraacetic Acid
ES	Effect size
ESR	Erythrocyte sedimentation time
Eto	Etoposide
ER	Endoplasmic reticulum
FACS	Fluorescent Activating Cell Sorting
FBS	Foetal bovine serum
FCgr1	Fcrγ receptor 1
FCS	Foetal calf serum
FGFR3	Fibroblast growth factor receptor
FMO	Fluorescence minus one
FSC	Forward scatter

GAS6	Growth arrest specific 6
GFP	Green fluorescent protein
H&E	Haematoxylin and Eosin
HDACi	Histone deacetylase inhibitor
HDM	High dose of melphalan
hFOb	Human foetal osteoblast cells
HSC	Hematopoietic stem cell
IC_{50}	Half maximal inhibitory concentration
Ig	Immunoglobulin
IgH	Immunoglobulin heavy chain
IL	Interleukin
IMiDs	Immunomodulatory drugs
IMS	Industrial methylated spirit
IMWG	International myeloma working group
IP	intra-peritoneal
IRE1 α	Inositol-requiring enzyme 1 α
IRF4	Interferon regulatory factor 4
IV	Intravenous
Ixa	Ixazomib
Len	Lenalidomide
Luc	Luciferase
mAbs	Monoclonal antibodies
MAPK	Mitogen-activated protein kinase
Mel	Melphalan
MFI	Mean fluorescence intensity
MGUS	Monoclonal gammopathy of undetermined significant
MHC II	Major histocompatibility complex class II
MM	Multiple myeloma
Mpeg1	Macrophage expressed gene 1
MRD	Minimal residual disease
mTORC1	Mammalian target of rapamycin complex 1
NaP	Sodium Phosphate
NEAA	Non-essential amino acids
NFκ β	Nuclear factor kappa B
NSD2	Histone-lysine N-methyltransferase
OV	Oncolytic virus
Pan	Panobinostat
PAX 5	Paired box genes 5
PBS	Phosphate Buffered Saline
PCa	Prostate cancer cell line
PCL	Plasma cell leukaemia
PCR	Polymerase chain reaction
PCs	Plasma cells
PET/CT	Positron emission tomography/computed tomographic scans
PIs	Proteosome inhibitors
PI	Propidium iodide
Pom	Pomalidomide
Prd	Prednisone
RANK	Receptor activator of nuclear factor κ B
RANKL	Receptor of activator of nuclear factor κ B -Ligand

RFU	Relative fluorescence intensity
ROI	Region of interest
RRMM	Relapse/refractory multiple myeloma patients
RT	Room temperature
SD	Standard deviation
SDF1	Stromal derived factor 1
SHM	Somatic hypermutation
SIPRA	Signal regulatory protein α1
SMaRT	Sheffield myeloma research team
SMM	Smouldering multiple myeloma
SoCs	Standard of care drugs
Spic	Spi-C transcription factor
SSC	Side scatter
Tb. N	Trabecular number
Tb. Th	Trabecular thickness
TGF-β	Transforming growth factor-β
Thal	Thalidomide
TNFα	Tumour necrosis factor α
TRIM44	Tripartite motif 44
uPAR	Urokinase-type plasminogen activator receptor
UPR	Unfolded protein response
VCAM1	Vascular cell adhesion molecule 1
Xbp1	X box-binding protein 1
YM155	Sepantronium Bromide

Chapter 1

Introduction

1.1 Multiple Myeloma

Multiple myeloma (MM) is the second most common B-cell haematological malignancy in the world, following non-Hodgkin's lymphoma, and it represents 10-15 % of all haematological malignancies. It is associated with hyper**c**alcemia, **r**enal failure, **a**naemia, and lytic **b**one disease (CRAB criteria), among other complications. Currently, it is an incurable condition that primarily affects the elderly, typically between the ages of 65 and 74, and is complicated (Ahmed Al-Anazi, 2023; van de Donk, Pawlyn, & Yong, 2021; Kane, 2020; Pinto et al., 2020; Nanni, Fanti, & Zanoni, 2019). MM is caused by an aberrant proliferation of plasma cells (PCs)

(fully differentiated antibody-producing B cells), which results in an overproduction of M-protein or paraprotein, which is responsible for the disease (monoclonal immunoglobulin heavy chains). Aside from bone marrow (BM), malignant plasma cells can be detected in the peripheral blood as well as other extramedullary sites such as soft tissue and organs. A further finding is that 15-20 % of patients produce monoclonal antibodies (mAbs) free light chains, whereas only 3 % of patients have no monoclonal protein secretion (Kumar et al., 2017). Additionally, this might result in the deterioration of various organs, such as the kidneys and the heart (Mahindra & Ng, 2016). These can lead to a number of complications (discussed in section 1.2). Myeloma cells reside in the BM, but in the later stages of the disease, they can also spread to peripheral blood and extramedullary locations, resulting in plasma cell leukaemia (PCL) and plasmacytomas (Kumar et al., 2017). Myeloma cells secrete cytokines and other factors that can lead to severe bone damage and bone pain.

Although the exact cause of MM is unclear, several studies have investigated the possibility of risk factors for this condition (Kumar et al., 2017; Pick, 2014). Twenty years after the atomic bombings of Hiroshima and Nagasaki, the incidence of MM was shown to be three times higher in individuals who had 0.5 Gy of radiation exposure compared to those who did not. On the other hand, data from 1950 to 1987 with 2,778,000 person-years of follow-up indicated that those who were exposed to 4 Gy of radiation did not have a significantly increased risk of MM when compared to those who were not exposed to radiation (Kumar et al., 2017). In addition, agricultural pesticides and perhaps petroleum chemicals. Rheumatoid arthritis patients or obese

patients have a higher risk of developing MM (body mass index of more than 30 kg per m^2). Most people with MM have no evident risk factors (Kumar et al., 2017; Nau & LeWis, 2008).

Current anti-MM treatments include proteasome inhibitors (PIs), e.g., bortezomib (Btz), histone deacetylase inhibitors (HDACis), e.g., Panobinostat (Pan), alkylating agents such as melphalan (Mel) and immunomodulatory drugs (IMiDs), e.g., pomalidomide (Pom) can initially reduce tumour burden (Kumar et al., 2017). However, patients usually succumb to disease relapse due to remaining minimal residual disease (MRD), drug resistance and/or dormant myeloma cells (DMCs). Currently, several approaches are employed to monitor MRD in MM, each technique has a set of limitations and advantages including next-generation flow cytometry, next-generation sequencing, polymerase chain reaction (PCR), and imaging techniques. The best approach will vary depending on the individual patient and the specific myeloma subtype. Therefore, novel treatment strategies are urgently required to eliminate all tumour cells.

1.2 Characteristics of Multiple Myeloma

Bone discomfort is reported by almost two-thirds of patients. As a primary cause of morbidity in people with myeloma, bone disease is a common symptom, and it can be evident in the lower back or the pelvis. Sudden attacks of pain may be experienced, especially in the case of pathological fractures. Radiographs of 75 % of patients reveal lytic lesions, osteoporosis, and fractures (Dispenzieri & Kyle, 2005). The myeloma-induced bone disease leads to hypercalcemia and debilitating bone damage. Osteoclast (OC) numbers increase during disease progression, causing bone resorption. On the other hand, osteoblasts (OB), the bone-builder cells, are inhibited and prevented from repairing bone. Around 80-90% of myeloma patients experience some form of bone destruction during their disease course, reducing their quality of life (Perfectionalis, 2018; Kumar et al., 2017). This imbalance of bone cells can lead to both bone damage and raised calcium levels in the blood and urine, resulting in hypercalcemia (Edwards, Zhuang, & Mundy, 2008) (Figure 1.1). Complications of this condition include kidney stones, renal failure, nervous system problems, osteoporosis, severe bone pain and arrhythmia (Mayo Clinic, 2020; Yadav, Cook, & Cockwell, 2016). Around half of patients develop renal impairment, with up to 5% requiring dialysis. Treating acute kidney injury is

challenging, but survival rates have improved with new drug treatments and the exploration of extracorporeal therapies (Yadav, Cook, & Cockwell, 2016). The secretion of abnormal monoclonal antibodies and the overproduction of free light chains by myeloma cells can increase total protein in the blood, resulting in hyperviscosity (Huang et al., 2024). This increase in proteins, along with myeloma cell infiltration, can then lead to renal failure due to their accumulation in the glomerulus and reabsorbed at the proximal tubule, the distal segment of the kidney nephrons (Perfectionalis, 2018; Kumar et al., 2017; Yadav, Cook, & Cockwell, 2016). Some myeloma patients can develop amyloidosis (a condition caused by a build-up of abnormal protein - amyloid), affecting the kidneys, heart and other organs (Kumar et al., 2017). In addition, as discussed above, hypercalcaemia can cause renal failure.

Anaemia is the most common diagnosis characteristic of MM. Due to the growth of plasma cells in the BM, most MM patients present with anaemia, whether it be normochromic or normocytic, and macrocytosis with a deficiency of vitamin B12 (Nau & LeWis, 2008; Dispenzieri & Kyle, 2005). High concentrations of serum immunoglobulin produce rouleaux formation, which increases erythrocyte sedimentation time (ESR). Anaemia and haemoglobin levels have a strong correlation with the percentage of myeloma cells in the BM. Furthermore, cytokines offer a rich environment in BM for MM cell proliferation but are unfunctional for erythropoiesis. For example, tumour necrosis factor-α (TNFα) and Interleukin 1 (IL-1) inhibit erythropoiesis. In myeloma patients, the level of erythroid apoptosis mediated by the Fas ligand is enhanced. For example, myeloma-induced renal insufficiency results in a relative erythropoietin deficiency, which is responsible for anaemia in MM patients (Perfectionalis, 2018; Dispenzieri & Kyle, 2005).

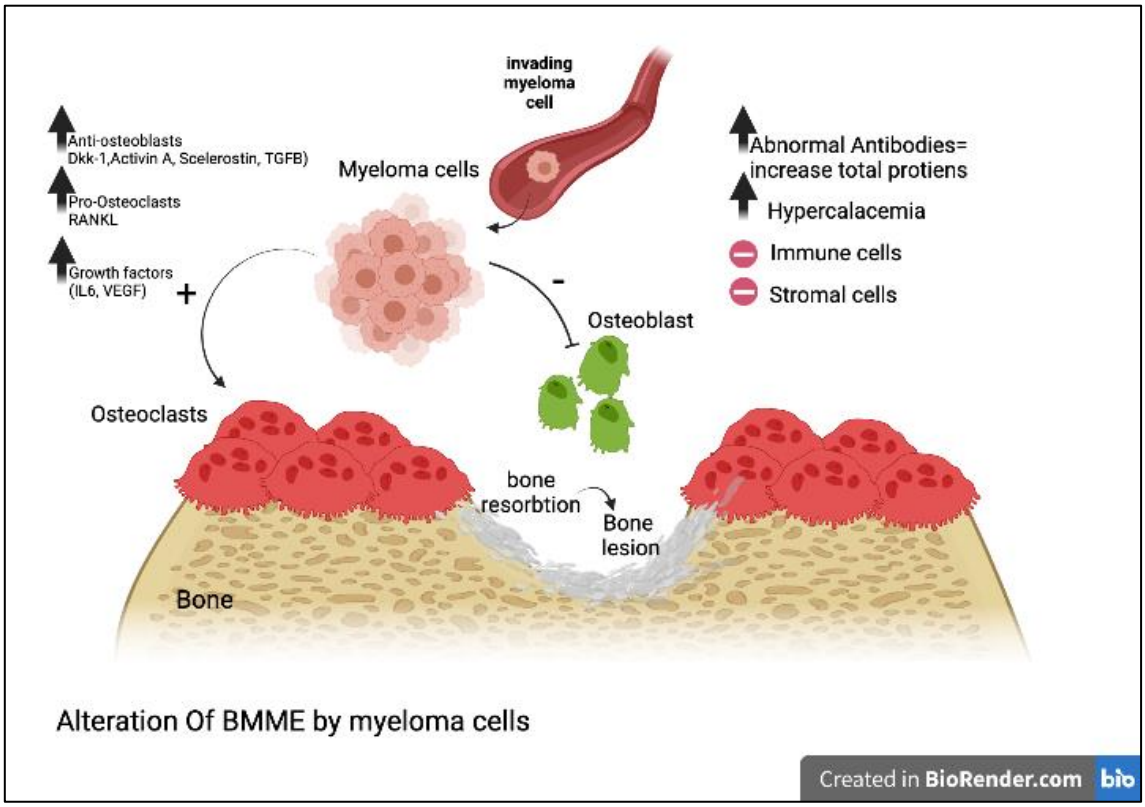

Figure 1.1: Alteration of the bone marrow microenvironment by Myeloma cells.

Myeloma cells play a huge role in manipulating the Bone marrow microenvironment (BMME) by increasing anti-osteoblasts (DKK-1, Activin A, Sclerostin, and Transforming growth factor-β (TGFB)) to inhibit osteoblast from rebuilding new bone, increase pro-osteoclast nuclear factor κ B ligand (RANKL), and growth factors (IL6, VEGF) to elevate osteoclasts for bone destruction. Hypercalcemia is a result of bone destruction, which may lead to kidney failure. Also, the increase of abnormal antibodies will raise blood total protein, resulting in hyperviscosity (Image adapted from (Lawson, 2017)).

1.3 Normal B Cell Development

B cell or B lymphocyte is the primary player in the adaptive immune response, responsible for humoral immunity. B cell production begins in the foetal liver during intrauterine development and continues in the BM after birth through the rearrangement of immunoglobulin (Ig) genes to produce a functional B-cell receptor precursor (Figure 1.2). Following this step, the naïve B cells migrate to the germinal centre to initiate activation. Protein antigen activation of B cells involves their functioning as antigen-presenting cells (APC), presenting protein epitopes on major histocompatibility complex class II (MHC II) to helper T cells. Some T-independent

antigens like polysaccharides, lipopolysaccharides, and other non-protein antigens can directly activate B cells without antigen processing and presentation to T cells (Althwaiqeb & Bruno, 2024; Morgan, Walker, & Davies, 2012). Next is the beginning of affinity maturation, and this step is done by presenting antigens from APC to the naïve B-cells. Somatic hypermutations (SHM) are produced by DNA encoding of the hypervariable region of the (IgH) to generate highly specific antibodies (Morgan, Walker, & Davies, 2012; González et al., 2007). The role of these antibodies is improved by class switch recombination (CSR), to produce antibodies of different immunoglobulin isotypes. In particular, activation-induced deaminase (AID) is required to activate SHM and CSR; they are also moderated by the generation of double-strand DNA breaks (DSBs) in the Ig loci11. As a result of the chromosomal translocation, a DSB is induced to undergo local repair and to be attached elsewhere in the genome (Althwaiqeb & Bruno, 2024; Morgan, Walker, & Davies, 2012; González et al., 2007). Moreover, chromosomal translocations are known as one of the molecular hallmarks of MM.

1.4 Normal Plasma Cells

PCs are part of the lymphoid line differentiated from the B lymphocytes, they are located in the BM and lymph nodes. They play a huge role in immune defence, providing the immune system with specific protection against pathogens, such as bacteria, viruses, fungi, and toxins. They are governed by the tight regulation of transcription factors to provide suitable immune reactions against pathogens. Stromal environments or niches that can control the differentiation, function, and survival of immune cells are usually provided by lymphoid tissues (Figure 1.2) (Imane, Meryem, & Moncef, 2024; Brookens et al., 2024; Moser et al., 2006). PCs differentiation has two pathways, short-lived and long-lived cells, and they differ according to their exposure to the appropriate stimuli for activation. Numerous cytokines have a fundamental role in PCs differentiation. For example, TNFα, CD40, IL2, IL4, IL5, IL6, IL10, IL21 and IL3 can upregulate X box-binding protein 1 (Xbp1) mRNA in mouse B cells, and Xbp1 is essential for PCs differentiation. In particular, IL4, a multifunctional cytokine, has an effect on T cells, mast cells, basophils and B cell differentiation and maturation. Regularly, IL4 stimulates Ig class switching to IgG and IgE, as well as preventing apoptosis. IL4 is involved in the differentiation of PCs and can lead to their survival. IL4 and CD40 have a similar

function in producing Ig in B cells (Oracki et al., 2010; Minges Wols et al., 2007; Moser et al., 2006; Iwakoshi et al., 2003; Rudge et al., 2002).

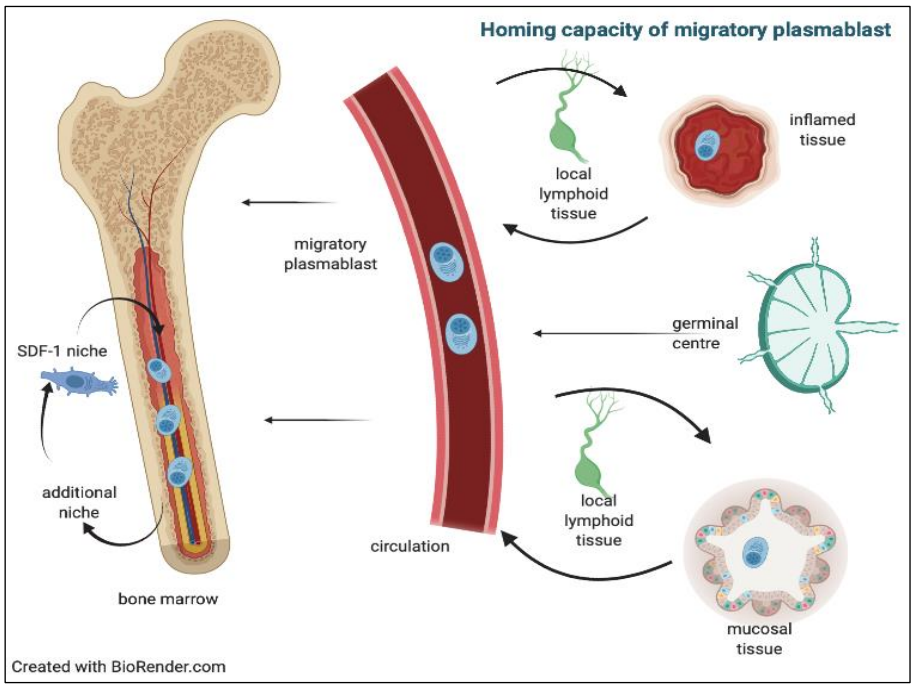

Figure 1.2: B cell development and the homing capacity of a migratory plasmablast

The impact of the stromal environment on the homing capacity of a migratory plasmablast will determine the terminal differentiation and survival of plasma cells. T-cell dependent or chemokines receptors (e.g. inflamed or mucosal sites) will stimulate the homing capacities of migratory plasma cell precursors. The germinal centre provokes plasmablasts to differentiate into long-lived plasma cells and their accumulation in the BM. (figure adapted from (Moser et al., 2006).

In vivo studies have shown IgG-positive (IgG^+) BM plasma cells are long-lived *in vivo* by stimulation of specific factors provided by T cells or dendritic cells, but when isolated *in vitro*, they undergo apoptosis. Stromal-derived factor-1 (SDF-1, also known as CXCL12), IL6 and CD44 are a combination of special survival factors and can rescue plasma cells *in vivo* from apoptosis (Moser et al., 2006). However, the BM contains stromal niches that can support long-term plasma cell survival. Interestingly, mice that have a genetic deletion in B cell lineage-specific SDF-1 receptor CXCR4, show delays in the accumulation of specific plasma cells in BM. Despite this, there is limited knowledge on the role of the different niches in BM and their function in controlling plasma cell response (Figure 1.2) (Moser et al., 2006).

1.5 Plasma Cell Differentiation

B lymphocyte-induced maturation protein (BLIMP1) has several key roles in plasma cell differentiation. BLIMP1 downregulates paired box genes 5 (PAX 5) to halt B cell maturation and upregulates XBP1, as well as cytokines that help plasma cell differentiation, as mentioned above. BLIMP1 also encourages c-myc to exit the cell cycle and initiate proliferation. It also upregulates CXCR1 to promote homing and maintenance of plasma cells (Khamyath et al., 2024; Abduh, 2024; Morgan, Walker, & Davies, 2012; Oracki et al., 2010; Tarlinton et al., 2008; Iwakoshi et al., 2003; Cruz et al., 2001). Expression of interferon regulatory factor 4 (IRF4), BLIMP1, and XBP1 are important for the ongoing survival of PCs, while XBP1 is a transcription factor that has a key role in intermediating the final stages of plasma cell development (Khamyath et al., 2024; Morgan et al., 2012; Oracki et al., 2010; Iwakoshi et al., 2003). Inositol-requiring enzyme 1α (IRE1α) is a key sensor of unfolded protein and cellular stress in the endoplasmic reticulum. IRE1α is responsible for XBP1 splicing to its active transcriptional state XBP1s (Morgan, Walker, & Davies, 2012). Moreover, XBP1s provide a fundamental role in growth and survival signals and stimulate the creation of genes necessary for Ig production and the unfolded protein response (UPR) (Khamyath et al., 2024; Morgan, Walker, & Davies, 2012; Carrasco et al., 2007; Iwakoshi et al., 2003). Overexpression of XBP1 in myeloma patients can prompt pathogenesis and has shown impaired outcomes such as an increase in myeloma cell growth and elevation in OC formation that can lead to the development of bone lesions (Yang et al., 2015; Iwakoshi et al., 2003).

The plasma cell membrane has many receptors for interaction with niche components, such as the CXCL12 receptor CXCR4. Also, plasma cell surfaces contain CD44 regardless of BLIMP1 existence. Establishment in the BM niche is determined by the level of receptors on the plasma cell membrane and their ability to home to BM (Khamyath et al., 2024; Abduh, 2024; Oracki et al., 2010). More recently, BLIMP-1 has been shown to regulate the size and fitness of plasma cells by controlling the mammalian target of rapamycin complex 1 (mTORC1), and the IRF4 controls the endoplasmic reticulum organisation and mitochondrial activity. This transcriptional program can control the epigenetic regulation (Khamyath et al., 2024).

1.6 Overview of Genetic Alternations in Multiple Myeloma

Progression of the genomic aberrations in MM begins within germline events (Figure 1.3). These may lead to disease development and resistance to treatment and can be divided into two incidents. The primary genomic events are chromosomal translocations and/or hyperdiploidy affecting immunoglobulin heavy chain (IgH) genes. They occur due to inaccuracies in VDJ recombination, a process involving chromosomal breakage and re-joining during B-cell development from the pre-pro-B phase to the pro-B cell phase. These translocations position oncogenes under the influence of potent enhancers located at IgH. The occurrence of IgH translocations is noted to escalate with the progression of the disease: 50% in Monoclonal Gammopathy of Undetermined Significance (MGUS) and smouldering MM (SMM), 60-65% in intramedullary MM, and 80% in extramedullary MM. While secondary events are more complex, they occur based on the primary events, such as gene mutations by chromosomal translocations, copy-number variations and single nucleotide variants (Wiedmeier-Nutor & Bergsagel, 2022; Barwick et al., 2019; Kumar et al., 2017; Manier et al., 2017; Morgan, Walker, & Davies, 2012). Moreover, the MYC gene is known to be affected by chromosomal translocations and copy-number variations and somatic mutations are known to affect mitogen-activated protein kinase (MAPK), NF-κB and DNA-repair pathways (Wiedmeier-Nutor & Bergsagel, 2022; Chng et al., 2007).

Morgan *et al.* (2012) pointed out that the characteristic features of myeloma cells involve an intimate relationship with the bone marrow microenvironment (BMME). In particular, plasma cells are supported in specialised niches to maintain their survival (Morgan, Walker, & Davies, 2012).

Translocations contain a limited number of repetitive common genes such as IgH and Histone-lysine N-methyltransferase 2 (NSD2), Fibroblast growth factor receptor 3 (FGFR3), and Cylclin D1 gene (CCND1) and express an essential class of primary actions identified in MGUS, SMM, and MM. In fact, the fusion of the IgH enhancer with other genes results in enhanced expression of partner genes (Table 1.3). (Wiedmeier-Nutor & Bergsagel, 2022; Heider et al., 2021; Barwick et al., 2019; Kumar et al., 2017).

Table 1.1: Chromosomal translocation and the genes involved in MM (taken from (Heider et al., 2021; Kumar et al., 2017))

Chromosomal translocation	Genes involved	Percentage in MM patients
t(11;14)	CCND1	14-15%
t(4;14)	NSD2, FGFR3	11-15%
t(14;16)	MAF	3-5%
t(14;20)	MAFB	1.5%
t(6;14)	CCND3	1-2%

Another form of mutation that may occur in MM patients is hyperdiploidy, and these patients are less likely to have primary IgH translocation. Nevertheless, patients with both IgH translocation and hyperdiploidy were identified in lesser numbers, 14-38% in patients between pseudodiploidy and hyperdiploidy. Moreover, Heider *et al.* (2021) mentioned that this percentage has increased to 50-60% (Heider et al., 2021; Kumar et al., 2017; Chretien et al., 2015). MM patients with hyperdiploidy are characterised by co-occurring trisomies in some chromosomes, including chromosomes 3, 5, 7, 9, 11, 15 and 19, and these are related to a good prognosis, while worse outcomes are correlated with trisomy 21 which is related to Down syndrome, nevertheless, it is a rare case (Kumar et al., 2017; Chretien et al., 2015).

Overall, some myeloma cells could escape from treatment, enter the dormant state, and cause the disease to relapse. Therefore, studying DMCs will provide us with a better understanding of their life cycle and how to eliminate these cells completely

1.7 Diagnosis of Multiple Myeloma

During the past decade, studying and understanding MM disease biology and the different classes of drugs with the role of supportive care have changed the style of treatment and management (Kumar et al., 2017). MM diagnosis follows the International Myeloma Working

Group (IMWG) criteria. IMWG is based on monoclonal protein levels, BM infiltration of clonal plasma cells, the validation of new biomarkers and CRAB features, followed by diagnostic tests for treatment response (Kumar et al., 2017). IMWG may soon lead the re-classification of high-risk patients with SMM to newly diagnosed myeloma (Chakraborty & Majhail, 2020). Imaging techniques have been developed to detect early disease, such as low-dose whole-body computed tomography (CT) and positron emission tomography/computed tomographic scans (PET/CT). Thus, patients will be observed for bone lesion changes and clonal BM PCs replacement in BM. In addition, the serum of free light chain (FLC) ratio can indicate the disease progression (Kumar et al., 2017; Mahindra & Ng, 2016; Dispenzieri & Kyle, 2005).

1.8 Treatment of Multiple Myeloma

Novel therapies have decreased mortality rates in MM, such as chimeric antigen receptor T cell (CAR T)- CD19 specific, proteosomes inhibitors (PIs), e.g., btz, HDACi e.g. Pan, IMiDs, e.g. Pom, and mAbs e.g. Daratumumab (anti-CD38), as well as autologous hematopoietic cell transplantation (AHCT) (Table 1.2) (Chakraborty & Majhail, 2020). Novel therapeutic developments improve and maintain a patient's quality of life, avoid organ damage, and increase long-term survival rates, yet disease relapse still occurs (Chakraborty & Majhail, 2020).

A hallmark of cancer is a higher rate of proliferation than healthy cells, and yet some cells can undergo dormancy during tumour growth and during treatment as a survival method (Komarova & Wodarz, 2007). Disease relapse following treatment leading to aggressive and drug-resistant cancers is the main clinical challenge. Yet, drug-resistant and/or DMCs are the major cause of disease recurrence, aggressiveness, and poor clinical outcome to primary treatment (Damen, van Rheenen, & Scheele, 2020; Komarova & Wodarz, 2007) .

Table 1.2: Drugs used in the clinical management of MM (adapted from (Kumar et al., 2017)

Type of drug	Drugs name	Mechanism of action
Proteasome inhibitors (PI)	Bortezomib (Btz) Carfizomib (Carf) Ixazomib (Ixa)	Block proteasome, a cellular machine that degrades damaged unwanted proteins. This leads to build up of

		unwanted proteins and disrupts normal functions causing them to die.
Immunomodulatory drugs (IMiDs)	Thalidomide (Thal) Lenalidomide (Len) Pomalidomide (Pom)	Regulate immune responses by targeting key pathways like cereblon-mediated protein degradation, cytokine modulation, and checkpoint inhibition. They enhance or suppress immune activity for treating cancer, autoimmune diseases, and inflammation.
Monoclonal antibodies (mAbs)	Daratumumab (anti-CD38) Elotuzumab (anti-SLAMF7 (signalling lymphocytic activation molecule family member 7))	Abs is produced to target specific proteins on myeloma cells to block the growth, deliver toxins directly and kill myeloma cells.
Histone deacetylase inhibitor (HDACi)	Panobinostat (Pan)	Block HDAC enzymes, increasing histone acetylation and leading to chromatin relaxation, which enhances gene transcription. This promotes tumour suppressor gene activation, cell cycle arrest, apoptosis, and reduced cancer cell proliferation.
Alkylating agents	Melphalan (Mel) Cyclophosphamide (Cyc) Bendamustine (Ben) Cisplatin (Cis)	Work by adding alkyl groups to DNA, causing crosslinking, strand breaks, and mispairing, which disrupts DNA replication and transcription. This leads to cell cycle arrest and apoptosis, primarily affecting rapidly dividing cancer cells.
Others	Dexamethasone (Dex) Prednisone (Prd)	A corticosteroid binds to glucocorticoid receptors, altering gene transcription, and inducing apoptosis in lymphoid cells making them useful for haematological malignancies.

	Etoposide (Eto)	Prevent DNA repair by stabilising the topoisomerase-II-DNA complex
	Doxorubicin (Dox)	Intercalates into DNA inhibiting topoisomerase-II leading to apoptosis.
	Chimeric antigen receptor T cell (CAR T)	Genetically engineered T cells express a synthetic receptor through several strategies e.g. targeting CD19, CD38, CS1or BCMA on B cells leading to death.

One reason why MM is so difficult to treat is its genetic heterogeneity, which includes genetic mutations, for example, copy number abnormality, DNA hypomethylation, and acquired mutations in some genes such as N-RAS, K-RAS, FGFR3 and TP53 (Damen, van Rheenen, & Scheele, 2020). Still, dormant myeloma cells, microenvironment protection, and genetic evolution are factors that allow the disease to resist treatments and undergo relapse, this explains that MM is incurable. More details are explained in the next section 1.9 and in chapter 4.

1.9 Stages of Multiple Myeloma Progression

MM has asymptomatic premalignant states, is associated with poor prognosis, and has a low survival rate (5-year survival rate is 53.2%) (Heider et al., 2021; Landgren et al., 2009). Disease progression can be continuous, but it is generally divided into different stages (Table 1.3). It can be initiated by MGUS, described by the production of abnormal immunoglobulin and infiltration of clonal plasma cells in the BM (Heider et al., 2021; Kane, 2020; Kumar et al., 2017; Mahindra & Ng, 2016). Patients with MGUS are usually asymptomatic but may have some clinical signs, for example, recurrent infection. MGUS can progress to SMM with a progression rate from 0.5-1% per year (Heider et al., 2021; Kane, 2020; Pratt et al., 2015; Landgren et al., 2009). SMM is defined as an intermediate condition with a higher percentage of clonal PCs than the MGUS. It is caused by higher levels of abnormal immunoglobulins or monoclonal M proteins in the BM. Both MGUS and SMM are asymptomatic and do not cause organ damage. Progression from SMM to overt MM can lead to a 10% increase in the first 5

years, followed by a 3% increase over the next five years, and a 1% increase in the 10 years after the initial diagnosis. SMM could take up to 15 years until its defined by CRAB criteria. Clinically the disease progresses sequentially between MGUS, SMM and MM, with a unique framework to incorporate the genomic development, treatment resistance, and recurrence (Figure 1.3) (Heider et al., 2021; Kane, 2020; Pratt et al., 2015; Landgren et al., 2009).

Table 1.3: Differences between MGUS, SMM, and MM (Heider et al., 2021; Kumar et al., 2017; Mateos & Landgren, 2016).

	MGUS	**SMM**	**MM**
Definition	Monoclonal gammopathy undetermined significance	Smouldering multiple myeloma	Multiple Myeloma
Symptoms	Asymptomatic premalignant stage	Asymptomatic Malignant stage	Symptomatic Malignant stage
Location	BM	BM	BM
Mutation	Hyperdiploidy	Hyperdiploidy	Aneuploidy
M-protein in serum (main key distinguishing between disease progression)	< 3 g/dl	≥ 3 g/dl	3 g/dl (or any level with symptoms)
CRAB criteria	Absence of CRAB features	amyloidosis	fatigue or dyspnoea related to anaemia, bone pain related to bone disease and neurological symptoms related to hypercalcaemia, hyperviscosity or spinal cord compression (due to spinal lesions)
Clonal bone marrow plasma cells (BMPC) infiltration	<10%	10-60%	≥ 10% or biopsy-proven plasmacytoma
Risk of progression	1% per year	10% per year	Active, requires treatment

Need of treatment	Only monitoring	Close observation	Immediate therapy required

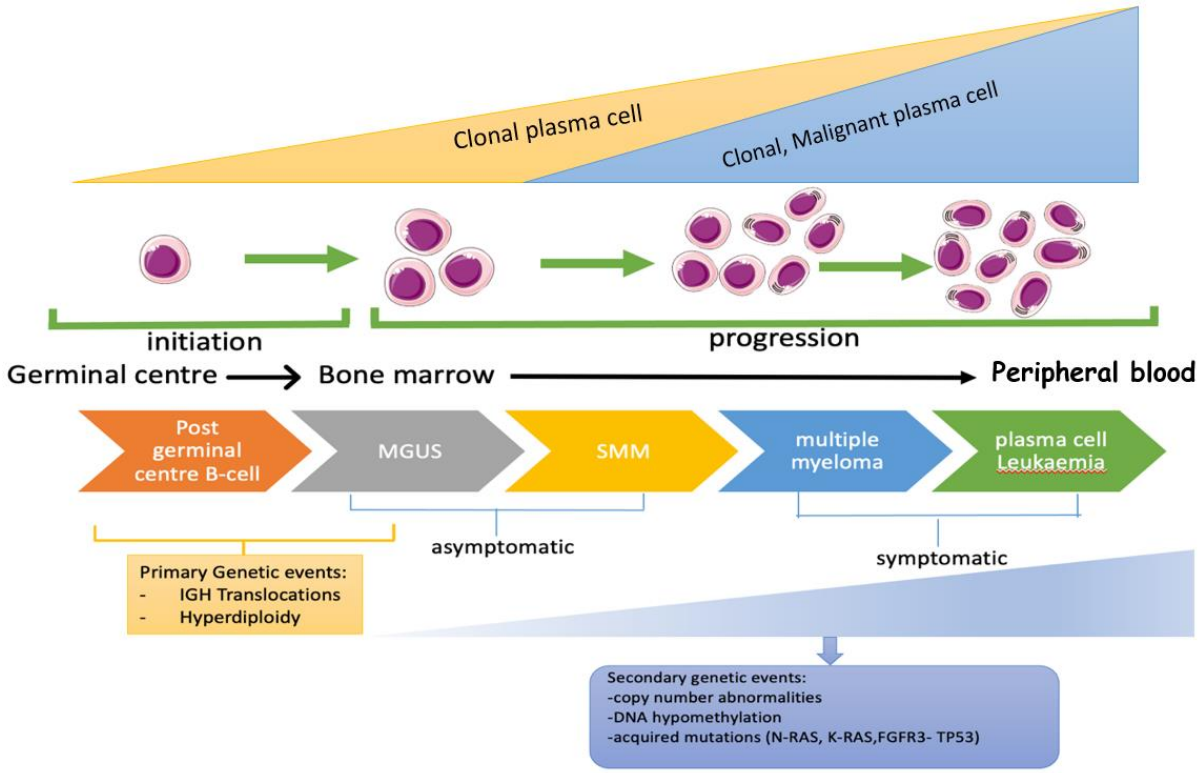

Figure 1.3: The stages of disease progression in MM

MM is a multistep process initiated with precursor disease states, such as MGUS and SMM. Clinically, there are a lot of similarities between MGUS, SMM, and MM but they are also well defined. MM can escape the BM in the later stages of the disease to extramedullary sites to become PCL. Primary genetic events in the development of MGUS, SMM and MM contain chromosomal translocation in IgH genes and hyperdiploidy. The progression to secondary genetic events can elevate to genetic aberrations such as copy number abnormality, DNA hypomethylation, and acquired mutations in some genes such as N-RAS, K-RAS, FGFR3 and TP53. (figure adapted from (Kumar et al., 2017)).

1.10 Dormant Tumour Cells

Tumour recurrence is a significant challenge in cancer therapy. Even years after the initial tumour has been removed, many people experience a return of cancer, often in a more

aggressive and metastatic form. The BM may play a role in homing some types of dormant cancer cells, creating a favourable environment for inactive cancer cells to settle and grow. In the case of solid tumours like prostate and lung cancers, secondary skeletal tumours can reappear in 6.9% of patients within 5 years. Meanwhile, MM patients experience a relapse rate of 16% within one year (Smith & Chai, 2024; Srour et al., 2020). This process has been seen in conjunction with the development of dormant cancer cells, which are characterised by cell cycle arrest and are mostly resistant to normal anti-cancer therapy. The majority of cancer cells are eliminated after cancer therapy at the primary site; nevertheless, some cancer cells may adopt a quiescent state in order to survive and cease reproducing, which is thought to be one of the causes of minimum residual disease (Wang et al., 2021; Phan & Croucher, 2020).

Disseminated cancer cells enter the dormant state through a niche-dependent reprogramming process, engaging with supportive niches such as BM and BMME. Upon the activation of cell-intrinsic and extrinsic stimuli, these rare and elusive cells may restore their proliferative powers, potentially promoting the growth of tumours and the development of metastases (Dadzie & Green, 2022; Li et al., 2021). The molecular processes underpinning the preservation of resistant dormant cells and their reactivation are vague, although they are still not understood at this point in time. However, growing data has lately revealed that cancer cells' metabolic changes significantly impact their ability to advance through the cell cycle.

Disease relapse can occur in several secondary metastatic cancers, and disseminated tumour cells are often the reason. They are typically found in small numbers and are often rare. Cells that originate from the primary tumour site or metastatic lesions can undergo dormancy, and they may persist as MRD following treatment and become resistant to therapy (Dadzie & Green, 2022; Khoo et al., 2019). The term dormant cancer cell is used to describe disseminated primary tumour cells with a latency period and hibernation until reactivation and repopulation under favourable conditions. Also, it is a process when tumour cells undergo G0-G1 cell cycle arrest and establish a non-proliferative state (Smith & Chai, 2024a; Klein, 2011). Dormant cells are frequently characterised by a general metabolic slowdown and an increased ability to cope with oxidative stress, but specific changes in dormant cells may be dictated by various factors such as extracellular matrix composition, stromal cell influence, and nutritional availability, ultimately leading to tumour relapse (Pranzini, Raugei, & Taddei, 2022; Li et al., 2021; Phan

& Croucher, 2020). Dormant cells may accumulate mutations in the early stages of tumorigenesis in a dynamic multistep process characterised by hyper-proliferative reactivation followed by a period of dormancy from which cancer cells may exit to undergo a final malignant transformation, ultimately resulting in tumour mass formation (Pranzini et al., 2022; Phan & Croucher, 2020). Unfortunately, the numbers of studies in this field are insufficient.

1.10.1 DMCs Interaction with BMME

The BMME contains various cells, such as osteogenic lineage cells, OC, OB, fibroblasts, and perivascular, endothelial, and hematopoietic cells. BMME usually provides a healthy environment to produce and maintain blood cells and bone homeostasis. During myeloma disease, the BMME is involved with myeloma cell survival, proliferation, and drug resistance (Smith & Chai, 2024; Dadzie & Green, 2022). Many types of cancer could send their dormant cells reside in the hematopoietic stem cell (HSC) niche as a survival process, such as MM, breast cancer and prostate cancer therefore, they could be modulated by the BMME (Lawson et al., 2015). However, the communication between niche components for long-term survival is still poorly understood. The pathogenesis of MM is influenced by the direct and indirect interaction between myeloma cells and the BMME (Dadzie & Green, 2022). In addition, HSCs residing in BM niches have a role in HSC dormancy, self-renewal, and mobilisation. Therefore, it has been speculated that dormant cancer cells also reside in similar niches (Phan & Croucher, 2020; Lawson et al., 2015; Aguirre-Ghiso, 2006).

Detailed knowledge about DMCs is limited, and there is little information from clinical studies as most studies have been done in murine models. Therefore, the remaining challenges in this area are finding ways to study the dynamic connections between dormant tumour cells and the BMME niche. The use of high-resolution deep tissue imaging through complete bone in live animals has provided some insight into the mechanisms of dormancy; however, further research is needed (Phan & Croucher, 2020; Lawson et al., 2015). Lawson *et al.* (2015) demonstrated an increase in myeloma cells when Receptor activator of nuclear factor κ B ligand RANKL was introduced to mice; they illustrated an elevation in OC, which decreased the DMCs in BM. Therefore, the OB and OC in the bone have been demonstrated to play a critical role in myeloma cell dormancy. BMME remodelling will cause DMCs to be switched

"on" and "off" (Lawson et al., 2015). OB maintain cells in a latent condition, while osteoclastic bone resorption drives their growth. (Phan & Croucher, 2020; Lawson et al., 2015). Key molecules expressed by dormant cells have been found; these include AXL receptor tyrosine kinase (Axl) and Tripartite motif 44 (TRIM44), which maintain MM dormancy in the BM niche (Figure 1.4) (Khoo et al., 2019; Chen et al., 2019; Yan et al., 2019; Zhu et al., 2019; Lawson et al., 2015).

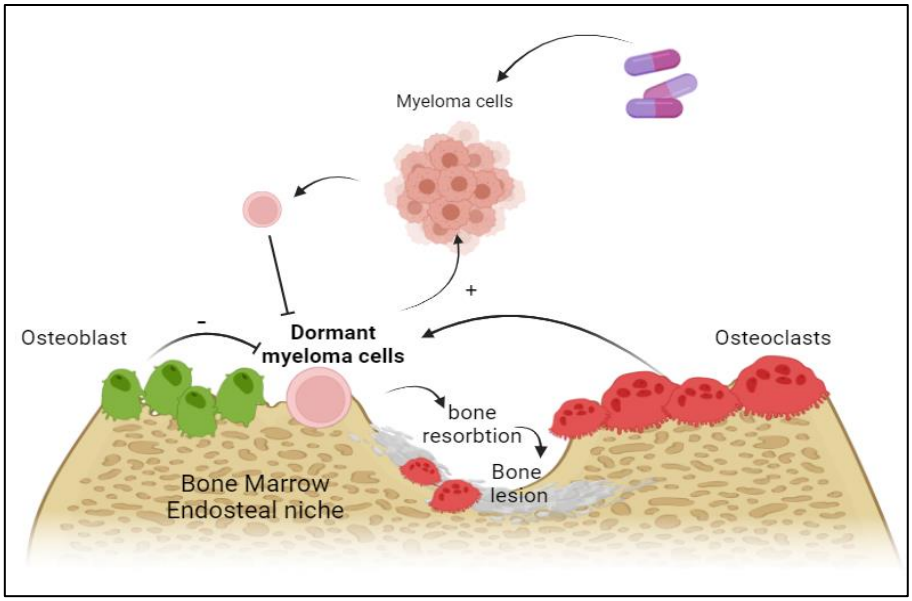

Figure 1.4: DMCs interaction with the BM cells.

The illustration shows how BMME influences disseminated myeloma cells to undergo a dormant state through OB interaction and, therefore, resist chemotherapy. OC can reactivate DMCs and cause relapse (image generated by biorender.com).

1.10.2 Hallmarks of Cancer Cells

Hanahan, 2000 was the first to distinguish between normal cells and cancer cells and explained a set of characteristics to understand the complex of cancer biology to develop a new cancer therapy. These hallmarks include uncontrolled cell growth, which means that cancer cells can stimulate their own growth and division, ignore signals to stop growing, resist and avoid programmed cell death (apoptosis). Cancer cells can achieve unlimited proliferation, unlike normal cells that have a limited number of divisions before going to senescence, and stimulate angiogenesis formation to supply cancer cells with nutrients and oxygen and metastasis to

occupy surrounding tissue or distance sites. These hallmarks arise due to genetic instability, which promotes the necessary genetic changes, and inflammation, which supports their development. More recently, additional hallmarks have been recognised and added to the previous: changes in energy usage through altering their metabolism to support rapid growth, the ability to evade and control the immune system to halt it from targeting the tumour cells, unlocking phenotypic plasticity, promoting inflammation to create a supportive microenvironment for tumour progression, non-mutational epigenetic reprogramming, polymorphic microbiomes (Hanahan, 2022; Hanahan & Weinberg, 2000). On the other hand, dormant cancer cells are essentially cancer cells that found a way to pause proliferation or slow down their growth by adapting or manipulating the classic cancer hallmarks to find a way to survive. The hallmarks of dormant cancer cells will be explained next in section 1.10.3.

1.10.3 Hallmarks of Dormant Cancer Cells

Dormant cancer cells exist in a unique cell state as part of coping and surviving a new situation, and that is partially regulated by the specific local environment of the niche where they reside. Therefore, it is believed that the following hallmarks can define a dormant cancer cell state: Niche dependence; this refers to the interactions and adaptations of cells to their specific microenvironment. Cell cycle arrest at the G0-G1 phase is demonstrated by the prolonged retention of high levels of a suitable intravital dye. Drug resistance is evidenced by the survival of cells following chemotherapy. Immune evasion is the ability of cells to evade immune destruction. Metastasis is the capacity of cells to form tumours after their release from BM control, but this is specialised to solid tumours. While blood cancer could spread to other organs like the liver, spleen, or lymph nodes (Figure 1.5) (Smith & Chai, 2024; Dias et al., 2021; Phan & Croucher, 2020).

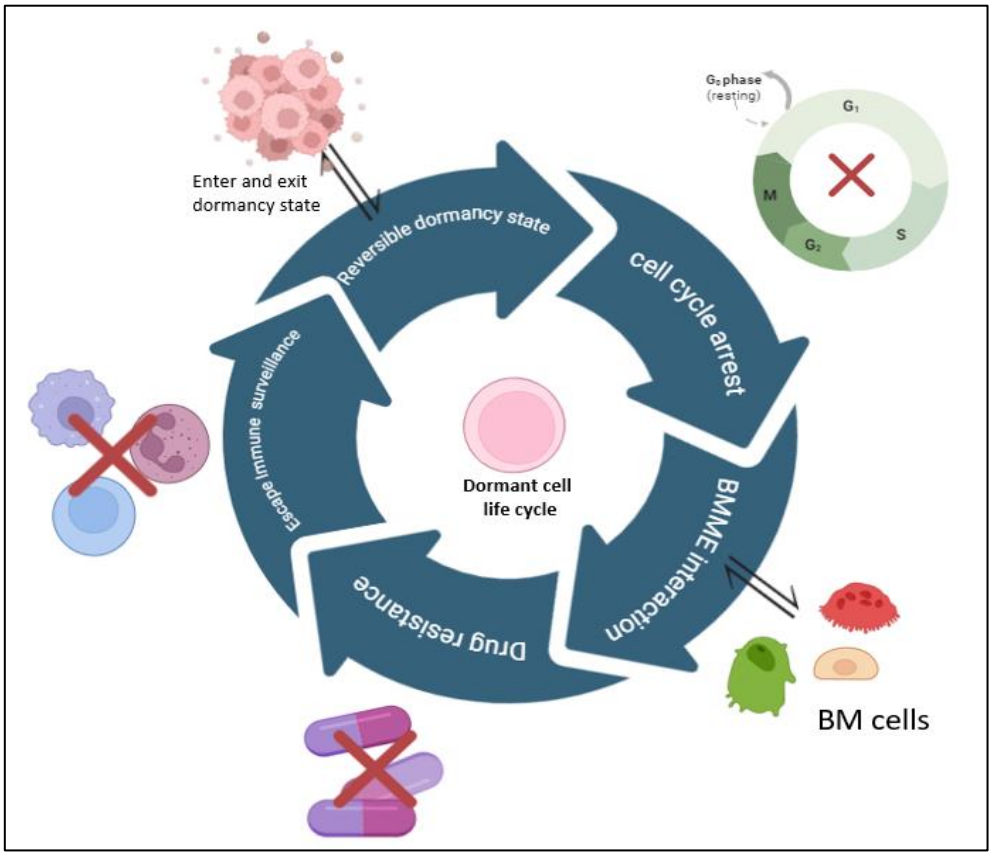

Figure 1.5: Cell dormancy hallmarks.

As a part of adaptation, cancer cells can force cells to reside in BM, halt the cell cycle in the G0-G1 phase, engage with the surrounding cells, resist therapy, hide from immune surveillance, and dormant cells will reactivate in favourable conditions. (Image adapted from (Smith & Chai, 2024)).

1.10.4 The Relation between Dormant Cancer Cells and Cancer Stem Cells

Dormant cancer cells and cancer stem cells (CSCs), while sharing some key characteristics, also exhibit significant differences. Both cell types can enter a state of dormancy or quiescence, characterised by decreased proliferation and metabolic activity, which unfortunately often correlates with drug resistance. Furthermore, both dormant cells and CSCs show activation of stemness-related signalling pathways like Notch, Wnt, and Hedgehog, promoting self-renewal, survival, and differentiation. Both cell types also interact with their microenvironment, including the extracellular matrix, to support survival and maintain their respective dormant or stem-like states (Quayle, Ottewell, & Holen, 2018; Weidenfeld & Barkan, 2018; Yu et al.,

2012). A key distinction lies in their surface markers. CSCs are typically identified by markers such as CD44, CD24, and EpCAM (Katoh, 2017), whereas dormant cancer cells express different markers, including Irf7, Spi-C transcription factor (Spic), Axl, Vascular cell adhesion molecule 1 (Vcam1), and Signal regulatory protein α1 (Sipra) (Khoo, et al., 2019). Finally, although they share some signalling pathways, their activity levels differ. Dormant cells exhibit heightened activity in stress response pathways compared to CSCs, while CSCs rely more heavily on pathways that promote self-renewal (Jalil et al., 2023; Quayle, Ottewell, & Holen, 2018; Katoh, 2017; Kleffel & Schatton, 2013). Thus, a deeper understanding of the biological mechanisms in dormant cancer cells and CSCs could lead to improved methods for uncovering and treating advanced tumours.

1.10.5 Life Cycle of Dormant Cancer Cells

Dormant cells have a life cycle to undergo dormancy, which Phan and Croucher (2020) have divided into different stages. **The first stage** begins with opting for the right niche. Disseminated cancer cells seek the right niche based on the primary tumour's tissue of origin and histological subtype. For instance, prostate cancer and breast cancer have an affinity for bone, while MM already initiate and resides in bone, triple-negative breast cancer prefers visceral organs. Still, there is little known about the mechanism of dormant cells homing the BM niche. Some studies have shown that certain cells, such as myeloma cells, are capable of replacing the entire BM cells completely as the disease progresses. The disseminated myeloma cells interact with the BMME during this progression through the CXCL12-CXCR4 signalling pathway (Smith & Chai, 2024; Dadzie & Green, 2022). This interaction facilitates the chemotaxis and invasion of tumour cells into the bone. Lawson *et al.* (2015) study used intravital imaging and revealed that myeloma cells circulate the body for several days before home to the BM endosteal niche (Lawson et al., 2015).

The second stage involves engaging and interacting with the BM niche cells; when MM, breast, and prostate cancer cells become dormant, they interact with the surrounding cells and their secreted molecules to induce dormancy. Lawson *et al.* (2015) co-cultured osteoblast-like cells (MC3T3) osteoblast precursor cells with 5TGM1 and illustrated a reduction in cell proliferation *in vitro* (Lawson et al., 2015). Dormancy could be induced through upregulation

of growth arrest-specific 6 (GAS6). It is a ligand of the TAM family receptor tyrosine kinase (TYRO3, AXL and MER). Studies have revealed that OB can produce GAS6 and prevent PC3 and myeloma cell proliferation. The GAS6-AXL signalling could induce dormancy in MM (Khoo et al., 2019; Yumoto et al., 2016).

The third stage is reprogramming and adaptation to the niche. It was thought that cancer would metastasise at the late stage of the disease, while studies have revealed that cancer cells can disseminate at an early stage during progression and then reactivate when needed (Phan & Croucher, 2020). Lawson *et al.* (2015) isolated 5TGM1 myeloma cells that have proliferated and lost their DID labelling *in vivo* and then labelled them with CMDiL and transplanted them in recipient mice. They observed that some of these cells proliferated, and a small fraction became dormant. This explains that dormancy could be initiated in a suitable environment and could be reversible (Lawson et al., 2015). Khoo *et al.* (2015) found that some genes were the major regulator of dormancy, over-expressed *in vitro* when co-cultured with MC3T3 cells and *in vivo*, such as interferon-regulatory factor 7 (IRF7), Spi-C transcription factor (SPIC), signal-regulatory protein α 1 (SIPRA), and vascular cell adhesion molecule 1 (VCAM1) and (tyrosine kinase receptor AXL) (Khoo et al., 2019). The study has suggested that these genes were associated with inducing dormancy inside the endosteal niche when myeloma cells get in contact with the BM cells (Phan & Croucher, 2020; Khoo et al., 2015).

The fourth stage is long-term dormancy establishment; this stage is related to how dormant cells can escape from immune cells and survive. Some genes like Fcγ receptor I (Fcgr1), macrophage-expressed gene 1 (Mpeg1), and SIPRA were associated with immune cells such as mast cells, monocytes, and macrophages, which will have a role in surviving immune surveillance. Regarding Khoo *et al.'s*. (2015) study, IFNγ has a role in immune-mediated dormancy in myeloma cells to express interferon signalling to control the expression of IRF7 and SPIC (Khoo et al., 2019). Surprisingly, IRF7 could induce MHC II gene expression to activate CD4 T^+ cells, while in DMCs, this could be linked to myeloid-lineage cells that may express interferons, allowing myeloma cells to disguise themselves as orthotopic immune cells within the niche. It is still unclear how MHC II and interferons interact during dormancy in disguise from immune cells; more studies are needed in this field (Smith & Chai, 2024; Weston & Barr, 2023; Dadzie & Green, 2022; Phan & Croucher, 2020; Lawson et al., 2015).

The fifth stage is the reactivation of dormant cells inside the niche. Previously, it was assumed that dormant cells have slowed metabolic rates and rely on glucose, glutamine, and fatty acid metabolism for energy, but it is still unclear if the dormant cells need cell-intrinsic adaptation to survive a poor-nutrient microenvironment. Some dormant cells, such as those in prostate cancer and oral cancer, have correlated reactivation of dormant cells with high expression of CD36, while it is still unclear whether dormant cells are in need of CD36 to survive in the niche. Whilst DMCs can be reactivated when they have stimulated the production of OC by RANKL, which decreases the number of DMCs and increases the proliferating myeloma cells. This confirms that dormant cells are influenced by the cell-extrinsic microenvironment to stay dormant or reactivate to reform tumour (Smith & Chai, 2024; Weston & Barr, 2023; Dadzie & Green, 2022; Phan & Croucher, 2020; Lawson et al., 2015).

1.10.6 Mechanisms of Dormancy in Multiple Myeloma

Studies have revealed that DMCs are encircled by fibronectin and can express integrins to downregulate proliferation signals such as Urokinase-type plasminogen activator receptor (uPAR) and the Raf-MeK-eRK pathway (Aguirre-Ghiso, 2007). Interestingly, though, some biomarkers that are associated with non-proliferating cells, such as Ki67-negative, TUNEL, M30, and members of the Transforming growth factor-β (TGFβ) family, are not specific dormant cell markers, nor senescent cell markers (Damen, van Rheenen, & Scheele, 2020; Miller et al., 2018).

1.10.6.1 Induction of Dormancy on the Intracellular Level

Different studies in dormancy on all cancers revealed that there are intrinsic factors that could have a role in promoting dormancy. Two levels of factors could influence dormancy; firstly, **at a transcriptional level**, like inhibiting cell cycle by reducing PI3K/AKT signalling, which is related to proliferation markers such as Ki67 and PCNA. Then, the Rb-E3f pathway has a role in the cell cycle and determines the cell fate, whether it could undergo proliferation, dormancy, or senescence. The Rb-E3f could set the depth of dormancy too. In addition, metabolic signalling will play a role in dormancy initiation and maintenance for example, inhibition of mTOR is affected by many factors like glucose deprivation, hypoxic environment, or binding to OC in the BM niche, which could promote dormancy survival (Damen, van

Rheenen, & Scheele, 2020). **At a post-transcriptional level,** the BM endothelial cells secrete micro-RNA-126 (miR)-126 to enhance dormancy in chronic myeloid leukaemia (CML). Also, the activation of MAPK could reduce or lose mitogenic signal to halt cell cycle progression. The activation of certain MAPK could lead to dormancy through a crosstalk with different pathways like Rb and AKT signalling that could determine the fate of the cell (Damen, van Rheenen, & Scheele, 2020). All these mechanisms on the intracellular level were studied in various cancers, not MM. Therefore, more studies are needed to understand the mechanism of dormancy in myeloma cell lines.

1.10.6.2 Induction of Dormancy on the Extracellular Level

A study has shown that tumour intrinsic IFN type I have an essential role in prostate cancer cell line (PCa) dormant cells to remain in a dormant state (Owen et al., 2020). Compared to DMCs, it was shown that co-culturing osteoblasts with myeloma cells increases dormancy genes. Khoo *et al.* (2015) study has highlighted the importance of the OB lineage for dormancy regulation in both murine and human myeloma cells; and revealed the signature genes expressed during dormancy included IRF7 and SPIC, in addition to AXL, VCAM1, and SIPRA (Khoo et al., 2019; Lawson et al., 2015).

In addition, GAS6/AXL causes prostate cancer cells to undergo dormancy and controls survival and self-renewal capacity in CML stem cells and myeloma cells (Smith & Chai, 2024; Dadzie & Green, 2022; De Veirman et al., 2019; Khoo, 2018; Shiozawa et al., 2010). The GAS6-AXL pathway was observed to decelerate cell cycling in HSCs, although it is proposed that this could exemplify a mechanism of quiescence in other tumours (Smith & Chai, 2024). *In vivo,* studies have shown that inhibiting AXL leads to the release of myeloma cells from dormancy and renders them sensitive to chemotherapy. Therefore, AXL is a potential target to treat MM dormancy and prevent relapse (Dadzie & Green, 2022; Khoo et al., 2019).

TRIM44 overexpression is exhibited in many kinds of cancer, such as gastric, breast, and non-small cell lung cancer, and can promote migration and invasion of cancer cells through Nuclear factor kappa β (NFκβ) signalling. TRIM44 has been shown to transform myeloma cells to a quiescence phenotype enhance myeloma cells' residence in BM niches, and maintain dormancy (Chen et al., 2019).

Several studies demonstrated the CXCR4/CXCL12 chemokine receptor required for homing and found in high levels in MM. CXCR4 plays a pivotal role in regulating the homing, invasion, migration and mobilisation of myeloma cells, in addition to drug resistance (Smith & Chai, 2024; Damen, van Rheenen, & Scheele, 2020; Phan & Croucher, 2020; Ullah, 2019; Di Marzo et al., 2016; Schueler et al., 2013; Fuhler et al., 2012). CXCR4/CXCL12 could be used as a biomarker target to detect DMC. On the other hand, CXCR4/CXCL12 could release DMCs from the endosteal niche and render them susceptible to chemotherapy.

Overall, various factors and interactions inside BM endosteal niches, such as OC, OB, and transcription factors, can regulate and maintain DMC; many reports have revealed different therapies to release dormancy and make them sensitive to drugs. This strategy could also ultimately lead to patient survival and a cure for MM.

Studying dormancy is challenging. Consequently, numerous studies have examined DMCs using a robust method to distinguish between inactive and actively dividing cancer cells necessary for imaging DMCs *in vivo.* Dyes such as carboxyfluorescein succinimidyl ester, which labels intracellular proteins, are not suitable for studying long-term cancer cell dormancy. CMDiL and CMI dyes could be appropriate for detecting dormant cells but may interfere with green fluorescent protein (GFP) labelling. Thus, myeloma cells were labelled twice, first with fixed genetic reporters and another with lipophilic membrane dye 1,1'-dioctadecyl-3,3,3',3'-tetramethylindodicarbocyanine (DID) (Ren et al., 2022; Quayle, Ottewell, & Holen, 2018; Lawson et al., 2015; Wang et al., 2015). Lawson *et al*. (2015) found that labelled cells dilute the DID dye during proliferation while the cells that retain the DID are dormant (Figure 1.6) (Lawson et al., 2015).

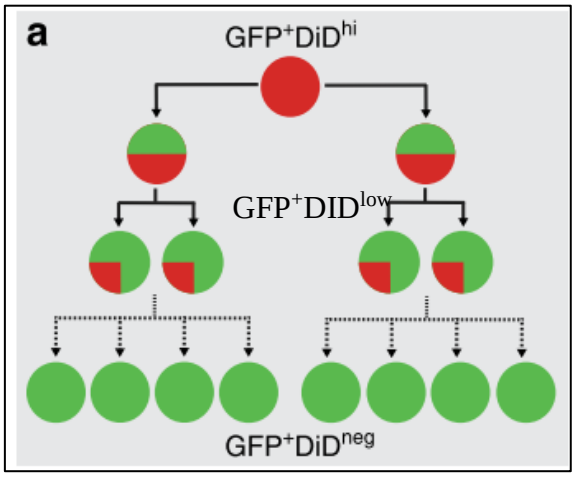

Figure 1.6: Labelling and tracking dormant cancer cells in vitro

Diagram identifying dormant and active labelled cells with GFP and DID, showing how cells lose their DID dye gradually during proliferation. (figure generated from (Lawson et al., 2015)).

1.10.7 Targeting Dormant Multiple Myeloma Cells with Current and Novel Therapies

Over the last few decades, MM treatment has undergone several changes due to an increased understanding of the disease's biology, and more effective classes of drugs have become available (Table 1.2). The goal of MM therapy is to have rapid and effective control of tumour burden whilst avoiding complications and to have the ability to collect stem cells in patients who are eligible for Allogeneic stem cell transplantation (ASCT). Remarkably, survival rates following ASCT have reached up to 86 % (Kumar et al., 2017). Still, there are not many investigations to eradicate the DMCs and stop disease relapse.

MM treatment regimens rely on the stage of the disease and whether the patient has SMM or MM, plus the disease progression and activity. Various factors are taken into consideration when applying specific treatments to MM patients, including age, comorbidities, and patient status. Yet treatment resistance and disease relapse are the major challenges. Clearly, preventing disease relapse at its early stage will be challenging. Thus, different kinds of combination therapies have been tested on MM patients and have given various promising results on overall survival (Abduh, 2024; Kumar et al., 2017; Lawson et al., 2008).

All novel treatments aim to manipulate myeloma cell-extrinsic pathways to prevent cell-intrinsic drug resistance. Various techniques and studies have been applied to understand the mechanism of MM dormancy in correlation with the microenvironment and therapy resistance.

Detecting the niche microenvironment biomarkers has been a target for many studies by searching for biomarkers associated with dormant cells. Several biomarkers have revealed a correlation with OB in the endosteal niche, like, AXL, *Irf7*, *Spic* and Vcam1 (Phan & Croucher, 2020; Damen et al., 2020; De Veirman et al., 2019a; Khoo et al., 2019; Lawson et al., 2015). AXL helps maintain dormant cells in a niche environment. Inhibiting AXL could reactivate these cells; thus, combining it with SoC could help achieve our goal (Suominen et al., 2015). Many studies have investigated AXL tyrosine kinase receptor inhibitors to reduce tumour burden and reach the OS (Zhu, Wei, & Wei, 2019).

Moreover, Chen *et al.* (2019) revealed that the TRIM44 protein's high expression in an osteoblastic niche can cause MM to undergo quiescence and compete with HSC to reside in the niche (Chen et al., 2019). More studies are needed to investigate more dormancy signature genes that may be used in therapy to maintain dormant cell status as they are or could be used as a prognostic marker for early detection of relapse.

Furthermore, the CXCR4/CXCL12 chemokine plays a pivotal role in regulating various functions in MM, including migration and mobilisation. It appears that CXCR4 can maintain OC (Damen, van Rheenen, & Scheele, 2020; Ullah, 2019; Di Marzo et al., 2016; Lawson et al., 2015; Schueler et al., 2013; Fuhler et al., 2012). Expanding studies in this field will allow us to use CXCR4 as a tool for migration and homing of DMC in and out of niche.

Recently, a lab member of the Sheffield Myeloma Research Team (SMaRT) has shown that current SoC myeloma therapies (Btz, Mel, Pom, and Pan) have synergistic effects when used in combination with a myeloma-specific oncolytic virus (OV) (personal communication, Dr Georgia Stewart). Currently, it is unknown if these combination therapies will have any effect on killing DMCs.

Ibrutinib and other Bruton's tyrosine kinase (BTK) inhibitors are now in clinical trials for MM. Critical concerns about the role of BTK in myeloma biology and treatment remain unanswered. Gu *et al.* (2017) demonstrated that a new BTK inhibitor may induce MM cell senescence,

prevent MM cell colony formation, and shrink xenografted tumours originating from MM cell lines *in vivo* (Gu et al., 2017).

Detecting MRD in MM patients is already difficult, and studying DMCs inside the human body is even harder due to their location in the bone. Exposure to frequent imaging may increase cancer risk. Patients who have a lot of repeated imaging usually have a lot of underlying illnesses, especially patients actively diagnosed with malignancy disease (Sodickson et al., 2009). Therefore, using live xenograft mice models is suitable for tracking DMCs, as we can monitor their colonisation, label myeloma cells, and induce them to undergo dormancy within weeks or months. However, further studies are required to investigate suitable murine models to look at DMCs, with the use of novel anti-cancer therapies (OV or others) in combination with conventional therapy (Table 1.2). Since dormant cells are resistant to therapy, a potential strategy involves reactivating dormant cells by manipulating the niche microenvironment and using RANKL (Phan & Croucher, 2020; Lawson et al., 2015). RANKL will increase OC bone resorption, and this has been shown to decrease DMC numbers (Lawson et al., 2015) (Figure 1.7). Hence, activating DMCs will render them sensitive to therapy and can be detected by immunosurveillance.

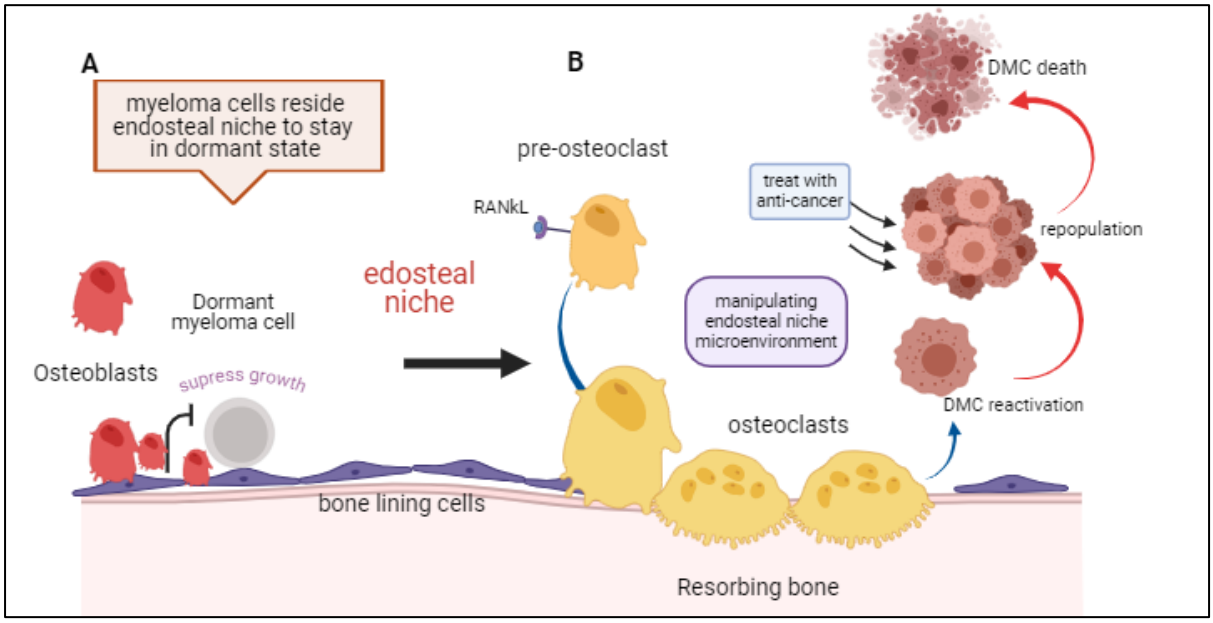

Figure 1.7: Remodelling the endosteal niche microenvironment and targeting dormant myeloma cells

(A) DMCs are disseminated from their population and reside in the endosteal niche; they are kept suppressed by the surrounding microenvironment to stay in a dormant state. (B) dormancy is a reversible state that is switched 'on' by engagement with bone-lining cells or OB and switched 'off' by OC remodelling the endosteal niche (Phan & Croucher, 2020; Lawson et al., 2015).

1.10.8 Combined Treatments on DMCs

We still have insufficient *in vivo* studies on combined therapy's effect on dormancy. Many studies investigated combined therapies to eradicate MRD and achieve a full survival rate by combining SoC drugs together or with novel treatments. Btz can inhibit OC differentiation by blocking the receptor activator NFκβ ligand (RANKL) and stimulating OB formation; Btz will increase bone anabolic activity and reduce tumour burden, this means that Btz has a role in bone remodelling (Wang et al., 2020; Accardi et al., 2015). However, Btz-resistant cells exist, and studies have investigated Btz combined with Len, Pan and Dex has improved in the *in vivo* experiments and enhanced patient's overall survival (Durie et al., 2017; Horton et al., 2006; Catley et al., 2006). Many novel therapies have combined different molecules to overcome Btz-resistance. For example, an *in vitro* study that combined Btz with a novel small molecule inhibitor Sepantronium Bromide (YM155) demonstrated robust cytotoxicity in U266, KMS-11 and KMS-12 myeloma cell lines at their G0/G1 phase. This suggests that these cells were in a dormant state, the study showed that the combination of Btz and YM155 have overcome the Btz-resistant cells and the combination also exhibited significant activity against primary MM patient cells, highlighting its potential as a promising therapeutic option for myeloma treatment (Ookura et al., 2017; Ueda et al., 2015)

A nitrogen mustard alkylating agent, Mel, has been used since 1942. Usually, a high dose of melphalan (HDM) combined with ASCT in newly diagnosed MM patients showed remission. Clinical trials suggested combining HDM-ASCT with Dox, Vincristine, or cyclophosphamide to disable remission (Poczta, Rogalska, & Marczak, 2021). Also, combining Mel with Btz, Len, Pom, or Dex showed longer progression-free survival (Gkotzamanidou et al., 2022). The study by Attal et al. (2017) reported approximately 60% of newly diagnosed MM patients achieved complete response after treatment with HDM combined with ASCT. This means that these patients showed no MRD (Attal et al., 2017). In addition, the side effects of HDM were the main problem that could increase mortality, and finding a better Mel derivative that could

reduce the toxicity could be a solution like melflufen has shown mediated toxicity *in vitro* and *in vivo* in single and in combination with Dex or Pom (Kapoor & Gonsalves, 2022; Poczta, Rogalska, & Marczak, 2021; Flanagan et al., 2019; Chauhan et al., 2013). Still, none of these studies examined their effect on DMCs. Besides, Lawson *et al*. (2015) observed that DMCs were mel-resistant (Lawson et al., 2015). Mel could stimulate OC formation, which causes bone loss but does not reduce OB numbers. This will disturb the niche microenvironment and may reactivate DMCs (Chai et al., 2017). Thus, combining Btz with Mel could cause balance and reduce DMCs' resistance to treatment and render them sensitive to Btz. At the same time, Mel could elevate bone loss while Btz could increase bone anabolic activity.

Pom is a potent immunomodulatory agent with high potential in targeting myeloma cells. It has a unique mechanism of action, including direct antiproliferative, pro-apoptotic, and angiogenic effects, in addition to indirect effect to maintaining bone resorption and immune cells by stimulating T cells, activating NK cells, and dendritic cells. Pom can cause cell-cycle arrest and apoptosis. Also, it could reduce OC production through downregulating transcription factor PU.1 (Lacy & McCurdy, 2013; Richardson, Mark, & Lacy, 2013; Chanan-Khan et al., 2013). The Pom combination with Dex, Pan or Btz enhances the survival rate with fewer side effects in relapse/refractory multiple myeloma patients (RRMM). Clinical trials have observed that combining Pom with Dex has enhanced Pom efficacy compared to Pom alone (Eleutherakis-Papaiakovou et al., 2020; Laubach et al., 2020; Katz et al., 2018; Offidani et al., 2014; Richardson, Mark, & Lacy, 2013; Lonial, 2010; Galustian et al., 2009). However, no studies investigated eliminating DMCs with Pom combined SoC agents.

Pan is a histone deacetylase inhibitor that has an anti-myeloma activity through modulating gene expression and protein function in myeloma cells. Pan increases the acetylation of histone proteins and other proteins that can induce cell cycle arrest and/or apoptosis of some transformed cells. Numerous studies have investigated the impact of Pan when used in combination with various therapeutic agents, both *in vitro* and *in vivo*. These studies have revealed that Pan synergises with a drug called MCL1-inhibitor, the MCL1 is a part of BCL2 family protein, IMiDs, Mel, Btz, and Dex to combat drug resistance, leading to improved survival rates among patients with RRMM. Further *in vivo* and *in vitro* research on the Pan effect on dormancy is crucial for a comprehensive understanding of this phenomenon (Tagoug

& Safra, 2023; Gkotzamanidou et al., 2022; Robinson et al., 2022; Eleutherakis-Papaiakovou et al., 2020; Imai et al., 2016; Laubach et al., 2015; Kikuchi et al., 2010; Atadja, 2009). Both pharmaceutical agents disrupt the normal function of cellular proteins, thereby inducing cell cycle arrest and apoptosis, which are recognised as cell death mechanisms. Nonetheless, knowing the precise impact of this drug combination on DMCs requires further comprehensive scientific investigation. To conclude this, we aim to assess the effect of these SoC agents on DMC viability *in vivo*.

Therefore, based on the above, there is limited data on SoC alone or combined on DMCs; therefore, adding knowledge to this field will form the basis of this PhD thesis.

1.11 Thesis Hypothesis and Aims

Based on previous methods used to assess DMCs *in vitro* and *in vivo* (Lawson et al., 2015), we **hypothesised** that DMCs would be targeted more effectively with current Standard of care drugs (SoCs) therapies in combination.

The main project aims to test this hypothesis are as follows:

1. To identify DMC populations *in vitro* over time in a panel of four myeloma cell lines (murine cell line 5TGM1), (human cell lines JJN3, OPM2, and U266). Cells will be labelled with a lipophilic membrane dye DID and then assessed with flow cytometry and fluorescent imaging (Chapter 3).
2. To assess the effects of current SoC therapies (Btz, Mel, Pom, and Pan) on DID-labelled DMCs *in vitro* (Chapter 4).
3. To assess the most effective combination therapy determined *in vitro* (aim 2) on DMCs *in vivo.* Drug effects on tumour burden and myeloma-induced bone disease will also be assessed with this combined treatment (Chapter 5).

Chapter 2 General

Material and Methods

2.1 Materials

2.1.1 Myeloma Cells

2.1.1.1 5TGM1/ 5TGM1-GFP Myeloma cells

The 5TGM1 cell line was generated from repeated passages from 5T33 MM by Garret (1997). The model first appeared in aged C57BL/KaLwRij mice and was later replicated in syngeneic mice. The 5TGM1 cell line is equipped with luciferase (Luc), allowing for bioluminescent imaging of cell growth in orthotopic environments. Following intravenous implantation into mice, 5TGM1-luc cells proliferate and can be observed in areas such as the BM, lungs, liver, spleen, spine, and brain (Al-Amer, 2015; Garrett et al., 1997). The murine 5TGM1 a kind of a gift from (Dr Oyajobi, University of Texas, San Antonio, TX, USA) myeloma. The BKAL mice injected with 5TGM1 cells have the ability to mimic human MM and lytic bone lesions, which is a potent tool for studying MM disease. Morphologically, the 5TGM1 was observed in single, rounded to oval cells. 5TGM1 was transfected with GFP and Luc. The cells were cultured in RPMI 1640 with 10% Foetal bovine serum (FBS), 1% non-essential amino acids (NEAA), 1% Sodium Phosphate (NaP), and 1% penicillin/streptomycin. They were passaged every 3-7 days and stored in T75 flasks until confluent. The cells were incubated at 37°C with 95% air and 5% CO_2.

The 5TGM1 has many chromosome abnormalities like aneuploidy gain in chromosomes 15, and 18 and frequently loses chromosome 16. The deletion could also be found in various regions (Holien et al., 2015; An et al., 2013).

2.1.1.2 JJN3/JJN3- GFP Myeloma cells

JJN3 is a cell line originating from a 57-year-old female diagnosed with PCL in 1987. Human JJN3 was ordered from (DSMZ, Germany). JJN3 is a subclone of the JJN1 parental cell line of PCL and is closely related to MM, making JJN3 a suitable model for studying plasma cell malignancies. JJN3 can produce independent IL6, leading to the generation of IgA1κ immunoglobulins. The JJN3 doubling time is approximately 24 hours, and it demonstrates stable microsatellite instability. NOD/SCID-GAMMA mice are the ideal model to study JJN3 and assess the efficacy of treatment and bone disease (Mehdi et al., 2021; Lawson et al., 2015). In terms of morphology, the JJN3 are rounded to oval cells exhibited in single-cells to multiple cells. JJN3 was transfected with GFP and Luc.

The cells were cultured in RPMI 1640 with 10% FBS, 1% NEAA, 1% NaP, and 1% penicillin/streptomycin. They were passaged every 3-7 days and stored in T75 flasks until confluent. The cells were incubated at 37°C with 95% air and 5% CO_2.

JJN3 is known as multi-drug resistance due to a combination of factors including chromosomal aberration, KRAS and TP53 mutations which are involved in cell signalling and apoptosis. The JJN3 often gain chromosomes 1q (specifically 1q21) and 11q and loses chromosome 13. The 1q21 significantly promotes cell growth and survival (Marianna D'Anca, 2016; Holien et al., 2015; An et al., 2013).

2.1.1.3 OPM2/OPM2- GFP Myeloma cells

The OPM2 human myeloma cell lines were established in 1982 from the peripheral blood of a 56-year-old female with PCL. Human OPM2 was ordered from (DSMZ, Germany). They have an IgG lambda and are known to carry the t(4;14) translocation, which leads to the IgH-FGFR3 (IGH-MMSET) fusion gene. Moreover, the deletion on chromosome 13 is common and leads to the loss of RB1 and MYC gene mutations in OPM2 representing a more aggressive form of myeloma. OPM2 demonstrated a hypertriploid/hypertetraploid karyotype characterised by the single, round-to-polygonal morphology in suspension culture. The whole exon sequencing of OPM2 has associated mutations with myeloma patients at relapse and OPM2 was transfected with GFP and Luc (Altogen labs, 2024; Lawson et al., 2015b).

The cells were cultured in RPMI 1640 medium with supplements and passaged every 3-7 days until confluent. They were stored in fresh RPMI and incubated at 37°C in a 95% air and 5% CO2 environment.

2.1.1.4 U266/ U266-GFP Myeloma cells

The cell line known as U266 was derived from the peripheral blood of a 53-year-old man with IgE-secreting PCL and was transfected with GFP and Luc in 1968. Human U266 was ordered from (LGC Standards, London, UK). The U266 cells are characterised by the secretion of lambda light and IgE-heavy immunoglobulin chains. They have the capability to produce IL6, leading to the generation of IgA1κ immunoglobulins. In the U266 cells, NRAS mutations are frequently observed and can trigger pathways that induce cell growth and survival. Furthermore, MYC gene translocations, particularly those involving deletion in chromosome

13, result in MYC overexpression and are resistant to programmed cell death (Holien et al., 2015). In terms of morphology, the U266 cells exhibit a round to polygonal shape and can grow as single cells or clusters in suspension cultures, with some loosely adherent cells (Lawson et al., 2015b).

The cells were cultured in RPMI 1640 with 10% FBS, 1% NEAA, 1% NaP, and 1% penicillin/streptomycin. They were passaged every 3-7 days and stored in T75 flasks until confluent. The cells were incubated at 37°C with 95% air and 5% CO_2.

2.1.2 NOD/SCID-GAMMA (NSG) Mice

NOD/SCID-GAMMA mice were purchased from Charles Rivers laboratories, UK, and housed in the University of Sheffield Biological Service located in Royal Hallamshire Hospital, Sheffield, UK. *In vivo* studies were carried out under the UK Home Office project licence PPL No: PP3267943, held by Dr Michelle Lawson. All animal work was performed by me (under UK Home Office Personal Licence PPL No: I74342304) and Alex Sprules. Individual study plans were approved by the Biological Services Unit veterinary team.

In an immunodeficient mouse strain, NOD/SCID-GAMMA mice lack adaptive immunity and have limited innate immunity. Myeloma cells can be successfully ingrafted from a primary patient tumour into NSG mice. They can secrete human IL6 associated with regulatory elements. This mouse model is ideal for *in vivo* studies of human myeloma cell lines such as JJN3, OPM2, and U266 (Lawson et al., 2015b).

2.1.3 Cell viability assay (AlamarBlue)

AlamarBlue™ cell viability reagent (Invitrogen by Thermo Fisher Scientific), is a non-toxic method used to assess cell viability and cytotoxicity by measuring cell activity. This method is based on resazurin dye converted into a fluorescent molecule called resorufin. When added to cells, resazurin undergoes reduction, causing a colour change from blue to red and fluoresces (Al-Nasiry et al., 2007). Cells were plated in a 96-well plate, and 2500 and 5000 cells/well were added to a 100 µl medium. Then, cells were treated with various concentrations of drugs in (section. 2.1.4) were then incubated for three days. The reaction was quantified and measured using a fluorescence-based microplate reader by adding 10% of the total volume (20

µl) to each well and incubating for four hours. The test changes the colour of a chemical, indicating how active the cells are. More details in (section 2.2.3).

2.1.4 SoC Drugs used in the study

2.1.4.1 Preparation of bortezomib

Btz was stored as a powder at -20°C, and vials containing 10 mM were prepared using 1.3013 ml Dimethyl sulfoxide (DMSO). 1µM solutions were made by diluting the stock solution 1 in 10 in Phosphate buffered saline (PBS) and stored at -80°C in 100 µl aliquots.

Btz concentrations ranging from 0.5, 1, 1.5, 2, 2.5, 5, 10, 20, and 30 nM were used to determined Btz IC_{50} value, and the drug was added to 2500 or 5000 cell/media mix at 2 x the required final concentration.

2.1.4.1.1 Administration of Btz to mice

0.01 mg/ml stock solution of Btz was prepared in DMSO and stored at -20°C. Before injection, the working concentration of Btz (0.5 mg/kg) was prepared by dissolving 50 µl of Btz in 50 µl of DMSO. The Btz was injected at 0.1 ml intra-peritoneal (IP) route into the lower abdominal part of the mouse.

2.1.4.2 preparation of melphalan

Mel, molecular weight 305.20, was stored at room temperature. Vials contained 5 mg. A 10 mM solution was prepared by adding 1.6383 ml of DMSO. Then, a 1 mM solution was made by diluting the 10 mM solution 1 in 10 in PBS. Aliquots of 500 µl were stored at -80°C. Mel concentrations were used 0.1, 1, 5, 10, 20, 50 µM. Mel was added to 100 µl of 2500 or 5000 cell/media mix.

2.1.4.3 Preparation of pomalidomide

Pom was stored at -20°C, and its molecular weight was 273.24. Vials were prepared by adding 1.8299 ml of DMSO. Based on previous studies, a range of Pom concentrations were used 0.001, 0.01, 0.1, 1, 10, 100 µM. Pom was added to 2500 or 5000 cell/media mix.

2.1.4.4 Preparation of panobinostat

Pan was stored as a -20°C powder and prepared in DMSO. A solution of 1 µM was diluted and stored at -80°C. Different concentrations of Pan were used in dilutions 5, 10, 15, 20, 50, and 100 nM and added to 2500 or 5000 cell/media mix.

2.1.4.4.1 Administration of Pan to mice

0.2 mg/ ml stock solution of Pan was prepared in DMSO and stored at -20°C. Before injection, the working concentration of Pan (20 mg/kg) was prepared by dissolving 3 µl of Pan in 997 µl of PBS. The Pan was injected at 0.1 ml IP into the lower abdominal part of the mouse.

2.2 General Methods

2.2.1 Cell Counting and Cell Viability with Trypan-Blue

10µl of cells in suspension and 10µl of trypan-blue (a diazo dye that stains cells with a distorted cell wall a dark blue colour) were mixed. A haemocytometer was prepared, and 10µl of the stained cell suspension was placed under the cover slip. The viability of cells (unstained) and non-viability of cells (blue stained) were determined by counting the four squares in (Figure 2.1).

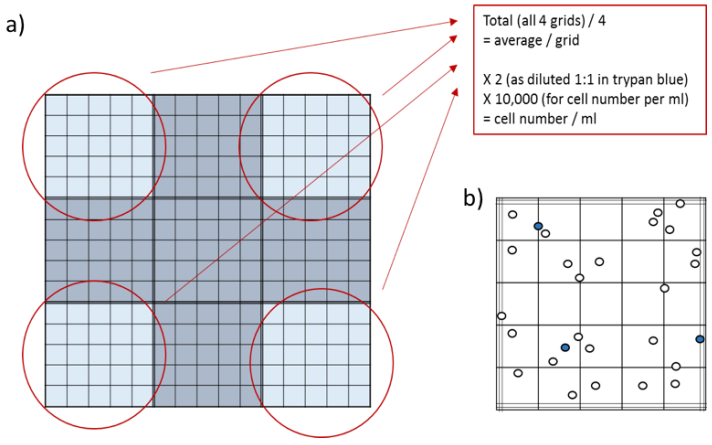

Figure 2.1: Using a haemocytometer grid for cell counting

In a haemocytometer, 10ul of cell suspension is mixed with 10ul of trypan blue stain and put under the cover slip. The haemocytometer is made up of nine discrete 5 × 5 grids inside a larger grid (a). Each 5 ×5 grid in each corner is used to count viable (unstained/clear) and non-viable (dark blue) cells. Cells that are inside the grid and in touch with the grid's top and

right sides are counted. Finding the mean viable cells in the four corner grids, multiplying by the dilution ratio (2), and multiplying by 10,000 to account for the coverslip region yields the cell count/ml (a). So, the equation will be a total number in the 4 squares divided by 4, then multiply dilution factor (×2) (trypan blue) and multiply them $\times 10^4$ to given cells/ml.

Cell count = Σ all squares ÷ 4 squares × 2 (dilution factor) × 10,000 = cells/ml.

2.2.2 Cryopreservation and Resuscitation of Cell Lines.

Cells were counted to 2×10^6 cells per ml, centrifuged at 1500 RPM for 5 min and suspended in a freezing medium of 90% Foetal calf serum (FCS) and 10% Dimethyl Sulfoxide (DMSO). Then, cells were suspended and transferred to tubes. 1 ml of freezing medium was added to the pellet and mixed, then topped up with 14 ml of freezing mixture. Aliquot in 1 ml in cryo-vials, then transferred to Mr Frosty and placed in -80°c freezer for 24 hours, then transferred in a collection box kept in -80°c.

To defrost the myeloma cells, cryovials were warmed for a couple of minutes and then transferred to a tube. 10 ml of media was added and mixed gently. Then, cells were centrifuged at 1500 RPM for 5 min. 10 ml of complete media was added and mixed for washing from the DMSO. The pellet was washed twice or more, then centrifuged at 1500 RPM for 5 min. 3 ml of complete media was added to the pellet, then transferred to the T25 flask and incubated at 37°C. cells maintained daily with media until confluent.

2.2.3 Determine Drugs' IC_{50} Values for The *In vitro* Study

To determine drug Half maximal inhibitory concentration (IC_{50}) values for each myeloma cell line, cells were placed in a 96-well plate at two densities. Various drug concentrations were added to each well, including vehicle, Btz, Mel, Pom, or Pan. Three plates were set up for assessment on days 0, 3 and 5. AlamarBlue was added to each well, and the plate was incubated before Relative fluorescence intensity (RFU) was determined on a SpectraMax 5e plate reader (Figure 2.2). Absorbance was measured at 570 nm and 600 nm wavelengths.

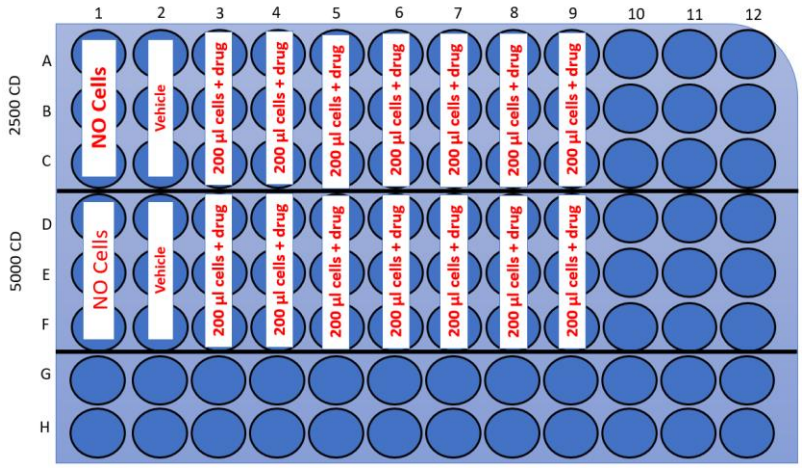

Figure 2.2: An example of a 96-well plate setup used to determine the IC_{50} values of Btz, Mel, Pom, and Pan for each myeloma cell line

Cells were seeded with varying drug concentrations at two densities (2500 and 5000/well). Cell viability was measured on days 0, 3, and 5 using an AlamarBlue assay. The experiment included three technical and biological repeats.

2.2.4 DID Labelling of Myeloma Cell Lines

Myeloma cells were labelled using 1,1'-dioctadecyl-3,3,3',3'-tetramethylindodicarbocyanine,4-chlorobenzenesulfonate salt dye (DID). The Vybrant™ Cell-Labelling solutions (Invitrogen by Thermo Fisher Scientific, Catalogue No. V22887) were utilised due to the high lipophilicity of the carbocyanine DID (Figure 2.3). Cells were suspended at a density of 1×10^6/ml with RPMI 1640 serum-free media. Then, 5 µM of DID labelling solution was added and incubated for 5 to 20 minutes at 37°c in a 5% CO_2 incubator. After that, cells were centrifuged, washed, and ready to be assessed by fluorescent microscope and flow cytometry within one hour.

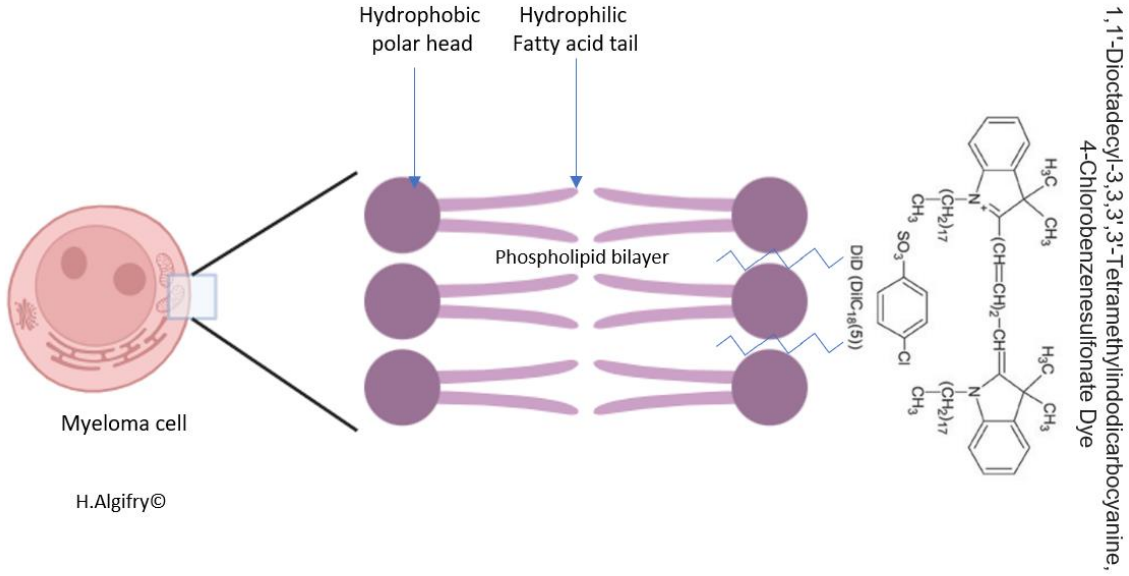

Figure 2.3: Labelling cell membrane by DID dye

DID refers to amphiphilic carbocyanine dyes featuring charged fluorescent head groups and lipophilic aliphatic tail groups. These dyes are conveniently inserted into the phospholipid bilayer of the cell membrane. Microscopy revealed that DID dye inserts into the cell membrane using its long lipophilic aliphatic tail chains, which anchor vertically into the membrane, with the fluorescent heads parallel to the cell surface membrane.

2.2.5 Fluorescence Microscopic Imaging

Myeloma cell lines were labelled with DID and analysed using the EVOS® FL Auto microscope with GFP and Cy5 filters at 10× and 20× magnification. Images of GFP and DID labelled cells were captured and can be seen in (Figure 2.4).

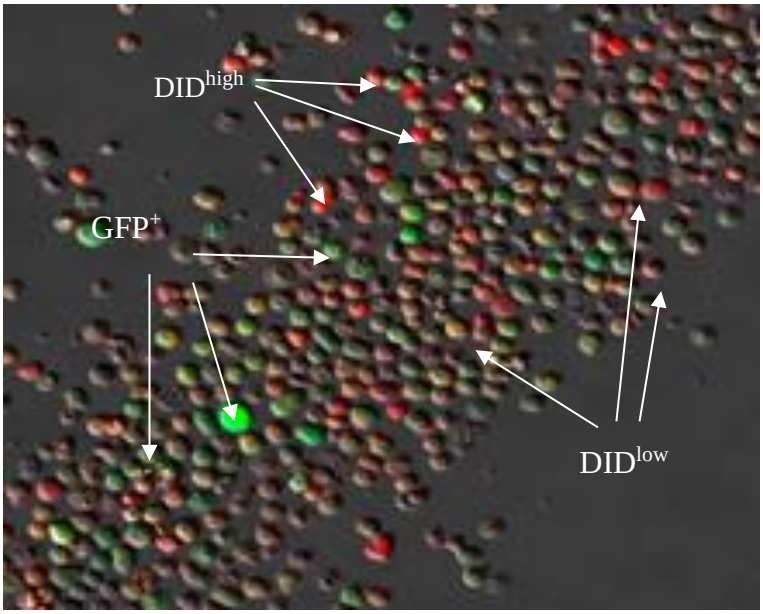

Figure 2.4: Representative fluorescent microscopic imaging with the MM cell line

Cells were stained with DID vybrant membrane dye and cultured for ten days. GFP^+ (green) DID^{high} (red) and DID^{low} (red and green) labelled cells are shown using the GFP filter and CY5 filter on an EVOS microscope (Cy5 exp.= 2ms, gain=0.0 db, light=100- GFP exp.=57 ms, gain= >3.0 db, light=100). Taken at 200 µm magnification.

2.2.6 Optimising DID-Vybrant Cell Labelling

DID dye was optimised for all myeloma cell lines (5TGM1, JJN3, OPM2, and U266) using different concentrations (1, 2, and 5 µM) and incubation times (5, 10, 15, and 20 minutes). The cells were suspended at 1×10^6/mL in serum-free media, dyed, and incubated. After centrifugation, the cells were assessed microscopically (Figure 2.4) and by flow cytometry (Figure 2.5).

The gating strategy used multiple steps to assess the presence of DMC. Initially, all cells were sorted based on their forward scatter (FSC) and side scatter (SSC) for differentiation to find all viable cell population (Figure 2.5-A). Next, single cells were isolated based on SSC and Blue 695/40-A nm laser refers to a far-red or near-infrared fluorophore (Figure 2.5-B). Then, GFP labelled cells were extracted from the single cell population for the GFP labelled cell population based on SSC and Blue 530/30-A nm laser, which refers to green fluorophore as a GFP detector (Figure 2.5-C). Non-dyed cells GFP^-DID^- were used as a control for negative dye and make sure the exact gating area (Figure 2.5-D). GFP^+DID^- and GFP^+DID^+ cells were used

as a control to distinguish between DID^{-} and DID^{+} locations on the flow cytometry dot plot based on SSC and Red 660/20-A nm laser, which refers to a far-red or near-infrared fluorophore as a DID dye detector (Figure 2.5-E & F). Mean fluorescence intensity (MFI) emitted by a population of cells was used for quantitative measurement.

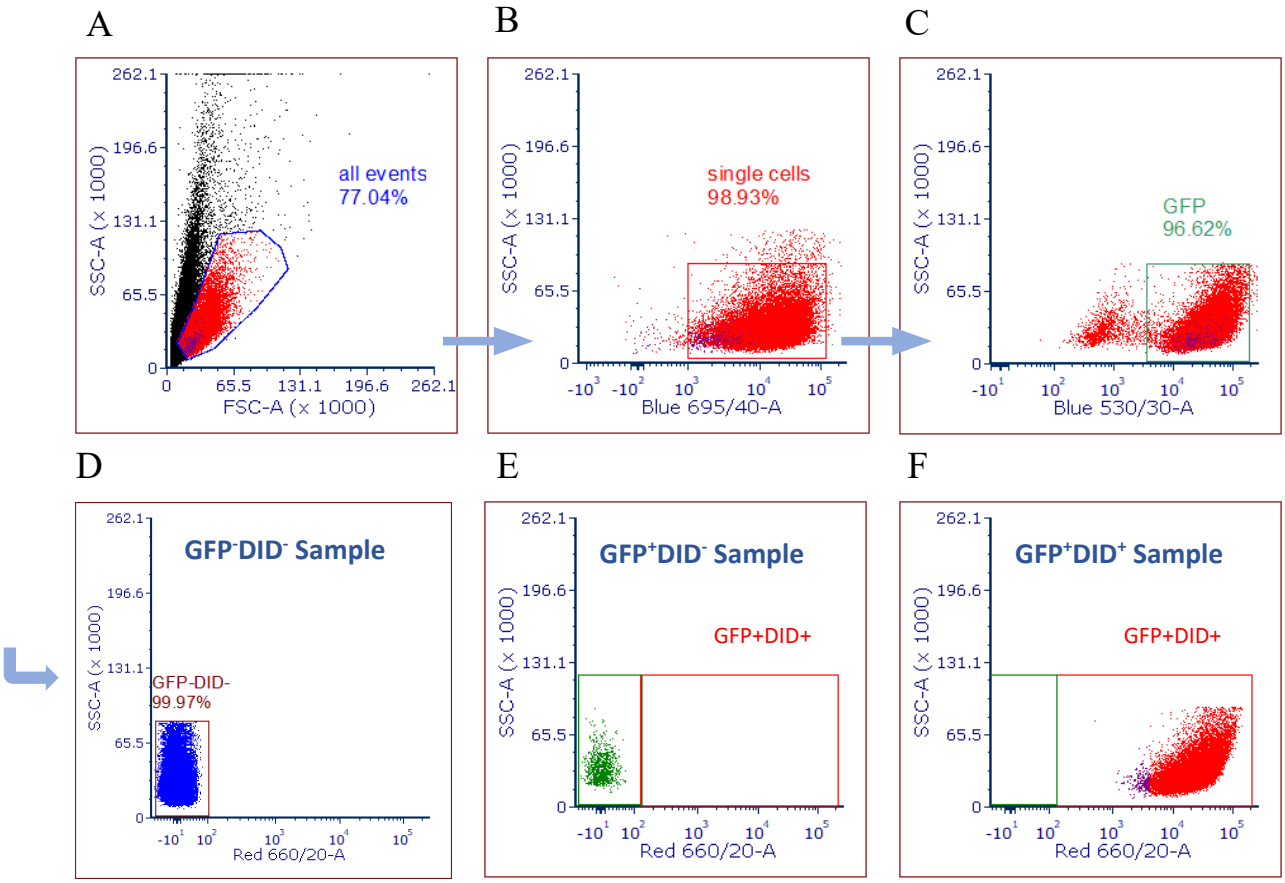

Figure 2.5: Representative flow cytometry explaining gating strategy to optimise DID dye

Flow cytometry graphs show the gating strategy used to track DMCs in monoculture. A) Polygon gate for double labelled JJN3-GFP-DID, SSC and FSC to distinguish live B lymphocytes (myeloma cells) and dead cells or lymphocyte debris. B) Gate are used to distinguish single cells to avoid doublets. C) Gates used to extract the GFP^{+} labelled cells from a single cell population. D) This gate determines GFP^{negative}-DID^{negative} cells as a control for non-dyed cells E) This gate determines the DID^{negative} cells to be used as a control for (no DID label) or proliferating cells. F) Gate used to determine DID label cells with DID^{high}. MFI is calculated to provide a quantitative measure.

2.2.7 Sorting/Isolating of DID^{high} Labelled Cells in MM Cell Lines

To isolate DID^{high} labelled cells in order to study the effect of single and combined SoC drugs, cells were isolated on days 7 or 10 using Fluorescent Activating Cell Sorting (FACS) BD FACSMelody cell sorter. A multiple gating strategy has been done on freshly DID-dyed cells to isolate the exact DID^{high} cells. To ensure the proper gating was placed on the flow cytometry graphs, unlabelled cells were used as a negative control for setting up the flow cytometer, a 488 nm laser was used to detect GFP^{+}DID^{-} cells as non-DID dye cells, and then a 635 nm laser was used to detect freshly DID dyed GFP^{+}DID^{+} were used as DID^{high} dyed cells (Figure 2.6).

Initially, all cells were sorted based on their FSC and SSC for differentiation between debris and viable cells (Figure 2.7-A). Then, the viable cell population were selected from all event cell populations (Figure 2.7-B). Afterwards, SSC and FSC singles were created to exclude cell doublets or aggregates and to ensure only single cells are included (Figure 2.7-C & D). Finally, the dot plot was set up regarding the GFP population using a 488 nm blue laser as a green channel and the DID population using a 635 nm red-diode laser for DID dye intensity (Figure 2.7-E). The DID^{high} cells were then collected in 1 ml of complete media, cultured in a T25 flask, and incubated at a 5% CO_2 incubator at 37°C.

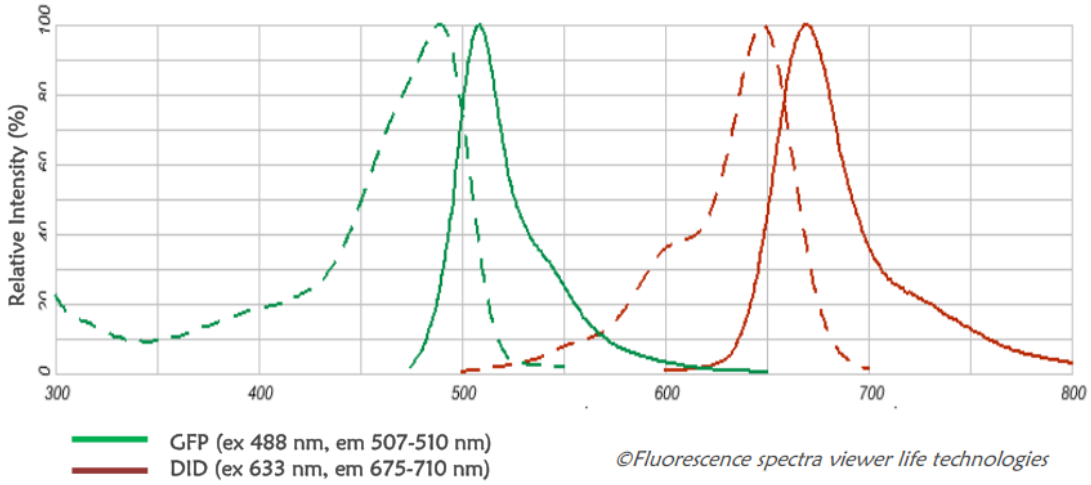

Figure 2.6: GFP and DID excitation and emission spectra

Fluorescence emission spectra for GFP (excitation at 488 nm, emission from 507 to 510 nm) and DID (excitation at 633 nm, emission from 675 to 710 nm) show significant spectral overlap between the two dyes.

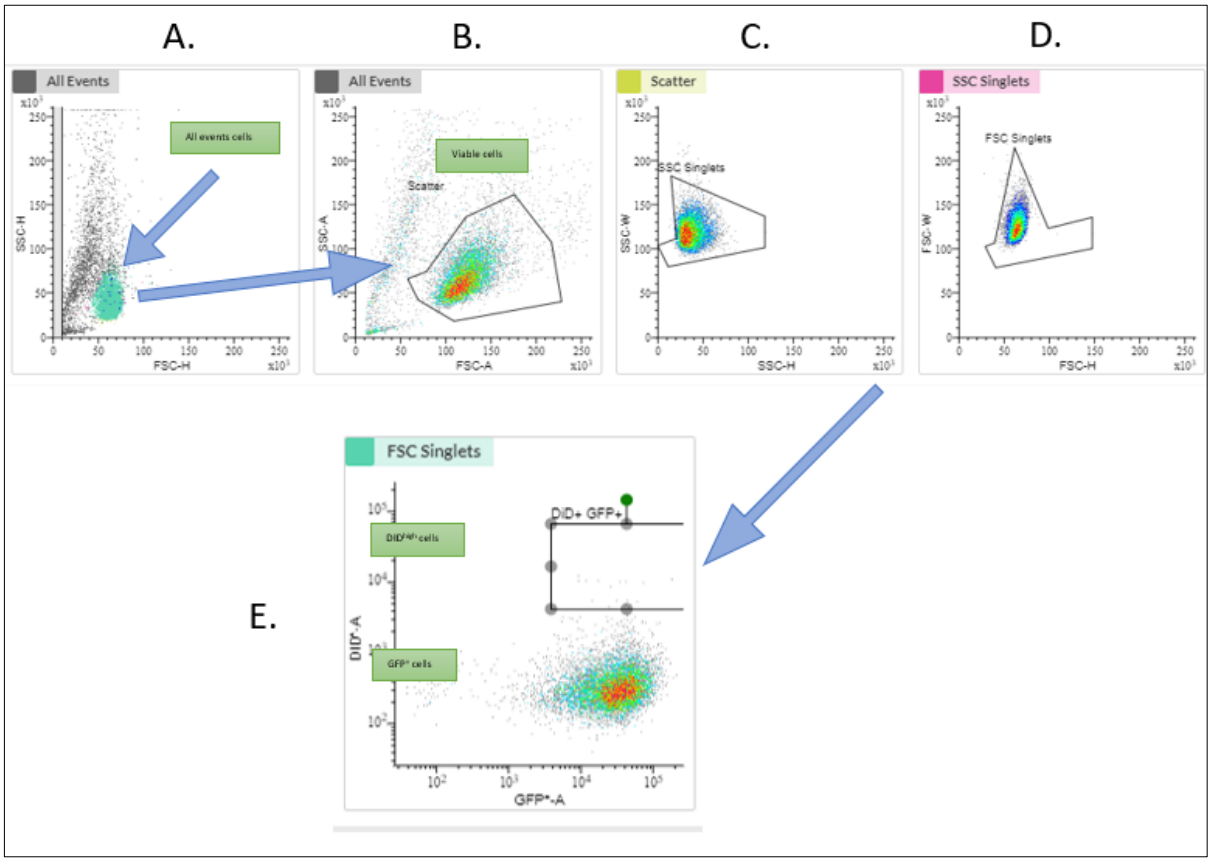

Figure 2.7: Representative FACS Melody explaining gating strategy to sort and isolate DID^{high} (potential DMCs).

Flow cytometry graphs show the gating strategy for isolating DID^{high} (potential DMCs). A) The gate for all events and distinguish live B lymphocytes (myeloma cells) and dead cells or lymphocyte debris. B) Polygon gate for viable cells, C) SSC to indicate cell granularity of the cells. D) FSC to indicate the cell size and exclude cell doublets. E) Gates used to determine the amount of DID^{negative}/GFP and DID^{high}. The procedure used BD FACSMelody™ cell sorter.

2.2.8 Determining sample size for the *in vivo* study

To achieve robust research, it is essential to calculate and determine the sample size in a study involving mice GPower 3.1.9.7 software was used. First, the minimum effect size (ES) will be determined to represent the difference we want to detect. Then, Alpha (α) was set to a significant level (usually 0.05). Next, choose the desired statistical power (1-β) of 80% or higher. Then, based on the research question, a t-test or ANOVA was selected from the test family (Figure 2.8). The mean values and standard deviation (SD) were extracted and

calculated using Microsoft Excel from a previous paper by Lawson *et al.* (2015), which studied the effect of Mel on DMCs and used 6-10 mice per group (Figure 2.9). The data were added to the GPower software (Figure 2.9- red arrows). The result gave a total sample size of 12 and 6 mice per group for two groups, then the sample size was adjusted to four groups (two single drug treatments, one combined treatment, and untreated group-vehicle), so to investigate DMCs which are typically present in low numbers within the BM, we increased the sample size to 13 per group with 5 mice per group for naïve (as a control for healthy mice) and have a total of 57 mice.

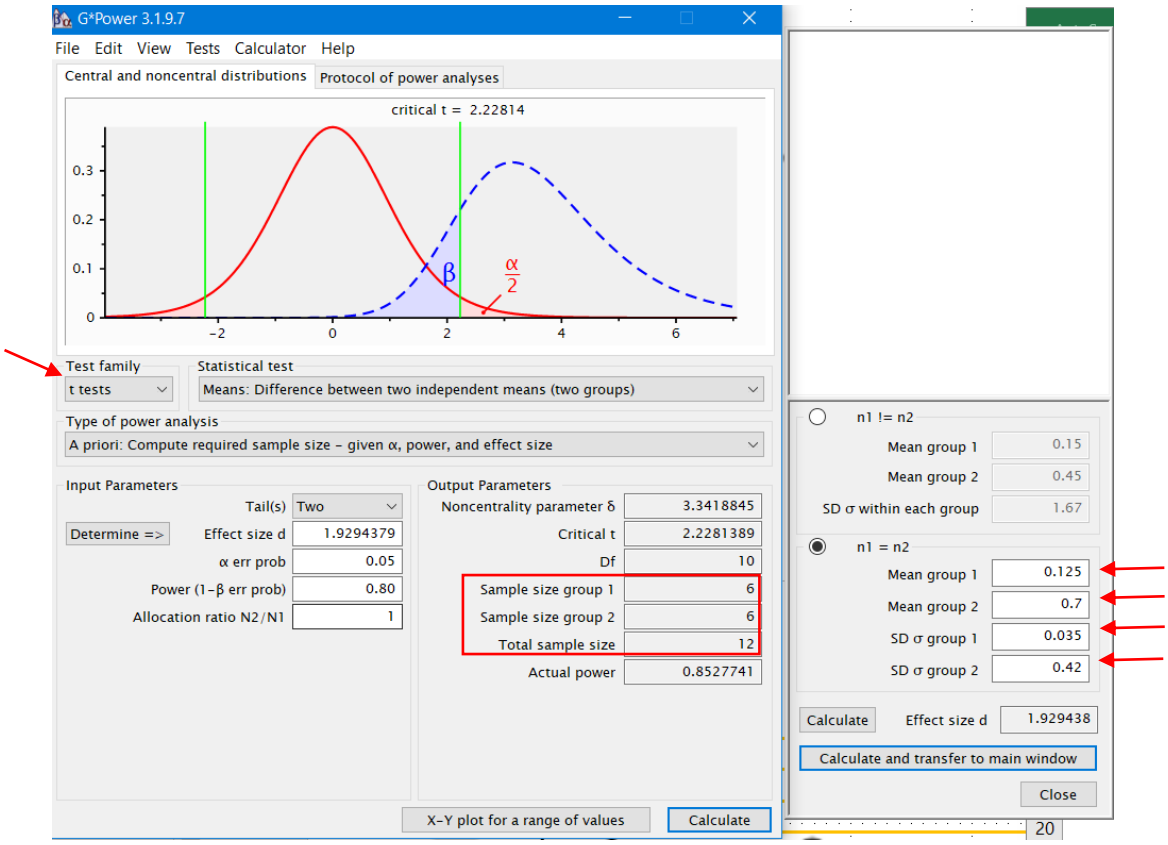

Figure 2.8: Determined sample size of the study by GPower application

GPower 3.1.9.7 application window were used to calculate the sample size for the in vivo study, data were extracted from Lawson et al. (2015) paper, mean value and SD were calculated and added to the GPower to calculate the sample size for our study.

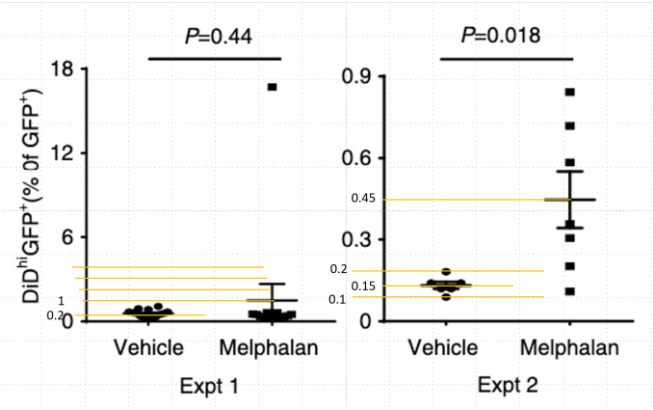

Figure 2.9: Extracting data from the previous study

These graphs show data extracted from Lawson et al.'s (2015) paper, which studied the effect of SoC Mel on 5TGM1-DID^{high} in a BKAL mouse model. Mean value and SD were calculated (Lawson et al., 2015).

2.2.9 Gating Strategy for Tracking the Presence of DMC in MM Cell lines *in vitro*

The gating strategy used multiple steps to assess the presence of DMC over 21 days. Initially, all cells were sorted based on their FSC and SSC for differentiation with PI to distinguish debris and live cells (Figure 2.10-A). Single cells were gated from all events based on SSC-A and blue 695/40-A to extract single cells and avoid aggregate (figure 2.9-B). Then, GFP was gated from the single cells gating as non-DID dye cells (Figure 2.9-C). Cells were already GFP transfected and dyed with DID and used as a control to distinguish DID^{+} and DID^{-} on the flow cytometry dot plot (Figure 2.10- D). We used the GFP transfected non-DID dyed cells and Red 660/20 channel for the DID dye to find the right gate for the DID^{-} cells. Therefore, the DID^{+} were used to determine the right location for the DID^{high} dyed cells. Then, the gap between the DID^{+} and the DID^{-} was determined for the slow-proliferating cells DID^{low} (Figure 2.10-D & E).

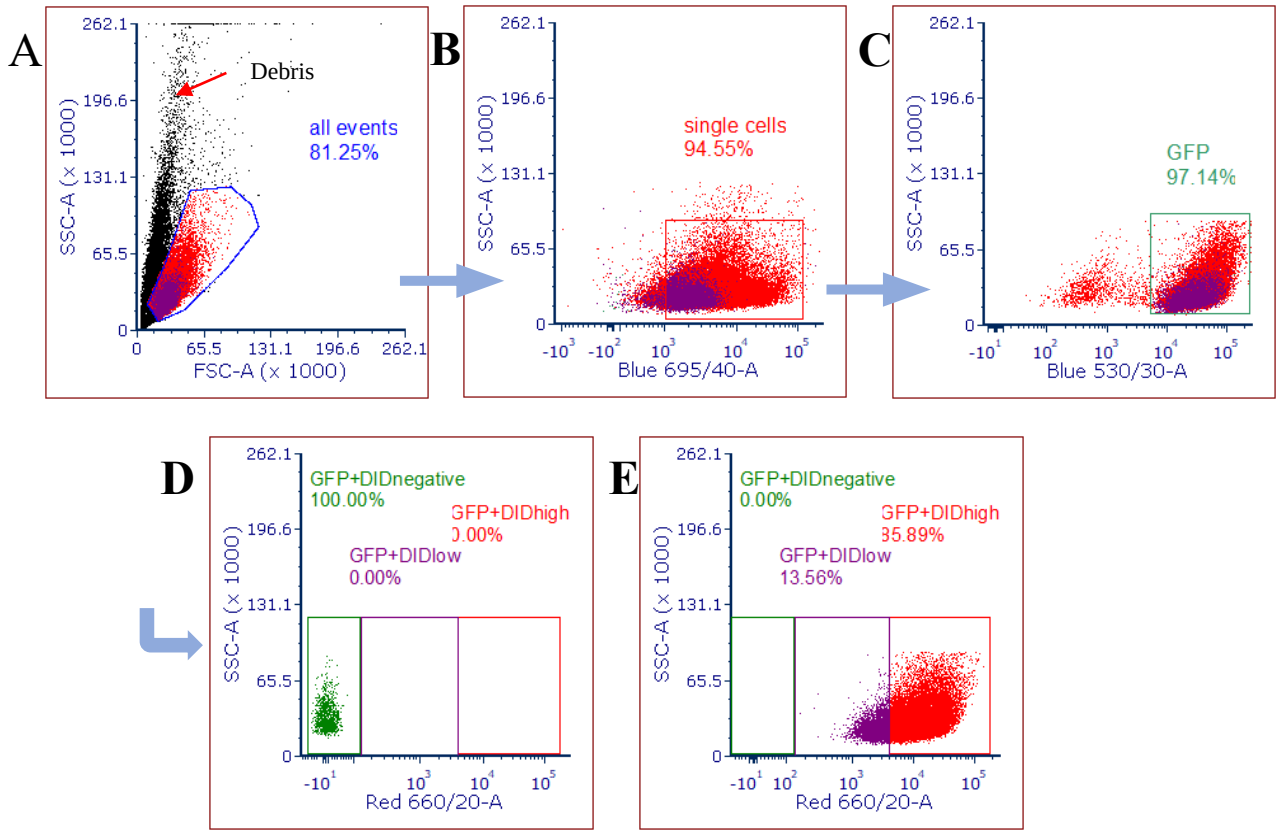

Figure 2.10: Representative flow cytometry explaining gating strategy to track the presence of DMC in MM cell lines over time

Flow cytometry graphs show the gating strategy to track DMCs in monoculture in 21 days. A) Polygon gate for double labelled JJN3-GFP-DID, SSC and FSC to distinguish live B lymphocytes (myeloma cells) and dead cells or lymphocyte debris. B) Gate are used to distinguish single cells to avoid doublets. C) Gates used to extract the GFP^{+} labelled cells from a single cell population. D) This gate determines the $DID^{negative}$ cells to be used as a control for (no DID label) or proliferating cells. E) Gate used to determine DID label cells with DID^{high} (potential DMCs) and DID^{low} (slow proliferating cells).

2.2.10 Injection of JJN3-GFP-DID into Mice Under Local Anaesthesia

Murine myeloma cells labelled with DID dye (JJN3-GFP-DID) were injected into mice via the lateral tail vein using a 1 ml insulin syringe. Prior to the injection, the tail was given analgesic using EMLA cream 5% (containing lidocaine & prilocaine), which was applied 15 minutes beforehand. The mice were placed in a 37 ˚C incubator for 5-10 minutes to dilate the vein. Subsequently, the mice were restrained, and 2×10^6 JJN3-GFP-DID cells suspended in 0.1 ml of sterile PBS were injected through the tail vein Intravenous (IV).

2.2.11 Cell Markers Used for The *In vivo* Study

Mice were sacrificed, and long bones were extracted. The BM was then flushed from both femurs by cutting the two ends of the long bone and flushing out with 1 ml of PBS. Afterwards, the cells were centrifuged at 500 g for 5 minutes. The supernatant was removed, and 1 ml of lysis buffer was added to lyse red blood cells. The tubes were then incubated at room temperature for 4-5 minutes. The cells were then centrifuged and resuspended in 2 ml of PBS. After two washes, 200 µl of extracellular antibodies (AXL, HLA, Annexin V, and Live dead/yellow) (Table 2. 1) were added and incubated on ice for 30 minutes. The supernatant will be washed twice and then fixed with PFA 4% or 100 µl permeabilisation solution buffer were added and then incubated at room temperature (RT) for 30 min; it can be kept overnight or followed by intracellular antibody staining. This was done by adding 100 µl of PBS with intracellular antibody (Ki67) followed by 30 minutes of incubation on ice (Table 2. 1). Finally, BM was washed and transferred to a flow cytometry tube for reading in the flow cytometry.

Table 2.1: Antibodies used for detecting the DMCs

Cell marker (Antibodies)	**Cat No. & supplier**	**Usage**	**Dormancy indication**	**Antibody location in the cell**
AXL monoclonal antibody (DS7HAXL), Super bright 436	62-1087-42 Invitrogen	As a dormant cell presence marker	AXL^{+}	Cell surface stain
HLA PE Mouse anti-human HLA-ABC	555553 BD Pharmingen	As an Indicator for human cells (JJN3)	HLA^{+}	Cell surface stain
Annexin V for flow cytometry	V13246 Invitrogen	As an apoptosis marker for	$AnnV^{-}$	Cell surface stain
LIVE/DEAD™ Fixable Yellow Dead Cell Stain Kit, for 405 nm excitation	L34959 Invitrogen	For cell viability	L/D^{+}	Cell surface stain
Ki-67 Monoclonal Antibody (20Raj1), PE-eFluor™ 610, eBioscience™	61-5699-42 Invitrogen	As a proliferation marker	$Ki67^{-}$	Intracellular staining (nucleus)
DID cell labelling solution	V22887 Invitrogen	As a dormant cell marker	DID^{+}	Cell surface stain

2.2.12 Detecting The Effect of Treatment on Proliferating Cells by Flow Cytometry *In vivo*

The gating strategy used multiple steps to assess the effect of single and combined treatment on proliferating cells *in vivo* after mice were inoculated with JJN3-GFP-Luc-DID cells, then treated with Btz and Pan in single and combined treatment. Initially, all cells were gated based on their FSC-A and SSC-A for differentiation between cells and debris regarding the area (Figure 2.11-A). Next, single cells were isolated based on FSC-H and SSC-A regarding cell size cell granulation to exclude doublets and select single cells (Figure 2.11-B). Then, viable cells were isolated from the single cells gating, and Live/Dead marker were used to distinguish cell viability (Figure 2.11-C). The HLA was gated from the viable cells to extract the human myeloma cell line JJN3-GFP-DID from mice BM cells (Figure 2.11-D). The majority of JJN3 loses their GFP expression post *in vivo* study, therefore, from the HLA gating Ki67 population extracted to look for the JJN3-Ki67^{+} myeloma cells to find that these cells were actively proliferating (Figure 2.11-F). To ensure accurate identification and gating of cell populations expressing specific markers, Fluorescence Minus One (FMO) controls were employed for each antibody. An FMO control for a given marker included all other fluorescently conjugated antibodies in the panel but lacked the antibody for the marker of interest. By analysing the FMO on a dot plot, we could visualise the background fluorescence and spillover from other channels into the channel for the missing marker. This allowed us to precisely define the negative population for that marker and accurately position the gates to distinguish between true positive cells and those exhibiting signal due to spectral overlap or autofluorescence. This step is crucial for reliable quantification or marker expression and identification of distinct cell populations.

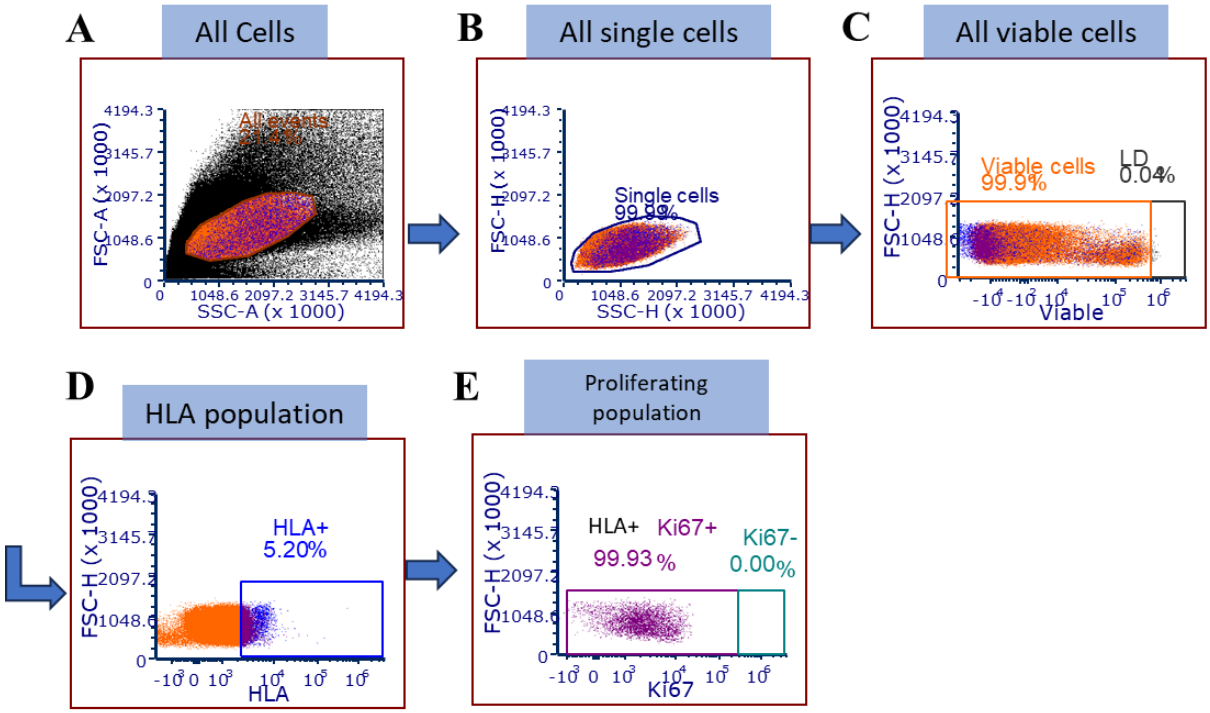

Figure 2.11: Flow cytometry gating strategy for the in vivo study to investigate the effect of (btz, pan, btz and pan) on proliferating cells

BM was flushed from femurs (right and left) of JJN3 NSG mice treated with vehicle or Btz, Pan, Btz and Pan after 7 and 19 days post-tumour inoculation. Cells were stained with AXL, HLA, Ki67, and Annexin V markers and then analysed by flow cytometry. A) FSC and SSC graph to select All events, B) Single cells, and C) live/dead antibody was used to select viable cells. D) The HLA+ population was gated from viable cells. E) $HLA^{+}Ki67^{+/-}$ marker gated as a proliferation indicator to identify non-proliferating cells. sample tubes were tested by Aurora 3 laser, Cytek Biosciences. FCSexpress software is used to generate graphs and data.

2.2.13 Detecting The Effect of Treatment on DMCs by Flow Cytometry *In vivo*

The gating strategy used multiple steps to assess the effect of single and combined treatment on DMCs *in vivo* after mice were inoculated with JJN3-GFP-DID cells, then treated with Btz and Pan in single and combined. Initially, all cells were sorted based on their FSC-A and SSC-A for differentiation between cells and debris regarding the area (Figure 2.12-A). Next, single cells were isolated based on FSC-H regarding the high viability signal and SSC-A to exclude doublets and select single cells (Figure 2.12-B). Then, viable cells were isolated from the single cells gating, and Live/Dead marker were used to distinguish cell viability (Figure 2.12-C). The

HLA population was gated from the viable cells to distinguish the human myeloma cell line JJN3-GFP-DID from the mice BM population (Figure 2.12-D). From the HLA gating, DID^+ was extracted to look for the dormant population (Figure 2.12-E). Then, $Ki67^-$, a proliferation marker, was gated from the DID^+ to find if this population were not proliferating (Figure 2.12-F). Then, the AXL^+ dormancy marker was gated from the DID^+Ki67^- population (Figure 2.12-G). Finally, Annexin V, an apoptosis marker, was gated from $DID^+Ki67^-AXL^+$ to investigate if cells had undergone apoptosis (Figure 2.12-H). FMO for each antibody was used to determine the exact location of each marker on the dot plot flow cytometry graphs.

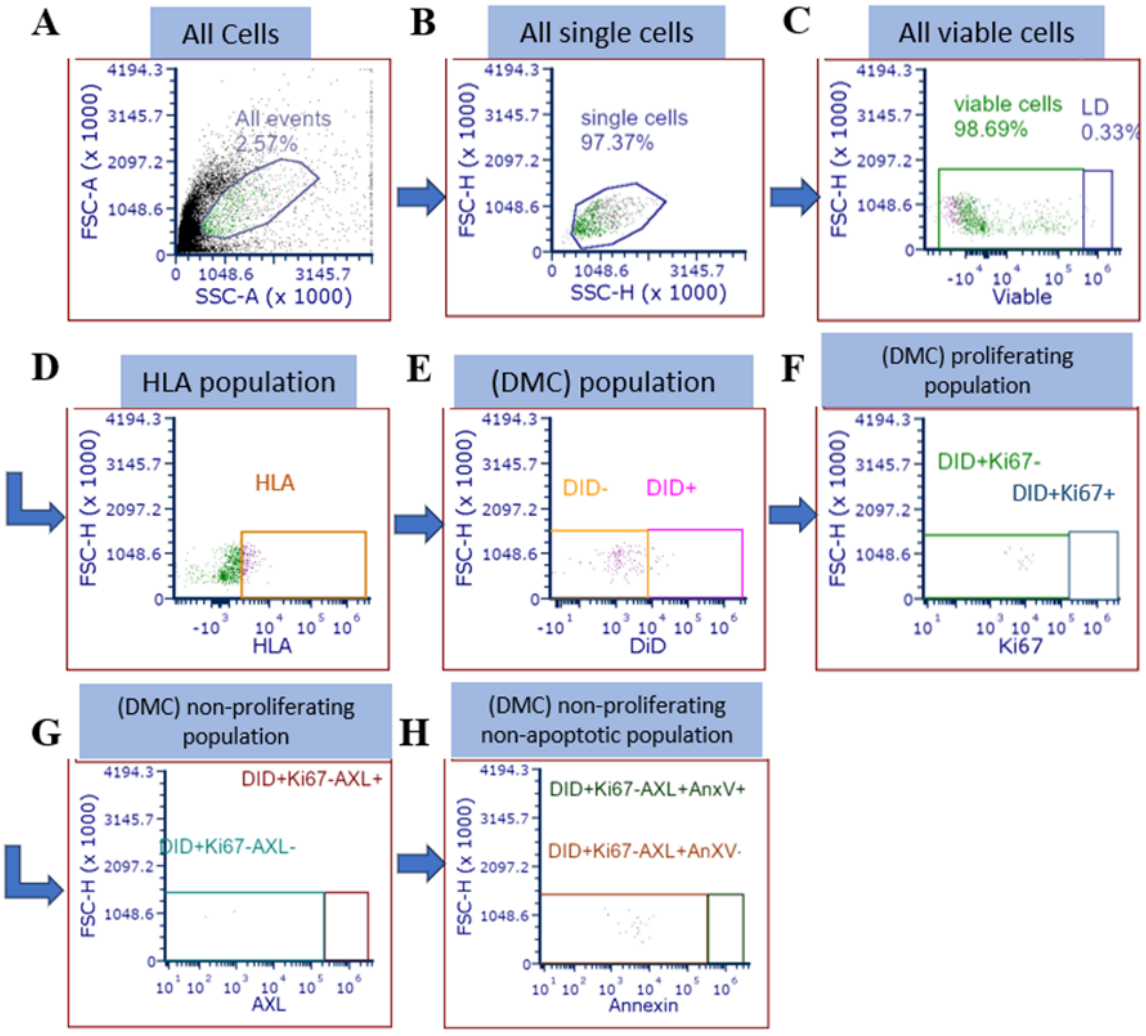

Figure 2.12: Flow cytometry gating strategy for the in vivo study to investigate the effect of (Btz, Pan, Btz and Pan) on DMCs

BM was flushed from femurs (right and left) of JJN3 NSG mice treated with vehicle or Btz, pan, Btz and Pan after 7 and 19 days post-tumour inoculation. Cells were stained with AXL, HLA, Ki67, and Annexin V markers and then analysed by flow cytometry. A) FSC and SSC graph to select All events, B) Single cells, and C) live/dead antibody was used to select viable cells. D) The HLA+ population was gated from viable cells. E) DID^{+} and DID^{-} populations determined from HLA^{+} F) $DID^{+}Ki67^{+/-}$ marker gated as a proliferation indicator to identify non-proliferating cells, G) $DID^{+/-}$ $Ki67^{+/-}$ $AXL^{+/-}$ used as a non-proliferation indicator potentially dormant cells, H) $DID^{+/-}Ki67^{+/-}AXL^{+/-}$ ANNEXIN V $^{+/-}$ to investigate any DMC going to apoptosis affected by Btz. sample tubes were tested by Aurora 3 laser, Cytek Biosciences. FCSexpress software is used to generate graphs and data.

2.2.14 Micro-Computed Tomography (µCT)

Micro-computed tomography (µCT) was conducted using a SkyScan 1272 desktop X-ray microtomography, which was designed and manufactured in Belgium. This equipment is a modified hospital computerised axial tomography (CAT-scan) capable of producing high-resolution cross-sectional images and non-destructively creating three-dimensional (3D) virtual models of objects. The cross-sectional images have a pixel size within the micrometre range, providing high resolution. The working principle involves using X-ray projection to capture multiple angular views of a 3D object using a cone beam microfocus X-ray source. A 2D x-ray planar detector is utilised to capture enlarged projection images, which are then processed by a computer to create 3D virtual cross-sections of the entire object. (Figure 2.13). The micro focus source produces a cone-shaped X-ray beam that illuminates the object area. The object is placed on a rotating turntable base, and planar projection images are collected by the detectors at multiple angles. The morphology of the trabecular and cortical components of the long bones was analysed using a medium-sized camera with 2000 × 1048 pixel resolution and an X-ray source powered by 50 kV and 200 µA electric current. A 0.5 mm aluminium filter was used to remove low-energy radiation. The tibia's proximal end was scanned at 4.3 µm pixels with a 0.7° rotation over 180˚.

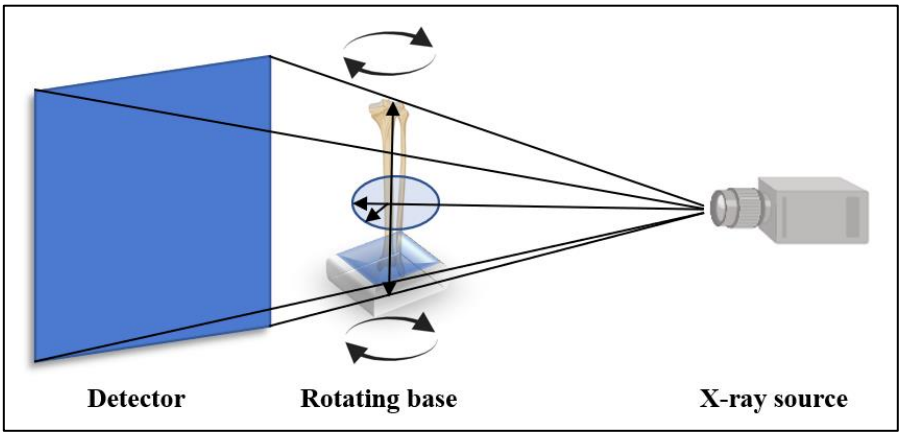

Figure 2.13: Principle of µCT imaging

Micro-computed tomography imaging is based on collecting magnified 2D image projections of the 3D object from a microfocus X-ray source.

Using NRecon software V 1.6.1.1 with a dynamic range of 0 to 0.16 and a ring artefact reduction factor of 1%. Reconstructed images were then analysed using CT Analyser V1.18.8.0. Analysis was done on the cross-sectional images of the tibiae by setting up the distance from the growth plate (reference point) at 1.2 mm. The proximal break in the growth plate was used as a standard reference point for both trabecular and cortical analysis. The analysis was done on a fixed region extending for 1 mm (Figure 2.14-A). The trabecular analysis bone was cautiously outlined on all cross-sectional images of the tibia, excluding cortical bone for the entire region of interest (ROI). Likewise, cortical bone was analysed (Figure 2.14-B). Analysis was done using CTAn Batch Manager (BatMan) software to measure the following parameters: trabecular bone volume (% BV/TV), trabecular thickness (Tb. Th), trabecular number (Tb. N), and cortical bone volume (Ct. V). The trabecular analysis binarised images were threshold between 80 and 255 and for the cortical bones, between 90 and 255.

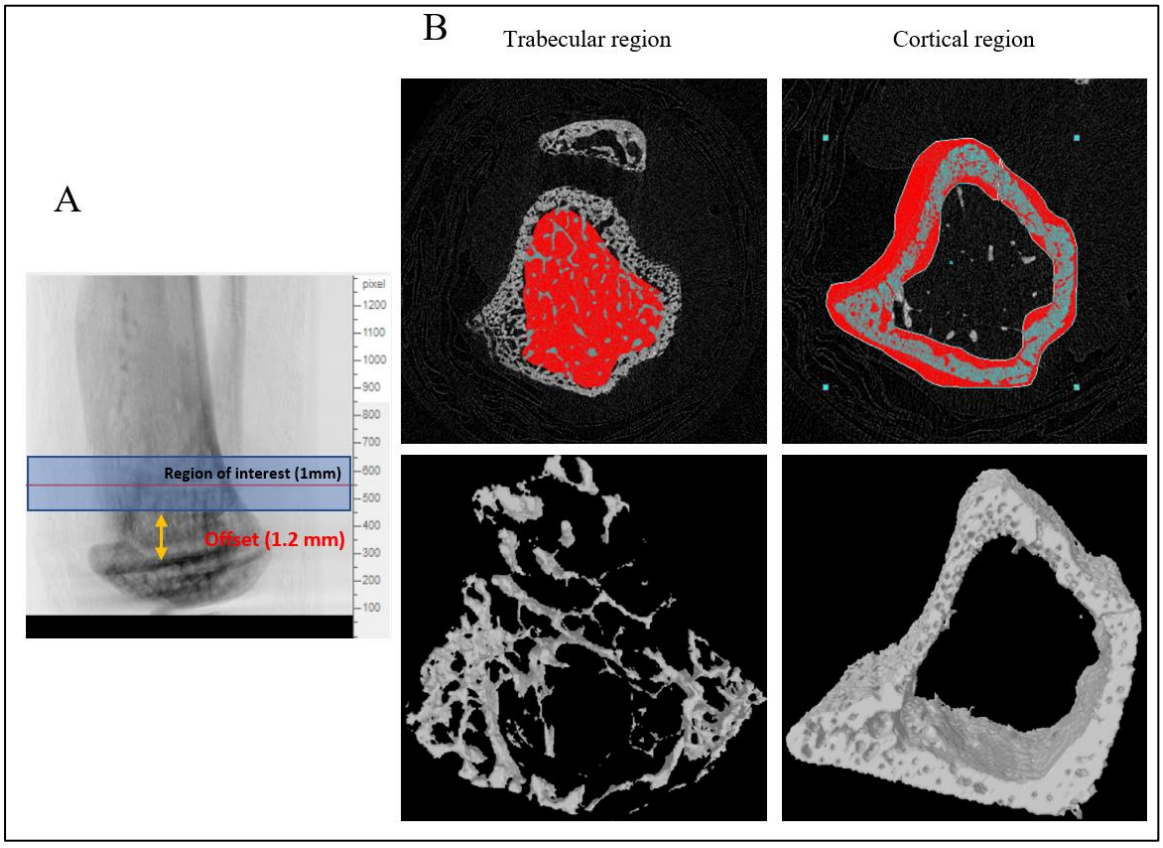

Figure 2.14: µCT image analysis and quantification

A) cross-section of the proximal tibial metaphysis, offset 1.2 mm from the distal end of the growth plate, 1 mm ROI for cortical and trabecular bone analysis. B) cortical and trabecular bone were analysed by tracing out boundaries (red) in the ROI, and the amount of bone (Ct. V & %BV/TV) and structural parameters were analysed using CTAn software.

2.2.15 Histology

2.2.15.1 Decalcification

Following the µCT analysis, the bones underwent a four-week decalcification process using Ethylenediaminetetraacetic Acid (EDTA) at room temperature, changing the EDTA solution once a week. After decalcification, the bone tissues were loaded onto labelled cassettes and washed with running water for 60 minutes in preparation for subsequent histomorphometry analysis.

2.2.15.2 Processing and Wax Embedding

The Bone Lab group, led by Orla G., conducted the tissue processing. The bones were dehydrated using alcohol gradients and infiltrated with paraffin wax. The processed tissue was then embedded in paraffin wax using metal moulds. For the tibiae samples, the crest was placed diagonally in the moulds, and melted paraffin wax was poured into the moulds and allowed to cool.

2.2.15.3 Section Cutting and Staining

Wax-embedded tissue blocks were cut using a Leica RM2135 rotary microtome. The cutting thickness was set at 3 μm. The wax moulds were trimmed until the BM was exposed. Serial sections were transferred to float onto a water bath set at 45°C, mounted on labelled slides appropriately, and dried overnight in a 37°C incubator.

2.2.15.4 TRAP and Haematoxylin and Eosin Stain

Initially, the slides were dewaxed and dried in an oven for 30 min. They were then submerged twice in xylene for 5 minutes to remove the paraffin. Then, slides were dipped in jars of serial concentration 99%, 95%, and 70% of industrial methylated spirit (IMS) for 5 minutes each to remove the xylene. The slides were then rinsed with running tap water.

A standard Napthol AS-BI phosphate post-coupling method was utilised for TRAP staining using hexazonium pararosaniline. To prepare a 1.2% acetic acid solution, 6 ml of absolute acetic acid (Analar Chemicals) was dissolved in 494 ml of distilled water (DW). To prepare the acetate buffer (0.2M), dissolve 4.6 g of sodium acetate trihydrate salt (Sigma S-9513) in 200 ml of DW. Adjust the pH to 5.2 by adding 50 ml of 1.2% acetic acid. Create the acetate-tartrate buffer by adding 4.6 g of Sodium tartrate (Sigma S-4797) and warm the buffer to 37°C for 2 to 4 hours. Then, incubate the dewaxed slides in the warm buffer at RT for 5 minutes. Prepare Solution A by dissolving 0.02 g of Napthol AS-BI phosphate (Sigma N-2250) in 1 ml of dimethyl formamide and mix with 50 ml of acetate tartrate buffer. Finally, incubate the slides in Solution A for 30 minutes at RT. To prepare a 4% Sodium nitrate solution, 80 g of sodium nitrate (Sigma S-2252) was added to 2 ml of DW. Then, 2 mL of pararosaniline (Sigma P-3750) was added to the 4% Sodium nitrate solution to form hexazonium pararosaniline. After that, Solution B was prepared by adding 2.5 mL of hexazonium pararosaniline/sodium nitrate

to 50 ml of pre-warmed acetate tartrate buffer. It's important to prepare this solution freshly and then incubate the slides in Solution B for 15 minutes at RT.

The slides were then rinsed and counterstained with Gills II (VW code 1.05175.0500) haematoxylin for 20 minutes and 20 seconds. They were then washed for blue under running tap water for 5 min. Eosin staining was dyed by dipping the slides in 1 % of aqueous solution of eosin containing 1% calcium carbonate for 5 min then washed in running tap water for 2-3 min. The slides were dehydrated quickly through ethanol and then cleared in xylene. Finally, mounted with DPX.

2.2.15.5 Scoring System for OB and OC Quantification

An Olympus BX53 microscope connected to a PC and Osteomeasure software was used to quantify the TRAP and haematoxylin and eosin (H&E) stained slides. Cells were first analysed at 10× magnification. TRAP stain was used to quantify OC, and H&E stain was used to quantify OB and tumour burden. Trabecular analysis was performed on a field size of 0.5625 mm^2, located 0.5 mm from the proximal margin of the growth plate. Histomorphometry assessment on the cortical-endosteal side was determined at 1.5 mm on each endosteal side, 0.5 mm from the growth plate (Figure 2.15). The statistic variable was measured as the total number of OC per unit area of trabecular bone (e.g., osteoclast index, $1/mm^2$) and the total number of OB per unit area of trabecular bone (e.g., osteoblast index, $1/mm^2$) were measured on the trabecular region. The total number of OC and OB per mm of cortico-endosteal (endocortical) bone surface (1/mm) was measured on the endocortical region. The TRAP staining was used to identify the morphological features of the OC, while the H&E staining was used to identify the OB as they are cuboidal in shape (Figure 2.16).

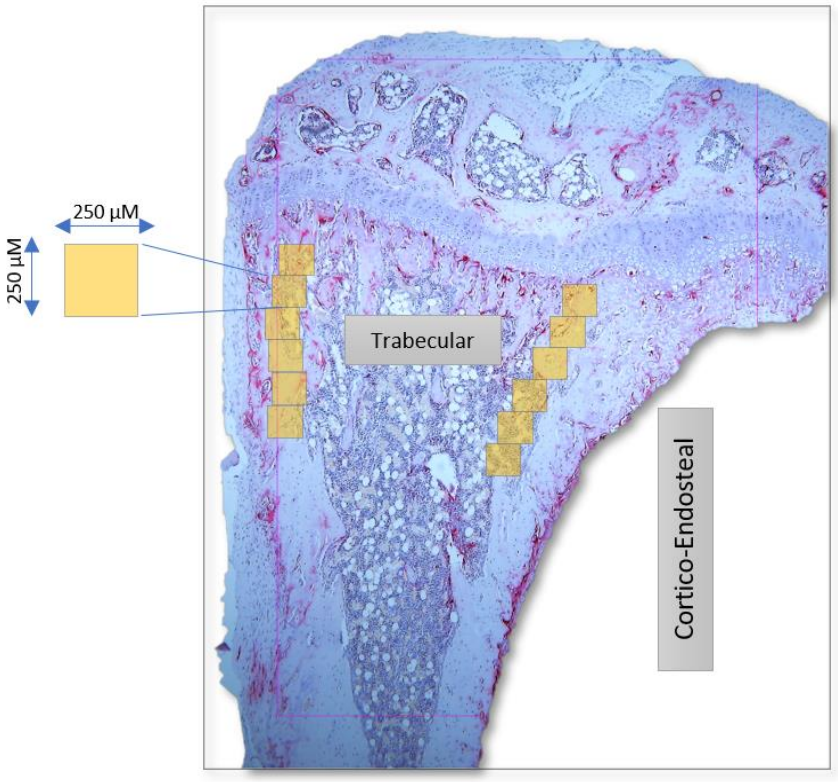

Figure 2.15: OCs and OBs analyses on tibial TRAP and H&E tissue sections

Osteomeasure software was used to quantify the number of OC and OB in the BM. The analysis was performed in the proximal tibial metaphysis, specifically 0.5 mm below the growth plate, using a 4× objective. For the trabecular region, a 3 × grid tile fashion was used, with each tile measuring 250×250 µM. For the endocortical analysis, 6 tiles were traced along the endocortical surface on both sides.

2.2.15.6 H&E Scoring System for Tumour Burden

An Olympus BX53 microscope connected to a PC and Osteomeasure software were used to quantify the H&E-stained slides. Cells were first analysed at 10× and 20× magnification. H&E stain was used to quantify the tumour burden. Trabecular analysis was performed on a field size of 0.5625 $mm^{2,}$ located 0.5 mm from the proximal margin of the growth plate. Histomorphometry assessment in the trabecular region was determined at 0.5 mm from the growth plate. By the Osteomeasure software, the normal BM area set as the whole BM and the normal cell area set were determined (Figure 2.16-A). The statistic variables were taken from the Osteomeasure software and calculated as follows:

$$\frac{\text{Total BM}}{\text{Total normal BM cells}} \times 100 = \% \text{ of normal BM region}$$

Tumour region = 100 - % of normal BM region

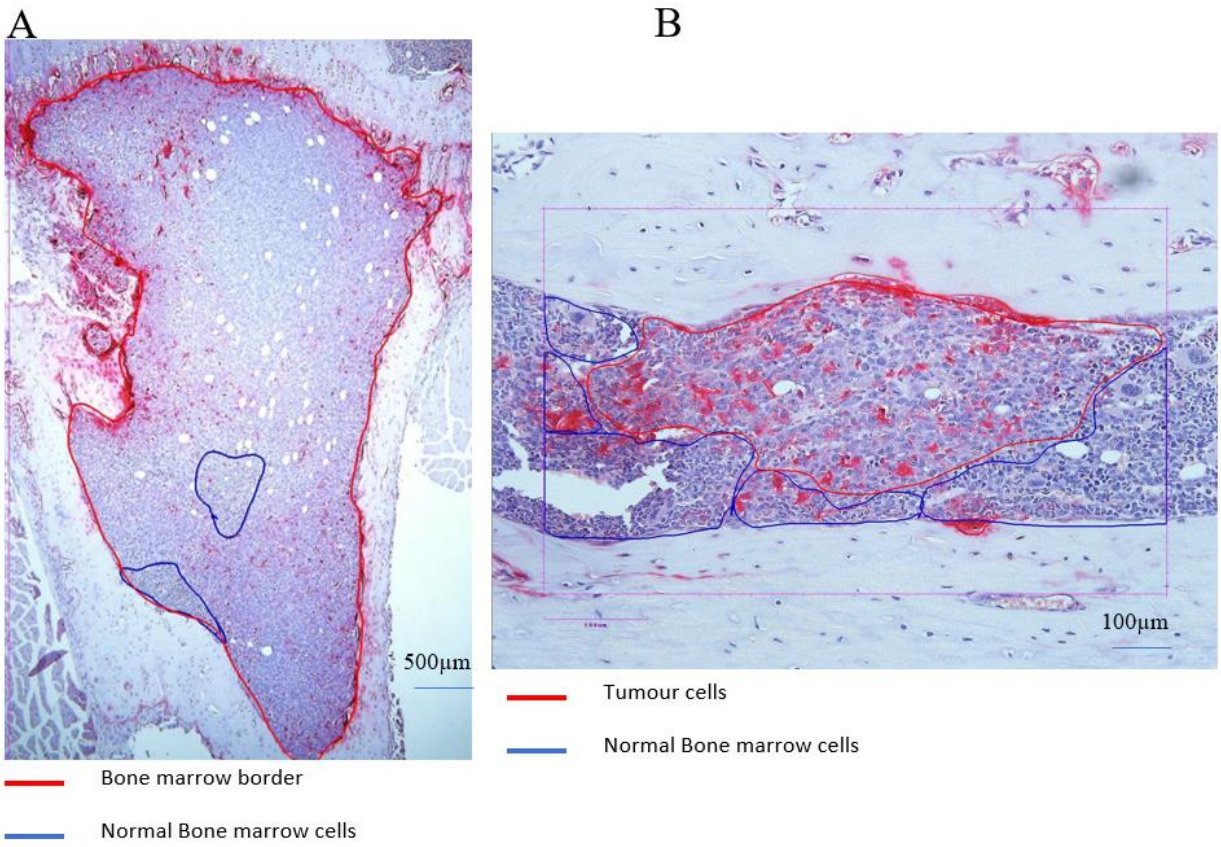

Figure 2.16: Scoring system for H&E slides

H&E-stained slides were scanned using an Olympus BX53 microscope. Images were loaded into OsteoMeasure7 V4.2.0.1 software. A) Showing normal BM and normal BM cells were selected in red and blue lines to calculate the tumour cells' replaced areas. Results were exported to Excel for analysis, scale bar 500 µm. B) Distinguishing tumour cells as the red area and normal BM cells as blue areas, scale bar 100 µm

Chapter 3 Optimising DID Dye and Tracking DMCs

3.1 Introduction

3.1.1 Dormant Tumour Cells

Myeloma is a blood cancer that is difficult to treat due to drug resistance and the likely presence of DMCs that reside in the BM; DMC is thought to remain inactive for long periods before being reactivated (Lawson et al., 2015), leading to clinical relapse. The small number of DMCs retained in the BM niche could be described as MRD (Li et al., 2021; Phan & Croucher, 2020), i.e. these are cells remaining post-treatment. DMCs can be switched on and off through their microenvironment (Lawson et al., 2015), and DMCs have been shown to have lower metabolic activity and higher oxidative resistance (Ikeda & Tagawa, 2021). Their behaviour may be influenced by factors such as tissue composition, stromal cells, and nutrient availability, potentially leading to tumour relapse (Pranzini, Raugei, & Taddei, 2022; Phan & Croucher, 2020; Lawson et al., 2015). DMCs can accumulate genetic mutations and inherit these mutations in their generations (Phan & Croucher, 2020; Khoo et al., 2019). To fully understand how tumour cells enter a state of dormancy, extensive research involving many patients would be necessary to gather sufficient information about dormant cells and how they repopulate. Additionally, discovering biomarkers to detect disseminated dormant cells early on could help prevent relapse (Aguirre-Ghiso, 2007). However, detecting dormant cells is challenging.

Using high-resolution deep tissue imaging through complete bone in live animals has provided some insight into dormancy mechanisms in myeloma (Phan & Croucher, 2020; Lawson et al., 2015). Lawson *et al.* (2015) demonstrated the critical role of OB and OC in the bone with regard to DMCs. OB in the 5TGM1 myeloma mouse model are responsible for maintaining cells in a latent condition, while osteoclastic bone resorption was shown to drive their growth (Lawson et al., 2015). The discovery of key molecules such as AXL and TRIM44, which play a vital role in maintaining DMCs in the BM niche, clearly confirms their presence in preclinical models, and there is now some evidence of these markers in patients which can affect myeloma patient outcomes (Chen et al., 2019b; Khoo et al., 2019; Yan et al., 2019; Lawson et al., 2015).

3.1.2 Mechanisms of Dormancy in Multiple Myeloma

DMCs are surrounded by fibronectin and can express integrins to reduce proliferation signals (Aguirre-Ghiso, 2007). Most markers used for dormancy may not be specific to DMCs. For

example, the $Ki67^{negative}$ marker can indicate cell quiescence, and TUNEL can identify cells undergoing apoptosis (Damen, et al., 2020; Miller et al., 2018).

According to a study by Lawson *et al.* (2015), culturing OB with myeloma cells can activate dormancy genes (Lawson et al., 2015). Studies conducted on murine myeloma models have demonstrated that the endosteal niche interacts with myeloma cells. This interaction leads to the activation of myeloid genes that regulate the process of dormancy. AXL, a receptor protein found on the cell surface, works as a regulator. It binds to the GAS6 receptor to activate signalling pathways that promote cell survival adhesion and resistance to cell death. It is crucial in controlling myeloma cells to undergo dormancy, whether in murine or human cells; for example, (GAS6)/AXL helps prostate cancer cells enter dormancy and maintains the survival and self-renewal capacity of CML stem cells (Khoo et al., 2019; Yan et al., 2019; Shiozawa et al., 2010). *In vivo* studies indicate that inhibiting AXL could be a potential target in treating MM dormancy and preventing relapse by releasing the cells from dormancy and rendering them sensitive to chemotherapy. These findings are a significant step forward in MM treatment and suggest the need for further research in this area. On the other hand, this procedure is not specific to myeloma cells only; it could be risky and could cause all tumour cells to re-grow (Khoo et al., 2019).

TRIM44 is a protein that is overexpressed in various cancers, including breast and gastric cancer. It promotes the spread of cancer cells and helps them survive in the BM. TRIM44 also plays a role in regulating the immune system and can keep cancer cells in a dormant state. (Chen et al., 2019).

Over expression of CXCR4 plays a role in various functions of myeloma cells, including their homing and survival that could be used as a biomarker for DMCs detection inside the BM (Damen, van Rheenen, & Scheele, 2020; Ullah, 2019; Di Marzo et al., 2016; Schueler et al., 2013; Fuhler et al., 2012).

The BM endosteal niches are home to DMCs that require specific factors and interactions to regulate and maintain them. OB and transcription factors are key players that enable DMCs to remain dormant. However, researchers have identified various therapy targets that can release dormancy and make DMCs sensitive to drugs. Still, this strategy could be harmful and could

release various cancer cells from dormancy or keeping them dormant forever could be much safer for patients.

3.1.3 Tracking Dormant Cells

Tracking DMCs within their niche was done by Lawson *et al.* (2015) using a multiphoton microscope *in vivo*, and *in vitro* studies have shown dormancy exists in monocultures using fluorescence labelling. Fluorescent dyes can be incorporated into live cells, avoiding damage to metabolic function and facilitating phenotype analysis through fluorescent imaging or flow cytometric analysis. There are three primary categories of fluorescent dyes based on what they bind to. These include (a) DNA binding dyes (e.g. Hoechst 33342), (b) cytoplasmic dyes (e.g. carboxyfluorescein succinimidyl ester (CFSE)), and (c) membrane dyes (e.g. DID). DNA binding dye is frequently used in cell cycle analysis, migration, and trafficking. However, prolonged exposure to the dye increases its cytotoxicity, making it unsuitable for long-term cell proliferation, which could harm proliferation. Cytoplasmic dyes are highly toxic to cells and can affect cellular functions. Therefore, for tracking DMCs, membrane-bound dyes are the preferred option as they are less toxic and well-recognised for their potential use in cell tracking, migration, and proliferation assays. This is due to their extended retention capabilities, making them a highly effective tool in these assays (Lawson et al., 2015; Yumoto, Janice E Berry, et al., 2014). Yumoto *et al.* (2014) compared the fluorescence retention of PCa cell lines stained with DID dye and CFSE dye over time. The results showed that cells containing DID dye retained their fluorescence significantly longer than those stained with CFSE dye (Yumoto, Janice E Berry, et al., 2014). According to Lawson *et al.* (2015), when 5TGM1-GFP cells were labelled with DID, daughter cells retain the DID, but it was gradually diluted as the cells proliferated, indicating cells were dividing. Cells that retain in the DID label are the non-dividing DMCs (Figure 1.6) (Lawson et al., 2015).

Therefore, to study DMCs and subsequently target them with SoC treatments, we first needed to optimise DID staining and then identify the presence of DID^{high} cells in a monoculture.

3.1.4 Aims, Hypothesis and Objectives

This chapter aims to optimise DID staining (concentration and incubation time) for four myeloma cell lines (5TGM1, U266, JJN3 and OPM-2) and then to track DID^{high} cells *in vitro* monocultures over time.

We Hypothesis that DMCs are present in all four myeloma cell lines when cultured alone.

The chapter objectives:

1. To determine the DID dye optimal concentration and incubation time in four MM cell lines (5TGM1, JJN3, OPM2, and U266).
2. To track DID labelled myeloma cells (5TGM1, JJN3, OPM2, and U266) over time to determine the number of DID^{high} cells after 0, 3, 7, 10, 14, 17 and 21 days of monoculture.
3. To determine the optimum time point to isolate DID^{high} labelled cells for subsequent treatment with SoC drugs.

3.2 Material and Methods

Detailed information on individual techniques performed can be found in Chapter 2 under General Material and Methods.

3.2.1 Determining the Optimal Vybrant DID Dye to Label MM Cell Lines

MM cell lines (5TGM1, JJN3, OPM2, and U266) were dyed using different concentrations of DID and then incubated for 20 min in a 37℃ incubator and washed 3 times; then, they could be assessed within an hour (details in chapter 2, section 2.2.6). Cells were labelled with different concentrations (1, 2, 5 µM) of DID to determine the optimal concentration and analysed in flow cytometry with propidium iodide (PI). Cell viability was determined, and the gating strategy is shown in (Figure 2.5).

GFP MM cell lines (5TGM1, JJN3, OPM2, and U266) were incubated with 5µM DID dye at 1×10^6 cell density for (5,10,15 and 20 minutes) at 37°C. After centrifugation, cell pellets were washed and resuspended in 500 µl PBS/flow buffer. Cell viability was determined by flow cytometry analysis with PI and gating strategy (Figure 2.5).

3.2.2 Tracking Dormancy Method in MM Cell Lines

To track the DMCs in (5TGM1, JJN3, OPM2, and U266) in a longitudinal experiment, cells were labelled with GFP and DID dye following the method in (Chapter 2 section 2.2.5). Four 6-well plates were seeded with 5000 cell density per well and incubated for 21 days. On days 0, 3, 7, 10, 14, 17, and 21, cells were imaged by the EVOS microscope and analysed by flow cytometry with PI to determine cell viability, and the percentage of viable cells was computed. The gating strategy is shown in (Figure 2.10).

3.2.3 Statistical Analysis

All data was analysed using GraphPad Prism (version 10). A student t-test or Ordinary one-way ANOVA was used when data was normally distributed. Data was expressed by presenting mean (+/- standard deviation).

3.3 Results

3.3.1 DID Optimisation

3.3.1.1 DID Optimisation in 5TGM1 Cell Line

5TGM1-GFP cells were labelled with different concentrations of DID dye to detect 5TGM1-GFP^{+} DID^{high} cells over time in a monoculture. After 5, 10 or 20 minutes, fluorescence images were taken (Figure 3.1-A.i). And using flow cytometry (Figure 3.1-Aii), mean fluorescence intensity (MFI) values were calculated for 3 technical and biological repeats and one-way ANOVA was performed. The chart shows that 5 µM/20 min. is the optimal concentration to dye 5TGM1 (Figure 3.1-B). The mean values for the MFI are 1 µM 32869 RFU (±3015), 2 µM 32625 RFU (±3151), and 5 µM 32812 RFU (±3244). MFI values for various incubation times: 32812 (±3244) RFU for 20 minutes, 32130 RFU (±3431) for 15 minutes, 32317 RFU (±3693) for 10 minutes, and 31929.72 RFU (±3431) for 5 minutes (Figure 3.1-B).

The percentage of DID concentration results showed no significant differences with values of 1 µM 99.3 %, 2 µM 99.9%, and 5 µM of DID 100 %. DID percentage for incubation time: 99.99 % for 20 minutes, 100 % for 15 minutes, 100 % for 10 minutes, and 99.99 % for 5 minutes (Figure 3.1-C). Based on the flow cytometry data, any concentration or time could be sufficient to dye the 5TGM1.

Cells were double labelled with GFP (green) and DID (red). The fluorescent imaging showed that DID concentrations < 5 µM with 20 minutes of incubation time have stained fewer cells than DID concentrations 5 µM. Then, the concentration at 5 µM with different incubation timing showed that all cells were stained with DID dye.

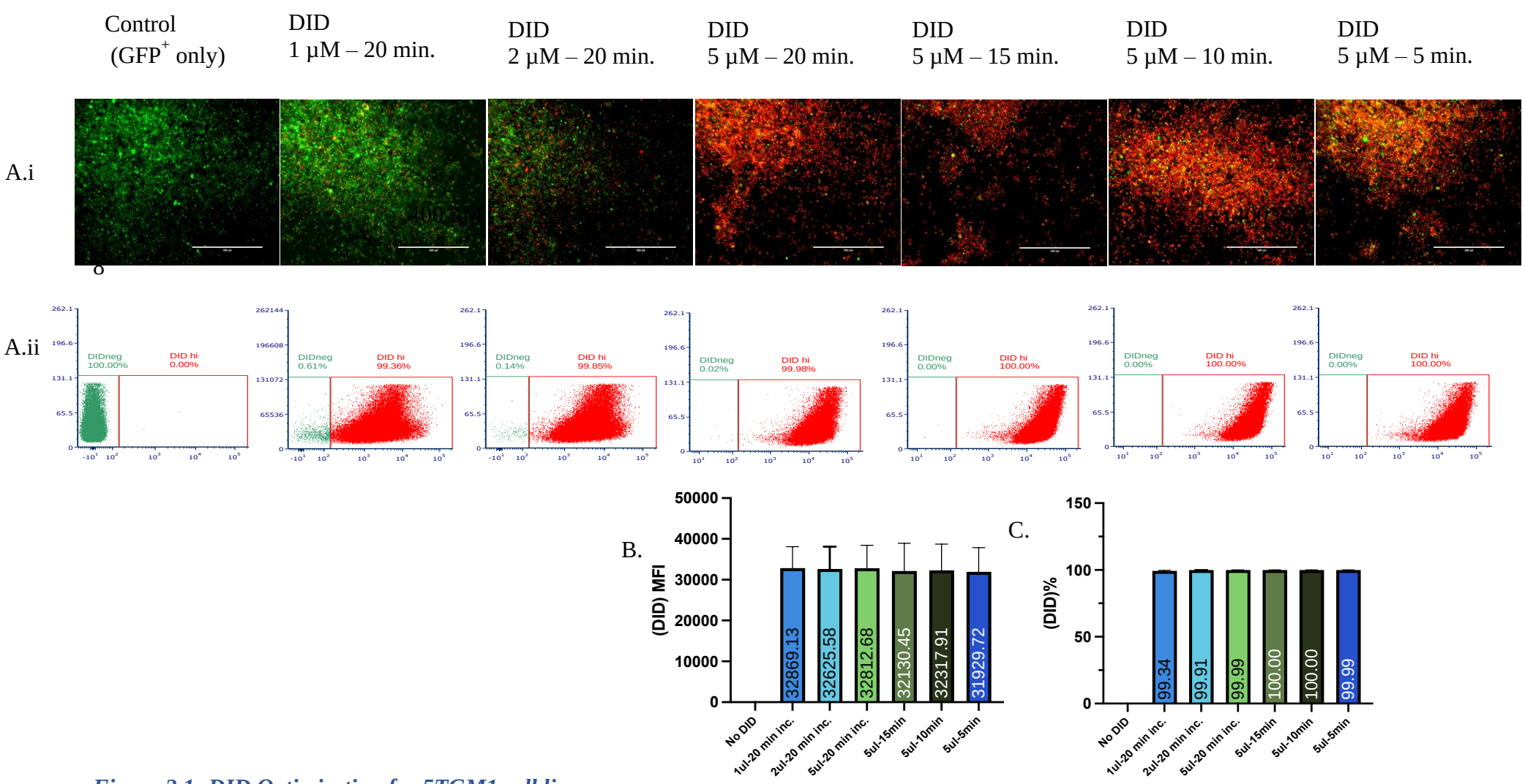

Figure 3.1: DID Optimisation for 5TGM1 cell line

(A.i) EVOS microscope images for 5TGM1 with filter (cy5, exp=2, Gain=0.0, light=100)- (GFP, exp=57, Gain=3.0, light=100)- scale bar 10×= 400 µm magnification apply to all panel. (A.ii) Dot plots for flow cytometry analysis showing DID dye optimisation for 5TGM1 using increased concentration of DID dye with different incubation times. (B) flow cytometry analysis of DID levels line chart showing DID dye optimisation for 5TGM1, calculating MFI mean values, one-way ANOVA were performed. (C) Bar chart showing DID Dye optimisation, calculating the percentage of cells regarding dye concentration and incubation time. 3 technical and biological repeats.

3.3.1.2 DID Optimisation in JJN3 Cell Line

JJN3-GFP cells were labelled with different concentrations of DID dye to detect JJN3-GFP^{+} DID^{high} cells over time in a monoculture. After 5, 10 or 20 minutes, fluorescence images were taken (Figure 3.2-A.i). Using flow cytometry (Figure 3.2-Aii), MFI values were calculated for 3 technical and biological repeats and one-way ANOVA was performed. The chart shows that 5 µM/20 min. is the optimal concentration to dye JJN3 (Figure 3.2-B). The mean values for the MFI are 1 µM 31994 RFU (±576), 2 µM 31459 RFU (±230), and 5 µM 31714 RFU (±862). MFI values for various incubation times: 31714 RFU (±862) for 20 minutes, 31632 RFU (±287) for 15 minutes, 31854 RFU (±728) for 10 minutes, and 3194 RFU (±754) for 5 minutes (Figure 3.2-B).

The percentage of DID concentration results showed no significant differences, with values of 1 µM 96.38 %, 2 µM 98.86 %, and 5 µM of DID 99.80 %. The DID percentage for incubation time was 99.99 % for 20 minutes, 100 % for 15 minutes, 100 % for 10 minutes, and 99.99 % for 5 minutes (Figure 3.2-C). Based on the flow cytometry data, any concentration or time could be sufficient to dye the JJN3.

Cells were double labelled with GFP (green) and DID (red). The fluorescent imaging showed that DID concentrations < 5 µM with 20 minutes of incubation time have stained fewer cells than DID concentrations 5 µM. Then, the concentration at 5 µM with different incubation timing showed that all cells were stained with DID dye.

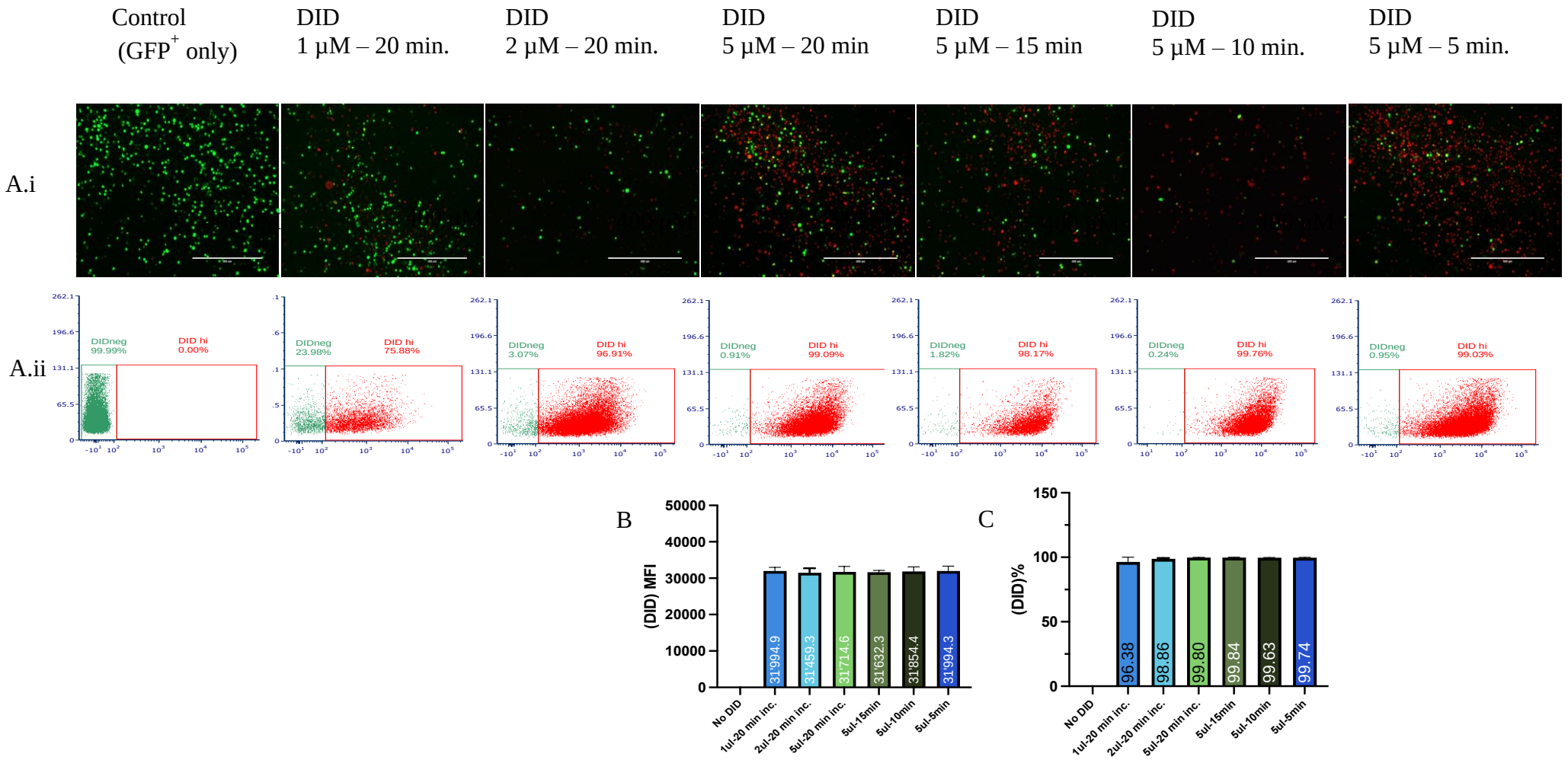

Figure 3.2: DID optimisation for JJN3 cell line

(A.i) EVOS microscope images for JJN3 with filter (cy5, exp=2, Gain=0.0, light=100)- (GFP, exp=57, Gain=3.0, light=100)- scale bar-10×= 400 µm magnification apply to all panel. (A.ii) Dot plots for flow cytometry analysis showing DID dye optimisation for JJN3 using an increased concentration of DID dye with different incubation times. (B) flow cytometry analysis of DID levels line chart showing DID dye optimisation for JJN3, calculating MFI mean values, one-way ANOVA were performed. (C) The bar chart shows DID dye optimisation, calculating the percentage of cells regarding dye concentration and incubation time. 3 technical and biological repeats.

3.3.1.3 DID Optimisation in OPM2 Cell Line

OPM2-GFP cells were labelled with different concentrations of DID dye to detect OPM2-GFP^{+} DID^{high} cells over time in a monoculture. After 5, 10 or 20 minutes, fluorescence images were taken (Figure 3.3-A.i). Using flow cytometry (Figure 3.3-Aii), MFI values was calculated for 3 technical and biological repeats and one-way ANOVA was performed. The chart shows that 5 µM/20 min. is the optimal concentration to dye OPM2 (Figure 3.3-B). The mean values for the MFI are 1 µM 50494 RFU (±6387), 2 µM 50811 RFU (±6781), and 5 µM 51321 RFU (±5530). MFI values for various incubation times: 51321 RFU (±5530) for 20 minutes, 4805 RFU (±8787) for 15 minutes, 51447 RFU (±5234) for 10 minutes, and 50699 RFU (±5413) for 5 minutes (Figure 3.3-B).

The percentage of DID concentration results showed no significant differences, with values of 1 µM 99.35 %, 2 µM 99.75%, and 5 µM of DID 99.97 %. The DID percentage for incubation time was 99.97 % for 20 minutes, 100 % for 15 minutes, 99.99 % for 10 minutes, and 99.97 % for 5 minutes (Figure 3.3-C). Based on the flow cytometry data, any concentration or time could be sufficient to dye the OPM2.

Cells were double labelled with GFP (green) and DID (red). The fluorescent imaging showed that DID concentrations < 2 µM with 20 minutes of incubation time have stained fewer cells than DID concentrations 5 µM. Then, the concentration at 5 µM with different incubation timing showed that all cells were stained with DID dye.

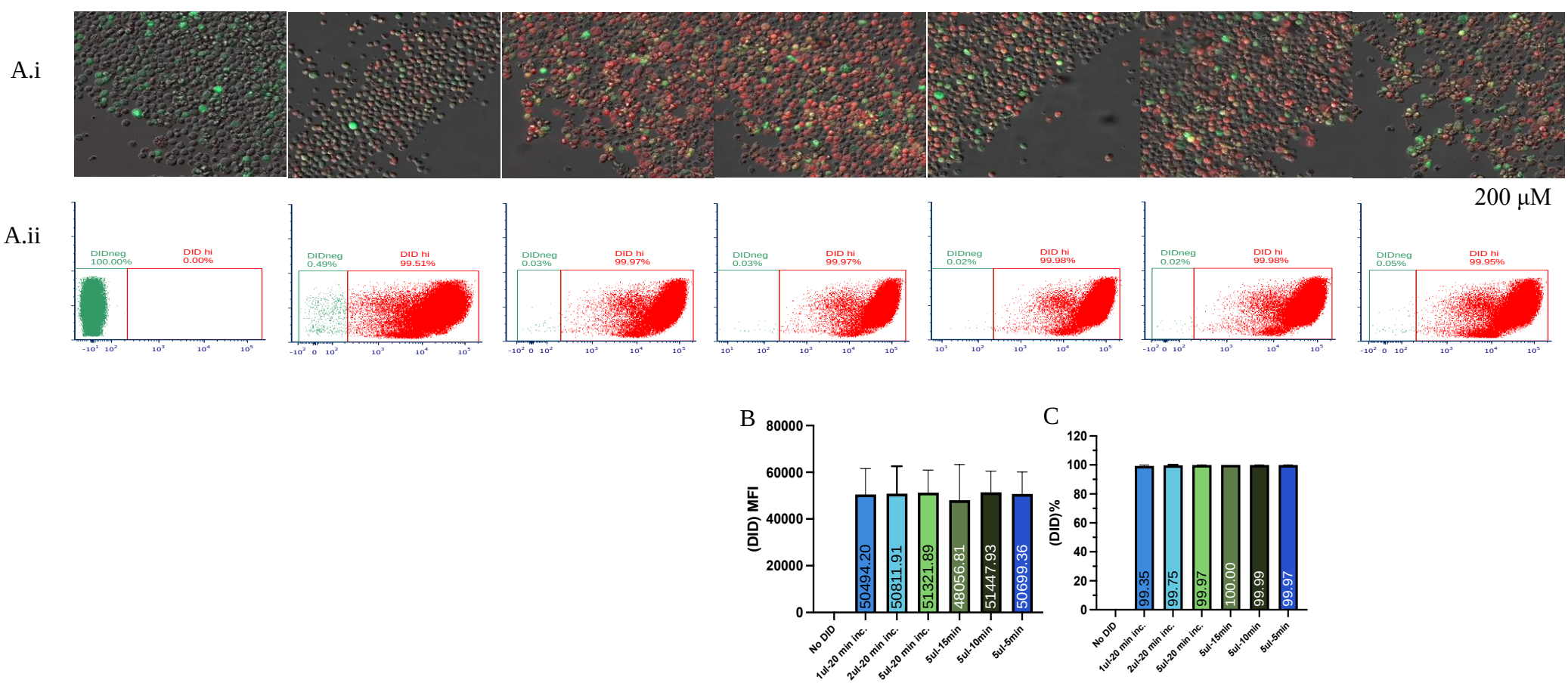

Figure 3.3: DID optimisation for OPM2 cell line

(A.i) EVOS microscope images for OPM2 with filter (cy5, exp=2, Gain=0.0, light=100)- (GFP, exp=57, Gain=3.0, light=100)- scale bar 200µM magnification apply to all panel. (A.ii) Dot plots for flow cytometry analysis showing DID dye optimisation for OPM2 using an increased concentration of DID dye with different incubation times. (B) flow cytometry analysis of DID levels line chart showing DID dye optimisation for OPM2, calculating MFI mean values, one-way ANOVA were performed. (C) Bar chart showing DID Dye optimisation, calculating the percentage of cells regarding dye concentration and incubation time. 3 technical and biological repeats.

3.3.1.4 DID Optimisation in U266 Cell Line

U266-GFP cells were labelled with different concentrations of DID dye to detect U266-GFP^{+} DID^{high} cells over time in a monoculture. After 5, 10 or 20 minutes, fluorescence images were taken (Figure 3.4-A.i). Using flow cytometry (Figure 3.4-Aii), MFI values were calculated for 3 technical and biological repeats and one-way ANOVA was performed. The chart shows that 5 µM/20 min. is the optimal concentration to dye U266 (Figure 3.4-B). The mean values for the MFI are 1 µM 30785 RFU (±2094), 2 µM 31119 RFU (±2147), and 5 µM 32799 RFU (±2862). MFI values for various incubation times: 32799 RFU (±2862) for 20 minutes, 37948 RFU (±2256) for 15 minutes, 32043 RFU (±2723) for 10 minutes, and 31832 RFU (±2089) for 5 minutes (Figure 3.4-B).

The percentage of DID concentration results showed no significant differences, with values of 1 µM 100 %, 2 µM 100 %, and 5 µM of DID 100 %. The DID percentage for incubation time was 100% for 20 minutes, 100 % for 15 minutes, 100 % for 10 minutes, and 100 % for 5 minutes (Figure 3.4-C).

Cells were double labelled with GFP (green) and DID (red). The fluorescent imaging showed that DID concentrations ≤ 5 µM with 20 minutes of incubation time have stained most of the cells than DID concentrations 5 µM. Then, the concentration at 5 µM with different incubation timing showed that all cells were stained with DID dye.

Based on the flow cytometry data and fluorescent images, any concentration or time was sufficient to dye the U266.

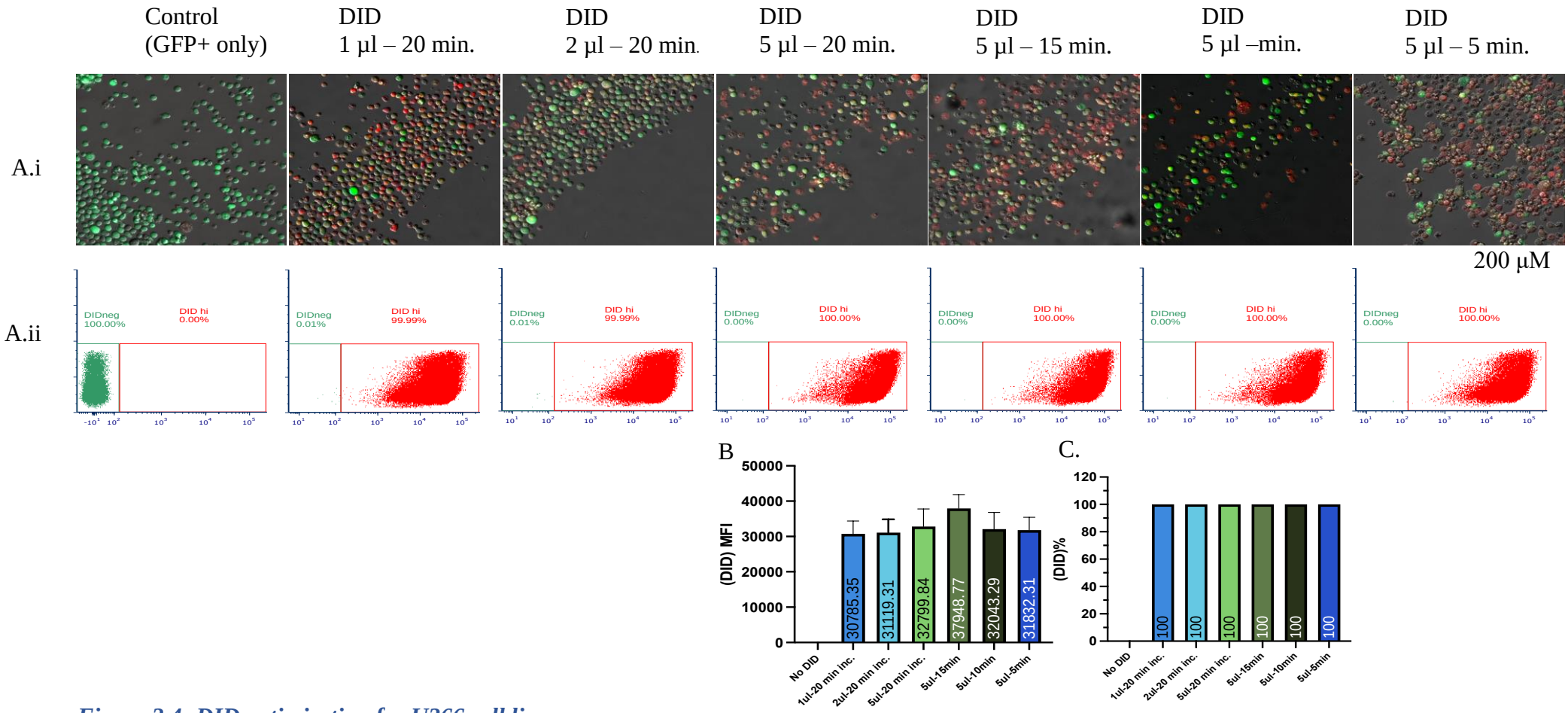

Figure 3.4: DID optimisation for U266 cell line

(A.i) EVOS microscope images for U266 with filter (cy5, exp=2, Gain=0.0, light=100)- (GFP, exp=57, Gain=3.0, light=100)- scale bar 10×= 400 µm magnification apply to all panel. (A.ii) Dot plots for flow cytometry analysis showing DID dye optimisation for U266 using an increased concentration of DID dye with different incubation times. (B) flow cytometry analysis of DID levels line chart showing DID dye optimisation for U266, calculating MFI mean values, one-way ANOVA were performed. (C) Bar chart showing DID Dye optimisation, calculating the percentage of cells regarding dye concentration and incubation time. 3 technical and biological repeats.

3.3.2 Dormancy tracking

3.3.2.1 Tracking Dormant Cells in the 5TGM1 Cell Line

5TGM1-GFP cells were labelled with DID dye, based on the manufacturer's protocol (5 µM of DID incubate with $1x10^6$ cells/mL for 20 mins) as no significant difference was observed with different DID concentrations or incubations times in (section 3.2.2) to track and visualise 5TGM1-GFP-DID^{high} cells in a monoculture for up to 21 days. The primary aim was to determine the optimum time point to sort and isolate DMCs (5TGM1-$GFP^{+}DID^{high}$) for subsequent treatment with SoCs alone or in combination.

The fluorescent imaging revealed a decrease in the number of DID^{high} labelled cells over 21 days. This was further validated using flow cytometric analyses, which showed the main cell population moved from the DID^{high} gate to the DID^{low} gate by seven days of culture; by 10 days of culture, the majority of cells were in the $DID^{negative}$ gate. This indicated that the majority of cells proliferated during the experiment, and only a limited number of cells stayed dormant (remained in the DID^{high} gate), suggesting DMCs were present in the 5TGM1 culture (Figure 3.5-A. i & A.ii).

The 5TGM1 DID^{high} percentage was reduced from 97% at the start of the culture (on day 0) to 32% after three days, and then it was reduced to only 3% by seven days of culture. The percentage of 5TGM1 DID^{high} cells continued to decrease until it reached less than 0.1% by day 21 (Figure 3.5-B). In comparison, the percentage of 5TGM1 DID^{low} cells (slow proliferating cells) started at around 2% (day 0) and increased to 67% on days 3 and 7. After this time, the 5TGM1 DID^{low} cells decreased from day 10 to 17, finishing with 12.5% DID^{low} after 21 days of culture (Figure 3.5-C).

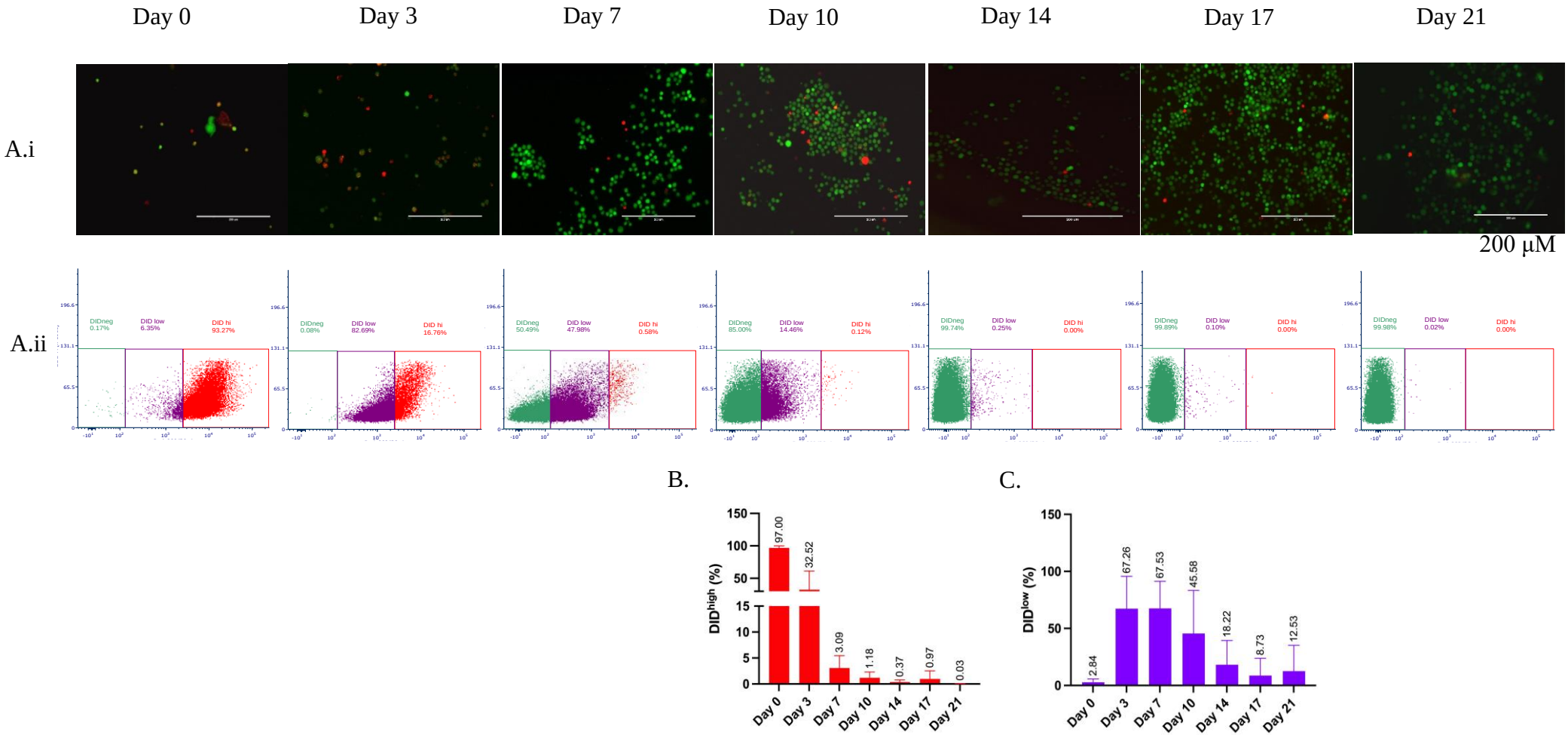

Figure 3.5: Tracking Dormancy in 5TGM1 cell line

(A.i) Fluorescent microscope images for 5TGM1 with filter (cy5, exp=2, Gain=0.0, light=100)- (GFP, exp=57, Gain=3.0, light=100)- scale bar 200 µM magnification apply to all panel. (A.ii) Dot plots of flow cytometry analysis showing DID^{high} labelled cells in a longitudinal experiment (21 days). (B) Bar chart showing DID^{high} labelled cells, calculating the percentage of cells over time (21 days). (C) The bar chart shows DID^{low}-labelled cells, calculating the percentage of cells over time (21 days). N=4.

3.3.2.2 Tracking Dormant Cells in The JJN3 Cell line

JJN3-GFP cells were labelled with DID dye, based on the manufacturer's protocol (5 µM of DID incubate with $1x10^6$ cells/mL for 20 mins) as no significant difference was observed with different DID concentrations or incubations times in (section 3.2.1) to track and visualise JJN3-GFP-DID^{high} cells in a monoculture for up to 21 days. The primary aim was to determine the optimum time point to sort and isolate DMCs (JJN3-$GFP^{+}DID^{high}$) for subsequent treatment with SoCs alone or in combination.

The fluorescent imaging revealed a decrease in the number of DID^{high} labelled cells over 21 days. This was further validated using flow cytometric analyses, which showed the main cell population moved from the DID^{high} gate to the DID^{low} gate by seven days of culture; by 10 days of culture, the majority of cells were in the $DID^{negative}$ gate. This indicated that most cells proliferated during the experiment, and only a limited number of cells stayed dormant (remained in the DID^{high} gate), suggesting DMCs were present in the JJN3 culture (Figure 3.6-A. i & A.ii).

The JJN3 DID^{high} percentage was reduced from 99% at the start of the culture (on day 0) to 61% after three days, and then it was reduced to only 12% by seven days of culture. The percentage of JJN3 DID^{high} cells continued to decrease until it reached less than 0.17% by day 21 (Figure 3.6-B). In comparison, the percentage of JJN3 DID^{low} cells (slow proliferating cells) started at around 0.7% (day 0) and increased to 39% on day 3 and 81% on day 7. After this time, the JJN3 DID^{low} cells decreased from day 10 to 17, finishing with 15% DID^{low} after 21 days of culture (Figure 3.6-C).

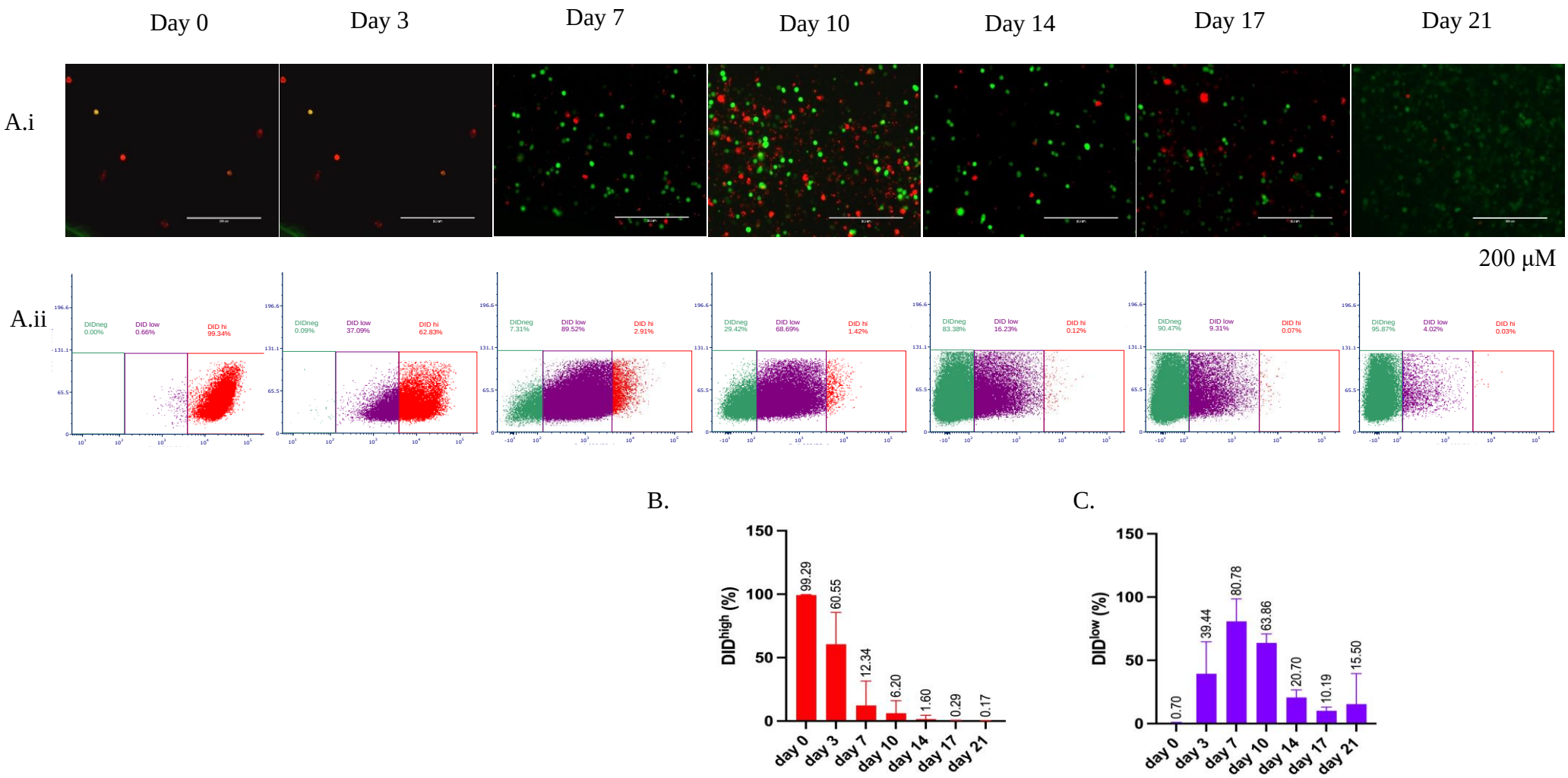

Figure 3.6: Tracking Dormancy in JJN3 cell line

(A.i) Fluorescent microscope images for JJN3 with filter (cy5, exp=2, Gain=0.0, light=100)- (GFP, exp=57, Gain=3.0, light=100)- scale bar 200 µM magnification apply to all panel. (A.ii) Dot plots of flow cytometry analysis showing DID^{high} labelled cells in a longitudinal experiment (21 days). (B) Bar chart showing DID^{high} labelled cells, calculating the percentage of cells over time (21 days). (C) Bar chart showing DID^{low} labelled cells, calculating the percentage of cells over time (21 days). N=4.

3.3.2.3 Tracking Dormant Cells in The OPM2 Cell Line

OPM2-GFP cells were labelled with DID dye, based on the manufacturer's protocol (5 µM of DID incubate with $1x10^6$ cells/mL for 20 mins) as no significant difference was observed with different DID concentrations or incubations times in (section 3.2.4) to track and visualise OPM2-GFP-DID^{high} cells in a monoculture for up to 21 days. The primary aim was to determine the optimum time point to sort and isolate DMCs (OPM2-$GFP^{+}DID^{high}$) for subsequent treatment with SoCs alone or in combination.

The fluorescent imaging revealed a decrease in the number of DID^{high} labelled cells over 21 days. This was further validated using flow cytometric analyses, which showed the main cell population moved from the DID^{high} gate to the DID^{low} gate by seven days of culture; by 10 days of culture, the majority of cells were in the $DID^{negative}$ gate. This indicated that the majority of cells proliferated during the experiment, and only a limited number of cells stayed dormant (remained in the DID^{high} gate), suggesting DMCs were present in the OPM2 culture (Figure 3.7 -A. i & A.ii).

The OPM2 DID^{high} percentage was changed from 95% at the start of the culture (on day 0) to 99% after three days, and then it was reduced to 47% by seven days of culture. The percentage of OPM2 DID^{high} cells continued to decrease until it reached less than 0.02% by day 21 (Figure 3.7-B). In comparison, the percentage of OPM2 DID^{low} cells (slow proliferating cells) started at around 3% (day 0), which was reduced to 0.2% on day three and then increased to 53% on day 7. After this time, the OPM2 DID^{low} cells decreased from day 14, finishing with 1.4% DID^{low} after 21 days of culture (Figure 3.7-C).

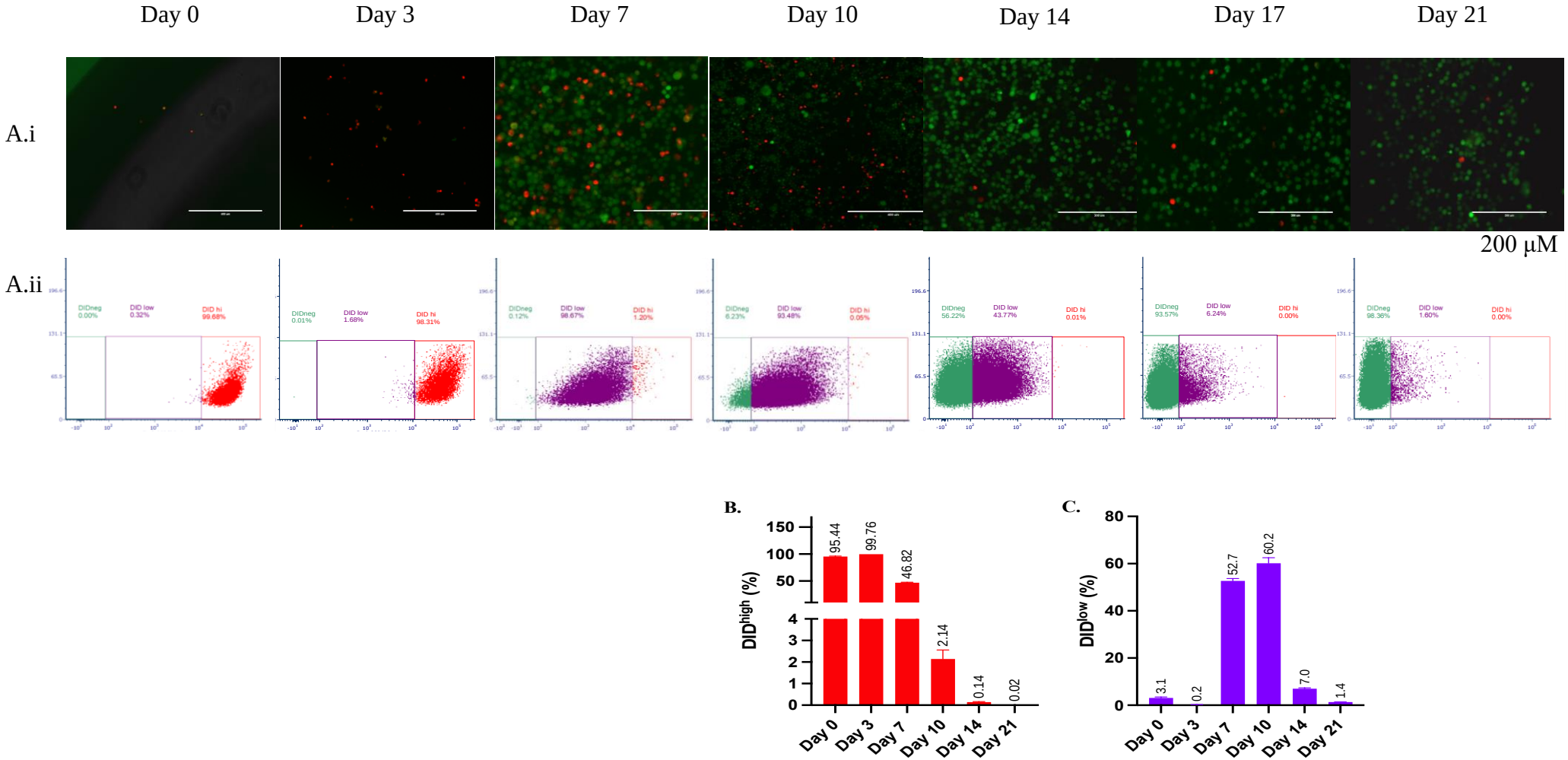

Figure 3.7: Tracking Dormancy in OPM2 cell line

(A.i) Fluorescent microscope images for OPM2 with filter (cy5, exp=2, Gain=0.0, light=100)- (GFP, exp=57, Gain=3.0, light=100)- scale bar 10X= 400 µm magnification apply to all panel. (A.ii) Dot plots of flow cytometry analysis showing DID^{high} labelled cells in a longitudinal experiment (21 days). (B) Bar chart showing DID^{high} labelled cells, calculating the percentage of cells over time (21 days). (C) Bar chart showing DID^{low} labelled cells, calculating the percentage of cells over time (21 days). N=4.

3.3.2.4 Tracking Dormant Cells in The U266 Cell Line

U266-GFP cells were labelled with DID dye, based on the manufacturer's protocol (5 µM of DID incubate with $1x10^6$ cells/mL for 20 mins) as no significant difference was observed with different DID concentrations or incubation times in (section 3.2.4) to track and visualise U266-GFP-DID^{high} cells in a monoculture for up to 21 days. The primary aim was to determine the optimum time point to sort and isolate DMCs (U266-$GFP^{+}DID^{high}$) for subsequent treatment with SoCs alone or in combination.

The fluorescent imaging revealed a decrease in the number of DID^{high} labelled cells over 21 days. This was further validated using flow cytometric analyses, which showed the main cell population moved from the DID^{high} gate to the DID^{low} gate by seven days of culture; by 10 days of culture, the majority of cells were in the $DID^{negative}$ gate. This indicated that the majority of cells proliferated during the experiment, and only a limited number of cells stayed dormant (remained in the DID^{high} gate), suggesting DMCs were present in the U266 culture (Figure 3.8-A. i & A.ii).

The U266 DID^{high} percentage was reduced from 99% at the start of the culture (on day 0) to 87% after three days, and then it was reduced to only 45% by seven days of culture. The percentage of U266 DID^{high} cells continued to decrease until it reached less than 1% by day 21 (Figure 3.8-B). In comparison, the percentage of U266 DID^{low} cells (slow proliferating cells) started at around 0.2% (day 0) and increased to 12% on day 3 and 54% on day 7. After this time, the U266 DID^{low} cells elevate from day 10 to 14, finishing with a reduction to 52% DID^{low} after 21 days of culture (Figure 3.8-C).

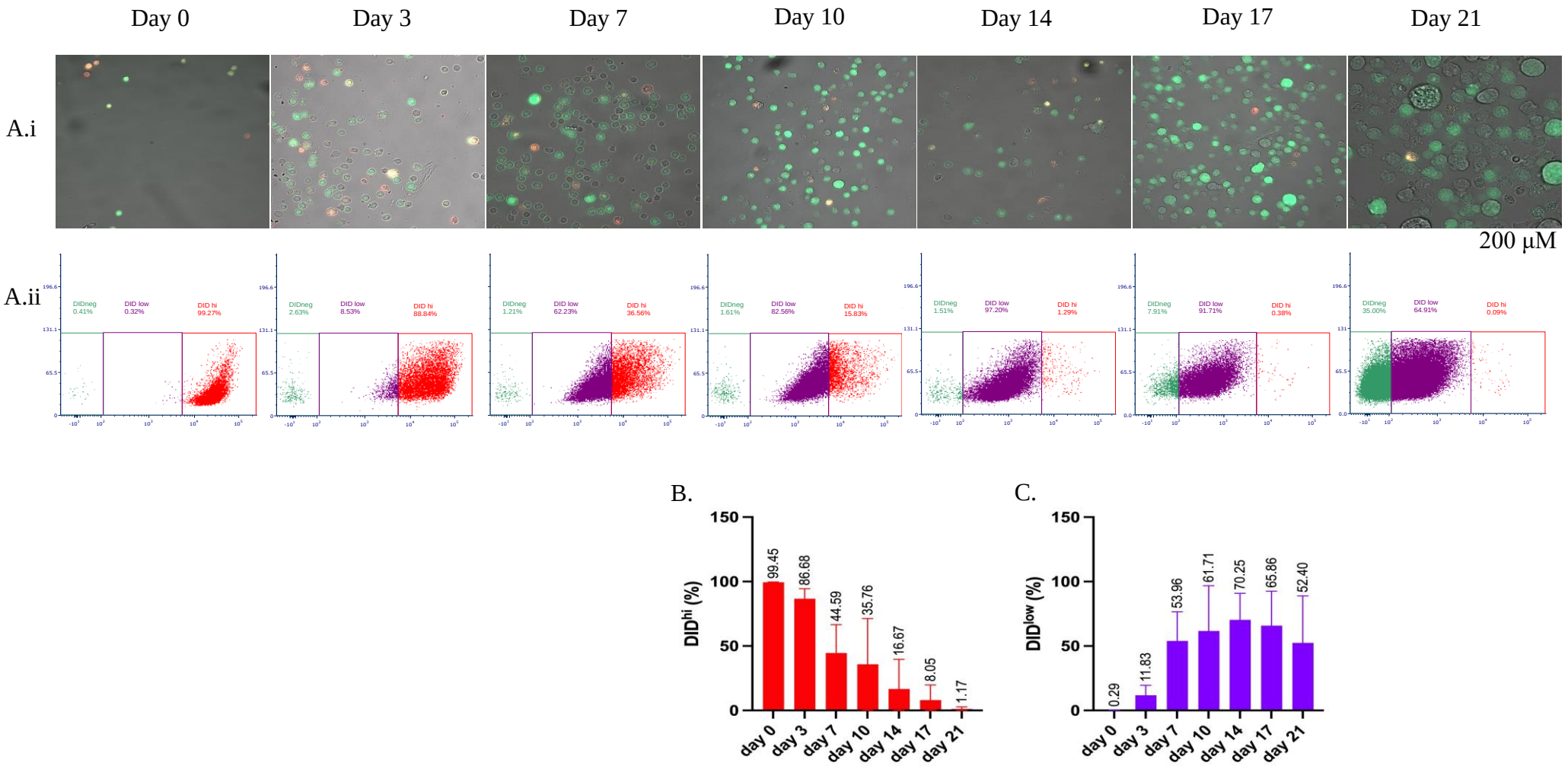

Figure 3.8: Tracking Dormancy in U266 cell line

(A.i) Fluorescent microscope images for U266 with filter (cy5, exp=2, Gain=0.0, light=100)- (GFP, exp=57, Gain=3.0, light=100)- scale bar 10X= 400 µm magnification apply to all panel. (A.ii) Dot plots of flow cytometry analysis showing DID^{high} labelled cells in a longitudinal experiment (21 days). (B) Bar chart showing of DID^{high} labelled cells, calculating the percentage of cells over time (21 days). (C) Bar chart showing of DID^{low} labelled cells, calculating the percentage of cells over time (21 days). N=4.

3.4 Discussion

This chapter aims to optimise the isolation of DID^{high} cells using DID dye for subsequent *in vitro* targeting DMCs. To establish optimal labelling conditions, we systematically evaluated various DID dye concentrations and incubation times across multiple MM cell lines (5TGM1, JJN3, OPM2, and U266).

To optimise the DID dye by labelling process, we systemically evaluated various DID concentrations and incubation times in MM-GFP^{+} cells with flow cytometry (detailed method in chapter 2 section 2.2.6). Flow cytometry was gated as DID^{negative} and DID^{high} populations, allowing us to calculate both the percentage of labelled cells and the MFI. Fluorescent microscopy images were employed to visually confirm successful DID labelling and to observe morphology. By carefully analysing DID percentage and MFI data, we determined that a wide range of concentrations and incubation times could be effectively employed to achieve our desired labelling outcomes. This flexibility is advantageous for accommodating diverse experimental conditions and requirements. A comparable strategy using DID labelling, along with concentration and timing as suggested by the manufacturer, was employed to analyse 5TGM1 over a 21-day *in vitro* period. DMCs were tracked successfully until their migration to the BM endosteal niche using two-photon microscopy *in vivo* (Lawson et al., 2015).

On the contrary, Yumoto *et al.* (2014) reported that a volume of 2 µM of DID was suitable for achieving optimal labelling for prostate cancer cells without affecting cell proliferation (Yumoto, Janice E. Berry, et al., 2014). While Yumoto *et al.* (2014) demonstrated the utility of DID for long-term, non-invasive monitoring of cell proliferation in both *in vitro* and *in vivo* models, our results suggest that the optimal DID volume may vary depending on the specific cell type and experimental conditions. It is important to note that DID can provide stable fluorescent labelling of live cells, which is useful for observing cell proliferation over time in both *in vitro* and *in vivo* studies without damaging cell proliferation. Additionally, this system does not require any genetic manipulation; the study indicates that DID can be a safe and powerful tool for identifying cell proliferation, although further analysis is necessary (Yumoto, Janice E. Berry, et al., 2014).

Our study complements previous research by Chen *et al.* (2019), who employed a different approach to track dormant cells using a PKH67 fluorescent tracker. PKH67, a lipophilic dye evaluated by flow cytometry, exhibits a similar mechanism of action to DID: proliferating myeloma cells lose the dye while quiescent cells retain it. Chen et al.'s findings provided valuable insights into the presence of dormant cell population within the BM niche and highlighted the crucial role of the microenvironment in regulating their growth and progression (Chen et al., 2019).

Likewise, Yu (2016) utilised the PKH dye method to track dormant cells in acute myeloid leukaemia (AML) by labelling cells as $CD45^{dim}CD34^{+}LAP^{+}PKH26^{high}$ and successfully targeted these dormant cells with chemotherapy. The advantages of using PKH26 has low toxicity profile and offers strong fluorescent signal which is preferred for long term cell tracking. Yu's (2016) study identified dormant AML cells *in vitro* and led to the discovery of novel agents capable of targeting chemotherapy-resistant cells (Yu, 2016). These findings collectively underscore the importance of targeting DMC populations in cancer therapy. By understanding the characteristics and behaviour of dormant cells, we can develop more effective treatment strategies that address both actively proliferating and quiescent cancer cells.

To investigate the long-term persistence of DID labelled DMCs, we closely monitored DID^{high} population in the monocultures of 5TGM1, JJN3, OPM2, and U266 for a period of 21 days. Our data was aligned with previous studies such as Lawson *et al.* (2015), Chen *et al.* (2019) and Khoo *et al.* (2019), which utilised lipophilic dyes like DID and PKH to track dormancy. Flow cytometry and fluorescent imaging assessed DMCs using DID dye over time. Likewise, Lawson *et al.* (2015) and Chen *et al.* (2019) demonstrated that dormant cells retain the dye while proliferating cells lose it, leading to its eventual disappearance (Figure 1.6) (Chen et al., 2019; Lawson et al., 2015). A similar approach was adopted by Wang *et al.* (2015), who tracked dormant PC3 prostate cancer cells by DID and revealed the presence of slow-growing/quiescent cells that express CXCR4, a protein involved in cell migration, as a characteristic of these cells (Wang et al., 2015).

To optimise the timing of cell sorting and isolation, we determined the growth rates of each cell line and identified the most favourable time point for harvesting DID^{high} labelled cells. We decided to isolate DMCs at their exponential/ log phase early before entering the plateau phase

to avoid losing all DID^{high} cells. The Murine 5TGM1 and human JJN3 cells are known for their fast growth rate, while human OPM2 and U266 are known for their low growth rate (Paton-Hough, Chantry, & Lawson, 2015). We suggest isolating the 5TGM1 and JJN3-DID^{high} on day seven and the OPM2 and U266-DID^{high} on day 10. This approach aimed to maximise the yield of DID^{high} cells while minimising label loss during cell proliferation.

Our study contrasts with Yu's (2016) study, which involved sorting dormant AML cells on day 12. Yu (2016) successfully identified a significant population of dormant AML using *in vitro* and discovered a novel agent that can target BM niche-mediated chemotherapy resistance (Yu, 2016). The sorting process is non-invasive, it could potentially impact cells through various factors. Mechanical stress induced by the fluid flow and nozzle pressure could cause membrane damage to cells or disrupt the intracellular structure. Additionally, temperature fluctuations during the sorting process, especially excessive heat generated from the laser, may contribute to cell damage. Although isolating DID^{high} cells differ regarding cell origin, type, cell behaviour, and culture condition, carefully optimising the sorting process is crucial to minimise cell damage.

3.4.1 Conclusion

This chapter aimed to identify and track DMCs using DID dye, then to determine the optimum time point to isolate DMCs for subsequent drugs assays. After optimising the dye concentration and incubation time, DMCs were monitored for 21 days and optimal time points to sort and isolate DID^{high} labelled cells for each cell line were determined. Our findings suggested isolating 5TGM1 and JJN3-DID^{high} cells on day seven and OPM2 and U266-DID^{high} cells on day 10 for single SoC and combined drug treatments (Chapter 4). Our research has demonstrated that DID labelling is a valuable tool for studying the dynamics of DMCs. As cells proliferate, the DID label is passed on to new daughter cells during cell division; therefore, the DID dye on the cell surface get progressively diluted until it eventually disappears. For cells that are not dividing and potentially DMCs the DID is retained (DID^{high}).

Chapter 4 Determining Drug IC_{50} Values for Myeloma Cell Lines and Their Effects on DMCs

4.1 Introduction

Previously, in chapter 3, we studied the presence of DMCs in monoculture by investigating the DID dye optimisation first for each cell line and determined the exact time point for each cell line to isolate potential DMC cells to investigate the efficacy of drugs in single and combined. Therefore, this chapter will investigate the most effective drug combination to target DMCs. We first wanted to determine the IC_{50} of each drug that can reduce the cell viability of proliferating myeloma cells. The IC_{50} measurement is a key indicator of a drug's potency, revealing the concentration necessary to inhibit a cellular process by 50%. A lower IC_{50} indicates a more potent drug, requiring a smaller dosage to achieve the desired outcome. Such precision is vital in developing effective treatments with fewer potential side effects. New types of therapies have led to a decrease in mortality rates in MM. These therapies include CAR-T therapy that targets CD19, PIs such as Btz, HDACis like Pan, IMiDs such as Pom, mAbs targeting CD38, and ASCT (Chakraborty & Majhail, 2020). In addition, bifunctional alkylating agents such as Mel used to be the first line of the standard MM treatments before approaching ASCT. Therefore, four types of anti-myeloma drugs were chosen based on their mechanism of action, target, and drug class. These were Btz, Mel, Pom, and Pan. These drugs were chosen because they have previously been used successfully and safely to target MM cell lines *in vitro* and *in vivo,* including patients. At the same time, there were insufficient studies targeting DMCs by single or combined treatments. Consequently, Lawson *et al.* (2015) studied 5TGM1-eGFP cells injected in BKAL male murine models of myeloma, then treated with Mel, and imaged by multiphoton microscope to find that DMCs were still detectable in murine BM, indicating that DMCs were resistant to Mel (Lawson et al., 2015). More studies are needed to investigate the effect of SoC drugs on DMCs.

4.1.1 Standard of Care Drugs

Btz is a reversible PIs that disrupts protein recycling, leading to accumulation and cell apoptosis. myeloma cells, with their high protein turnover, are particularly susceptible to Btz as it interferes with protein metabolism and removal within the cell, prompting a proapoptotic signal (Laubach et al., 2015). Btz has a robust anti-neoplastic effect by lowering myeloma cells' constitutively high proteasome activity. It is also approved as a first-line therapy for MM

patients. Although Btz is known to target proliferating myeloma cells, reducing tumour burden *in vivo* and in patients, there is limited data regarding Btz's effects on DMCs (Lawson et al., 2015). Lawson *et al.* showed that Btz treatment did not significantly reduce DMCs compared to vehicle-treated mice in the 5TGM1 model of myeloma. However, to date, no further research has assessed the effects of Btz alone or in combination with SoCs on DMCs in other murine models of myeloma or on patient DMCs. Therefore, further research in this area is needed.

Novel PIs have been developed to defeat Btz's resistance. In the past few years, there has been a fast discovery of innovative drugs targeting tumour-specific pathways in MM; nevertheless, when used as monotherapy, these targeted medications have often demonstrated limited effectiveness due to the multi-step process of tumorigenesis on proliferating cells (Lawson et al., 2015; Accardi et al., 2015; Chauhan et al., 2013; Kapoor, Ramakrishnan, & Rajkumar, 2012; Adams et al., 1999). Therefore, in this thesis, we intend to combine Btz with other anti-myeloma drugs to target DMCs with various mechanisms of action (Chen, Garssen, & Redegeld, 2021; Suominen et al., 2015; Kikuchi et al., 2014; Ocio et al., 2010).

Mel is a type of chemotherapy drug that is used to treat MM as a standard treatment for MM involves high-dose therapy (HDT), followed by ASCT. Mel is an alkylating agent that works by binding to biological molecules. It can create different types of DNA adducts. These DNA adducts include mono-adducts at the N7 of guanine and the N3 of adenine, as well as interstrand cross-links and pre-mutagenic lesions. These chemical changes are believed to contribute to the toxic and carcinogenic effects of Mel (Gkotzamanidou et al., 2022; Chauhan et al., 2013). In addition, gene mutations, epigenetic changes, DNA repair alteration, BMME interaction, and disease relapse have been linked to patients undergoing Mel-based therapies (Poczta et al., 2022; Poczta, Rogalska, & Marczak, 2021).

Chai *et al.,* 2017 approved that treatment with Mel can reactivate DMCs through the RANKL protein that binds to its receptor RANK and activates signalling molecules that are necessary for the differentiation of OC. These signalling molecules include transcription factors such as NFκβ. myeloma cells also produce RANKL and induce its production in the surrounding BMME. This can lead to increased osteoclastic bone resorption and bone loss. However, Mel treatment can also activate DMCs to MM proliferating cells, which may have implications for disease progression. This will explain disease relapse and short-term survival rate (Chai et al.,

2017). In addition, Lawson *et al*., 2015 confirm that DMCs were resistant to Mel (Lawson et al., 2015). Therefore, in this chapter, we will combine Mel with other anti-myeloma drugs to potentially target DMCs *in vitro*, then subsequently, in chapter 5, assess the efficacy of targeting DMCs within their niche *in vivo*.

Pom is a potent second-generation IMiD with antiproliferative, pro-apoptotic, anti-angiogenic properties, bone resorption, and immune system modulatory effects. Pom aims to enhance treatment options available for patients who suffer from RRMM. *In vitro* and *in vivo* experiments showed that Pom is more potent than other IMiDs, such as thal or len (Table 1.2), whilst being less harmful as it is used at lower doses. Moreover, Pom has a dual action on the BMME and malignant plasma cells (Lacy & McCurdy, 2013; Richardson et al., 2013; Chanan-Khan et al., 2013; Schey & Ramasamy, 2011). Pom directly and indirectly affects immune cells, such as NK cells, and enhances NK cell cytotoxicity to target myeloma cells (Chanan-Khan et al., 2013). Plus, Pom has the ability to inhibit NFκβ activation, which is critical in improving chemo-susceptibility by promoting apoptosis. However, in solid tumours, these effects and mechanisms remain unknown (Saito et al., 2018). Most of the Pom studies targeted proliferating cells, and several papers have investigated the effectiveness of combining Pom with chemotherapies and RRMM. However, we still have limited knowledge of the effect of Pom on DMCs. Therefore, further studies are needed in this field (Gay et al., 2013; Schey & Ramasamy, 2011). Hence, this chapter will focus on assessing Pom's potential to target DMCs *in vitro* alone and combined with other SoC drugs.

Pan is a HDACi. Histone acetylation plays an essential role in regulating the accessibility of transcription factors to DNA, controlling the cell cycle arrest of myeloma cells, and inducing cell apoptosis. Apart from causing cell death in plasma cells taken from MM patients, Pan is also being developed clinically for the treatment of hematologic and solid tumours (Laubach et al., 2015; Ocio et al., 2010; Growney et al., 2007; Maiso et al., 2006). Pan can target a wide range of Deacetylase (DAC) enzymes, and investigations have shown that MM patients overexpress DACs. Pan is considered to provide broad anti-cancer effects through epigenetic gene expression control and protein metabolism inhibition. Reducing class I, II and IV histone deacetylases, which target histones and transcription factors like p53, may aid in the reactivation of epigenetically repressed tumour suppressor genes. Pan has also been proven to

work in combination with PIs such as Btz. Btz inhibits proteasome function, resulting in the accumulation of misfolded proteins and the formation of aggresome. Therefore, Pan disrupts aggresome pathways, increases the acetylation of microtubules and makes them less efficient for transportation, so this combination has the ability to trap unwanted proteins within the cell, which leads to stronger proapoptotic signal and increases cytotoxicity in myeloma cells (Laubach et al., 2015). However, most studies on Pan were conducted on dividing cells, leaving DMCs un-investigated. In this chapter, we will focus on investigating the potential of Pan to target DMCs, whether it's alone or in combination with SoC drugs.

4.1.2 Combined Treatment to Target DMCs

Regardless of advances in anti-MM therapies, patients still suffer from disease relapse largely due to drug resistance. Some combined therapies have been approved to overcome drug resistance and disease relapse with improved safety and better clinical outcomes *in vitro* and *in vivo* and on MM patients with regards to toxicity, such as combining Pan, Dex, Dox, and Btz with Mel. However, more studies are needed in this field (Gkotzamanidou et al., 2022; Lacy & McCurdy, 2013). Therefore, few *in vivo* studies investigated the efficacy of SoC drugs on DMCs, such as Lawson *et al.* 2015 study that used murine models of myeloma, have shown that single SoC agents such as Btz or Mel are often insufficient to eliminate all myeloma cells (Lawson et al., 2015), Therefore, since limited research has been done on assessing SoC drug efficacy on DMCs alone and in combination, this research will assess these drugs alone and combined.

The next chapter will assess the most promising drugs, alone or in combination, to affect DMCs in an *in vivo* model of myeloma.

4.1.3 Aims, Hypothesis and Objectives

The aim of this chapter was to determine the IC_{50} values of four SoC drugs (Btz, Mel, Pom and Pan) on four myeloma cell lines (5TGM1, U266, JJN3 & U266). Then use the determined drug IC_{50} values in the subsequent *in vitro* studies to assess their efficacy against DMCs when used alone or in combination.

We hypothesised that Btz, Mel, Pom and Pan would effectively inhibit myeloma cell viability after 3 days of culture and target DMCs when the drug IC_{50} values are used in combination.

The objectives:

1. To determine IC_{50} values of Btz, Mel, Pom, and Pan using drug titration assays on four MM cell lines (5TGM1, U266, JJN3 & U266).
2. To assess the effect of drug IC_{50} values when used alone or in combination on DMCs from the four MM cell lines.

4.2 Material and Methods

Detailed information on individual techniques performed can be found in Chapter 2 under General Materials and Methods.

4.2.1 Drug Preparations

Btz concentrations used were 0.5, 1, 1.5, 2, 2.5, 5, 10, 20, and 30 nM, Mel concentrations used were 0.1, 1, 5, 10, 20, 50 µM, Pom concentrations used were 0.001, 0.01, 0.1, 1, 10, 100 µM, and Pan concentrations used were 5, 10, 15, 20, 50, and 100 nM. Drugs were then added to 2500 or 5000 cell/media mix, for further details see section 2.2.3.

4.2.2 Cell Viability Assay (AlamarBlue) and Drug Titration Assays to Determine IC_{50} Values

To measure cell viability, a titration assay was performed to determine IC_{50} values for each drug. Cells were exposed to different drug concentrations, including Btz, Mel, Pom, Pan, and vehicle (Details in Chapter 2 section 2.1.3).

4.2.3 Targeting DMCs with SoC Drugs

4.2.3.1 Flow Cytometry and Sorting/Isolating GFP-DID^{high} Labelled Cells

To sort DMCs (GFP^+DID^+), MM cell lines were labelled with DID, and flow cytometry was used with a FlowMelody (details in section 2.2.6).

4.2.3.2 Targeting DID^{high} Labelled Cells by SoC

The sorted/isolated DID^{high} cells were seeded in a 96-well plate, 5000 cells/well. Drugs were added to cells at their IC_{50} values in single or combined form. Then, the cells were incubated at 37°C in a 95% air and 5% CO_2 environment. After three days, the cells were resuspended in a buffer solution containing 500 µl of FBS and then analysed using flow cytometry. Three technical and biological repeats were done. The gating strategy is explained in (Figure 4.1).

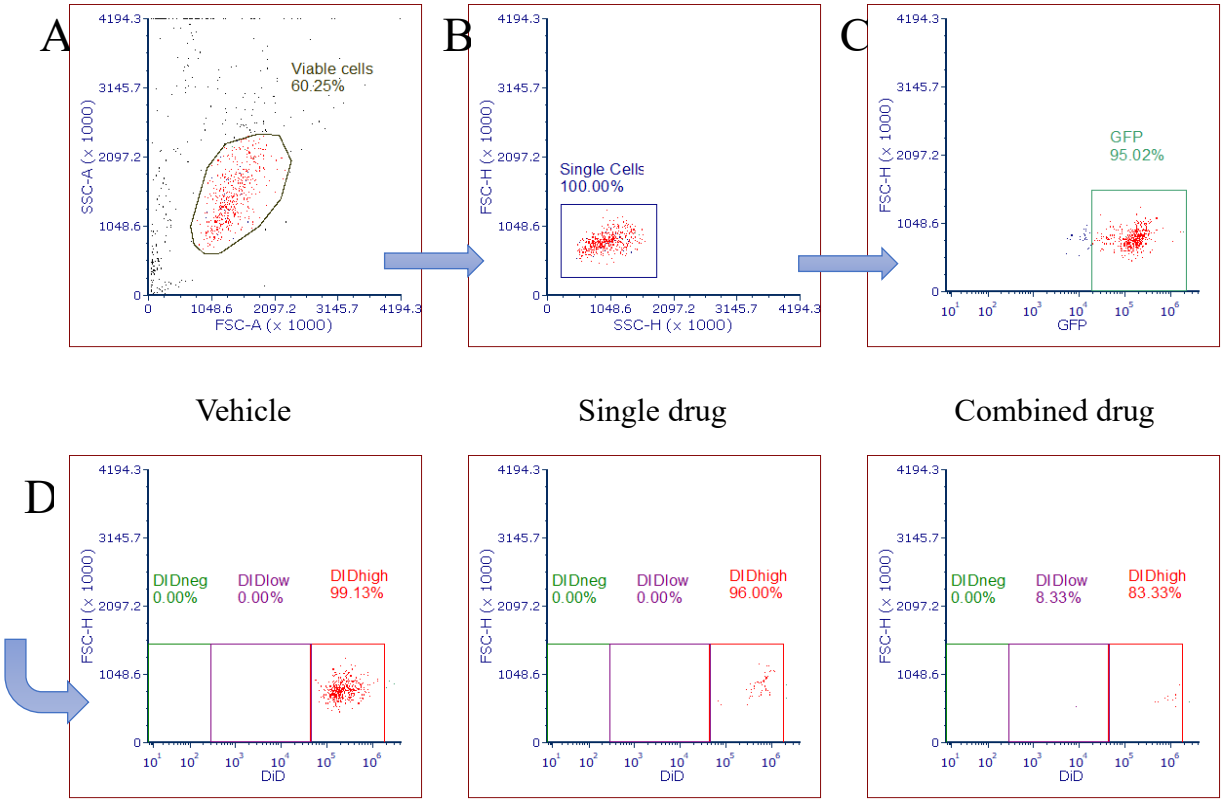

Figure 4.1: Representative flow cytometry explaining the gating strategy to target sorted DID^{high} (DMCs).

Flow cytometry graphs show the gating strategy to target DID^{high} (DMCs) with alone or combined drugs in monoculture 3 days post-treatment. A) Polygon gate for double labelled JJN3-GFP^{+}DID^{high}, SSC and FSC to distinguish live B lymphocytes (myeloma cells) and dead cells or lymphocyte debris. B) Gates used FSC and SSC to extract single cells. C) Gate extracted from the single cells population to extract GFP labelled cells. D) DID gate was extracted from GFP population to find the effect of treatments on DID^{high} sorted cells.

4.2.4 Statistical Analyses

Data was analysed using GraphPad Prism 9.1/10. For normally distributed data, one-way ANOVA with Tukey's multiple comparison tests was performed. Mean (+/- standard deviation) was presented. IC_{50} values were calculated using GraphPad Prism 9.3/10. Data was transformed to log values and normalised to 100%. Non-linear regression was used to find the dose-response versus inhibition, and a sigmoidal curve was drawn to illustrate the IC_{50} value for each drug using each cell line.

4.3 Results

4.3.1 Bortezomib Titration Studies to Determine IC_{50} Values on Four Myeloma Cell Lines

4.3.1.1 To Determine the IC_{50} Values of Bortezomib on 5TGM1 Cells Using a Cell Viability Assay (AlamarBlue)

The IC_{50} values of Btz were initially determined so they could be used to target 5TGM1 DMCs in subsequent studies (Chapter. 5). Two 5TGM1 cell densities (2500 cells/well and 5000 cells/well) were used and assessed with various concentrations of Btz 0.5, 1, 1.5, 2, 2.5, 5, 10, 20, and 30 nM (Details in chapter 2, section. 2.2.3).

For the 2500 cell density, day 0 was done as a baseline control to make sure the assay was set up correctly; after 3 days of treatment, 5TGM1 cell viability was significantly decreased compared to the vehicle using 2, 2.5, 5, 10, 20, and 30 nM Btz concentrations. After five days of treatment, cell viability was significantly reduced compared to the vehicle using 1.5, 2, 2.5, 5, 10, 20 and 30 nM Btz concentrations (Figure 4.2-A, i, ii, iii, C). These data were calculated using GraphPad Prism, and the Btz IC_{50} value for 2500 cell density was 40.25 nM. This value is considered out of range because it is higher than the maximum concentration tested in the experiment, indicating that a 50% inhibitory effect was not achieved within the concentration range used. Suggesting expanding the concentration values.

For the 5000 cell density, day 0 was done as a baseline control to ensure the assay was set up correctly; after 3 days of treatment, 5TGM1 cell viability significantly decreased compared to the vehicle, using 5, 10, 20, and 30 nM Btz concentrations. After 5 days of treatment, cell viability was significantly reduced compared to the vehicle using 2, 2.5, 5, 10, 20 and 30 nM Btz concentrations (Figure 4.2-B, i, ii, iii, C). These data were calculated using GraphPad Prism, and the Btz IC_{50} value for 5000 cell density was 3.08 nM.

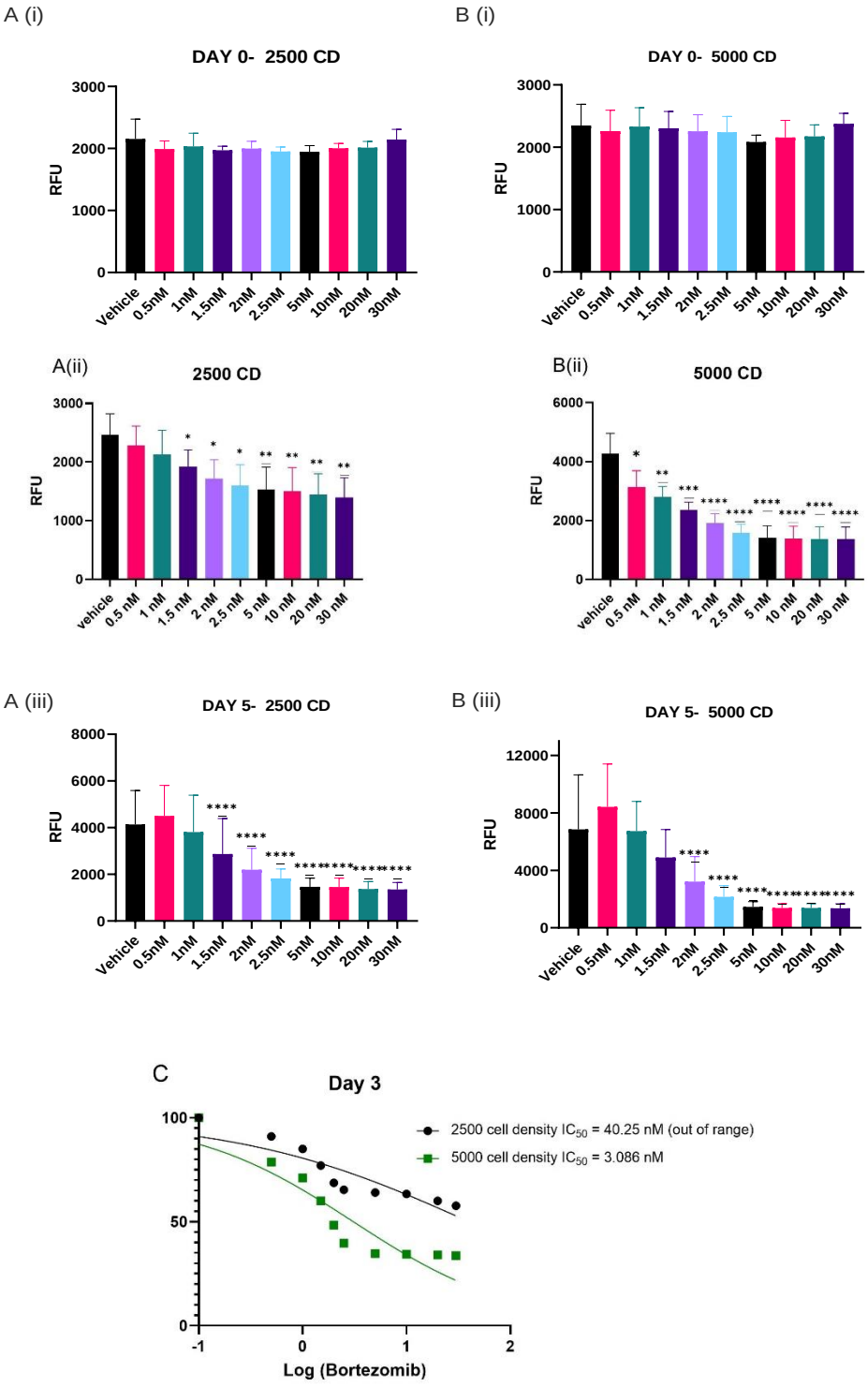

Figure 4.2:Determining the IC_{50} values of Btz on murine 5TGM1 cells using two cell densities

*5TGM1 cells were cultured at (A-i, ii, iii) 2500 cells/ well or (B-i, ii, iii) 5000 cells/well in 96 well plates with different concentrations of Btz (0.5, 1, 1.5, 2, 2.5, 5, 10, 20, and 30 nM) or vehicle control for up to 5 days. Cell viability was assessed using an AlamarBlue® assay on days 0 (baseline), 3 and 5 on a plate reader (580 nm excitation, 610 nm emission with a cut-off at 590nm) to determine RFU. The findings were reported using one-way ANOVA, and P-values were determined compared to vehicle, where *<0.01, **<0.001, ***<0.0001, ****<0.00001. N=3. (C) Using GraphPad Prism, calculating Btz IC_{50} for two 5TGM1 cell densities (2500 and 5000), non-linear regression was performed on day 3 post-treatment. For the 2500 cell density, IC_{50} = 40.25 nM. For the 5000 cell density, IC_{50} = 3.08 nM.*

4.3.1.2 To Determine the IC_{50} Values of Bortezomib on JJN3 Cells using a Cell Viability Assay (AlamarBlue)

Next, IC_{50} values of Btz were determined for JJN3 cells. Two JJN3 cell densities (2500 cells/well and 5000 cells/well) were used and assessed with various concentrations of Btz 0, 1, 2, 2.5, 5, 10, 20, and 30 nM (Details in chapter 2, section 2.2.3).

For the 2500 cell density, day 0 was done as a baseline control to make sure the assay was set up correctly; after 3 days of treatment, JJN3 cell viability was significantly decreased compared to the vehicle using 1, 1.5, 2, 2.5, 5, 10, 20, 30 nM Btz concentrations. After 5 days of treatment, cell viability was significantly reduced compared to the vehicle using 0.5, 1, 1.5, 2, 2.5, 5, 10, 20 and 30 nM Btz concentrations (Figure 4.3-A, i, ii, iii, C). These data were calculated using GraphPad Prism, and the Btz IC_{50} value for 2500 cell density was 19.49 nM.

For the 5000 cell density, day 0 was done as a baseline control to make sure the assay was set up correctly; after 3 days of treatment, JJN3 cell viability was significantly decreased compared to the vehicle, using 1, 1.5, 2, 2.5, 5, 10, 20, and 30 nM Btz concentrations. After 5 days of treatment, cell viability was significantly reduced compared to the vehicle using 0.5, 1, 1.5, 2, 2.5, 5, 10, 20 and 30 nM Btz concentrations (Figure 4.3-B, i, ii, iii, C). These data were calculated using GraphPad Prism, and the Btz IC_{50} value for 5000 cell density was 12 nM.

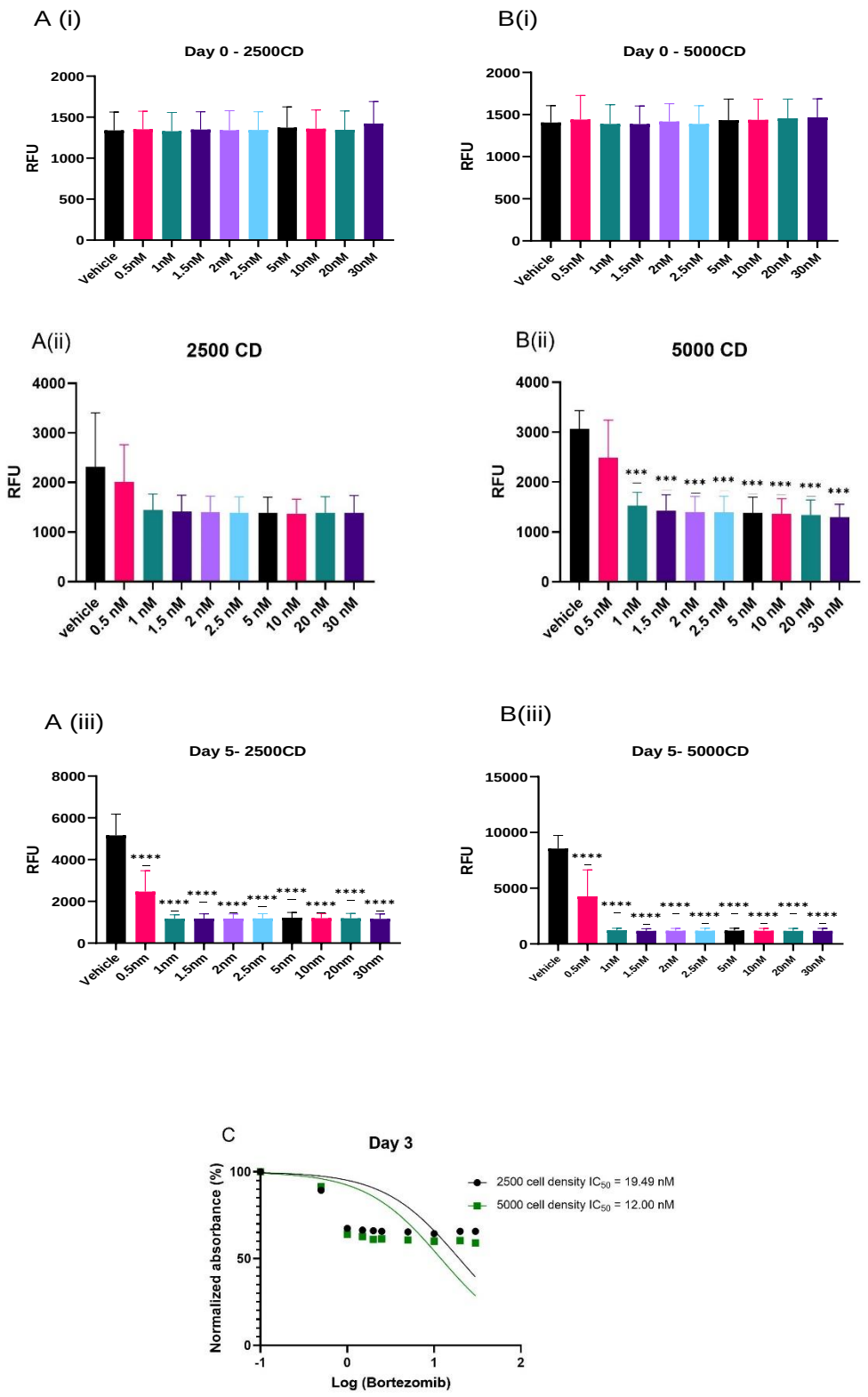

Figure 4.3: Determine the effect of Btz IC_{50} on the JJN3 cell line with two cell densities

*JJN3 cells were cultured at (A-i, ii, iii) 2500 cells/ well or (B-i, ii, iii) 5000 cells/well in 96 well-plates with different concentrations of Btz (0.5, 1, 1.5, 2, 2.5, 5, 10, 20, and 30 nM) or vehicle control for up to 5 days. Cell viability was assessed using an AlamarBlue® assay on days 0 (baseline), 3 and 5 on a plate reader (580 nm excitation, 610nm emission with a cut-off at 590nm) to determine RFU. The findings were reported using one-way ANOVA, and P-values were determined compared to vehicle, where *<0.01, **<0.001, ***<0.0001, ****<0.00001. N=3. (C) Using GraphPad Prism, calculating Btz IC_{50} for two JJN3 cell densities (2500 and 5000), non-linear regression was performed on day 3 post-treatment. For the 2500 cell density, IC_{50} = 19.49 nM, and for the 5000 cell density, IC_{50} = 12 nM.*

4.3.1.3 To Determine the IC_{50} Values of Bortezomib on OPM2 Cells Using a Cell Viability Assay (AlamarBlue)

Then, we investigated the IC_{50} values of Btz for OPM2. OPM2 cell densities used were (2500 cells/well and 5000 cells/well) and assessed with various concentrations of Btz 0.5, 1, 2, 2.5, 5, 10, 20, and 30 nM (Details in chapter 2, section 2.2.3).

For the 2500 cell density, day 0 was done as a baseline control to make sure the assay was set up correctly; after 3 days of treatment, OPM2 cell viability was significantly decreased compared to the vehicle using 0.5, 1, 1.5, 2, 2.5, 5, 10, 20, and 30 nM Btz concentrations. After 5 days of treatment, cell viability was significantly reduced compared to the vehicle using 1, 1.5, 2, 2.5, 5, 10, 20 and 30 nM Btz concentrations (Figure 4.4-A, i, ii, iii, C). These data were calculated using GraphPad Prism, and the Btz IC_{50} value for 2500 cell density was 18.53 nM.

For the 5000 cell density, day 0 was done as a baseline control to make sure the assay was set up correctly; after 3 days of treatment, OPM2 cell viability was significantly decreased compared to the vehicle, using 1.5, 2, 2.5, 5, 10, 20, and 30 nM Btz concentrations. After 5 days of treatment, cell viability was significantly reduced compared to the vehicle using 1, 1.5, 2, 2.5, 5, 10, 20 and 30 nM Btz concentrations (Figure 4.4-B, i, ii, iii, C). These data were calculated using GraphPad Prism, and the Btz IC_{50} value for 5000 cell density was 6.29 nM.

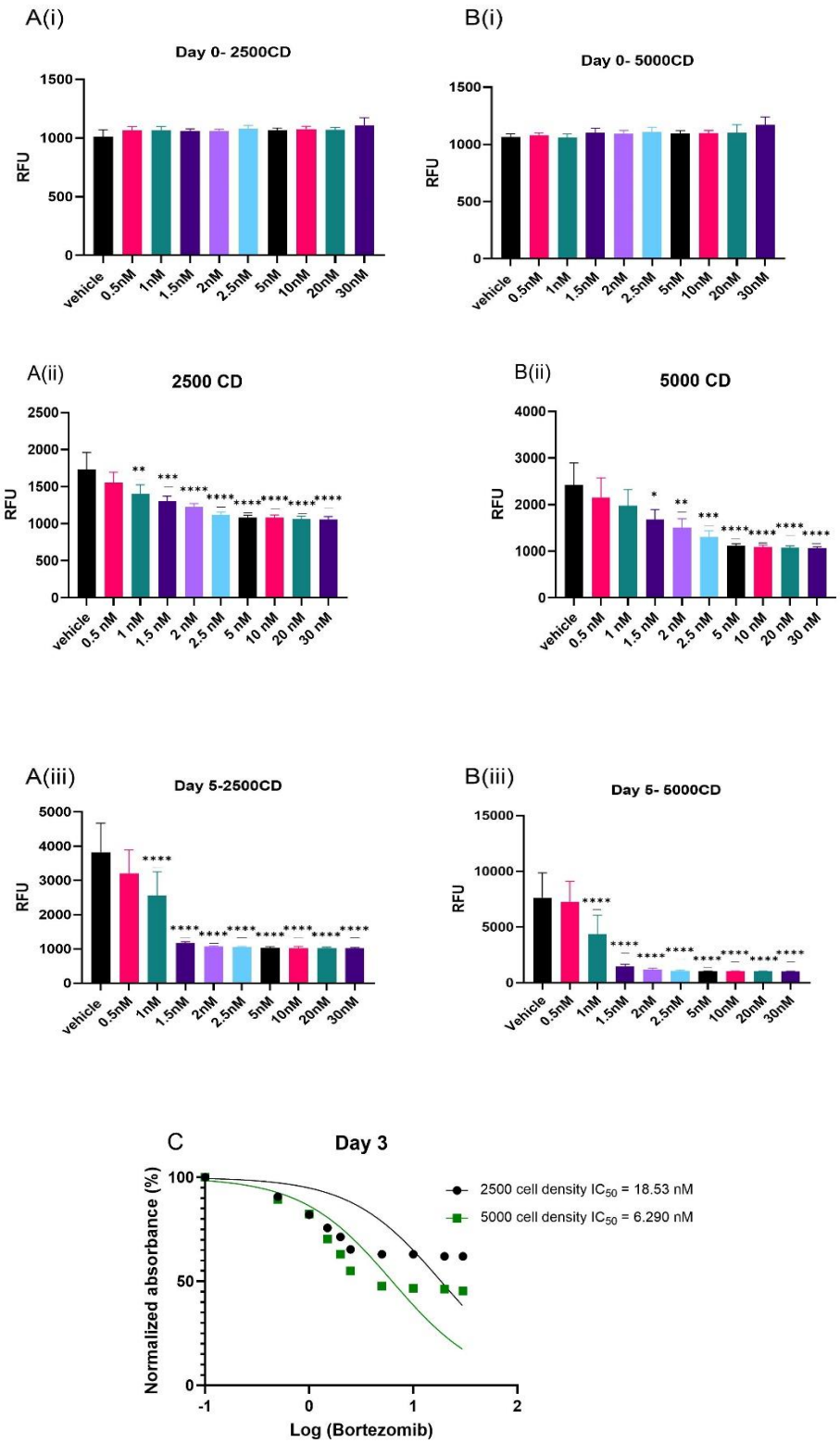

Figure 4.4: Determine the effect of Btz IC_{50} on the OPM2 cell line with two cell densities

*OPM2 cells were cultured at (A-i, ii, iii) 2500 cells/ well or (B-i, ii, iii) 5000 cells/well in 96well plates with different concentrations of Btz (0.5, 1, 1.5, 2, 2.5, 5, 10, 20, and 30 nM) or vehicle control for up to 5 days. Cell viability was assessed using an AlamarBlue® assay on days 0 (baseline), 3 and 5 on a plate reader (580 nm excitation, 610 nm emission with a cut-off at 590nm) to determine RFU. The findings were reported using one-way ANOVA, and P-values were determined compared to vehicle, where *<0.01, **<0.001, ***<0.0001, ****<0.00001. N=3. (C) Calculating Btz IC_{50} for two OPM2 cell densities (2500 and 5000), non-linear regression was performed on day 3 post-treatment. The 2500 cell density IC_{50} = 18.53 nM, and the 5000 cell density IC_{50} = 6.29 nM.*

4.3.1.4 To Determine the IC_{50} Values of Bortezomib on U266 Cells Using a Cell Viability Assay (AlamarBlue)

Subsequently, the IC_{50} values of Btz were found for two U266 cell densities (2500 cells/well and 5000 cells/well). U266 were tested with different concentrations of Btz 0, 1, 2, 2.5, 5, 10, 20, and 30 nM (Details in chapter 2, section 2.2.3).

For the 2500 cell density, day 0 was done as a baseline control to make sure the assay was set up correctly; after 3 days of treatment, U266 cell viability was significantly decreased compared to the vehicle using 1, 1.5, 2, 2.5, 5, 10, 20, and 30 nM Btz concentrations. After 5 days of treatment, cell viability was significantly reduced compared to the vehicle using 0.5, 1, 1.5, 2, 2.5, 5, 10, 20 and 30 nM Btz concentrations (Figure 4.5-A, i, ii, iii, C). These data were calculated using GraphPad Prism and the Btz IC_{50} value for 2500 cell density, which was 9.84 nM.

For the 5000 cell density, day 0 was done as a baseline control to make sure the assay was set up correctly; after 3 days of treatment, U266 cell viability was significantly decreased compared to the vehicle using 1, 1.5, 2, 2.5, 5, 10, 20, and 30 nM Btz concentrations. After 5 days of treatment, cell viability was significantly reduced compared to the vehicle using 0.5, 1, 1.5, 2, 2.5, 5, 10, 20 and 30 nM Btz concentrations (Figure 4.5-B, i, ii, iii, C). These data were calculated using GraphPad Prism, and the Btz IC_{50} value for 5000 cell density was 6.18 nM.

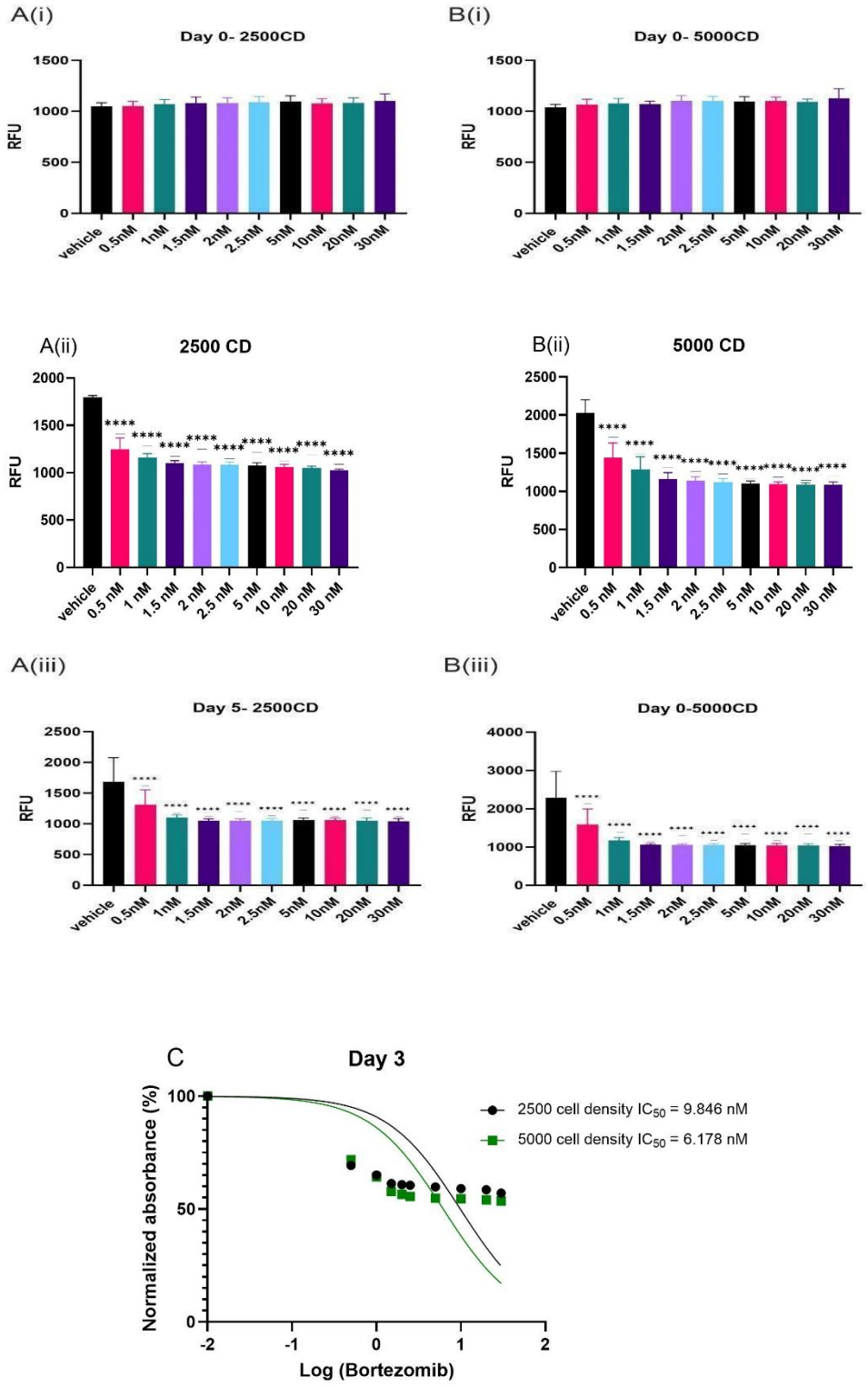

Figure 4.5: Determine the effect of Btz IC_{50} on the U266 cell line with two cell densities

*U266 cells were cultured at (A-i, ii, iii) 2500 cells/ well or (B-i, ii, iii) 5000 cells/well in 96well plates with different concentrations of Btz (0.5, 1, 1.5, 2, 2.5, 5, 10, 20, and 30 nM) or vehicle control for up to 5 days. Cell viability was assessed using an AlamarBlue® assay on days 0 (baseline), 3 and 5 on a plate reader (580 nm excitation, 610 nm emission with a cut-off at 590nm) to determine RFU. The findings were reported using one-way ANOVA, and P-values were determined compared to vehicle, where *<0.01, **<0.001, ***<0.0001, ****<0.00001. N=3. (C) Calculating Btz IC_{50} for two U266 cell densities (2500 and 5000), non-linear regression was performed on day 3 post-treatment. For the 2500 cell density, IC_{50} = 9.84 nM, and for the 5000 cell density, IC_{50} = 6.19 nM.*

4.3.2 Melphalan Titration to Determine IC_{50} Values

4.3.2.1 To Determine the IC_{50} Values of Melphalan on 5TGM1 Cells Using a Cell Viability Assay (AlamarBlue)

The next drug to determine its IC_{50} values was Mel for the 5TGM1 cell line. Two 5TGM1 cell densities (2500 cells/well and 5000 cells/well) were used and assessed with various concentrations of Mel 1, 5, 10, 20, 50, and 100 µM. (Details in chapter 2, section 2.2.3).

For the 2500 cell density, day 0 was done as a baseline control to ensure the assay was set up correctly; after 3 days of treatment, 5TGM1 cell viability significantly decreased compared to the vehicle using 5, 10, 20, 50, and 100 µM Mel concentrations. Cell viability was significantly reduced after 5 days of treatment compared to the vehicle using 1, 5, 10, 20, 50, and 100 µM Mel concentrations (Figure 4.6 -A, i, ii, iii, C). These data were calculated using GraphPad Prism, and the Mel IC_{50} value for 2500 cell density was 94.08 µM.

For the 5000 cell density, day 0 was done as a baseline control to ensure the assay was set up correctly; after 3 days of treatment, 5TGM1 cell viability was significantly decreased compared to the vehicle using 5, 10, 20, 50, and 100 µM Mel concentrations. After 5 days of treatment, cell viability was significantly reduced compared to the vehicle using 1, 5, 10, 20, 50, and 100 µM Mel concentrations (Figure 4.6-B, i, ii, iii, C). These data were calculated using GraphPad Prism, and the Mel IC_{50} value for a 5000 cell density was 12.14 µM.

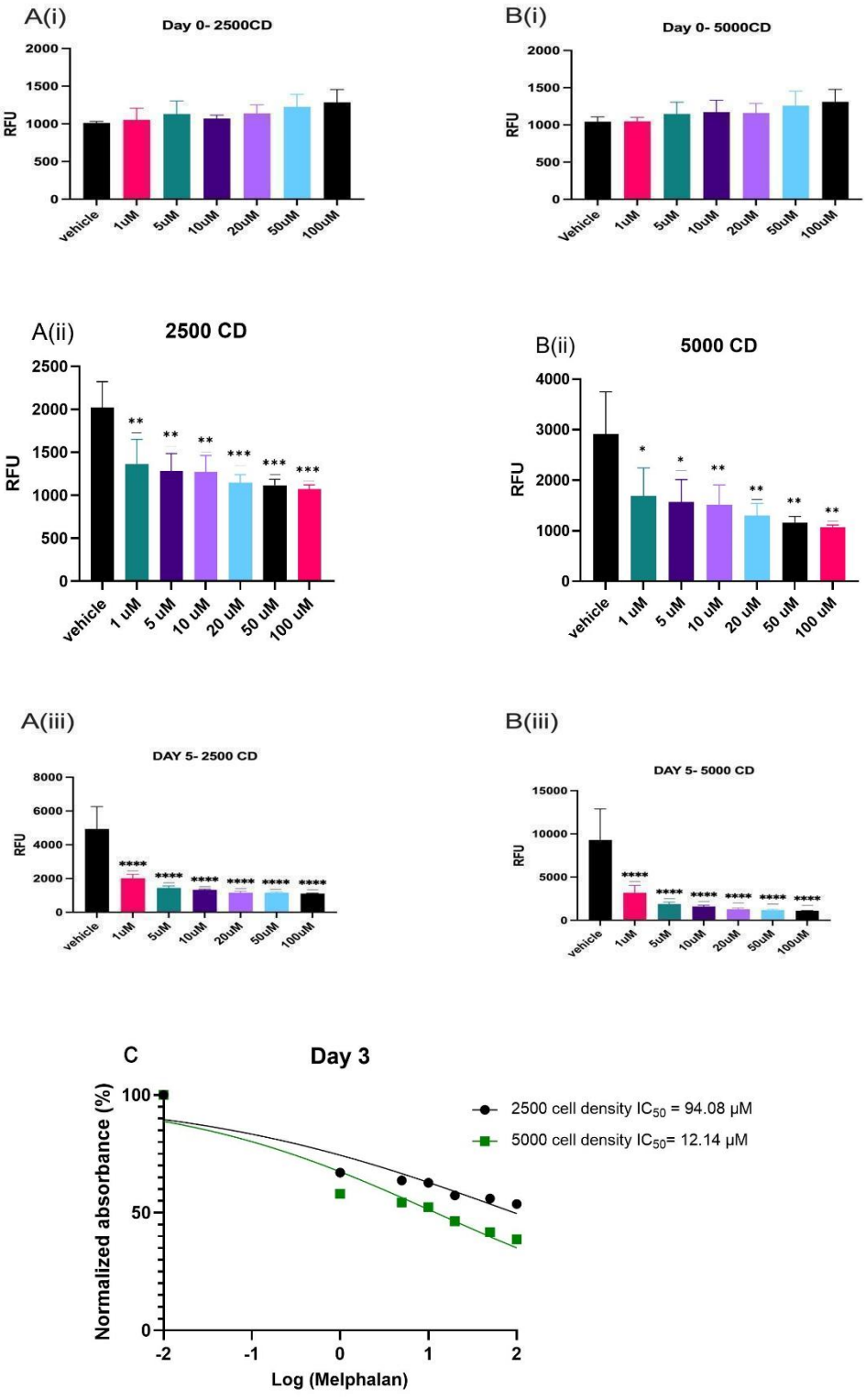

Figure 4.6. Determine the effect of Mel IC_{50} on the 5TGM1 cell line with two cell densities

*5TGM1 cells were cultured at (A-i, ii, iii) 2500 cells/ well or (B-i, ii, iii) 5000 cells/well in 96 well plates with different concentrations of Mel (1, 5, 10, 20, 50, and 100 µM) or vehicle control for up to 5 days. Cell viability was assessed using an AlamarBlue® assay on days 0 (baseline), 3 and 5 on a plate reader (580 nm excitation, 610 nm emission with a cut-off at 590nm) to determine RFU. The findings were reported using one-way ANOVA, and P-values were determined compared to vehicle, where *<0.01, **<0.001, ***<0.0001, ****<0.00001. N=3. (C) Calculating Mel IC_{50} for two 5TGM1 cell densities (2500 and 5000), non-linear regression was performed on day 3 post-treatment. For the 2500 cell density, IC_{50} = 94.08 µM, and for the 5000 cell density, IC_{50} = 12.14 µM.*

4.3.2.2 To Determine the IC_{50} Values of Melphalan on JJN3 Cells Using a Cell Viability Assay (AlamarBlue)

Consequently, IC_{50} values of Mel for two JJN3 cell densities (2500 cells/well and 5000 cells/well) were used and valued with various concentrations of Mel 1, 5, 10, 20, 50, and 100 µM (Details in chapter 2, section 2.2.3).

For the 2500 cell density, day 0 was done as a reference control to ensure the assay was set up correctly; after 3 days of treatment, JJN3 cell viability was significantly decreased compared to the vehicle using 1, 5, 10, 20, 5, and 100 µM Mel concentrations. Cell viability was significantly reduced after 5 days of treatment compared to the vehicle using 1, 5, 10, 20, 50, and 100 µM Mel concentrations (Figure 4.7-A, i, ii, iii, C). These data were calculated using GraphPad Prism, and the Mel IC_{50} value for 2500 cell density was 31.44 µM.

For the 5000 cell density, day 0 was done as a baseline control to ensure the assay was set up correctly; after 3 days of treatment, JJN3 cell viability was significantly decreased compared to the vehicle using 1, 5, 10, 20, 50, and 100 µM Mel concentrations (figure 7 -B, i, ii, iii, iv). Cell viability was significantly reduced after 5 days of treatment compared to the vehicle using 1, 5, 10, 20, 50, and 100 µM Mel concentrations (Figure 4.7-B, i, ii, iii, C). These data were calculated using GraphPad Prism, and the Mel IC_{50} value for 5000 cell density was 7.06 µM.

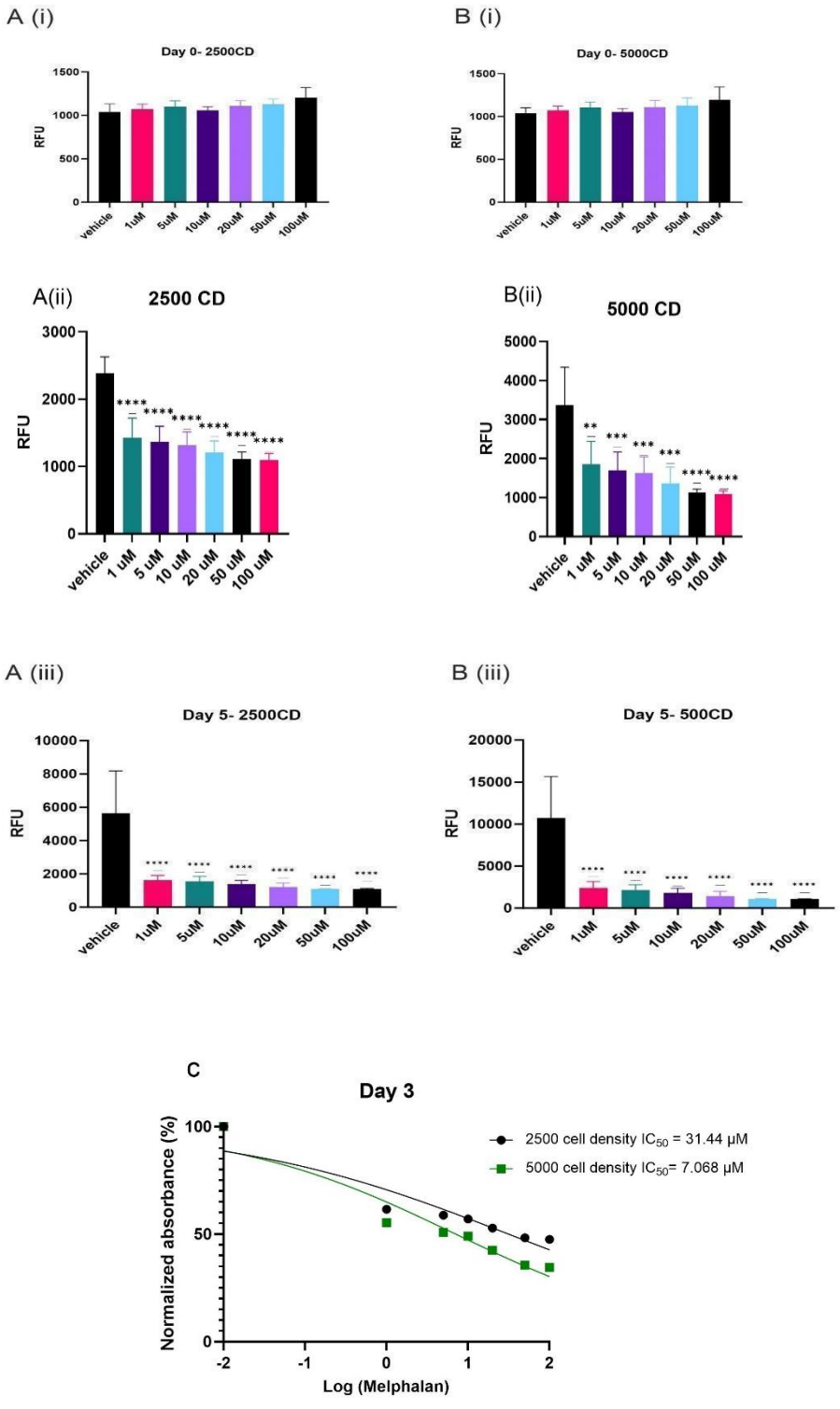

Figure 4.7: Determine the effect of Mel IC_{50} on the JJN3 cell line with two cell densities

*JJN3 cells were cultured at (A-i, ii, iii) 2500 cells/ well or (B-i, ii, iii) 5000 cells/well in 96 well-plates with different concentrations of Mel (1, 5, 10, 20, 50, and 100 µM) or vehicle control for up to 5 days. Cell viability was assessed using an AlamarBlue® assay on days 0 (baseline), 3 and 5 on a plate reader (580 nm excitation, 610 nm emission with a cut-off at 590nm) to determine RFU. The findings were reported using one-way ANOVA, and P-values were determined compared to the vehicle, where *<0.01, **<0.001, ***<0.0001, ****<0.00001. N=3. (C) Calculating Mel IC_{50} for two JJN3 cell densities (2500 and 5000), non-linear regression was performed on day 3 post-treatment. For the 2500 cell density, IC_{50} = 31.44 µM. For the 5000 cell density, IC_{50} = 7.06 µM.*

4.3.2.3 To Determine the IC_{50} Values of Melphalan on OPM2 Cells Using a Cell Viability Assay (AlamarBlue)

Next, IC_{50} values of Mel were determined for OPM2. Two OPM2 cell densities (2500 cells/well and 5000 cells/well) were used and valued with various concentrations of Mel 1, 5, 10, 20, 50, and 100 µM (Details in chapter 2, section 2.2.3).

For the 2500 cell density, day 0 was done as a baseline control to ensure the assay was set up accurately; after 3 days of treatment, OPM2 cell viability was significantly decreased compared to the vehicle using 1, 5, 10, 20, 5, and 100 µM Mel concentrations. After 5 days of treatment, cell viability was significantly reduced compared to the vehicle using 1, 5, 10, 20, 50, and 100 µM Mel concentrations (Figure 4.8-A, i, ii, iii, C). These data were calculated using GraphPad Prism, and the Mel IC_{50} value for 2500 cell density was 13.33 µM.

For the 5000 cell density, day 0 was done as a baseline control to ensure the assay was set up correctly; after 3 days of treatment, OPM2 cell viability significantly decreased compared to the vehicle using 1, 5, 10, 20, 50, and 100 µM Mel concentrations. After 5 days of treatment, cell viability was significantly reduced compared to the vehicle using 1, 5, 10, 20, 50, and 100 µM Mel concentrations (Figure 4.8-B, i, ii, iii, C). These data were calculated using GraphPad Prism, and the Mel IC_{50} value for a 5000 cell density was 6.76 µM.

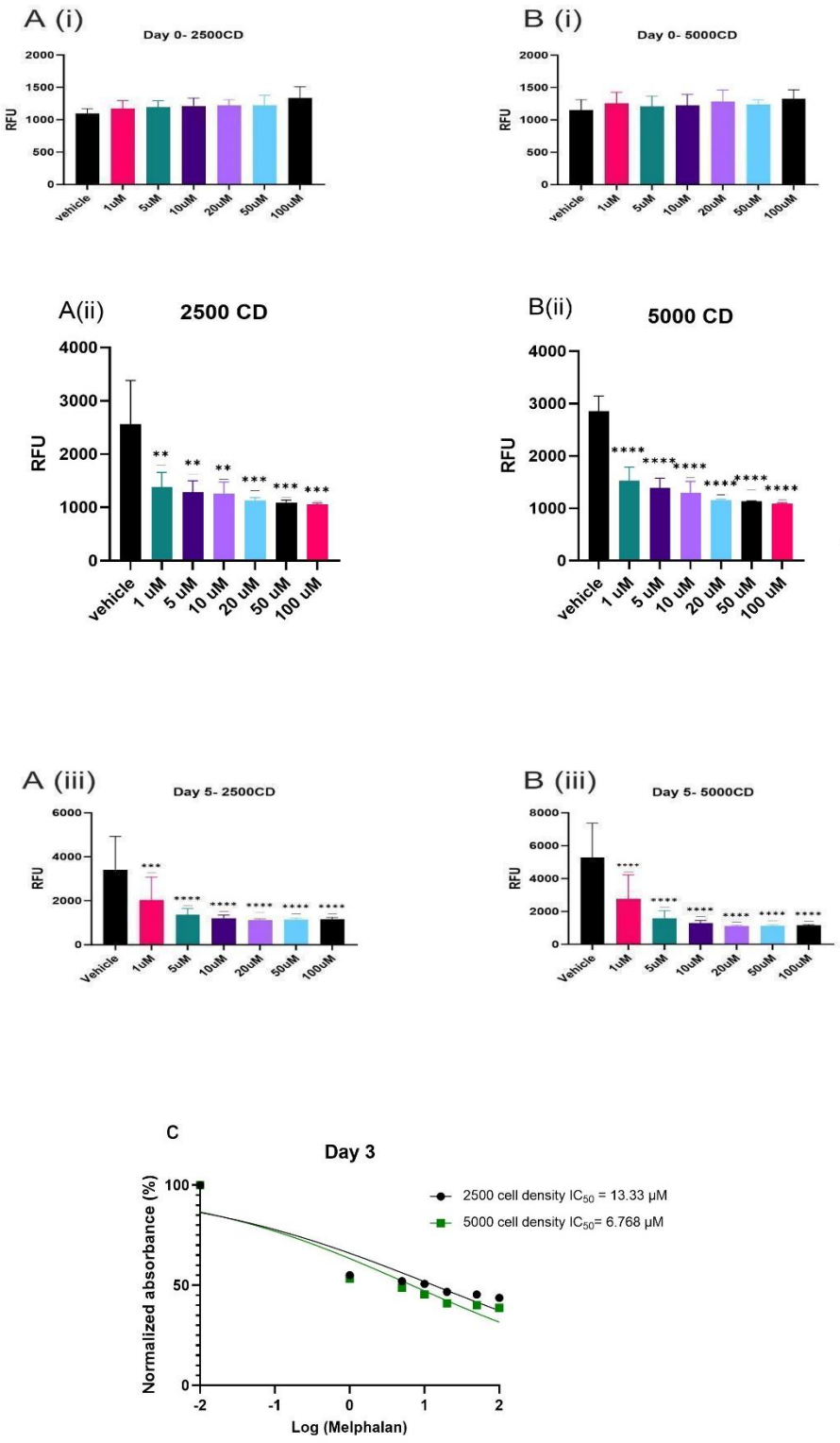

Figure 4.8: Determine the effect of Mel IC_{50} on the OPM2 cell line with two cell densities

*OPM2 cells were cultured at (A-i, ii, iii) 2500 cells/ well or (B-i, ii, iii) 5000 cells/well in 96 well-plates with different concentrations of Mel (1, 5, 10, 20, 50, and 100 µM) or vehicle control for up to 5 days. Cell viability was assessed using an AlamarBlue® assay on days 0 (baseline), 3 and 5 on a plate reader (580 nm excitation, 610nm emission with a cut-off at 590nm) to determine RFU. The findings were reported using one-way ANOVA, and P-values were determined compared to vehicle, where *<0.01, **<0.001, ***<0.0001, ****<0.00001. N=3. (C) Calculating Mel IC_{50} for two OPM2 cell densities (2500 and 5000), non-linear regression was performed on day 3 post-treatment. For the 2500 cell density, IC_{50} = 13.33 µM. For the 5000 cell density, IC_{50} = 6.76 µM.*

4.3.2.4 To Determine the IC_{50} Values of Melphalan on U266 Cells Using a Cell Viability Assay (AlamarBlue)

The IC_{50} values of Mel were initially determined so they could be used to target U266 DMCs in subsequent studies (Chapter 5). Two U266 cell densities (2500 cells/well and 5000 cells/well) were used and assessed with various concentrations of Mel 0.01, 1, 5, 10, 20, 50, and 100 µM (Details in chapter 2, section 2.2.3).

For the 2500 cell density, day 0 was done as a baseline control to ensure the assay was set up correctly; after 3 days of treatment, U266 cell viability was decreased compared to the vehicle using 1, 5, 10, 20, 5, and 100 µM Mel concentrations. After 5 days of treatment, cell viability was significantly reduced compared to the vehicle using 5, 10, 20, 50, and 100 µM Mel concentrations (Figure 4.9-A, i, ii, iii, C). These data were calculated using GraphPad Prism, and the melphalan IC_{50} value for 2500 cell density was 12.66 µM.

For the 5000 cell density, day 0 was done as a baseline control to make sure the assay was set up correctly; after 3 days of treatment, U266 cell viability was significantly decreased compared to the vehicle using 1, 5, 10, 20, 50, and 100 µM Mel concentrations. After 5 days of treatment, cell viability was significantly reduced compared to the vehicle using 5, 10, 20, 50, and 100 µM Mel concentrations (Figure 4.9-B, I, ii, iii, C). These data were calculated using GraphPad Prism, and the Mel IC_{50} value for a 5000 cell density was 12.23 µM.

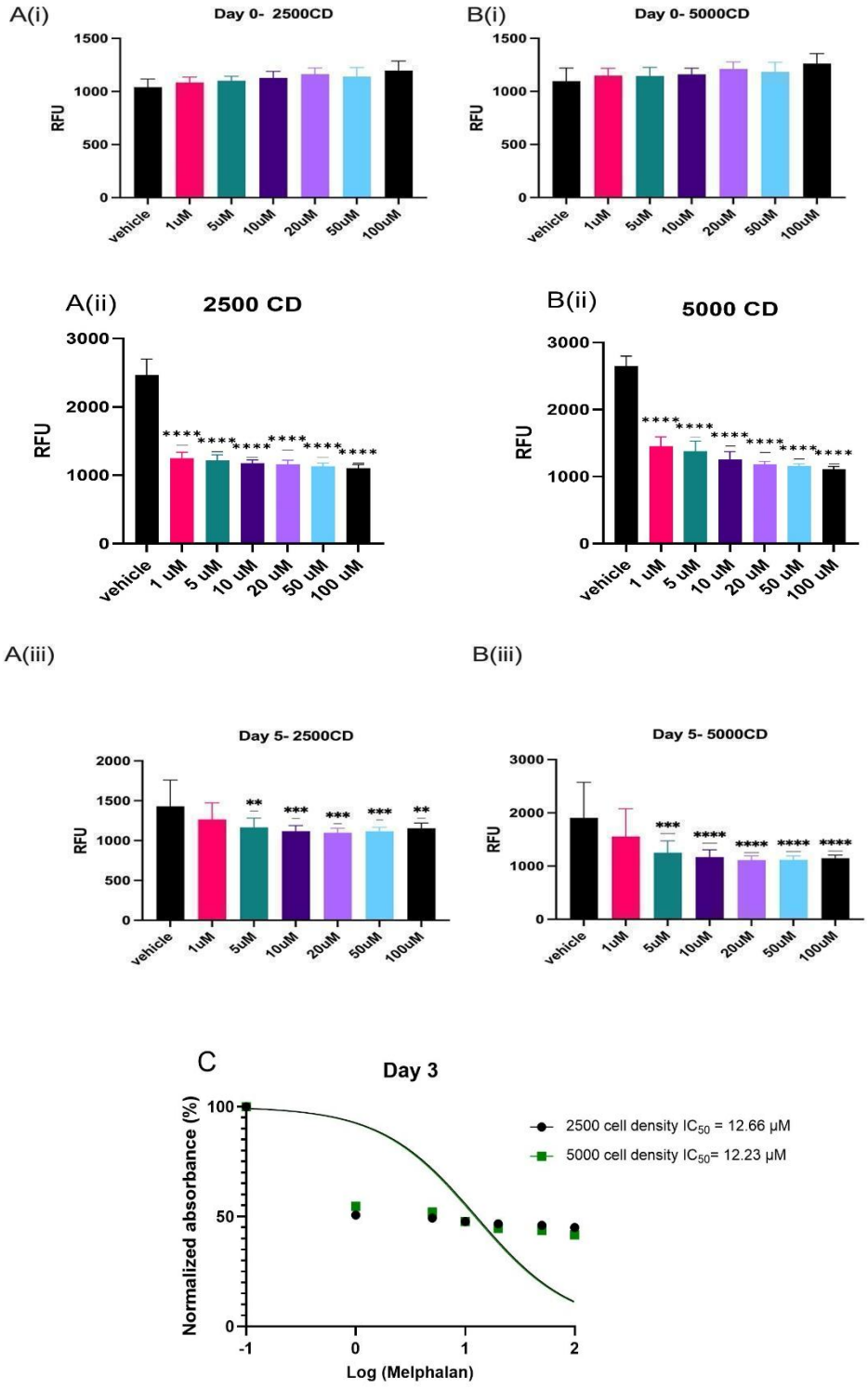

Figure 4.9: Determine the effect of Mel IC_{50} on the U266 cell line with two cell densities

*U266 cells were cultured at (A-i, ii, iii) 2500 cells/ well or (B-i, ii, iii) 5000 cells/well in 96 well-plates with different concentrations of Mel (0.01, 1, 5, 10, 20, 50, and 100 µM) or vehicle control for up to 5 days. Cell viability was assessed using an AlamarBlue® assay on days 0 (baseline), 3 and 5 on a plate reader (580 nm excitation, 610nm emission with a cut-off at 590nm) to determine RFU. The findings were reported using one-way ANOVA, and P-values were determined compared to vehicle, where *<0.01, **<0.001, ***<0.0001, ****<0.00001. N=3. (C) Calculating Mel IC_{50} for two U266 cell densities (2500 and 5000), non-linear regression was performed on day 3 post-treatment. For the 2500 cell density, IC_{50} = 12.66 µM. For the 5000 cell density, IC_{50} = 12.23 µM.*

4.3.3 Pomalidomide Titration to Determine IC_{50} Values

4.3.3.1 To Determine the IC_{50} Values of Pomalidomide on 5TGM1 Cells Using a Cell Viability Assay (AlamarBlue)

The IC_{50} values of Pom were initially determined so they could be used to target 5TGM1 DMCs in subsequent studies (Chapter 5). Two 5TGM1 cell densities (2500 cells/well and 5000 cells/well) were used and assessed with Pom 0.1, 0.01, 0.001, 1, 10, and 100 µM concentrations (Details in chapter 2, section 2.2.3).

For both the 2500 and 5000 cell densities, day 0 was done as a baseline control to ensure the assay was set up correctly; after 3 and 5 days of treatment at both densities, no significant difference was observed in 5TGM1 cell viability to compare them with the vehicle at day 3 and 5 post-treatment. (Figure 4.10-A & B, i, ii, iii, iv, v). No significant difference in cell viability compared to the vehicle, so IC_{50} values could not be determined.

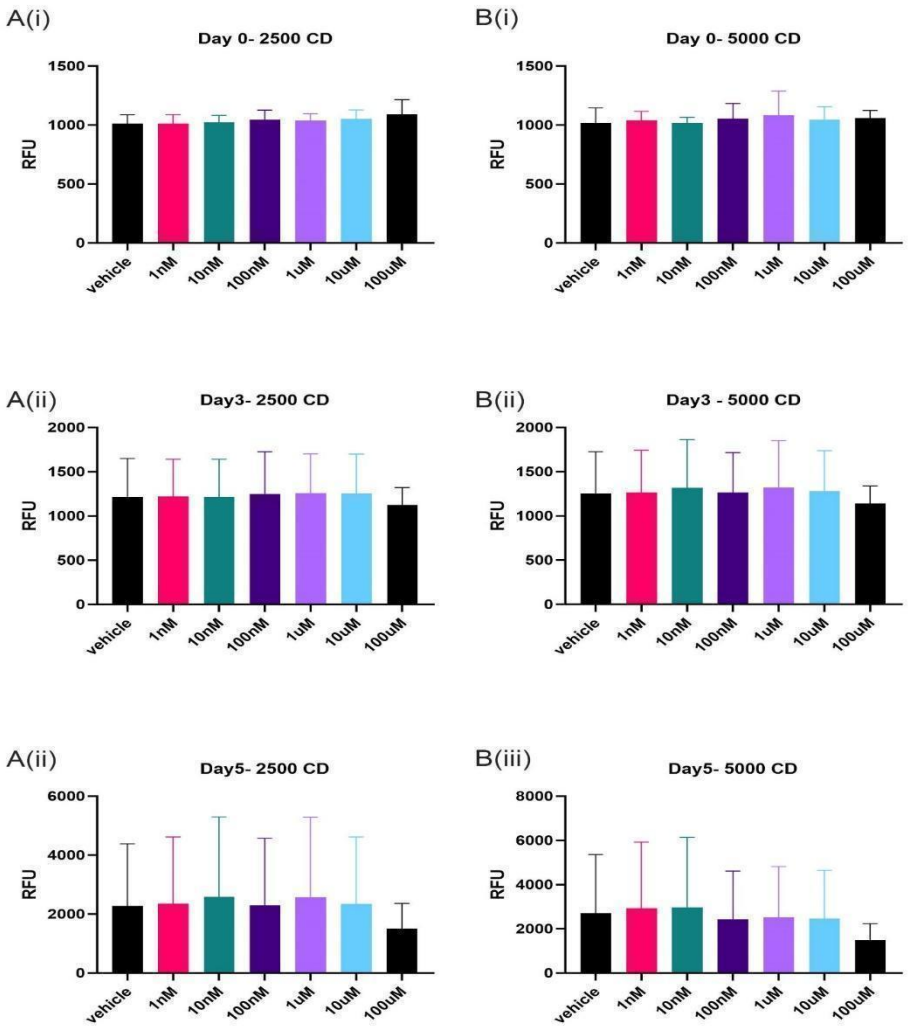

Figure 4.10: Determine the effect of Pom on the 5TGM1 cell line with two cell densities

5TGM1 cells were cultured at (A-i, ii, iii) 2500 cells/ well or (B-i, ii, iii) 5000 cells/well in 96 well-plates with different concentrations of Pom (0.1, 0.01, 0.001, 1, 10, and 100 µM) or vehicle control for up to 5 days. Cell viability was assessed using an AlamarBlue® assay on days 0 (baseline), 3 and 5 on a plate reader (580 nm excitation, 610 nm emission with a cut-off at 590nm) to determine RFU. The findings reported that no IC_{50} values can be calculated. N=3.

4.3.3.2 To Determine the IC_{50} Values of Pomalidomide on JJN3 Cells Using a Cell Viability Assay (AlamarBlue)

The IC_{50} values of Pom were initially determined so they could be used to target JJN3 DMCs in subsequent studies (Chapter 5). Two JJN3 cell densities (2500 cells/well and 5000 cells/well) were used and assessed with Pom 0.1, 0.01, 0.001, 1, 10, and 100 µM concentrations (Details in chapter 2, section 2.2.3).

For both the 2500 and 5000 cell densities, day 0 was done as a baseline control to ensure the assay was set up correctly; after 3 and 5 days of treatment at both densities, no significant difference was observed in JJN3 cell viability to compare them with the vehicle at days 3 and 5 post-treatment. (Figure 4.11-A & B, i, ii, iii, iv, v). No significant difference in cell viability compared to the vehicle, so IC_{50} values could not be determined.

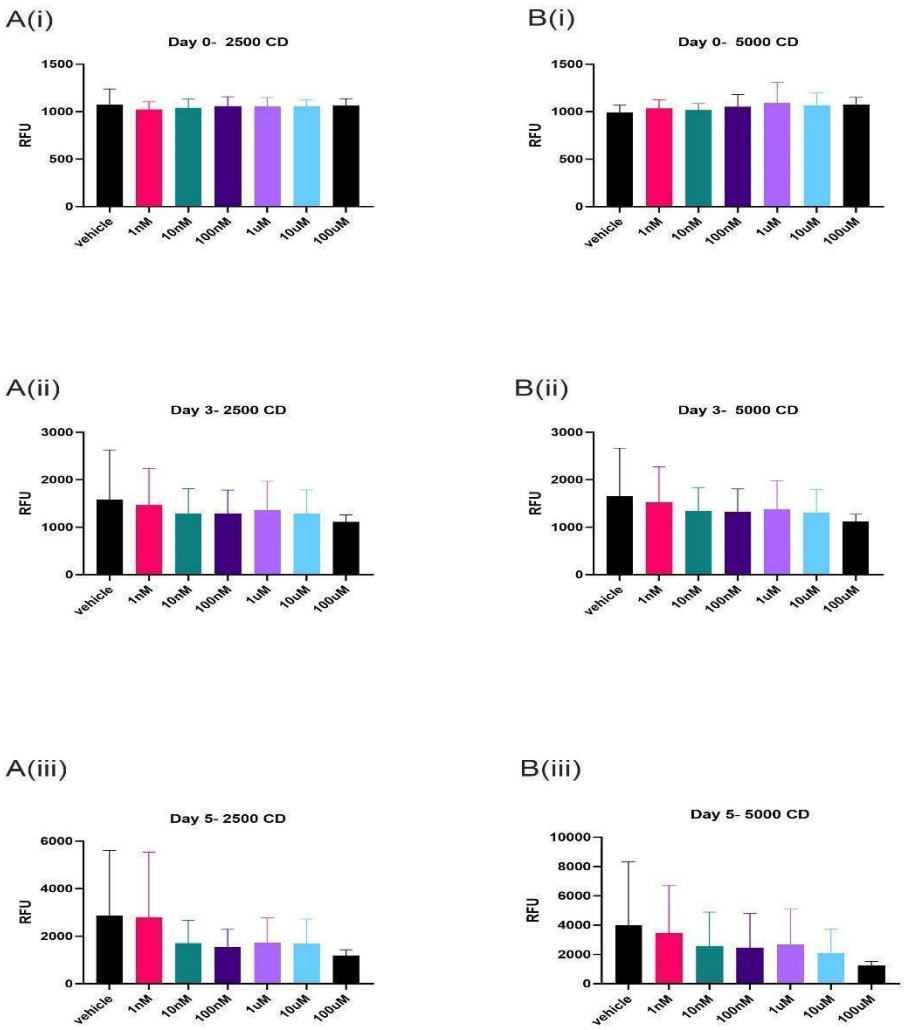

Figure 4.11: Determine the effect of Pom on the JJN3 cell line with two cell densities

JJN3 cells were cultured at (A-i, ii, iii) 2500 cells/ well or (B-i, ii, iii) 5000 cells/well in 96 well-plates with different concentrations of Pom (0.1, 0.01, 0.001, 1, 10, and 100 µM) or vehicle control for up to 5 days. Cell viability was assessed using an AlamarBlue® assay on days 0 (baseline), 3 and 5 on a plate reader (580 nm excitation, 610 nm emission with a cut-off at 590nm) to determine RFU. The findings reported that no IC_{50} values can be calculated. N=3.

4.3.3.3 To Determine the IC_{50} Values of Pomalidomide on OPM2 Cells Using a Cell Viability Assay (AlamarBlue)

The IC_{50} values of Pom were initially determined so they could be used to target OPM2 DMCs in subsequent studies (Chapter 5). Two OPM2 cell densities (2500 cells/well and 5000 cells/well) were used and assessed with different concentrations of Pom 0.1, 0.01, 0.001, 1, 10, and 100 µM (Details in chapter 2, section 2.2.3).

For the 2500 cell density, day 0 was done as a baseline control to ensure the assay was set up correctly; after 3 days of treatment, OPM2 cell viability was not significantly decreased compared to the vehicle using 100 µM Pom concentration. After 5 days of treatment, cell viability was significantly reduced compared to the vehicle using 0.1, 0.01, 0.001, 1, 10, and 100 µM Pom concentrations (Figure 4.12-A, i, ii, iii, iv, v). These data were calculated using GraphPad Prism, and Pom IC_{50} values for 2500 CD at day 5 were 0.30 µM.

For the 5000 cell density, day 0 was done as a baseline control to ensure the assay was set up correctly; after 3 days of treatment, OPM2 cell viability was decreased compared to the vehicle using 10, 100 nM and 100 µM Pom concentrations. After 5 days of treatment, cell viability was significantly reduced compared to the vehicle using 0.1, 0.01, 0.001, 1, 10, and 100 µM Pom concentrations (Figure 4.12-B, i, ii, iii). These data were calculated at day 5 post-treatment using GraphPad Prism, and the Pom IC_{50} value for a 5000 cell density was 0.06 µM.

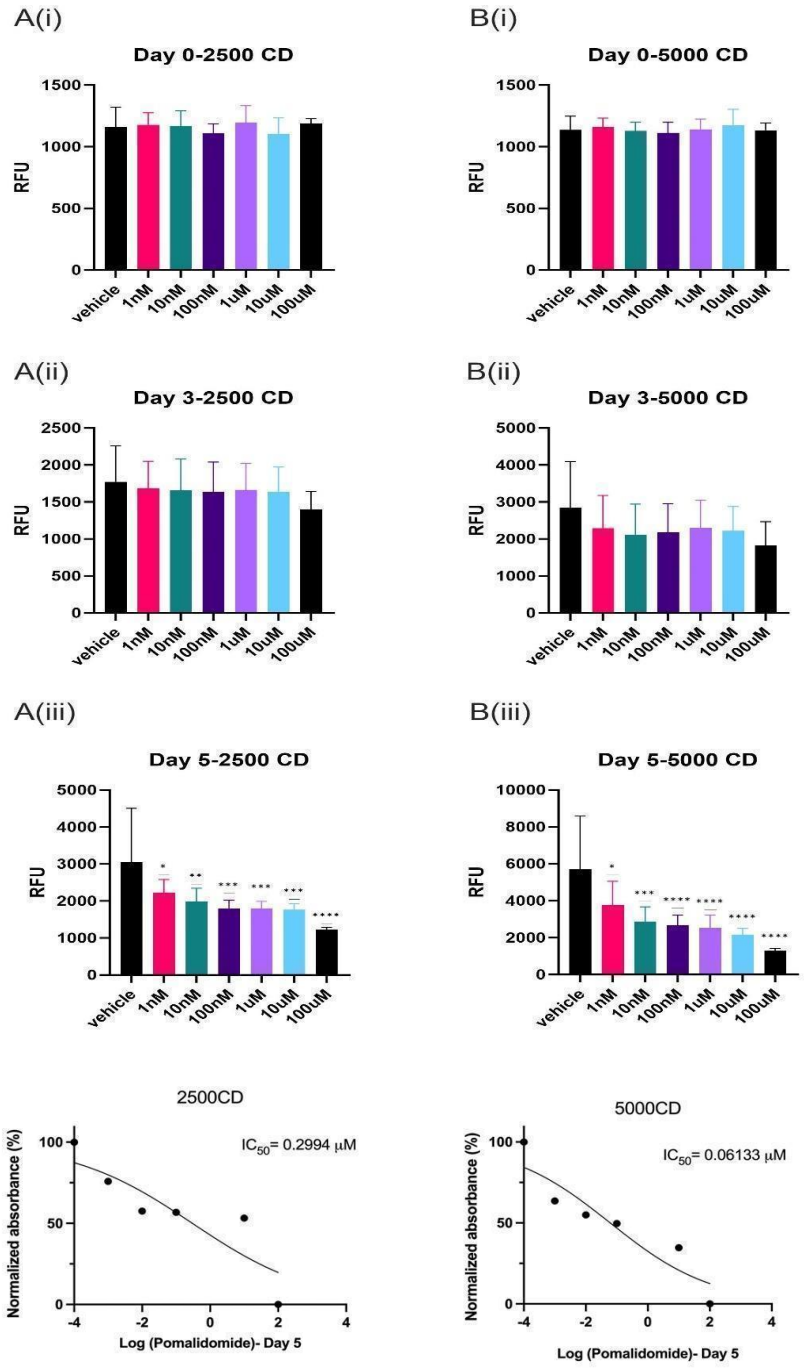

Figure 4.12: Determine the effect of Pom IC_{50} on the OPM2 cell line with two cell densities

OPM2 cells were cultured at (A-i, ii, iii) 2500 cells/ well or (B-i, ii, iii) 5000 cells/well in 96 well-plates with different concentrations of Pom (0.1, 0.01, 0.001, 1, 10, and 100 µM) or vehicle control for up to 5 days. Cell viability was assessed using an AlamarBlue® assay on days 0 (baseline), 3 and 5 on a plate reader (580 nm excitation, 610 nm emission with a cut-off at 590nm) to determine RFU. The findings were reported using one-way ANOVA, and P-

*values were determined compared to vehicle, where *<0.01, **<0.001, ***<0.0001, ****<0.00001. N=3. (A, B (iv)) Non-linear regression was performed using GraphPad Prism to calculate Pan IC_{50} for two OPM2 cell densities (2500 and 5000) at day 5. For the 2500 cell density, IC_{50} = 0.30 µM. For the 5000 cell density, IC_{50} = 0.06 µM.*

4.3.3.4 To Determine the IC_{50} Values of Pomalidomide on U266 Cells Using a Cell Viability Assay (AlamarBlue)

The IC_{50} values of Pom were initially determined so they could be used to target U266 DMCs in subsequent studies (Chapter 5). Two U266 cell densities (2500 cells/well and 5000 cells/well) were used and assessed with Pom 0.01, 0.1, 1, 10, and 100 µM concentrations (Details in chapter 2, section 2.2.3).

For both the 2500 and 5000 cell densities, day 0 was done as a baseline control to ensure the assay was set up correctly; after 3 and 5 days of treatment at both densities, no significant difference was observed in U266 cell viability to compare them with the vehicle at days 3 and 5 post-treatment. (Figure 4.13-A & B, i, ii, iii, iv, v). No significant difference in cell viability compared to the vehicle, so IC_{50} values could not be determined.

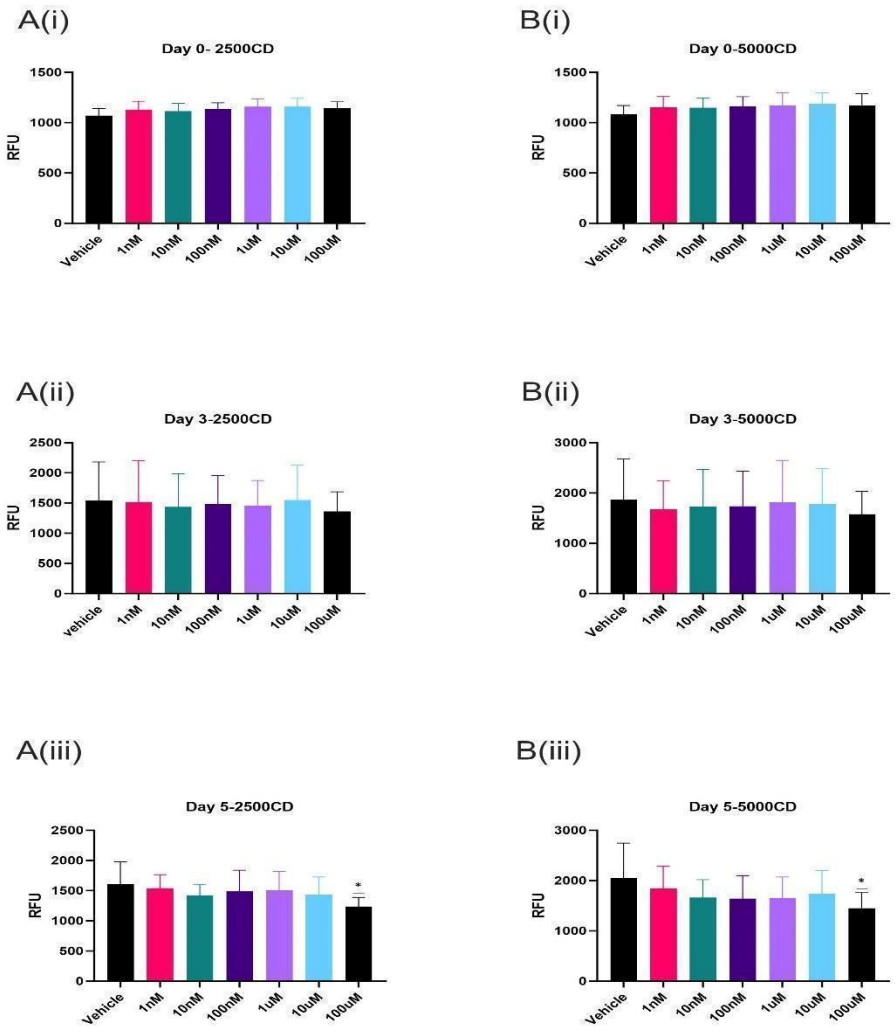

Figure 4.13: Determine the effect of Pom on the U266 cell line with two cell densities

U266 cells were cultured at (A-i, ii, iii) 2500 cells/ well or (B-i, ii, iii) 5000 cells/well in 96 well-plates with different concentrations of Pom (0.01, 0.1, 1, 10, and 100 µM) or vehicle control for up to 5 days. Cell viability was assessed using an AlamarBlue® assay on days 0 (baseline), 3 and 5 on a plate reader (580 nm excitation, 610 nm emission with a cut-off at 590nm) to determine RFU. The findings reported that no IC_{50} values can be calculated. N=3.

4.3.4 Panobinostat Titration to Determine IC_{50} Values

4.3.4.1 To Determine the IC_{50} Values of Panobinostat on 5TGM1 Cells Using a Cell Viability Assay (AlamarBlue)

The IC_{50} values of Pan were initially determined so they could be used to target DMCs in subsequent studies (Chapter 5). Two 5TGM1 cell densities (2500 cells/well and 5000 cells/well) were used and assessed with different Pan 5, 10, 15, 20, 50, and 100 nM concentrations (Details in chapter 2, section 2.2.3).

For the 2500 cell density, day 0 was done as a baseline control to ensure the assay was set up correctly; after 3 days of treatment, cell viability was significantly decreased compared to the vehicle, using 5, 10, 15, 20, 50, and 100 nM Pan concentrations. After 5 days of treatment, cell viability was significantly reduced compared to the vehicle using 5, 10, 15, 20, 50, and 100 nM Pan concentrations (Figure 4.14-A, i, ii, iii, C). These data were calculated using GraphPad Prism, and the Pan IC_{50} value for 2500 cell density was 24.33 nM.

For the 5000 cell density, day 0 was done as a baseline control to ensure the assay was set up correctly; after 3 days of treatment, cell viability was significantly decreased compared to vehicle, using 5, 10, 15, 20, 50, and 100 nM Pan concentrations. Cell viability was significantly reduced after 5 days of treatment compared to vehicle using 5, 10, 15, 20, 50, and 100 nM Pan concentrations (Figure 4.14-B, i, ii, iii, C). These data were calculated using GraphPad Prism, and the Pan IC_{50} value for a 5000 cell density was 19.13 nM.

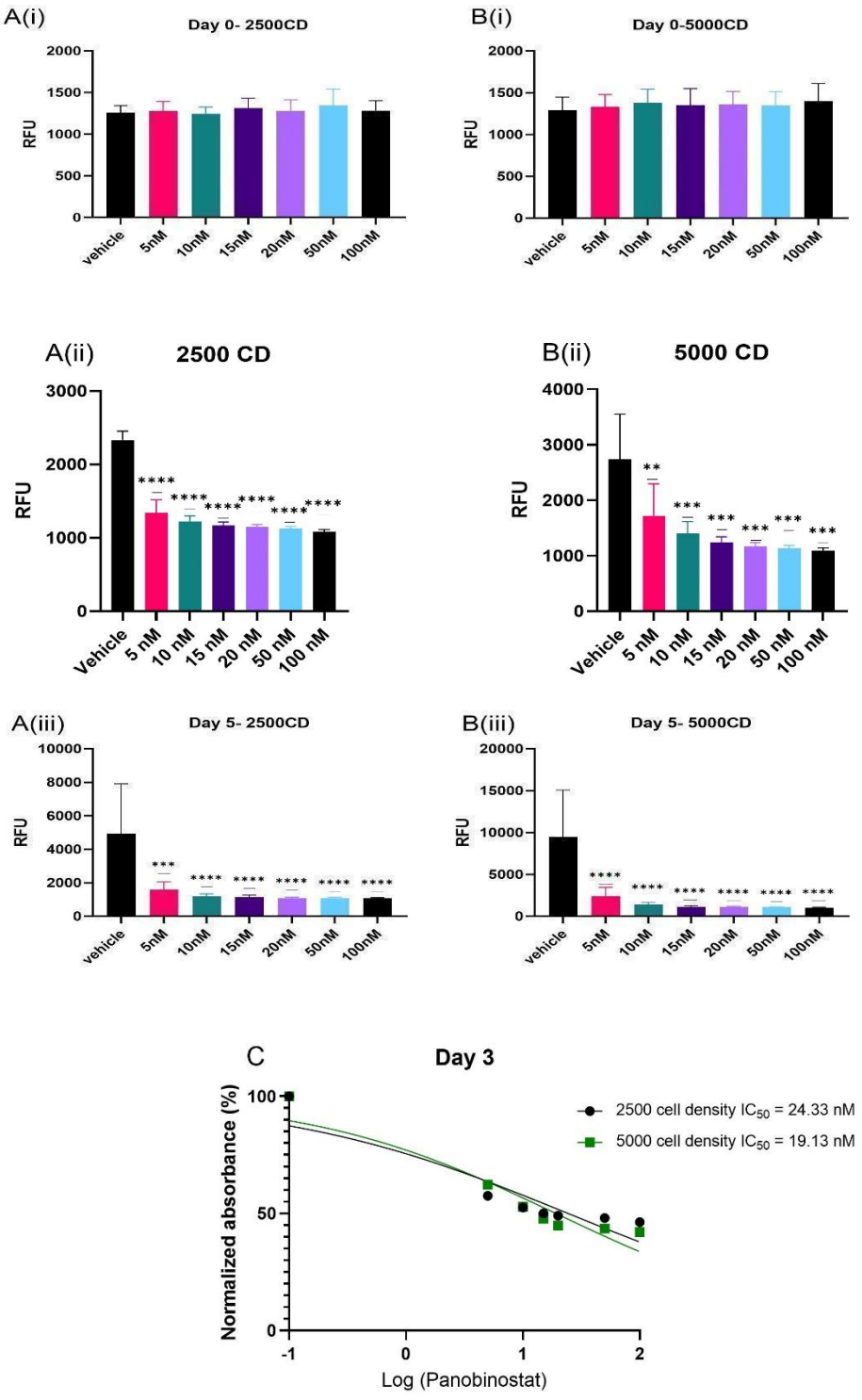

Figure 4.14: Determine the effect of Pan IC_{50} on the 5TGM1 cell line with two cell densities

5TGM1 cells were cultured at (A-i, ii, iii) 2500 cells/ well or (B-i, ii, iii) 5000 cells/well in 96 well-plates with different concentrations of Pan (5, 10, 15, 20, 50, and 100 nM) or vehicle

*control for up to 5 days. Cell viability was assessed using an AlamarBlue® assay on days 0 (baseline), 3 and 5 on a plate reader (580 nm excitation, 610 nm emission with a cut-off at 590nm) to determine RFU. The findings were reported using one-way ANOVA, and P-values were determined compared to vehicle, where *<0.01, **<0.001, ***<0.0001, ****<0.00001. N=3. (C) Non-linear regression was performed using GraphPad Prism to calculate Pan IC_{50} for two 5TGM1 cell densities (2500 and 5000). For the 2500 cell density, IC_{50} = 24.33 nM. For the 5000 cell density, IC_{50} = 19.13 nM.*

4.3.4.2 To Determine the IC_{50} Values of Panobinostat on JJN3 Cells Using a Cell Viability Assay (AlamarBlue)

Then, the IC_{50} values of Pan were initially determined so they could be used to target JJN3 DMCs in subsequent studies (Chapter 5). Two JJN3 cell densities (2500 cells/well and 5000 cells/well) were used and assessed with different concentrations of Pan 5, 10, 15, 20, 50, and 100 nM (Details in chapter 2, section 2.2.3).

For the 2500 cell density, day 0 was done as a baseline control to ensure the assay was set up correctly; after 3 days of treatment, JJN3 cell viability was significantly decreased compared to the vehicle, using 10, 15, 20, 50, and 100 nM Pan concentrations. After 5 days of treatment, cell viability was significantly reduced compared to the vehicle using 5, 10, 15, 20, 50, and 100 nM Pan concentrations (Figure 4.15-A, i, ii, iii, C). These data were calculated using GraphPad Prism, and the Pan IC_{50} value for 2500 cell density was 16.56 nM.

For the 5000 cell density, day 0 was done as a baseline control to make sure the assay was set up correctly; after 3 days of treatment, JJN3 cell viability was significantly decreased compared to the vehicle using 5, 10, 15, 20, 50, and 100 nM Pan concentrations. After 5 days of treatment, cell viability was significantly reduced compared to vehicle using 10, 15, 20, 50, and 100 nM Pan concentrations (Figure 4.15-B, i, ii, iii, C). These data were calculated using GraphPad Prism, and the Pan IC_{50} value for a 5000 cell density was 22.12 nM.

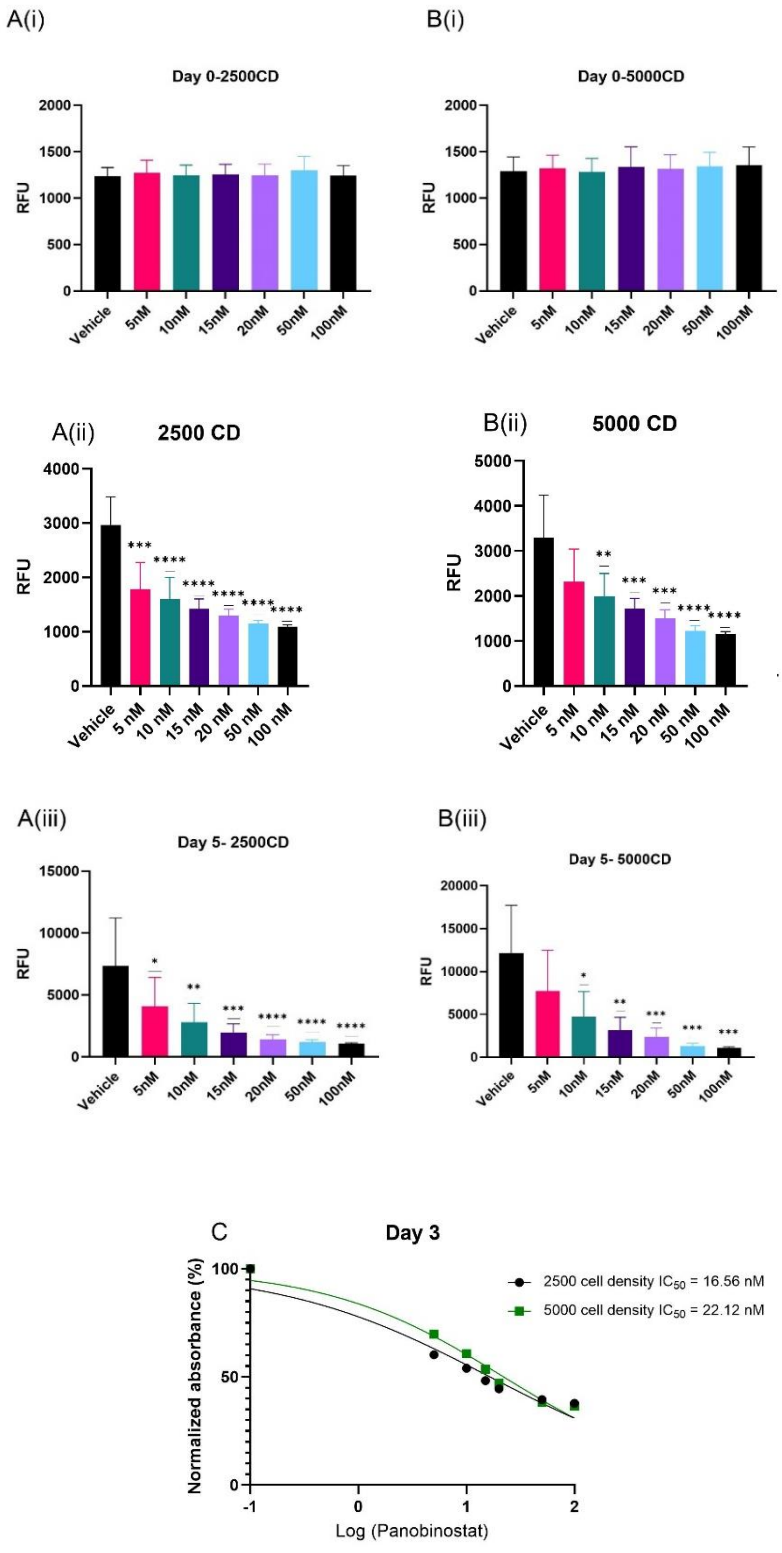

Figure 4.15: Determine the effect of Pan IC_{50} on the JJN3 cell line with two cell densities

*JJN3 cells were cultured at (A-i, ii, iii) 2500 cells/ well or (B-i, ii, iii) 5000 cells/well in 96 well-plates with different concentrations of Pan (5, 10, 15, 20, 50, and 100 nM) or vehicle control for up to 5 days. Cell viability was assessed using an AlamarBlue® assay on days 0 (baseline), 3 and 5 on a plate reader (580 nm excitation, 610 nm emission with a cut-off at 590nm) to determine RFU. The findings were reported using one-way ANOVA, and P-values were determined compared to vehicle, where *<0.01, **<0.001, ***<0.0001, ****<0.00001. N=3. (C) Non-linear regression was performed using GraphPad Prism to calculate Pan IC_{50} for two JJN3 cell densities (2500 and 5000). For the 2500 cell density, IC_{50} = 16.56 nM. For the 5000 cell density, IC_{50} = 22.12 nM.*

4.3.4.3 To Determine the IC_{50} Values of Panobinostat on OPM2 Cells Using a Cell Viability Assay (AlamarBlue)

Next, the IC_{50} values of Pan were determined on OPM2 myeloma cells. Two OPM2 cell densities (2500 cells/well and 5000 cells/well) were used and assessed with different concentrations of Pan 5, 10, 15, 20, 50, and 100 nM (Details in chapter 2, section 2.2.3).

For the 2500 cell density, day 0 was done as a baseline control to ensure the assay was set up correctly; after 3 days of treatment, OPM2 cell viability significantly decreased compared to the vehicle, using 20, 50, and 100 nM Pan concentrations. After 5 days of treatment, cell viability was significantly reduced compared to vehicle using 10, 15, 20, 50, and 100 nM Pan concentrations (Figure 4.16-A, i, ii, iii, C). These data were calculated using GraphPad Prism, and the Pan IC_{50} value for 2500 cell density was 26.69 nM.

For the 5000 cell density, day 0 was done as a baseline control to ensure the assay was set up correctly; after 3 days of treatment, OPM2 cell viability was significantly decreased compared to the vehicle using 15, 20, 50, and 100 nM Pan concentrations. After 5 days of treatment, cell viability was significantly reduced compared to vehicle using 10, 15, 20, 50, and 100 nM Pan concentrations (Figure 4.16-B, i, ii, iii, C). These data were calculated using GraphPad Prism, and the Pan IC_{50} value for a 5000 cell density was 26.64 nM.

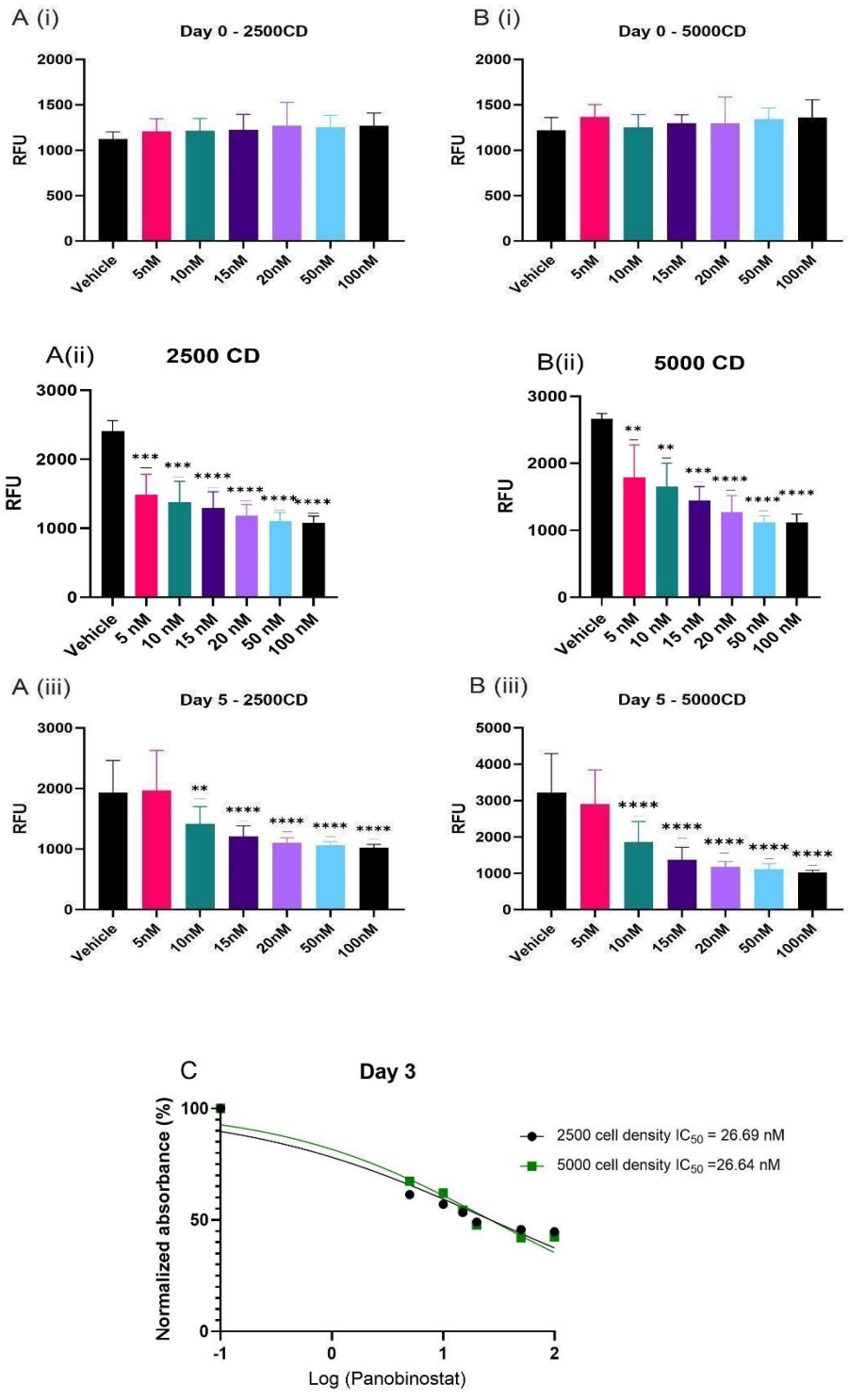

Figure 4.16: Determine the effect of Pan IC_{50} on the OPM2 cell line with two cell densities

OPM2 cells were cultured at (A-i, ii, iii) 2500 cells/ well or (B-i, ii, iii) 5000 cells/well in 96 well-plates with different concentrations of Pan (5, 10, 15, 20, 50, and 100 nM) or vehicle

*control for up to 5 days. Cell viability was assessed using an AlamarBlue® assay on days 0 (baseline), 3 and 5 on a plate reader (580 nm excitation, 610 nm emission with a cut-off at 590nm) to determine RFU. The findings were reported using one-way ANOVA, and P-values were determined compared to vehicle, where *<0.01, **<0.001, ***<0.0001, ****<0.00001. N=3. (C) Non-linear regression was performed using GraphPad Prism to calculate Pan IC_{50} for two OPM2 cell densities (2500 and 5000). For the 2500 cell density, IC_{50} = 26.69 nM. For the 5000 cell density, IC_{50} = 26.64 nM.*

4.3.4.4 To Determine the IC_{50} Values of Panobinostat on U266 Cells Using a Cell Viability Assay (AlamarBlue)

The last investigation was the IC_{50} values of Pan for two U266 cell densities (2500 cells/well and 5000 cells/well), which were used and assessed with different concentrations of Pan 5, 10, 15, 20, 50, and 100 nM (Details in chapter 2, section 2.2.3).

For the 2500 cell density, day 0 was done as a baseline control to ensure the assay was set up correctly; after 3 days of treatment, U266 cell viability was significantly decreased compared to the vehicle, using 10, 20, 50, and 100 nM Pan concentrations. After 5 days of treatment, cell viability was significantly reduced compared to the vehicle using 5, 10, 15, 20, 50, and 100 nM Pan concentrations (Figure 4.17-A, i, ii, iii, C). These data were calculated using GraphPad Prism, and the Pan IC_{50} value for 2500 cell density was 16.69 nM.

For the 5000 cell density, day 0 was done as a baseline control to ensure the assay was set up correctly; after 3 days of treatment, U266 cell viability significantly decreased compared to the vehicle, using 10, 15, 20, 50, and 100 nM Pan concentrations. Cell viability was significantly reduced after 5 days of treatment compared to vehicle using 5, 10, 15, 20, 50, and 100 nM Pan concentrations (Figure 4.17-B, i, ii, iii, C). These data were calculated using GraphPad Prism, and the Pan IC_{50} value for a 5000 cell density was 15.67 nM.

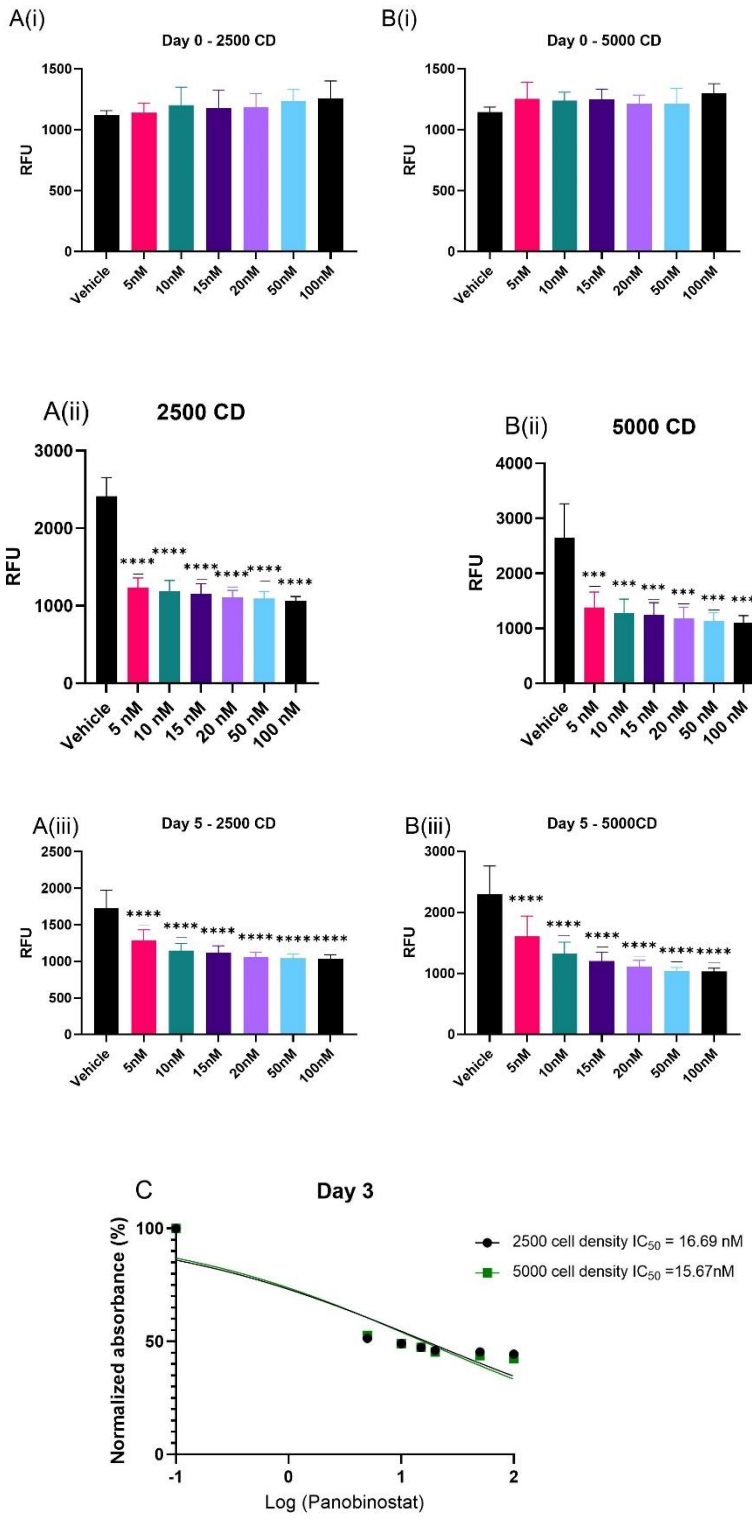

Figure 4.17: Determine the effect of Pan IC_{50} on the U266 cell line with two cell densities

*U266 cells were cultured at (A-I, ii, iii) 2500 cells/ well or (B-i, ii, iii) 5000 cells/well in 96 well-plates with different concentrations of Pan (5, 10, 15, 20, 50, and 100 nM) or vehicle control for up to 5 days. Cell viability was assessed using an AlamarBlue® assay on days 0 (baseline), 3 and 5 on a plate reader (580nm excitation, 610 nm emission with a cut-off at 590nm) to determine RFU. The findings were reported using one-way ANOVA, and P-values were determined compared to vehicle, where *<0.01, **<0.001, ***<0.0001, ****<0.00001. N=3. (C). Calculating Pan IC_{50} for two U266 cell densities (2500 and 5000), non-linear regression was performed using GraphPad Prism. For the 2500 cell density, IC_{50} = 16.69 nM. For the 5000 cell density, IC_{50} = 15.67 nM.*

Table 4.1: Determining the IC_{50} values (Btz, Mel, Pan, and Pom) with MM cell lines using two cell densities

Drugs **Cell line**	**Bortezomib (nM)**		**Melphalan (µM)**		**Pomalidomide (µM)**		**Panobinostat (nM)**	
Cell density	2500	5000	2500	5000	2500	5000	2500	5000
5TGM1	40.25	3.08	94.08	12.14	ND*	ND*	24.33	19.13
JJN3	19.49	12.00	31.44	7.06	ND*	ND*	16.56	22.12
OPM2	18.53	6.29	13.33	6.76	0.37	0.02	26.69	26.64
U266	9.84	6.18	12.66	12.23	ND*	ND*	16.69	15.67

*ND = Not Determined

4.3.5 Targeting DMCs by Single and Combined Drug Treatments

4.3.5.1 Pilot Study to Target Unsorted OPM2 DMCs at Days 17 and 21

Once the IC_{50} values for each drug were determined, we next assessed single and combined treatments to investigate their effect on DMCs. This pilot study aimed to identify the optimal day to target DMCs and determine whether assessing unsorted DMCs was viable. Therefore, OPM2 $GFP^{+}DID^{+}$ cells were cultured for up to 21 days, and then 96 well-plates were seeded with 5000 cells/well. On day 17, cells were treated with drug IC_{50} values previously determined in (Table 4.1), using single Btz or Mel or combined Btz with Mel. Cells were assessed by flow cytometry after 3 days of treatment. The same experiment was repeated with the whole cell population after 21 days of culture. Each assay was repeated once.

OPM2 DID^{high} cells showed no significant difference between the vehicle compared to single doses of Btz or Mel on day 17. And no significant difference between single doses compared to combined drugs (Figure 4.18-Ai). OPM2 DID^{low} cell numbers were significantly decreased with single treatments of Btz or Mel when compared to the vehicle, and a significant reduction was observed between single Btz treatment and combined Btz and Mel (Figure 4.18-Aii). Comparing the vehicle and a single treatments, OPM2 $DID^{negative}$ cells exhibited a significant reduction in cell numbers at single treatments compared to vehicle. There was no significant difference when comparing combined treatment to single doses (Figure 4.18-Aiii).

OPM2 DID^{high} cells showed no difference between the vehicle compared to single or combined doses of Btz and Mel on day 21 (Figure 4.18-Bi). OPM2 DID^{low} cell numbers showed no significant difference with single treatments Btz or Mel when compared to the vehicle, and no significant reduction was observed between single Btz or Mel treatment and combined Btz and Mel (Figure 4.18-Bii). Comparing the vehicle and single treatments, OPM2 $DID^{negative}$ cells exhibited a significant decrease in cell numbers when comparing vehicle to single treatments. While there is no significant difference when comparing combined treatment to single doses (Figure 4.18-Biii).

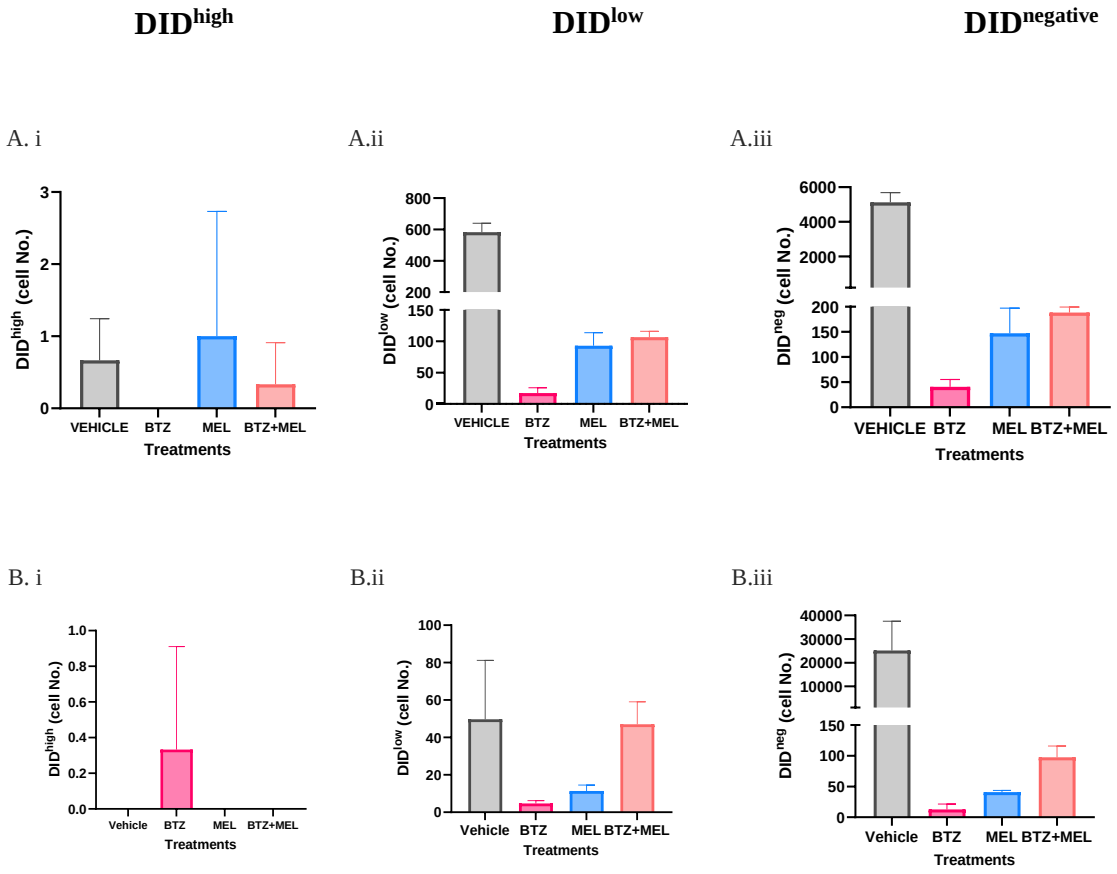

Figure 4.18: Pilot study: Unsorted OPM2 DID labelled cells treated with single and combined Btz or Mel after 17 and 21 days of in vitro culture

A) Bar charts showing unsorted OPM2 GFP$^+$ DID^{high} (potential DMCs) cells, OPM2 GFP$^+$ DID^{low} (slow proliferating) cells, and OPM2 GFP$^+$ DID^{negtive} (proliferating) cells treated with single drugs (Btz or Mel) and combined (Btz, Mel), assessed after 17 days of culture. B) Bar charts showing unsorted OPM2 GFP$^+$ DID^{high} (potential DMCs) cells, OPM2 GFP$^+$ DID^{low} (slow proliferating) cells, and OPM2 GFP$^+$ DID^{negtive} (proliferating) cells treated with single drugs (Btz or Mel) and combined (Btz, Mel), assessed after 21 days of culture. N=1.

4.3.5.2 Targeting Sorted OPM2 DMCs

In the previous study, DMCs could not be affected by drugs at days 17 or 21 due to the small number of DID^{high} cells in the whole population; concerning our results in previous chapter 3, most of the cells proliferated and lost their DID labelling over time. Cells inherit the DID labelling to their daughter cells, but the dye gets diluted through proliferation in the meantime. Thus, we decided to sort and isolate DID^{high}-labelled cells and then treat them with single and combined drugs. In chapter 3, we suggested treating DMCs on days 7 or 10 of the culture as it showed that these days had the highest number of DID^{high} cells, regarding cell culture behaviour

and before we lose the DID^{high} labelling. Thus, OPM2 DID^{high} cells were isolated using a FACS Melody cell sorter. The isolated cells were seeded in a 96-well plate, 5000 cells/well, then treated with a single or combination of drugs before being assessed by flow cytometry analysis. The flow cytometry was performed 3 days after treatment to determine the effectiveness of the drugs on the cells. Each assay was repeated three times.

OPM2 DID^{high} sorted cells treated with single or combined drugs after DMCs isolation on day 10 of culture showed that the single drugs (Btz or Mel) demonstrated a significant reduction compared to the vehicle, and when comparing single drugs, the graph shows a significant reduction between (Btz and Mel), while the combination treatment with (Btz and Mel) showed a significant decrease compared to single Btz, and while no significant effect showed when compared to Mel (Figure 4.19-A.i).

Then, OPM2 DID^{high} cells treated with single or combined drugs after DMCs isolation on day 10 of culture showed that the single drugs (Btz or Pan) demonstrated a significant reduction compared to the vehicle, and when comparing single drugs, the graph shows a significant reduction between (Btz and Pan), while the combination treatment with (Btz and Pan) showed a significant decrease compared to single Btz, and while no significant effect showed when compared to Pan (Figure 4.19-A.ii).

Then, OPM2 DID^{high} cells treated with single or combined drugs after DMCs isolation on day 10 of culture showed that the single drugs (Mel or Pan) demonstrated a significant reduction compared to the vehicle, and when comparing single drugs, the graph shows a significant reduction between (Mel and Pan), while the combination treatment with (Mel and Pan) showed a significant decrease compared to single Mel, and while no significant effect showed when compared to Pan (Figure 4.19-A.iii).

The results of treating slow proliferating cells OPM2 DID^{low} with single and combined drugs showed a significant reduction in comparison to the vehicle (Figure 4.19 B.i, ii, iii). While comparing combined treatment with single drugs, it was observed that there was a decrease, but this was not significant (Figure 4.19-B.i, ii, iii).

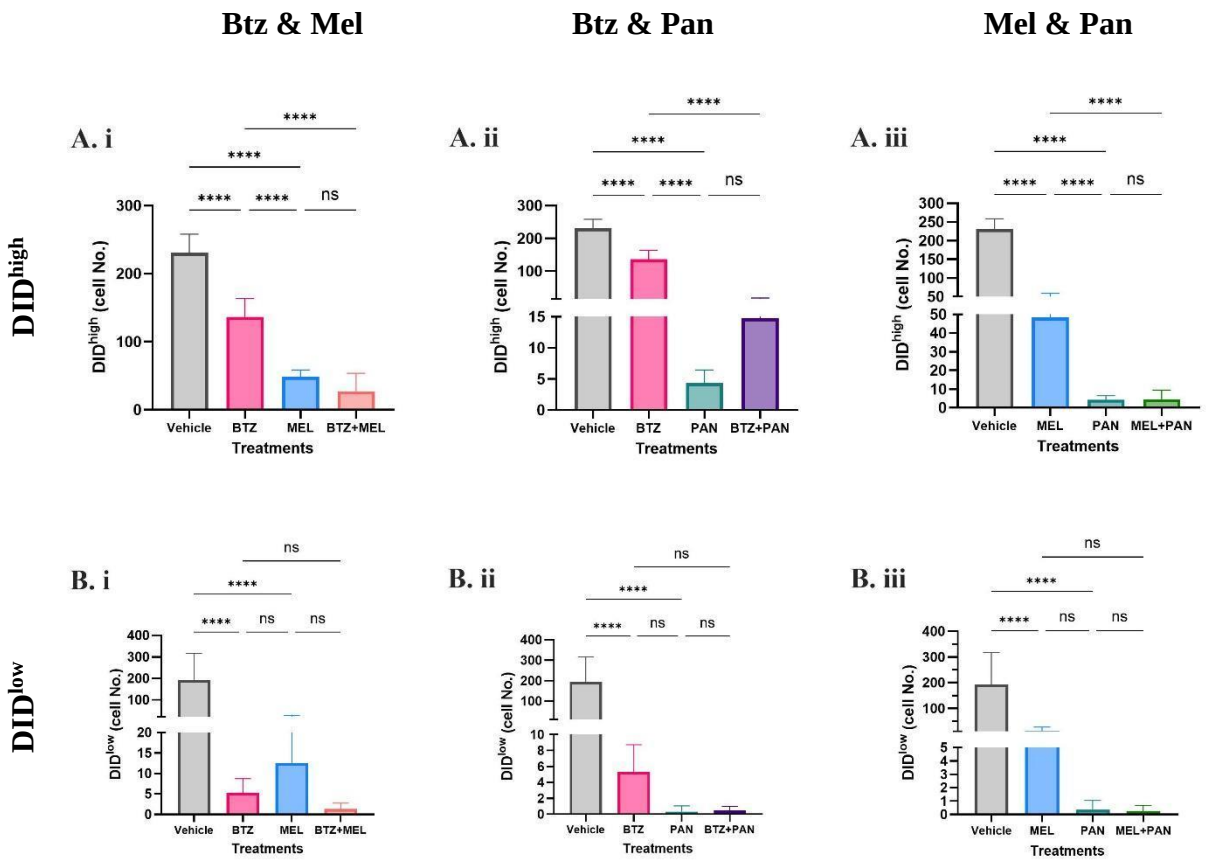

Figure 4.19: Assessment of sorted OPM2 DID^{high} cells treated on day 10 with single and combined drugs in vitro

A) Bar charts showing all isolated and treated on day 10 OPM2 GFP^{+} DID^{high} (potential DMCs) cells treated with single drugs (Btz, Mel, and Pan) and combined (Btz, Mel)— (Btz, Pan)— (Mel, Pan). B) Bar charts showing all sorted OPM2 GFP^{+} DID^{low} (slow proliferating) cells treated with single drugs (Btz, Mel, and Pan) and combined (Btz, Mel)— (Btz, Pan)— (Mel, Pan). Flow cytometry assessment on day 3 post-treatment. Statistical analysis used ordinary one-way ANOVA, N=3.

4.3.5.3 Targeting Sorted JJN3 DMCs

Next, we sorted and isolated JJN3-DID^{high} labelled cells and then treated them with single and combined drugs. On day 7 of the culture, JJN3 DID^{high} cells were isolated using the FACS Melody cell sorter. The isolated cells were seeded in a 96-well plate of 5000 cells/well, then treated with a single and a combination of drugs before being assessed by flow cytometry analysis. The flow cytometry analysis was performed three days after treatment to determine the effectiveness of the drugs on the cells. Each assay was repeated three times.

Firstly, JJN3 DID^{high} treated with single or combined drugs after DMCs isolation on day 7 of culture showed that the single drugs Btz, Mel, or Pan demonstrated a significant reduction compared to the vehicle, and when comparing single drugs, the graph shows no significant reduction between single drugs. The combination of (Btz and Mel) and (Mel and Pan) showed no significant effect compared to single Btz, Mel or Pan (Figure 4.20-A. i, A.iii). A significant reduction was illustrated in (Btz and Pan) combined in comparison to Btz (Figure 4.20 A.ii).

The results of treating slow-proliferating cells, JJN3 DID^{low,} with single drugs showed a significant reduction in comparison to the vehicle (Figure 4.20- B.i, ii, iii). When combined treatment with single drugs was compared, a decrease was observed, but no significant effect was noticed. (Figure 4.20- B.i, ii, iii).

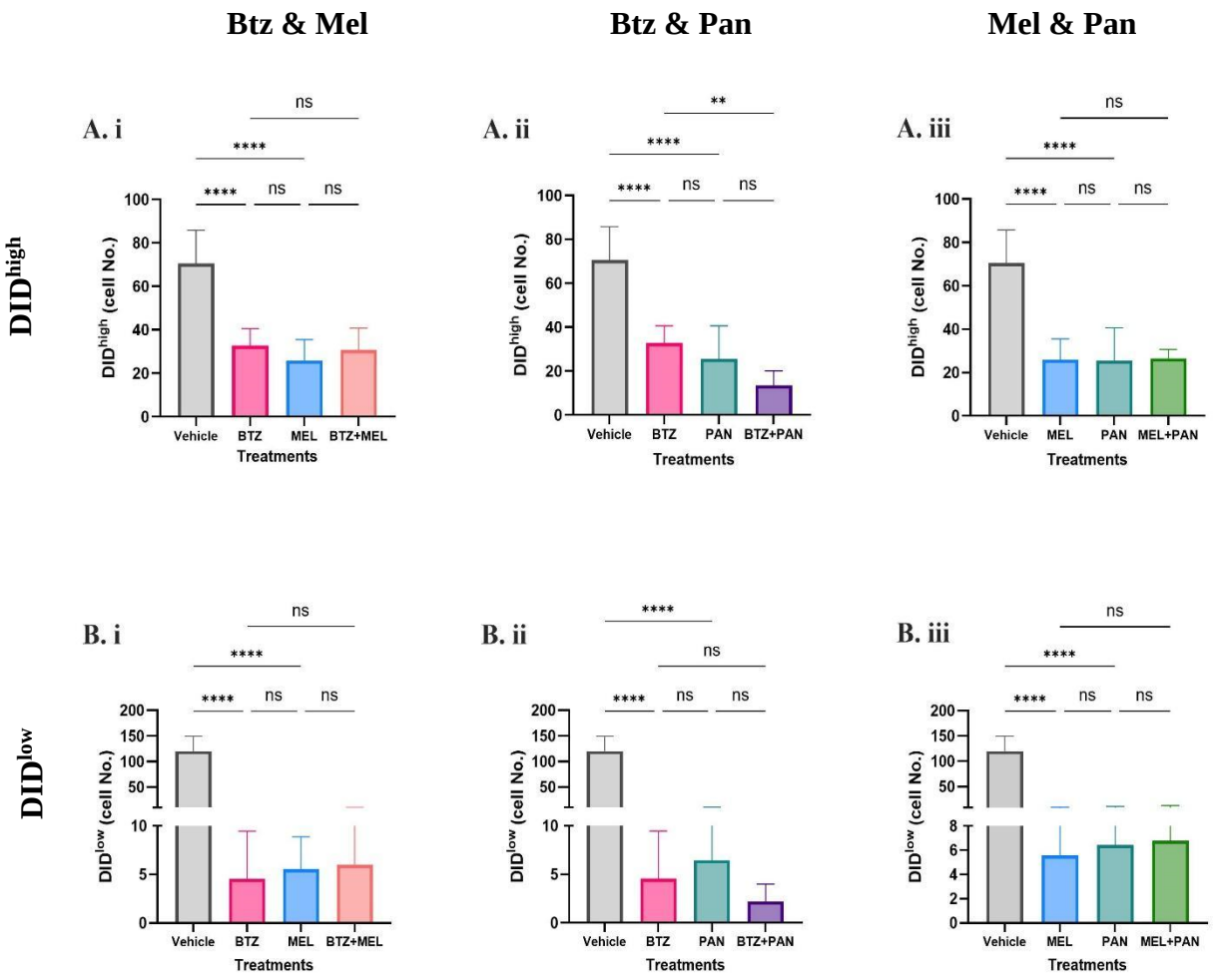

Figure 4.20: Representative graphs for flow cytometry results to study sorted JJN3 DID^{high} cells treated with single and combined drugs in vitro

A) Bar charts showing all isolated JJN3 GFP^{+} DID^{high} (potential DMCs) cells treated with single drugs (Btz, Mel, and Pan) and combined (Btz, Mel)— (Btz, Pan)— (Mel, Pan). B) Bar charts showing all sorted JJN3 GFP^{+} DID^{low} (slow proliferating) cells treated with single drugs (Btz, Mel, and Pan) and combined (Btz, Mel)— (Btz, Pan)— (Mel, Pan). Statistical analysis used ordinary one-way ANOVA, N=3.

4.4 Discussion

In this chapter, we aimed to determine the IC_{50} values of four SoC drugs, Btz, Mel, Pom, and Pan and assess their subsequent effects on DMCs *in vitro* when used alone and in combination.

A broad range of drug concentrations is crucial in determining drug IC_{50} values, as it provides an understanding of a drug's effect on MM cell lines. Dose-response curves facilitate the identification of the optimal therapeutic dose regarding myeloma cells' sensitivity to the drug. Different genetic variability may affect cell response to the drug, which could make it more resistant or sensitive (Tessoulin et al., 2017). Furthermore, to effectively identify threshold effects, account for individual differences, and maintain statistical reliability, a comprehensive range of concentrations is indispensable. By carefully considering the breadth of exposure levels, we can gain a more nuanced understanding of the relationship between the variable of interest and its outcomes. Therefore, IC_{50} value investigations are fundamental to developing effective and safe treatments in drug research. Thus, based on previous literature and personal communication (lab group colleague Dr Georgia Stewart) (Stewart et al., 2021), we chose a wide range of drug concentrations for each drug (Btz 0.5-30 nM, Mel 1-100 µM, Pom 0.1-100 µM, and Pan 5-100 nM) (Lawson et al., 2015). Then, we studied the effect of single and combined treatment on DMCs using the IC_{50} values we determined for each drug. Several experiments were conducted in order to determine the appropriate concentration and culture conditions.

4.4.1 Bortezomib

Initially, we determined the IC_{50} values of Btz with the four MM cell lines, and each displayed sensitivity to Btz, with IC_{50} values ranging from 3.08 to 40.25 nM for both cell densities (refer to Table 4.1 for data). Zhou *et al.* (2020) used a similar method to our value ranges, the MTT viability assay, to explore inhibitors called ZY-2 and ZY-3 IC_{50} values, comparing them with the Btz effect on myeloma cells such as U266 and then assessed them after 24 hours. IC_{50} values were found for Btz with U266 12.5 nM (Zhou et al., 2020). In the same way, Horton *et al.* (2006) evaluated Btz IC_{50} values for different types of haematological malignancies. Horton *et al.* (2006) found Btz IC_{50} values between 9 to 20 nM for the MM1.S myeloma cell line. Moreover, both studies used assays to measure the metabolic activity, which is similar to the

AlamarBlue method, with the only difference being the cell density of 2500 and 5000 cells/well used in our study. However, Horton *et al.* (2006) study differed from ours when using 10,000 cells/96 well-plates, where we used less than 10,000 cells (Horton et al., 2006). The 5TGM1 IC_{50} value hasn't fully elucidated the dose-response curve in the experiment. This indicates that the drug might be less potent, or the cells might possess some resistance to Btz. So, we suggest expanding the range of concentrations and testing higher doses. Also, consider alternative assays. Also, the JJN3, OPM2, and U266 have lost the sigmoidal curve. The insufficient concentration range has rapidly reached the plateau effect. These cells could have accumulated mutations in the proteosome that increase resistance to Btz (Kozalak et al., 2023). In addition, cell seeding density variation could lead to numerous errors in measuring absorbance values, fluctuation in the absorbance reading from the plate reader, or minor variations in the quality of the cell culture media or assay reagents. Therefore, the reported IC_{50} values are predictions based on the model used in the GraphPad Prism application. Higher ranges of concentrations or different fitted curves are suggested to be used in future work.

Above all, our main aim is to study the effect of Btz, whether it is in single or combination treatment, on DMCs (see section 4.4.5).

4.4.2 Melphalan

Next, we determined the IC_{50} values of Mel with the four MM cell lines, a wide range of Mel concentrations from 1 to 100 µM, used on our MM cell lines at two different cell densities of 2500 and 5000; the results were tested using the AlamarBlue assay. We calculated Mel's IC_{50} values from 6.76 to 94.08 µM (please see Table 1 for data). A similar method was conducted by Poczta *et al.* (2022) using the MTT assay to determine Mel and its derivatives IC_{50} values within 96 hours to confirm Mel cytotoxicity on MM cell lines of anti-cancer properties with the Mel derivatives. The study involved various leukemic cell lines, including RPMI8226 myeloma cells, with a range of Mel concentrations from > 4 to > 9 µM. The results showed a Mel IC_{50} value of 8.9 µM with the RPMI8226 cell line; the cell density used in the study was much higher at 15,000 cells/ well in a 96 well-plate (Poczta et al., 2022). Sonneveld *et al.* (2005) have determined an IC_{50} value within the range of our values for MM1S 1.9 µM and a

higher value for MM1MEL2000 50 µM. The paper did not mention the cell density or viability assay used (Sonneveld et al., 2005).

A study by Xiong *et al.* (2015) determined different values of Mel IC_{50} in RPMI-8226 and RPMI-8226/R, 4.79 µM and 20.43 µM, respectively, to find the effect of combining Mel with a small molecule called PJ4 that can inhibit PARP. Xiong *et al.* (2015) used the CCK-8 assay and had a higher cell density of 10,000 cells/well in a 96-well plate. Drugs were added after 24 hours (Xiong et al., 2015). Moreover, CCK-8 have some similarities to AlamarBlue, like the non-toxicity on cells, and the detection method of absorbance. Therefore, CCK-8 are more sensitive than AlamarBlue (Vichai & Kirtikara, 2006).

In the approaches of Poczta *et al.* (2022) and Xiong *et al.* (2015), the MTT, CCK-8, and AlamarBlue are colourimetric assays that measure metabolic activity and cell viability (Poczta et al., 2022; Xiong et al., 2015; Vichai & Kirtikara 2006). The obvious difference is the cell density, as we used less than 10,000 cells per 96-well plate, which explains why we had our values as described above (section 4.4.1). Low cell density facilitates optimal distribution of drugs and nutrients among cells, enhancing overall efficacy. Higher cell density can lead to drug depletion, increase cell-cell interaction that promotes survival and alter cell cycle distribution, which reduces drug effectiveness (Thurley et al., 2015). Our hypothesis is using Mel alone or in combination with other SoC drugs may help target DMCs *in vitro* and *in vivo* (see section 4.4.5).

4.4.3 Pomalidomide

Next, we determined the IC_{50} values of Pom with the four MM cell lines using the AlamarBlue assay. For each cell line, two cell densities of 2500- 5000 cells /well were used with a range of Pom concentrations from 0.001 to100 µM, which were then assessed after 3 and 5 days of treatment. No reduction in cell viability was observed for 5TGM1, JJN3 and U266 cell lines after 3 and 5 days post-treatment, except for the OPM2 cell line. After 5 days, a significant decrease was observed in cell viability in OPM2, so IC_{50} values were determined for two cell densities of 0.30 and 0.06 µM, respectively.

In a study similar to ours by Guglielmelli *et al.* (2015), Pom's IC_{50} value was determined using the MTT assay with RPMI8226 and OPM2 cell lines. The study used a range of Pom

concentrations similar to ours with OPM2 from 0.01 to 50 µM set up in 96-well plates and incubated for 24 to 48 hrs. Pom showed cell viability reduction within 48 hrs and determined IC_{50} values of RPMI-8226 were 8 and for the OPM2 10 µM, but cell densities used in the study were not mentioned (Guglielmelli et al., 2015).

According to a study by Panga *et al.* (2018) used a similar method to ours, U266B1 and RPMI6228 myeloma cells had IC_{50} values of 6.12 and 15.54 µM, respectively. These were determined by the MTT assay using cell densities of 5000 cells seeded in a 96-well plate to evaluate Pom and its derivatives (Panga, Podila, & Ciddi, 2018).

In contrast to our study, Matyskiela *et al.* (2018) used the TR-FRET cereblon binding assay to find IC_{50} values for Pom and Len and compare them with a cereblon modulator called compound 6 to enhance cellular and biochemical effectiveness. This study used MF15 and OPM2 myeloma cell lines and found IC_{50} values for Pom at 1.5 and 1.2 µM, respectively. Again, no cell densities were cited in the paper (Matyskiela et al., 2018).

Panga *et al.* (2018) had a similar cell density to our study, while Guglielmelli *et al.* (2015) did not mention the cell density used in their paper. Both studies used assays to assess metabolic activity and cell viability, employing a method akin to the AlamarBlue method (Panga, Podila, & Ciddi, 2018; Guglielmelli et al., 2015). Pom exhibits both direct effects through cell cycle arrest and triggering programmed cell death and indirect cytotoxicity effect through modulation of the BMME and activates immune effector cells, such as NK cells and T cells and their co-stimulation cytokines, which might not be captured in our *in vitro* assay lacking immune components, this will be considered in future studies to enhance Pom effect of myeloma cells (Cruz, 2016; Richardson, Mark, & Lacy, 2013; Chanan-Khan et al., 2013). In addition, with a higher cell density, the proximity of cells to each other reduces drug accessibility, potentially leading to microenvironment changes in cell signalling and communication *in vitro*. This can result in biological variability, a common occurrence in research experiments, influenced by factors such as varying cell lines, cell culture conditions, technical errors, and the differential responses of myeloma cell lines to Pom, thereby causing fluctuations in IC_{50} values (Mura et al., 2019; Young, Hung, & Hsu, 2004).

Our main aim is to assess the effect of Pom alone or combined with SoC agents to target DMCs *in vitro* (see section 4.4.5).

4.4.4 Panobinostat

The last drug assessed was the HDACi Pan, a novel treatment to target histone and p53; anti-cancer effects come from how it controls gene expression and stops protein metabolism (Laubach et al., 2015). A wide range of Pan concentrations from 5 to 100 nM was assessed using the AlamarBlue assay on day three post-treatment. Our experiments determined Pan IC_{50} values between 16 to 26.70 nM for all four MM cell lines (see Table 4.1). Various studies have determined similar values to ours with equivalent assessment methods. Lemaire *et al.* (2012) used AlamarBlue for viability assay after 72 hours, which is similar to our method, and demonstrated IC_{50} values of 2.8 to 16 nM for MM cell lines OPM2, LP-1, Karapas707, and RPMI8226, respectively. The paper did not state what the cell density was used (Lemaire et al., 2012). Tagoug & Safra (2023) also had similar results to ours when using a JJN3 cell line with values of 13. The study used a range of Pan concentrations from 3.125 to 25 nM and a cell density of 10,000 cell/well in a 96-well plate and assessed after 48 hours by Cell-Titer-Glo viability assay, they suggested that the combination of Pan and MCL-1 inhibitor (S63845) has significant antitumor activity in MM (Tagoug & Safra, 2023). The MCL-1 inhibitor enhances the cytotoxic effect of Pan and decreases the viability of human cell lines and primary myeloma patient cells; non-dividing cells were not mentioned in the paper. This combination may be a promising therapeutic target for myeloma patients that should be explored further on DMCs (Tagoug & Safra, 2023). Comparable to our findings, a study by Ramakrishnan *et al.* (2014) examined Pan and RADOO1 inhibitor agents on various myeloma cell lines, including OPM2 and U266. They found a range of Pan IC_{50} values from 5 to 15 nM. The study assessed the cell viability by MTT assay within 48 hours in a 96-well plate with bone marrow stromal cells (BMSCs) seeded overnight before seeding the myeloma cells, which differs from our method as we used monoculture (Ramakrishnan et al., 2014). Our main target is to find the Pan IC_{50} value for our MM cell lines in order to be used for combined treatments to target DMCs.

Moreover, we observed significant variability in drug sensitivity across different MM cell lines. That may refer to different factors, such as genetic variations: myeloma cell lines have different

genetic mutations that may affect their sensitivity or resistance to drugs. Individual cell characteristics: cells may respond to drugs differently in the same cell line, which may lead to a residual sub-population of cells (Mitra et al., 2015). Drug interactions: Myeloma cells are influenced by drug interactions and cell sensitivity; the analysis of mutational status and signalling protein profiling holds great potential for predicting drug sensitivities and identifying resistance markers in MM (Giliberto et al., 2022). In summary, our study has determined that the IC_{50} values for Btz, Mel, and Pan were significantly effective in reducing the viability of myeloma-proliferating cells. The Pom IC_{50} could not be determined in most of our cell lines except the OPM2 due to its mechanism of action in monoculture. We believe that these SoCs have the potential to target DMCs when combined based on their mechanism of action. Therefore, we examined their impact on DMCs in the following section.

4.4.5 Targeting DMCs with Single and Combined Drugs

Next, we studied the effect of single and combined anti-myeloma drugs *in vitro on DMCs*. In Chapter 3, we showed that the remaining DID^{high} cells on days 17 and 21 could be dormant as they have retained the DID dye, and based on that, a pilot study was conducted to target DMCs. On days 17 and 21 of culture, unsorted OPM2 DID cells were treated with a single Btz or Mel and a combination of both. Our study showed no effect on OPM2 DID^{high} cells. Assessing unsorted cells on day 17 or 21 of the experiment is challenging because they have proliferated and lost their DID labelling, leaving a low number of DID^{high} cells. As Lawson *et al.* (2015) reported, the DID-labelled cells lose their label during proliferation as they inherit the lipophilic membrane dye to their daughter cells, leading to dilution through expansion (Lawson et al., 2015). This phenomenon likely explains the limited number of DID^{high} cells observed in our study that could be proliferated over time and become sensitive to therapy. Regarding this result, we decided to isolate the DID^{high} cells at earlier time points before they lose all the DID^{high} cells and treat them with single or combined drugs.

Based on our previous studies in chapter three, we isolated the DID^{high} cells by FACS Melody on day 7 and day 10 for JJN3 and OPM2, respectively. This is followed by treatment with Btz, Mel, and Pan at their IC_{50} values determined in (Table 4.1) individually and in combination.

Cell viability was assessed by flow cytometry three days post-treatment. It is important to note that the effect of these anti-myeloma drugs varies depending on the cell type.

The OPM2 DID^{high} showed sensitivity to single drugs and to the combination of Btz with Mel compared to Btz, Btz with Pan compared to Btz, and Mel with Pan compared to Mel. Meanwhile, the JJN3 DID^{high} was sensitive to a single treatment of Btz, Mel, and Pan and the combination of Btz and Pan compared to Btz. The observed variation can be clarified by the behaviour of the cells and cell culture conditions, e.g., seeding density or number of isolated cells. Furthermore, it should be noted that the sorting process has had a noteworthy impact on cells. This is an important aspect to consider when analysing the experiment's outcomes (Cheetham et al., 2024a). Our findings showed that Pan and Btz become potent when combined. As we demonstrated, OPM2 DID^{high} and JJN3 DID^{high} (potentially dormant cells) were sensitive to Pan and Btz together, which supports Laubach *et al.'s* (2015) findings on proliferating cells. However, Pan paired with Btz showed synergy, but nothing was mentioned regarding DMCs (Laubach et al., 2020). Moreover, OPM2 DID^{high} were significantly sensitive to the other combinations of Btz and Mel and Pan and Mel. Most studies demonstrated the power of a single treatment with SoCs on proliferating cells. Other research suggests using combination therapy to enhance the killing effect on proliferating cells. This could rely on the different molecular mechanisms that could increase the cell's sensitivity to combined treatments. While the Btz blocks the proteasome activity and accumulates misfolded proteins, Pan will alter chromatin acetylation, increase the transcription of apoptotic genes, and disrupt protein homeostasis. Moreover, the Pan can modulate BMME, reduce survival signals, and increase the vulnerability of DMCs. The combination of Btz and Pan will increase the endoplasmic reticulum (ER) stress, leading to apoptosis. However, there is a lack of studies targeting DMCs in this research area (Ramakrishnan et al., 2014; Ocio et al., 2010; Horton et al., 2006). Khoo *et al.,* 2019 discovered the dormancy gene signature (Khoo et al., 2019). Therefore, to improve our study in future, we could confirm the dormancy status by examining the expression of dormancy genes for the myeloma cell lines and then treating the cells with single or combined SoC agents.

However, most studies have limited focus on targeting DMCs by SoC, while Dadzie & Green., Chen *et al.,* Khoo *et al.,* and Lawson *et al.* were the early investigators in understanding

dormancy in order to target DMCs (Dadzie & Green, 2022a; Chen et al., 2019; Khoo et al., 2019; Lawson et al., 2015). Furthermore, Lawson *et al.* (2015) were the only study investigating targeting DMCs and found that Btz could target cells in their slow proliferative or dormant state. It has been thought that Btz can prompt apoptosis in quiescent myeloma cells by activating pro-apoptotic pathways. However, the effectiveness of Btz in targeting dormant cells is still constrained, and further research is required (Lawson et al., 2015). Therefore, we focused on using the JJN3 cell line and treating it with Btz and Pan to find the effect on DMCs in subsequent *in vivo* studies (see Chapter 5).

4.4.6 Conclusion

In conclusion, in this chapter, we determined the IC_{50} values for three of the SoC drugs (Btz, Mel, and Pan) on four myeloma cell lines (5TGM1, JJN3, OPM2 and U266). Regarding Pom treatment, we could not determine its IC_{50} because there was no significant reduction in cell viability on 3 of the cell lines, except with OPM2 cells, which showed a significant reduction by day 5 (refer to Table 4.1). The differences between our study and others may be due to many factors such as cell density, culture conditions, type of MM cell line, proliferation state, cell cycle stage, and drug concentration used.

With regards to targeting DMCs, the OPM2 DID^{high} cells showed variable effects to treatment with single and combined Btz, Mel, and Pan; however, these results were not significant and needed more repeats. Meanwhile, the JJN3 DID^{high} cells were only sensitive to the combination of Pan and Btz.

Chapter 5 Assess the Effects of Bortezomib and Panobinostat on DMCs in the JJN3 Murine Model of Myeloma

5.1 Introduction

In the previous chapter, we studied the effect of single and combined anti-myeloma drugs on DMCs *in vitro* for OPM2 and JJN3 cell lines. We initially examined the impact of the drugs on unsorted DID^{high} cells on days 17 and 21. Unfortunately, we could not target the DMCs due to low cell counts, as most of the DID-labelled cells had proliferated and lost their DID labelling. Consequently, we opted to isolate the JJN3-DID^{high} cells on day seven and the OPM2-DID^{high} on day ten before we lost most of the DID labelling and analysed the drugs' effect on DMCs. Our findings reveal a distinct difference in drug effects on DMCs across different cell lines. OPM2 DMCs demonstrated significant sensitivity to all single drugs Btz, Mel, and Pan compared to vehicle, and combined treatments of Btz and Mel, Btz and Pan compared to Btz, and Mel and Pan compared to Pan. In contrast, the JJN3 DMCs were responsive to single Btz, Mel, and Pan compared to vehicles, but only Btz and Pan combined.

The understanding of MM cell dormancy and how to effectively target it is still in its beginning. Our research, which investigates the effect of SoC drugs on DMCs, is a significant step towards filling this research gap. Limited studies have investigated the effect of SoC drugs on DMCs. Some studies have looked into the presence of DMCs in BM and found that these cells reside in the BM endosteal niche and interact with the microenvironment. As in chapters 3 and 4, here to study dormancy *in vivo,* these cells will be detected with a lipophilic dye DID (Khoo et al., 2019; Lawson et al., 2015).

Determining an appropriate mouse model is a crucial aspect of our comprehensive study of the effects of drugs on DMCs *in vivo*. In a study by Lawson *et al.* 2015, it was demonstrated that dormant 5TGM1 murine myeloma cells in C57BL/BKAL (BKAL) mice were resistant to Mel, while Btz showed no significant effect when used as monotherapies (Lawson et al., 2015). Moreover, the 5TGM1 cell line was developed by passaging 5T33 cells repeatedly in BKAL mice until a bone phenotype was observed, which typically develops monoclonal B cells (5TGM1 cells), making it an ideal model for studying MM (Arber et al., 2016; Al-Amer, 2015; Garrett et al., 1997). Another study by Lawson *et al.,* 2015b, concluded that immune-suppressed NOD/SCID-GAMMA (NSG) mice are the ideal animal model for studying anti-myeloma therapies (Lawson et al., 2015b). Highlighting the importance of their choice of mice

model to study the effect of drugs on DMCs. Therefore, we have chosen to expand the knowledge on targeting DMCs with SoC agents in single and combined to find their effect on other types of MM cell lines like JJN3, OPM2, and U266 in NSG mice. In this chapter, we specifically focused on the human myeloma cell line JJN3, which is known to be an aggressive, short-term model. However, studies targeting DMCs in this model are limited.

Regarding our results in chapter 4, Btz and Pan were two promising therapies for treating DMCs *in vitro*. Btz is a PI that triggers apoptosis in myeloma cells. It inhibits the 26S proteasome, a protein complex that degrades ubiquitinated proteins and disrupts their interaction with the BMME (Liu et al., 2023; Di Lernia et al., 2020; Ghiaur et al., 2015; Pitcher et al., 2015; Kapoor et al., 2012). We still have insufficient *in vivo* studies on the Btz effect on dormancy. On the other hand, Pan is an HDACi that has shown anti-myeloma activity by modulating gene expression and protein function in myeloma cells, leading to increased acetylation of histone proteins. This accumulation of acetylated histones and other proteins can induce cell cycle arrest and/or apoptosis of some transformed cells. Many studies have explored the effect of Pan when combined with different therapeutic agents *in vitro*, *in vivo* and on patients' peripheral blood; they have observed that Pan works in synergy with many drugs, including Btz to overcome drug resistance; these studies have improved survival in RRMM patients. Studying the effect of Pan on dormancy is important for understanding this phenomenon (Tagoug & Safra, 2023; Gkotzamanidou et al., 2022; Robinson et al., 2022; Eleutherakis-Papaiakovou et al., 2020; Imai et al., 2016; Laubach et al., 2015; Atadja, 2009). Both pharmaceutical agents disrupt the normal function of cellular proteins, thereby inducing cell cycle arrest and apoptosis, which are recognised as cell death mechanisms. Nevertheless, knowing the precise impact of this drug combination on DMCs requires further comprehensive scientific investigation. To conclude this, we aim to assess the effect of SoC agents on DMC viability *in vivo*.

5.1.1 Aims, Hypothesis and Objectives

The aim of this chapter was to assess the effect of combined SoC agents Btz and Pan on dormant JJN3 DID-labelled cells *in vivo* compared to monotherapy.

We hypothesised that combined Btz and Pan would be more effective than monotherapy at inhibiting DMCs, inside their BM endosteal niche, in NSG mice injected by JJN3-GFP-DID.

The chapter objectives were as follows:

1. To determine the effect of single and combined Btz and Pan on DMCs in the JJN3-NSG model of MM.
2. To assess the effect of single and combined treatments of Btz and Pan on total tumour burden and myeloma-induced bone disease.

5.2 Material and Methods

Detailed information on individual techniques performed is given in Chapter 2, General Material and Methods.

5.2.1 *In vivo* Experimental Design to Study the Effect of Single and Combined Btz and Pan on DMCs in the JJN3 Murine Model

JJN3-GFP-Luc cells were labelled with DID as described in chapter 2 (section 2.2.4), then 2×10^6 of JJN3- GFP-Luc-DID were injected via tail vein in 6-8 week old female NSG mice, a total of 57 mice randomised based on various body weights in each group of 13 mice per tumour group, and 5 mice were naïve group injected with 100 µl PBS and used as tumour-free control. Mice were treated with either PBS, single Btz, single Pan, or Btz and Pan combined. All animals were regularly monitored for signs of illness or the development of hind limb difficulties. The study design schematic representation is shown below (Figure 5.1). Treatments were initiated on day 5 through the IP route.

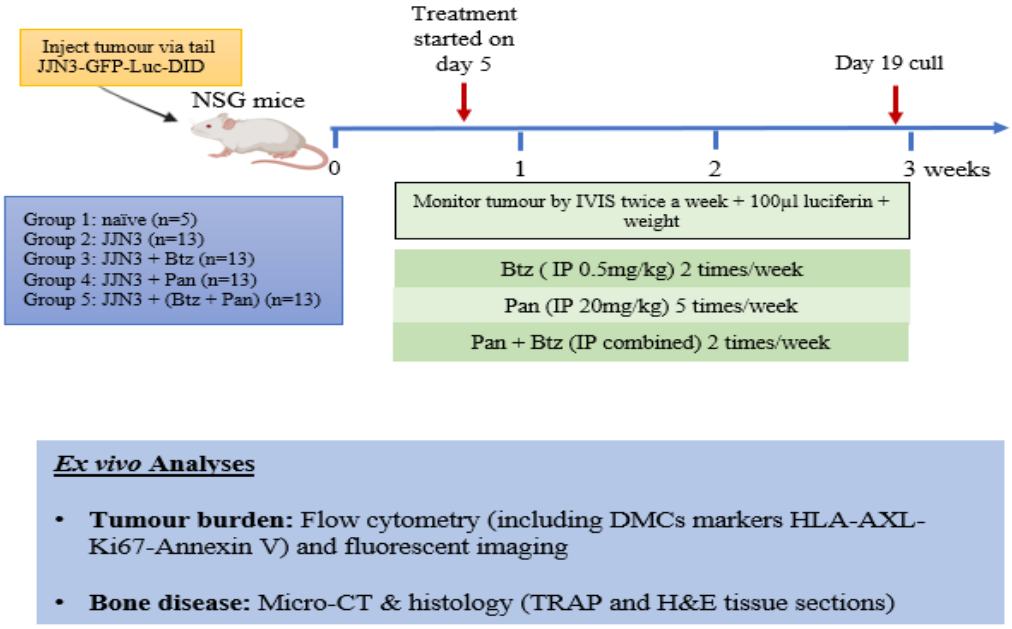

Figure 5.1: In vivo study schematic to assess tumour burden and bone disease in the JJN3 model.

PBS or JJN3-GFP-Luc cells labelled with DID dye were injected into NSG mice via the tail vein. 5 groups of mice (13 mice in each tumour treatment group and 5 mice in the naïve group) were treated with PBS (naïve group 1 and JJN3 group 2), Btz (IP 0.5 mg/kg, 2 times a week, group 3), Pan (IP 20 mg/kg, 5 times a week, group 4) or Pan and Btz combined (group 5). The study lasted for 3 weeks, with inoculation on day 0, and all treatments started 5 days later. Tumour progression was monitored by IVIS + 100µl luciferin twice a week. Ex-vivo samples analysed were femurs for tumour burden (including DMCs) and tibias for bone disease.

5.2.2 Statistical Analysis

GraphPad Prism 9.1/10.1 was used to plot the graphs, and values were represented as Mean SD was used to compare parameters between tumour-free mice, untreated JJN3-GFP-Luc-DID, and Btz, Btz, and Pan combined-treated JJN3-GFP-Luc-DID tumour-bearing animals. Ordinary one-way ANOVA was performed with Tukey's multiple comparison tests and unpaired t-tests. The findings were reported using one-way ANOVA, and P-values were determined compared to vehicle where *<0.01, **<0.001, ***<0.0001, ****<0.00001.

5.3 Results

5.3.1 Monitoring Tumour Progression Over Time

5.3.1.1 New Experiment Design

Mice were injected with JJN3-GFP-Luc-DID via the tail vein, and then the plan was to treat them with PBS, Btz, Pan, or combined Btz and Pan for 18 days. Treatment was initiated on day 5 post tumour injection, but by day 7, mice groups treated with Pan alone or Pan combined with Btz showed toxicity to the drugs, such as hunching posture, reduced movements, loss of appetite, ruffled fur, and laboured breathing. Therefore, the experimental design had to be altered as all Pan-treated mice needed to be euthanised. Groups of 8 mice from the vehicle and Btz were culled, and all mice from Pan and the combination of Btz and Pan were culled on day 7. After this time point, the treatment schedule continued as planned but with only naïve, vehicle and Btz groups until day 19 (Figure 5.2).

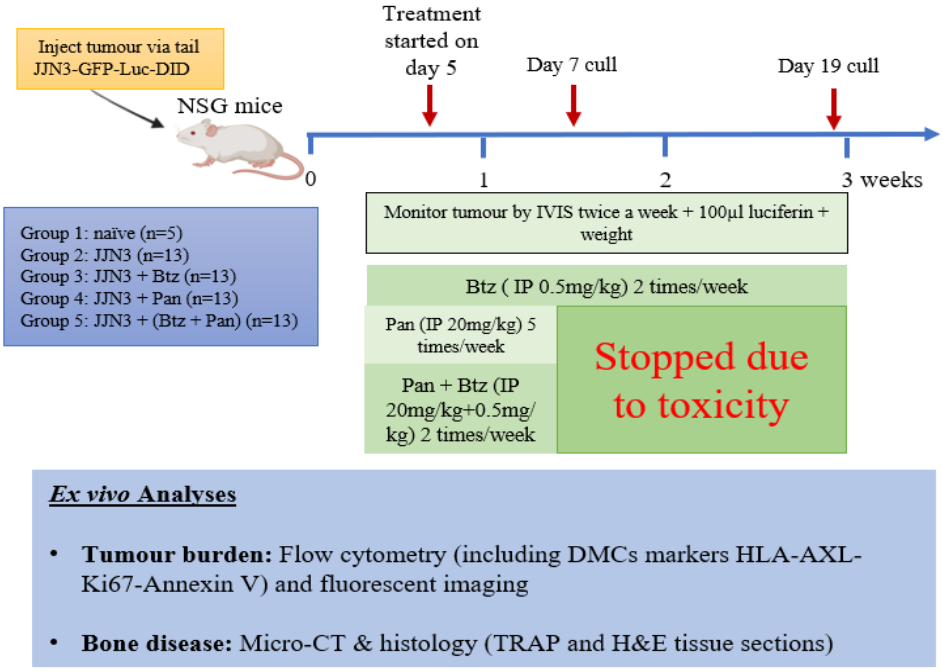

Figure 5.2: Modified in vivo study schematic (due to Pan toxicity) to assess tumour burden and bone disease in the JJN3 model.

PBS or JJN3-GFP-Luc cells labelled with DID dye were injected into NSG mice via the tail vein. 5 groups of mice (13 mice in each tumour treatment group and 5 mice in the naïve group) were treated with PBS (naïve group 1 and JJN3 group 2), Btz (IP 0.5mg/kg, 2 times a week,

group 3), Pan (IP 20mg/kg, 5 times a week, group 4) or Pan and Btz combined (group 5). The study was planned to last for 3 weeks, with inoculation on day 0, and all treatments started 5 days later. However, 42 mice were culled on day 7 due to Pan toxicity (8 from group 2, 8 from group 3, 13 from group 4, and 13 from group 5), then 15 mice (5 from group 1, 5 from group 2, and 5 from group 3) were culled on day 19. Tumour progression is monitored by IVIS + 100µl luciferin twice a week. Ex-vivo samples analysed were femurs for tumour burden (including DMCs) and tibias for bone disease.

5.3.1.2 Monitoring Mouse Weight

Following tumour cell injection and subsequent treatment, mice were weighed every four days to ensure their health. Weight loss greater than 20% was sacrificed using the Schedule 1 method. Naïve mice were tumour-free and healthy have not lost weight (Figure 5.3-A). Vehicle mice developed tumour, as they were only treated with PBS, but their weight has remained stable throughout the study. The group treated with Btz also showed stable weight during the experiment (Figure 5.3- B & C). The Pan group and combination group of (Btz and Pan) showed stable weight throughout the experiment. However, due to the toxicity of Pan in two groups (Pan alone and the combination of Btz and Pan groups) was that the mice were hunching, lacking locomotion, losing appetite, and ruffling fur. All these mice had to be euthanised on day 7, in addition to 8 mice from the vehicle group and 8 mice from Btz only group were euthanised with the Pan groups to find the effect of drugs on DMCs at the early stage of the disease (day 7) (Figure 5.3-D&E).

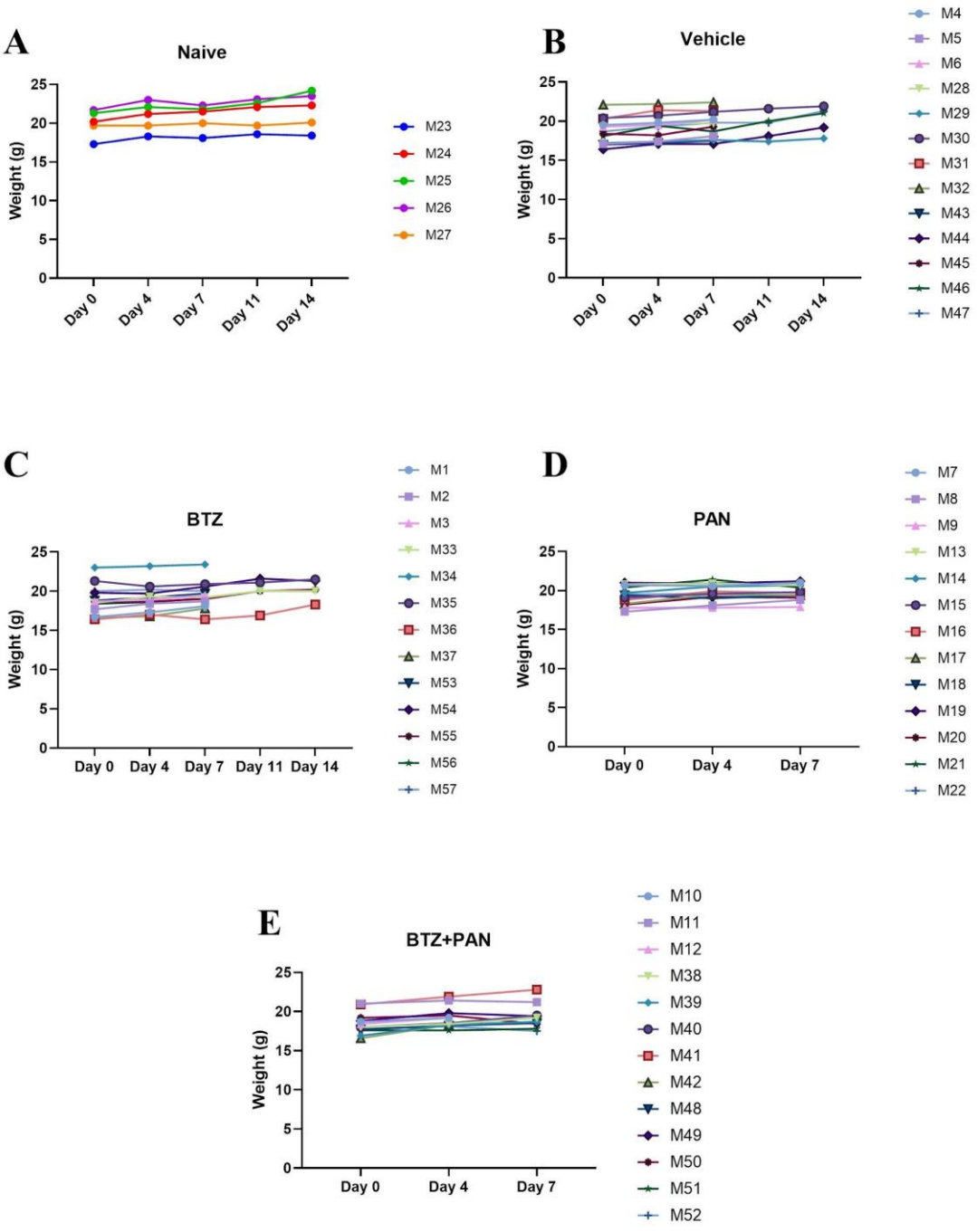

Figure 5.3: Group body weights over time.

Murine body weight changes during the in vivo study over 19 days in the five treatment groups: A) Naïve group, B) Vehicle/ tumour group, C) Btz tumour-treated group, D) Pan tumour-treated group, and E) Btz & Pan tumour-treated group. 8 mice from vehicle and Btz treated groups and

13 mice from Pan treated group and Btz combined with Pan group were culled on day 7due to Pan toxicity.

5.3.1.3 Monitoring Tumour Progression by BLI

Tumour cells were labelled with luc, so IVIS was used to measure bioluminescence imaging (BLI) over time; this allowed visual monitoring of tumour progression twice a week. However, the Pan group and the Btz with Pan combination group were culled on day seven due to the mouse intolerance to the toxicity of Pan (Figure 5.4-C, D).

The results of the study clearly demonstrated a significant difference in tumour progression between the vehicle and the Btz groups; however, due to Pan toxicity, BLI was monitored only in the vehicle and Btz groups post 4 days. The vehicle group showed a significant increase in tumour burden, starting from day 11 in limbs until day 18. The tumour burden was significantly increased in the vertebrate, calvaria and the whole body from day 11 until day18 (Figure 5.4-A). In contrast, the Btz group exhibited less tumour progression in all body sites (limbs, vertebrates, calvaria and the whole body) and was only detected from day 14 and continued to increase until the end of the experiment slowly (Figure 5.4-B).

The graphs illustrated the difference in increased tumour progression in the vehicle group in the whole body, vertebrate, calvaria, and limbs, compared to the Btz group (Figure 5.4-E).

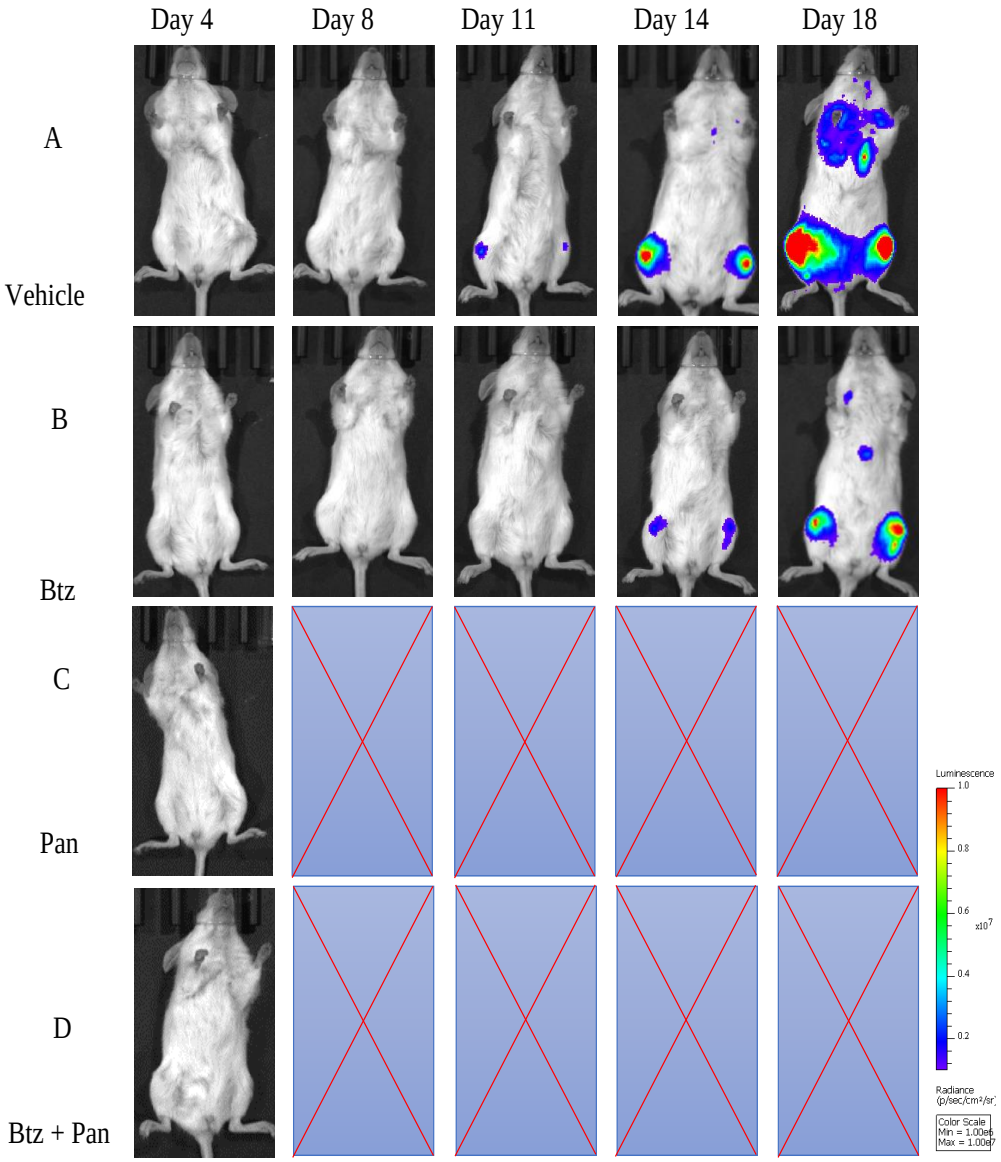
Day 4
Day 8
Day 11
Day 14
Day 18
A
Vehicle
B
Btz
C
Pan
D
Btz + Pan
Luminescence
1.0
0.8
0.6
x10^7
0.4
0.2
Radiance
(p/sec/cm²/sr)
Color Scale
Min = 1.00e6
Max = 1.00e7

E

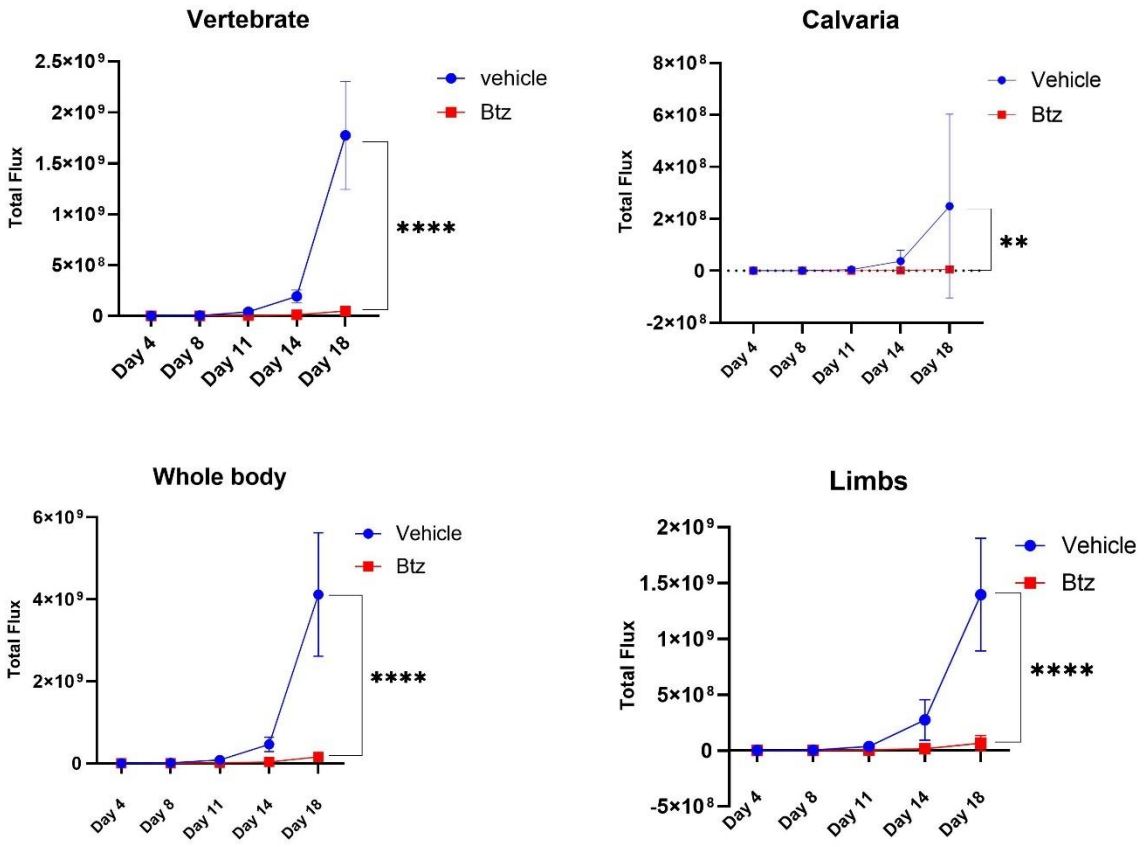

Figure 5.4: Tumour progression monitoring over time by bioluminescence imaging in the vehicle and Btz-treated mice.

*Representative IVIS images of tumour progression over time in NSG mice injected with JJN3-GFP-Luc-DID cells and then treated with vehicle, Btz, Pan, and Btz and Pan. Tumour growth over time in the whole body, vertebrae, calvaria, and long bones. The findings were reported using one-way ANOVA, and P-values were determined compared to vehicle where *<0.01, **<0.001, ***<0.0001, ****<0.00001.*

5.3.1.4 End-stage assessment of tumour burden by histology

Next, tibias were collected for decalcification, 3 µm sections were cut, and tissue sections were processed for TRAP and H&E staining to study tumour and bone histology.

The naïve group was used as a control for healthy BM. The images illustrated a well-preserved non-pathological bone and BM architecture on day 19. The cellular heterogeneity is obvious, with nucleated cells. Naïve BM showed a good structure of haematopoietic cells in addition to adipose tissue. There were no signs of dysplasia or malignancy (Figure 5.5-A & B).

The vehicle–untreated group, in the early stage of the disease (day 7), showed BM with a few cellular regions of myeloma cells starting to replace the normal marrow elements (Figure 5.5-C). H & E analysis showed no significant increase in the MM cells when comparing vehicle to naïve, Btz, Pan and the combination of Btz and Pan (Figure 5.6- A). In the end stage of the disease, the BM region shows an obvious replacement with myeloma cells. Compared to the early stage of the disease (day 7), the bone structure was distorted (Figure 5. 5-D). H & E analysis showed a significant increase in myeloma cells compared to the naïve and Btz-treated group (Figure 5.6-B).

The Btz-treated group, in the early stage of the disease (day 7), illustrated a BM with fewer myeloma cells. There were obvious normal BM cells such as adipose cells, some haematopoietic cells, well-structured bone (Figure 5.5-E). H& E analysis showed no significant difference in tumour progression when comparing vehicle to other groups (Figure 5.6-A). In the late stage of the disease (day 19), dense myeloma cells with BM cells were observed compared to the early stage of the disease (day 7) and the vehicle at the late stage of the disease (day 19) (Figure 5.5- F). H & E analysis illustrated a significant decrease in myeloma cells compared to naïve and vehicle groups (Figure 5.6-B).

The Pan-treated group, in the early stage of the disease (day 7), showed unhealthy BM with increased atrophic, more haematopoietic cells; H& E analysis illustrated no significant difference in tumour cells compared to naïve, vehicle, Btz and the combination of Btz and Pan (Figure 5.5-G & H) (Figure 5.6-A). Due to Pan's toxicity, day 19 images were unavailable in these treatment groups, as mice were culled on day 7 due to adverse effects on animals. (Figure 5.5-G & H).

The Btz and Pan combined group, in the early stage of the disease (day 7), showed unhealthy BM with increased atrophic, more haematopoietic cells; H& E analysis illustrated no significant difference in tumour cells compared to naïve, vehicle, and Btz groups (Figure 5.5-I & J) (Figure 5.6-A). Due to Btz and Pan's toxicity, day 19 images were unavailable in these treatment groups, as mice were culled on day 7 due to adverse effects on animals. (Figure 5.5-I & J).

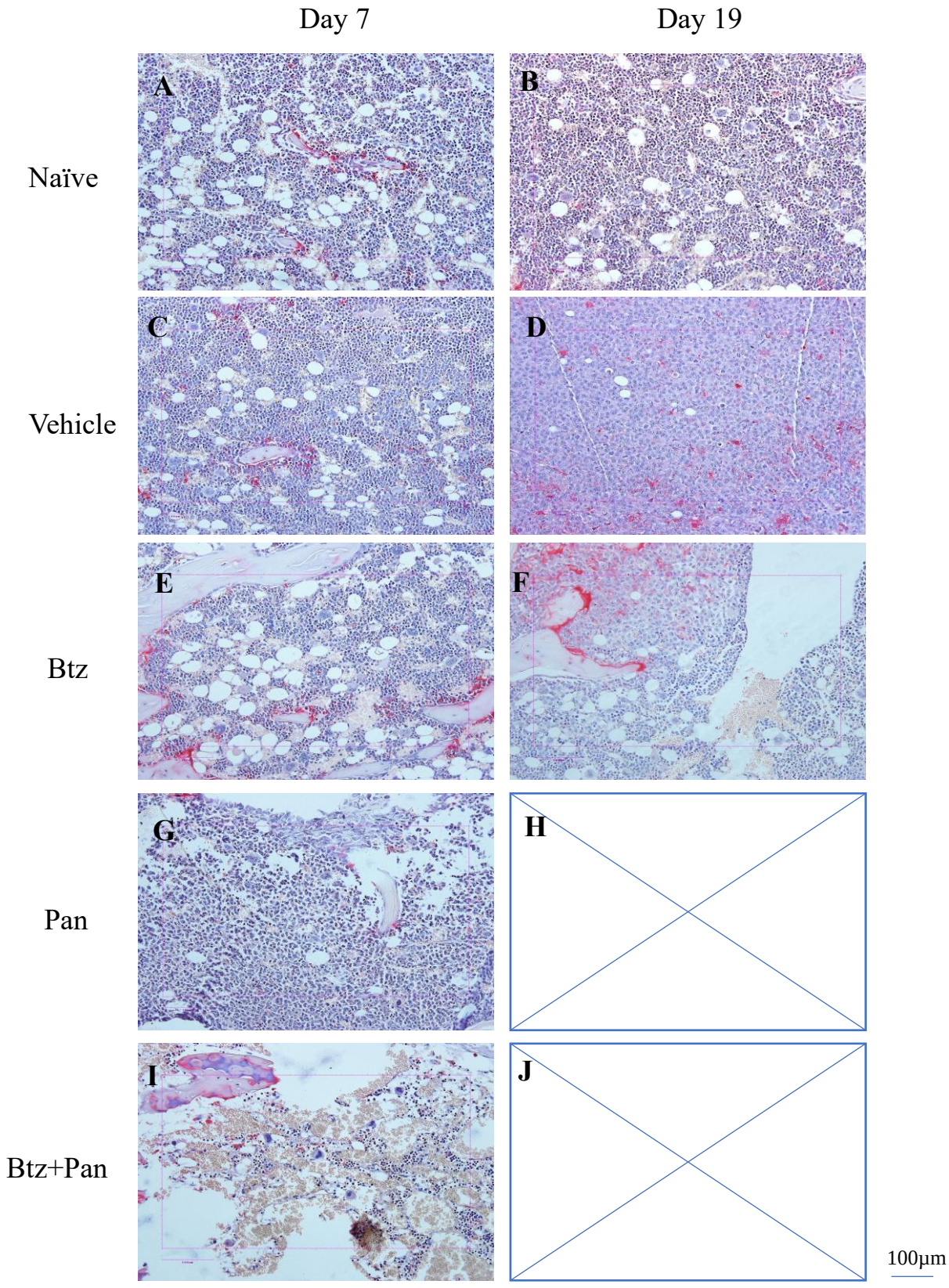
Day 7
Day 19
Naïve
Vehicle
Btz
Pan
Btz+Pan
A
B
C
D
E
F
G
H
I
J
100μm

Figure 5.5: H&E stain showing the tumour burden at days 7 and 19.

Representative H&E stained images of tibial sections of A & B) naïve non-tumour at days 7 and 19, C & D), Vehicle group of mice after JJN3 inoculation at days 7 and 19 days, E & F) Btz treated group of mice after JJN3 inoculation at days 7 and 19, G & H), Pan treated group of mice after JJN3 inoculation at day 7 (no image for day 19 as this group was culled on day 7), I & J), and Btz &Pan treated group of mice after JJN3 inoculation at day 7 (no image for day 19 as this group was culled on day 7).

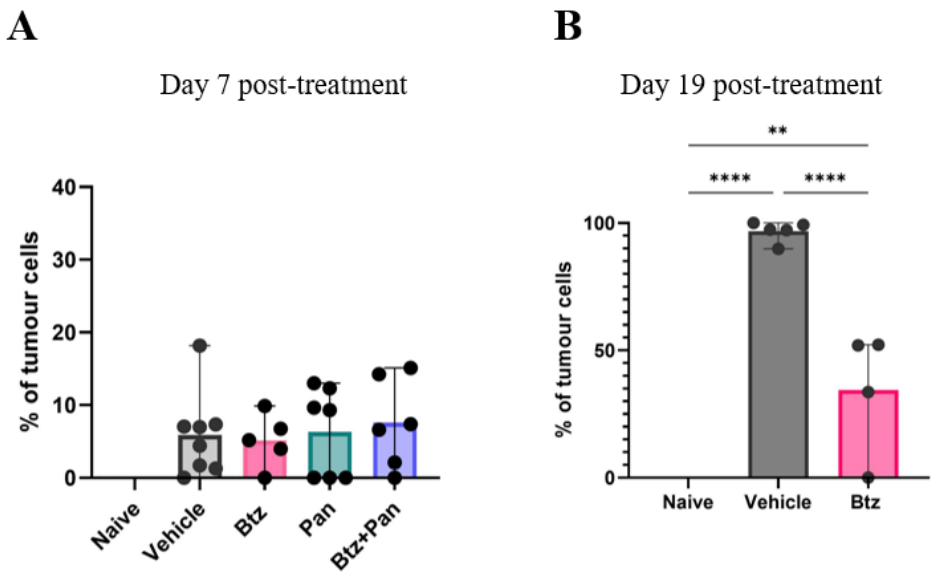

Figure 5.6: Histomorphology analysis detecting tumour burden.

*H&E stained tibial sections to detect tumour burden in BM. A) The effect of treatment at the early stage of the disease (day 7 post-treatment) for naïve, vehicle, Btz, Pan, and a combination of Btz & Pan groups. B) The effect of treatment at the late stage of the disease (Day 19 post-treatment) for naïve, vehicle, and Btz groups. The findings were reported using one-way ANOVA, and P-values were determined compared to vehicle where *<0.01, **<0.001, ***<0.0001, ****<0.00001.*

5.3.2 Treatment effects on proliferating and dormant tumour cells in the BM using flow cytometry

As mentioned, above groups of mice were culled at two time points: day 7, the early stage of the disease, and day 19, the late stage of the disease. At both cull time points, soft tissue was removed from the femurs before the BM was flushed out for flow cytometric analysis. This was to study the effect of Btz and /or Pan on proliferating cells and DMCs. Different markers

were used to label the tumour cells to distinguish between cells in a dormant state (not dividing) or proliferating (actively dividing). This procedure is detailed in Chapter 2.

In our gating strategy, we employed multiple steps to assess the impact of treatments on proliferating cells. Initially, all cells were sorted based on their FSC and SSC properties for differentiation (Figure 5.7-A). Subsequently, we isolated the single-cell population from the entire population (Figure 5.7-B). Next, viable cells were identified by gating them based on FSC and their viability using a live-dead antibody to exclude any non-viable cells (Figure 5.7-C). Further, we gated the HLA^+ population from the viable cells to distinguish the human myeloma cell line, JJN3, from mouse BM cells (Figure 5.7-D). As the JJN3 cells were double labelled with GFP and DID and most of the cells lost their GFP labelling, so we isolated the $Ki67^+$ population from the HLA^+ population (Figure 5.7-E). Finally, we focused on the HLA^+Ki67^+ population to specifically investigate the proliferating JJN3 cells.

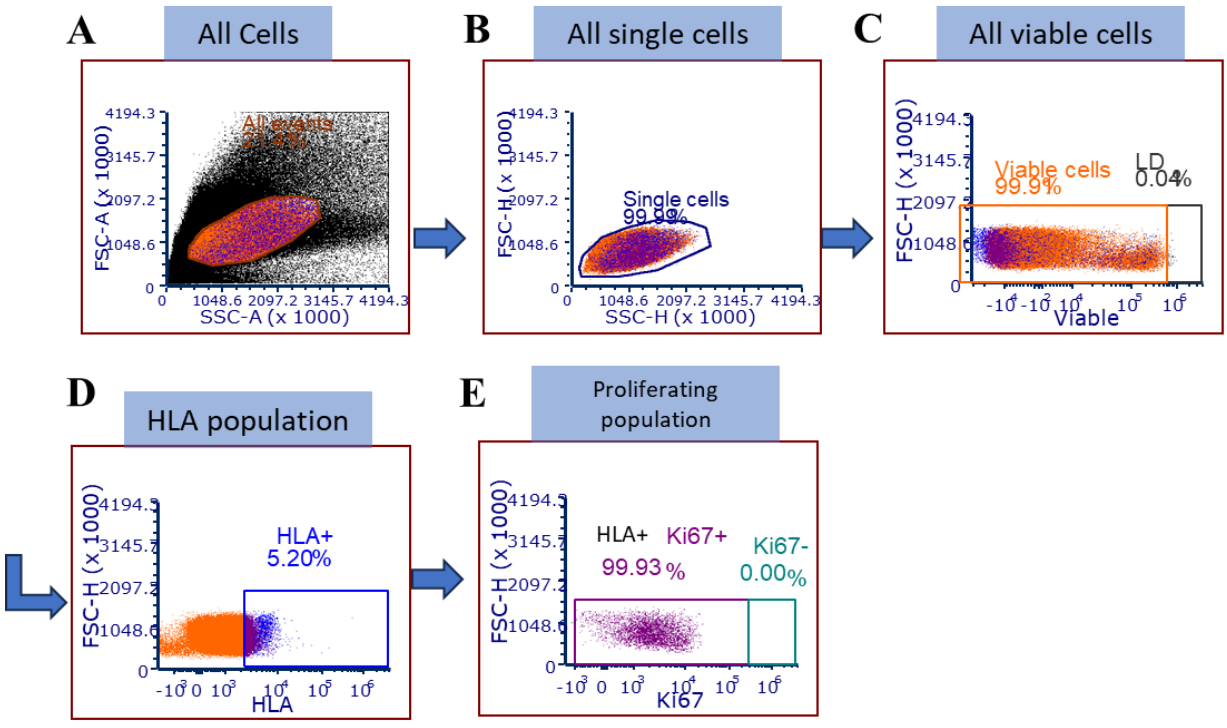

Figure 5.7: Flow cytometry gating strategy for the in vivo study to investigate the effect of (Btz, Pan, Btz and Pan) on proliferating cells.

BM was flushed from femurs (right and left) of JJN3, NSG mice treated with vehicle, Btz, Pan, or Btz and Pan after 7 and 19 days post-tumour inoculation. Cells were stained with AXL, HLA, Ki67, and Annexin V markers and then analysed by flow cytometry. A) FSC and SSC graph to

select All events, B) Single cells, and C) live/dead antibody was used to select viable cells. D) The HLA^+ population was gated from viable cells. E) $HLA^+Ki67^{+/-}$ marker gated as a proliferation indicator to identify proliferating cells. sample tubes were tested by Aurora 3 laser, Cytek Biosciences. FCSexpress software is used to generate graphs and data.

In our gating strategy to study DMCs, we employed multiple steps to assess the impact of treatments on non-proliferating cells. Initially, all cells were sorted based on their FSC and SSC properties for differentiation (Figure 5.8-A). Subsequently, we isolated the single-cell population from the entire population (Figure 5.8-B). Next, viable cells were identified by gating them based on FSC and their viability using a live-dead antibody to exclude any non-viable cells (Figure 5.8-C). Further, we gated the HLA^+ population from the viable cells to distinguish the human myeloma cell line JJN3 from mouse BM cells (Figure 5.8-D). As the JJN3 cells were double labelled with GFP and DID and most of the cells lost their GFP labelling, so we isolated the DID^+ population from the HLA^+ population (Figure 5.8-E). Then, we focused on the DID^+Ki67^- population from the DID^+ population to investigate the non-proliferating JJN3 cells (Figure 5.8-F) specifically. Therefore, to discover that cells were dormant, we investigated the presence of AXL^+ as it is over-expressed in DMCs (personal communication Dr Alanna Green (Dadzie & Green, 2022)). We then gated AXL^+ from the DID^+Ki67^- (Figure 5.8-G). Finally, we assessed whether these cells had undergone apoptosis by labelling them with Annexin V. Therefore, our DMC population was gated/selected as $DID^+Ki67^-AXL^+AnxV^-$ (Figure 5.8-H).

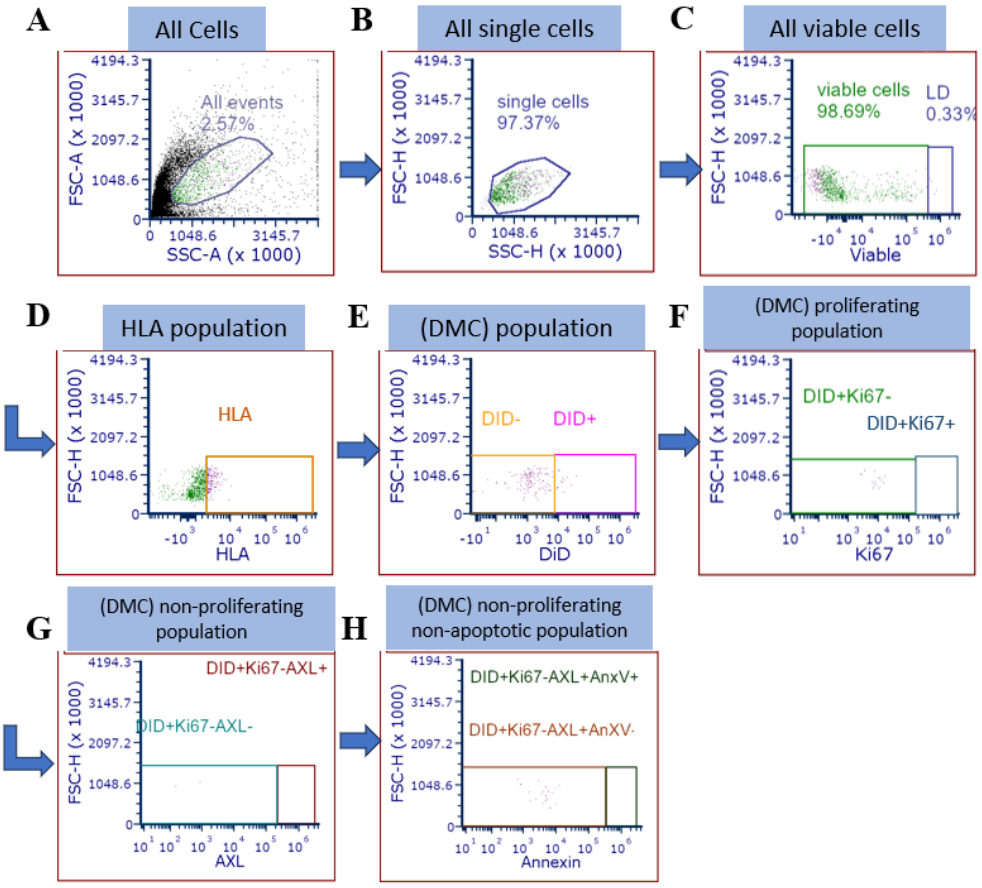

Figure 5.8: Flow cytometry gating strategy for the in vivo study to investigate the effect of (Btz, Pan, Btz and pan) on DMCs in the BM.

BM was flushed from femurs (right and left) of JJN3, NSG mice treated with vehicle, Btz, Pan, or Btz and Pan after 7 and 19 days post-tumour inoculation. Cells were stained with AXL, HLA, Ki67, and Annexin V markers and then analysed by flow cytometry. A) FSC and SSC graph to select All events, B) Single cells, and C) live/dead antibody was used to select viable cells. D) The HLA^+ population was gated from viable cells. E) DID^+ and DID^- populations determined from HLA^+ F) $DID^+Ki67^{+/-}$ marker gated as a proliferation indicator to identify non-proliferating cells, G) $DID^{+/-}$ $Ki67^{+/-}$ $AXL^{+/-}$ used as a non-proliferation indicator potentially dormant cells, H) $DID^{+/-}Ki67^{+/-}AXL^{+/-}$ ANNEXIN V $^{+/-}$ to investigate any DMC going to apoptosis affected by Btz. sample tubes were tested by Aurora 3 laser, Cytek Biosciences. FCSExpress software is used to generate graphs and data.

5.3.2.1 Assessing the effect of treatment on Proliferating cells

At day 7, no significant effect was demonstrated on JJN3 proliferating cells (HLA^+Ki67^+) when treated with Btz, Pan, and their combination compared to the vehicle (Figure 5.9-A). There

were no samples at the late stage of the disease (day 19), in groups treated with Pan alone or in combination with Btz as these mice were culled due to toxicity, so the experiment continued with naïve, vehicle and the Btz treatment only groups. At day 19, a significant effect was demonstrated on JJN3 proliferating cells (HLA^+Ki67^+) when treated with Btz compared to the vehicle (Figure 5.9-B).

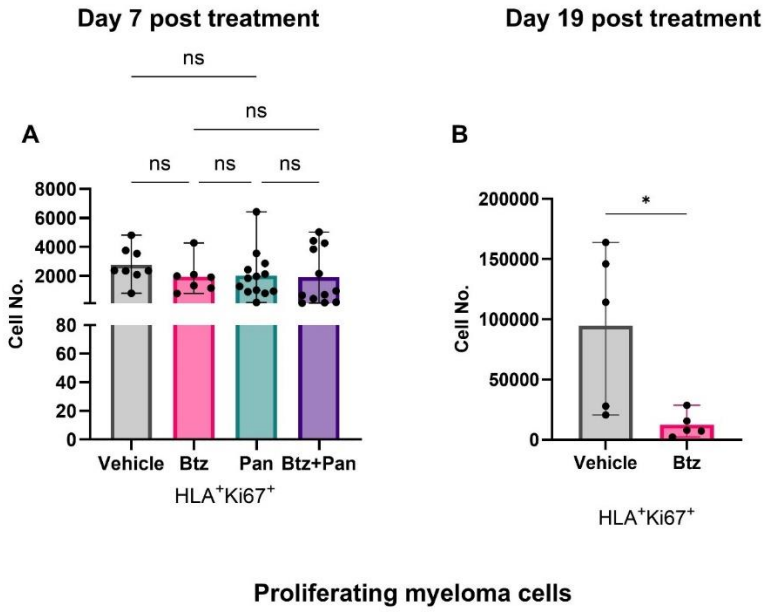

Figure 5.9: Flow cytometry assessing viable JJN3 HLA^+Ki67^+ cells in mice after 7 and 19 days of treatment.

*A) Number of HLA^+Ki67^+cells (proliferating cells) were treated by vehicle, Btz, Pan or Btz, and Pan on day 7 post-treatment. B) Number of HLA^+Ki67^+cells (proliferating cells) by vehicle or Btz on day 19 post-treatment. Bar charts were analysed and calculated using GraphPad prism. The findings were reported using one-way ANOVA, and student t-test. P-values were determined compared to vehicle where *<0.01, **<0.001, ***<0.0001, ****<0.00001.*

5.3.2.2 Assessing the effect of treatment on DMCs

At day 7, no significant effect was observed on JJN3 DMCs ($DID^+Ki67^-AXL^+AnxV^-$) when treated with Btz, Pan, or their combination compared to the vehicle (Figure 5.10-A). The combined drugs reduced the DMCs, but the decrease was not significant. At day 19, no significant effect was observed on JJN3 DMCs ($DID^+Ki67^-AXL^+AnxV^-$) when treated with Btz compared to the vehicle (Figure 5.10-B).

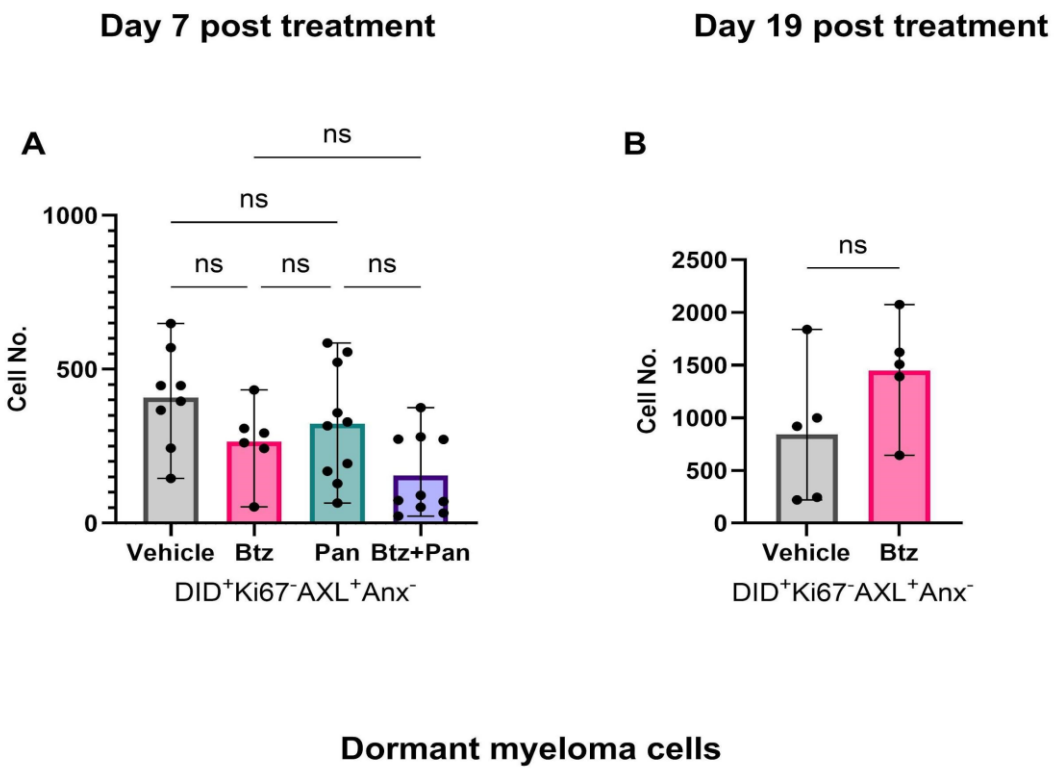

Figure 5.10: Flow cytometry assessing JJN3 DMCs in BM samples after 7 and 19 days of treatment.

*A) Number of DID$^+$Ki67$^-$AXL$^+$AnxV$^-$cells (DMCs) were treated by vehicle, Btz, Pan or Btz, and Pan on day 7 post-treatment. B) Number of DID$^+$Ki67$^-$AXL$^+$AnxV$^-$cells (DMCs) treated by vehicle or Btz on day 19 post-treatment. Bar charts were analysed and calculated using GraphPad prism. The findings were reported using one-way ANOVA, and student t-test. P-values were determined compared to vehicle where *<0.01, **<0.001, ***<0.0001, ****<0.00001.*

5.3.3 Analysis of Bone Disease at end stage

5.3.3.1 Assessing Myeloma-induced Bone Disease with µ-CT

Next, we investigated the myeloma-induced bone disease by assessing the long bone structure, as myeloma cells typically reside in the BM and cause lesions. As mentioned in Chapter 2 (section 2.2.14), µ-CT scanning was performed on the proximal tibial metaphysis to evaluate the structural changes after treatment with either Naïve, Vehicle, Btz, Pan, or a combination of Btz and Pan at two different time points during the disease progression. Several bone parameters were analysed, including BV/TV and Ct. V, Tb. N, Tb. Th, and the percentage of

bone lesions (% lesions). Bone loss was assessed the tibia, including the trabecular and cortical regions (Figure 5.11-A). At day 7, images and analysis illustrate no lesions observed on Vehicle, Btz, Pan, or a combination of Btz and Pan compared to naïve. No significant number of osteolytic lesions were detected compared to naïve (Figure 5.11- A, B). No significant difference was observed in CT. V, Tb. N, Tb. Th and TB/TV. This suggests that myeloma growth in the BM after 7 days has not yet affected the actual bone structure (Figure 5.11- C, D, E, & F).

At day 19, lesions were observed in the vehicle and Btz-treated group compared to the naïve group (Figure 5.12-A). There was a significant increase in the number of bone lesions in the vehicle group compared to naïve, while the Btz-treated group had fewer lesions compared to the vehicle (Figure 5.12-B). No significant difference was observed in CT. V, while the Tb. N showed a significant decrease in the vehicle group compared to the naïve and a significant increase in the Btz-treated group compared to the vehicle group (Figure 5.12- C, D). Tb thickness did not show a significant difference between the three groups. However, TB/TV revealed a significant decrease in the vehicle group compared to the naïve group and a significant increase in the Btz-treated group compared to the vehicle group (Figure 5.12- E, F).

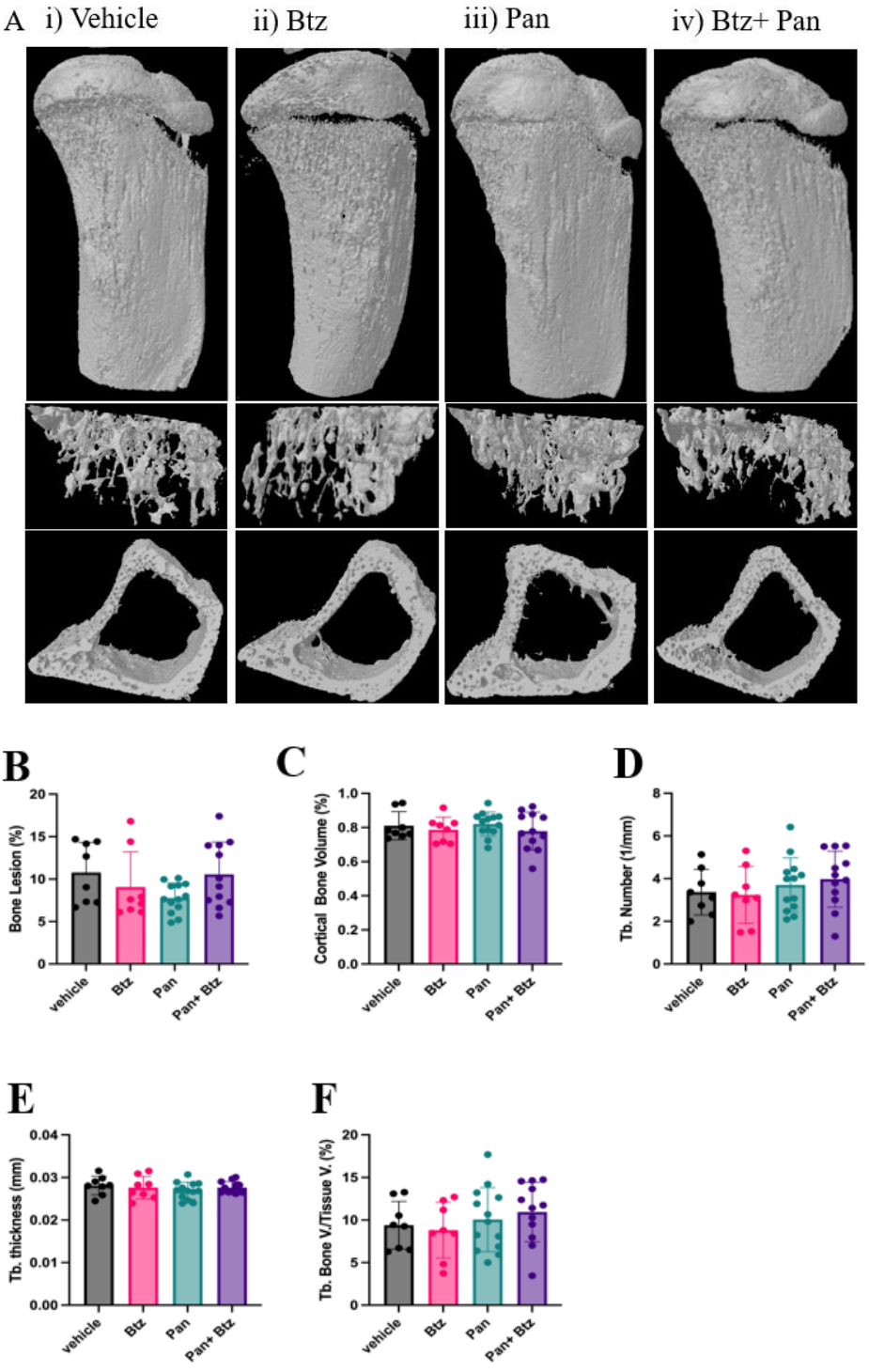

Figure 5.11: Effect of treatments on bone disease in tibias at day 7 post tumour inoculation.

A) Representative 3D reconstruction μ-CT images (upper) left tibia, (lower) trabecular and cortical bone. A-i, ii, iii, iv, and v) Images showing treatment groups for naïve, vehicle, Btz, Pan, Btz & Pan combo. B) Representative graph of the percentage of bone lesions. C)

*Representative graph of percentage of cortical bone volume. D) Representative graph of trabecular number. E) Representative graph of trabecular thickness. F) Representative graph of percentage of trabecular bone volume to tissue volume. All data are represented as mean ±SD, one-way ANOVA test, *p≤ 0.05, **p≤ 0.01, ***p≤0.001 and ****p≤0.0001.*

A i) Naïve ii) Vehicle iii) Btz

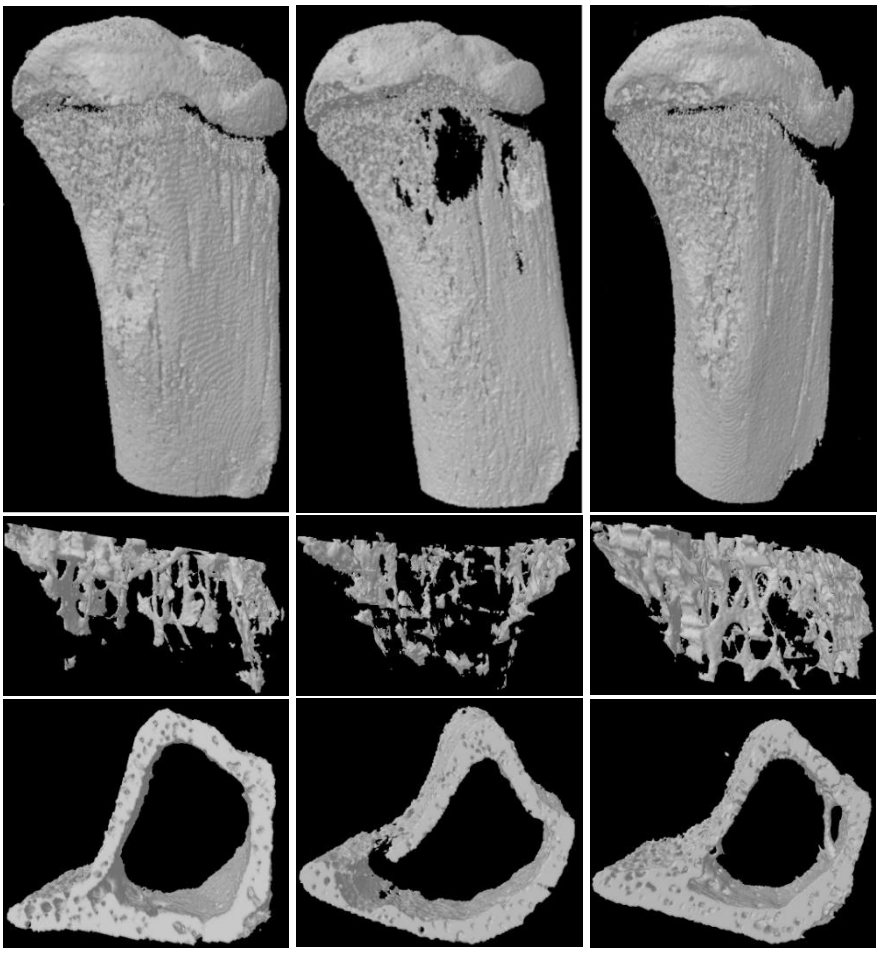

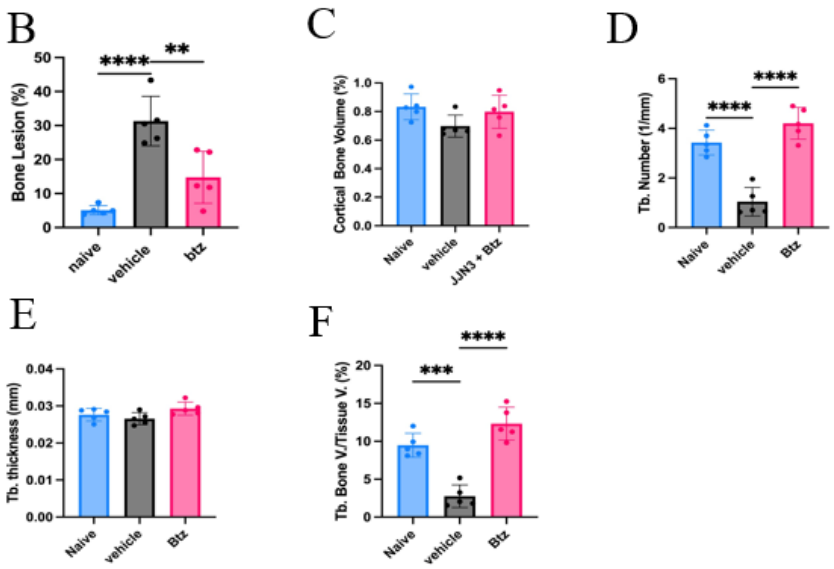

Figure 5.12: Effect of treatment on bone disease in tibias at day 19 post-tumour inoculation.

*A) Representative 3D reconstruction µ-CT images (upper) left tibia, (lower) trabecular and cortical bone. A-i, ii, iii, iv, and v) Images showing Naïve, Vehicle, and Btz treatment groups. B) Representative graph of the percentage of bone lesions. C) Representative graph of percentage of cortical bone volume. D) Representative graph of trabecular number. E) Representative graph of trabecular thickness. F) Representative graph of percentage of trabecular bone volume to tissue volume. All data are represented as mean ±SD, one-way ANOVA test, *p≤ 0.05, **p≤ 0.01, ***p≤0.001 and ****p≤0.0001.*

5.3.3.2 Assessing Myeloma-induced Bone Disease by Histomorphometry (Osteoclast and Osteoblast analyses)

Lastly, the impact of treatments on bone cells was evaluated on tibias from NSG mice by examining changes in the number of OB and OC in the BM. TRAP staining was used as outlined in Chapter 2. The images illustrated the changes in OB and OC numbers (Figure 5.13). For description, OBs are cubed cells found lining the BM cavity (endosteal) and on the outer surface (periosteal) and attached directly to the bone surface. At the same time, the OC are large, multinucleated, TRAP-stained (red) rounded cells found attached directly to the bone surface.

At the early stage of the disease (day 7), there was no significant difference in OB number in single-treated Btz, Pan, and Btz and Pan combined groups compared to the naïve and vehicle groups (figure 5.13-A & Bi). And no significant difference in OC number in single-treated Btz,

Pan, and Btz and Pan combined groups compared to the naïve and vehicle groups (Figure 5.13- A & Bii).

At the late stage of the disease (day 19), the Btz-treated group showed a significant elevation in OB numbers compared to the vehicle group (Figure 5.14– A&B). The Btz-treated group had a significantly reduced number of OCs compared to the vehicle groups (Figure 5.14- A & B).

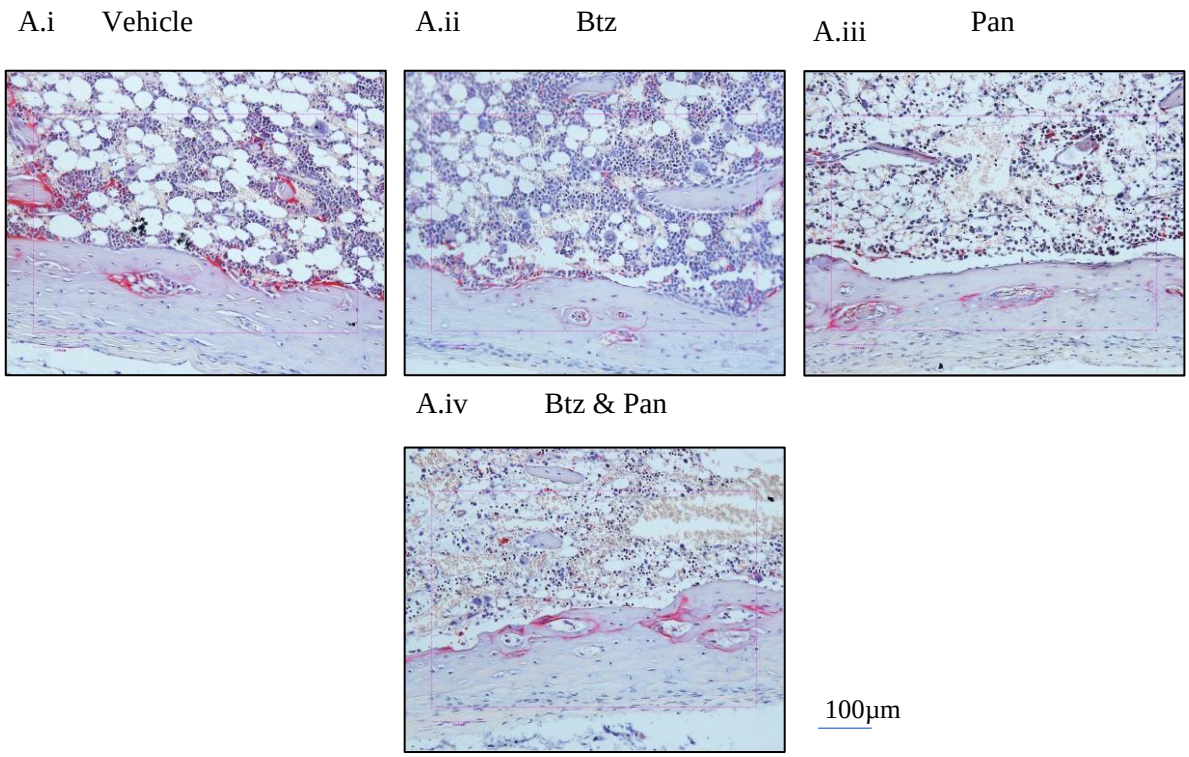

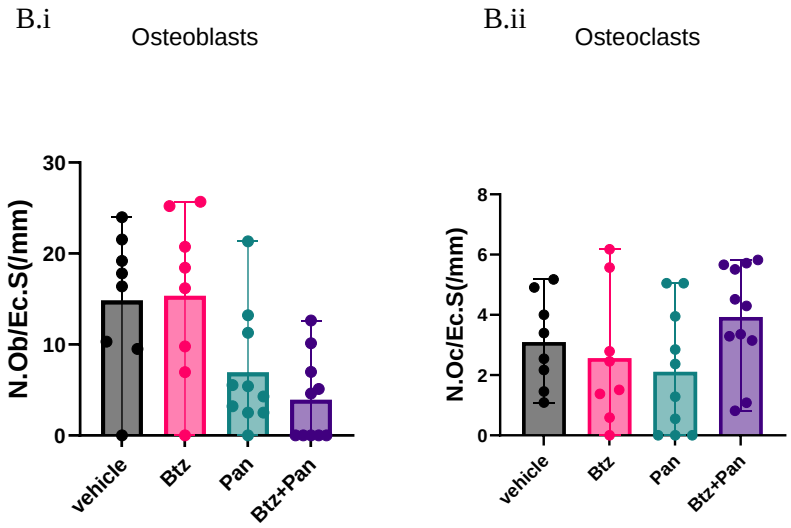

Figure 5.13: Osteoclast and osteoblast analysis of left tibias 7 days post-tumour inoculation.

A) Representative images of tibial sections stained with TRAP and haematoxylin (scale bar100µm); analyses were done in the proximal tibial metaphyseal region. In control vehicle-treated mice, Btz-treated mice, Pan-treated mice, and Btz & Pan-treated mice. B.i & ii) Bar

*charts calculating OB and OC numbers pre mm. The findings were reported using one-way ANOVA, and P-values were determined compared to vehicle where *<0.01, **<0.001, ***<0.0001, ****<0.00001.*

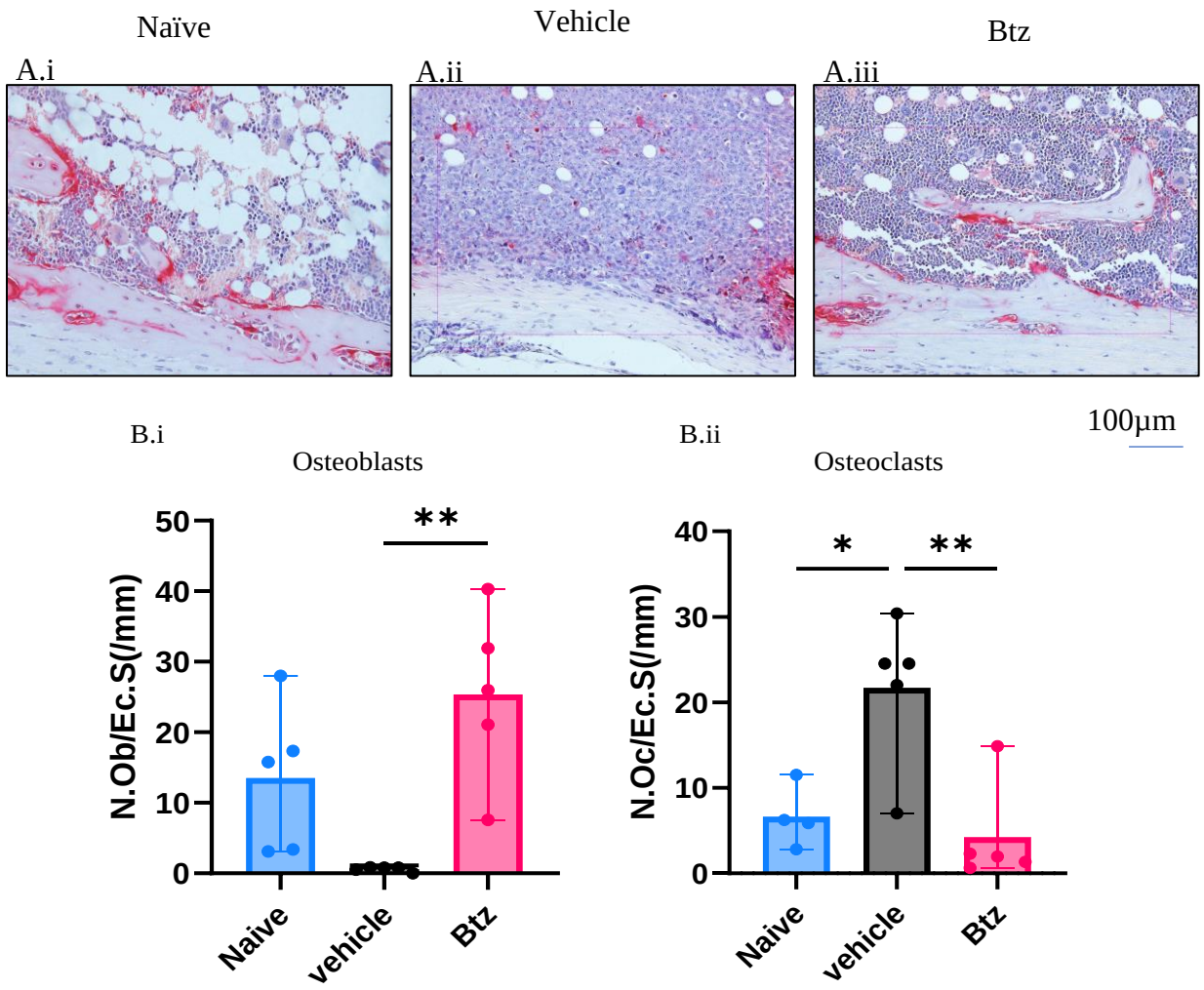

Figure 5.14: Representative images of TRAP stain of left tibias 19 days following treatment.

*A) Images show magnified (100µm) proximal tibial metaphyseal region. In control vehicle-treated mice, Btz-treated mice. B.i & ii) Bar charts calculating OB and OC numbers pre mm. The findings were reported using one-way ANOVA, and P-values were determined compared to vehicle where *<0.01, **<0.001, ***<0.0001, ****<0.00001.*

5.4 Discussion

The previous chapter 4 determined that Btz and Pan combined were an efficient combination to target JJN3 DMCs *in vitro*. Therefore, in this chapter, an *in vivo* model of myeloma was used where the tumour growth in bone is caused by injecting the JJN3-GFP-Luc-DID human myeloma cell line into the tail vein of young (6-8 weeks) female NSG mice. This resulted in mimicking human myeloma disease and allowed the assessment of Btz, Pan monotherapy and in combination on DMCs.

At the early stage (day 7), the disease progressed slowly and did not affect the BM or bone structure. This applied to all the groups of treated and untreated mice. At the later stage (day 19), myeloma cells spread in the BM, replacing normal components. Notably, there was spongy bone loss and outer layer bone within three weeks of tumour introduction. Additionally, JJN3 development in the bone led to increased OC and bone lesions in the untreated mice. On the other hand, the Btz-treated have controlled the tumour growth with fewer bone lesions, and this could be explained by Wang *et al.* (2020) and Vallet & Raje. (2011) described that Btz could work as an anabolic agent that lowers tumour burden and elevates the OB numbers (Wang et al., 2020; Vallet & Raje, 2011).

Based on previous studies, which used six to eight weeks-old mice to ensure a longer health span for experiments, female mice showed less unstructured variance compared to males (Smarr & Kriegsfeld, 2022; Liu et al., 2022; Lawson et al., 2015; Lawson et al., 2015b). The study utilised 57 female mice, aged between six and eight weeks, to establish a stable and consistent baseline for the MM study. The mice were randomly assigned to groups of 13 each. By using the GPower 3.1 application was employed to determine the appropriate sample size for the study based on data extracted from previous research for Lawson *et al.* (2015), who studied the effect of Mel on 5TGM1 DMCs in C57BL/6 mice model (Lawson et al., 2015). The treatment with Btz and Pan combined *in vitro* showed a significant effect on JJN3 DID^{high} cells (potentially dormant) in Chapter 4. Thus, this study was carried out to illustrate the effect of combined treatment on DMCs in NSG mice model injected with JJN3-GFP-DID.

In the late stage of the disease (day 19), myeloma cells were expanded in the BM, progressively replacing normal BM components. Notably, significant trabecular and cortical bone loss was

observed within three weeks following tumour inoculation. In addition, the development of JJN3 in bone was associated with a significant increase in OC numbers and bone lesions in the vehicle-untreated group of mice. Based on Lawson *et al.'s* (2015b) study, the NSG mice strain is the most effective strain for evaluating and treating myeloma bone disease. The JJN3 human cell line exhibited an aggressive myeloma model characterised by rapid progression in NSG mice within a span of three weeks (Lawson et al., 2015b). Our data conform to Lawson *et al.'s* (2015b) study, as the tumour burden has increased aggressively in the vehicle group throughout the body, while the tumour progression in the Btz-treated group has controlled the tumour growth with a lower tumour burden. Sadly, the Pan-treated group and the combination of Btz with Pan ended at the early stage of the disease (day 7) due to the toxicity of Pan, and no significant changes in bone were observed at this time point.

Regarding the significant increase in tumour burden in the vehicle group, an increase in bone lesions and a decrease in BV/TV and Tb.Th have been observed. These data were similar to studies that had comparable results to ours and involved studying NSG and C57BL/6 mice with JJN3, U266, OPM2 and 5TGM1 in order to find the ideal murine model for evaluating the effectiveness of antimyeloma drugs on bone disease (Paton-Hough et al., 2019; Lawson et al., 2015b; Paton-Hough, Chantry, & Lawson, 2015; Miyakawa et al., 2004). The group treated with Btz showed an improvement in BV/TV and Tb.Th while having fewer bone lesions. Similar to other studies, it was observed that Btz affects the microenvironment of myeloma cells and positively impacts bones, promoting bone formation by stimulating OB (Wang et al., 2020; Paton-Hough et al., 2019; Lawson et al., 2015b; Hurchla et al., 2013; Ocio et al., 2010). On the other hand, Pan has the ability to decrease bone lesions but also will reduce trabecular density (Wang et al., 2020; Accardi et al., 2015; Ocio et al., 2010). Unfortunately, no signs of bone alteration were observed at the early stage of the disease (day 7) with all treatments, and the research study had to discontinue the Pan treatment due to its severe toxicity in mice, leading to the cessation of the Pan and the combination of Btz with Pan groups. Our histological analysis revealed a significant reduction in tumour cells with Btz treatment compared to the vehicle group. At the same time, the Pan and Btz with Pan combined had adverse effects on the BM. Moreno *et al.* (2022) and Homan *et al.* (2021) avoid using a high dosage of Pan due

to the harmful side effects observed (Moreno et al., 2022; Homan et al., 2021). Consider using lower doses of Pan to improve this study.

The drug's dosages used were based on previous research. The Btz IP route was 0.5 mg/kg twice a week, and the Pan IP route was 20 mg/kg five times per week, and the combination of Btz and Pan were (Btz 0.5 mg/kg twice a week, Pan 20 mg/kg five times a week) (Robinson et al., 2022; Savvidou et al., 2022; Imai et al., 2016; Lawson et al., 2015; Sanchez et al., 2013; Ocio et al., 2010). Unfortunately, with the harmful effect of Pan and the combined drugs of Btz with Pan on the BM, the procedure stopped at an early time point. Moreno *et al.* (2022) treated NSG mice with a lower dose of 5 mg/kg dose of Pan to avoid its side effects, such as splenomegaly, weight loss and central nervous system abnormalities. (Moreno et al., 2022). In addition, Homan *et al.* (2021) used a 15 mg/kg IV administration dose to prevent Pan toxicity (Homan et al., 2021). Thus, using a lower dosage could overcome this issue in future.

The observed toxicity in the current study is consistent with the known toxic profile of the Pan in preclinical models. Pan, a histone deacetylase inhibitor, exerts its anti-tumour effects by disrupting the balance of histone acetylation and deacetylation, thereby affecting gene expression. However, this mechanism of action is not entirely specific to tumour cells, leading to off-target effects and toxicity. It is known that Pan inhibition of HDACs can disrupt normal function of various cell types including those in BM, gastrointestinal tract, heart, and liver. Therefore, applying a lower dose should be considered. Pan can induce several cytotoxic effects at the cellular level, such as cell cycle disruption, apoptosis induction, increase of oxidative stress, and DNA damage (Smith et al., 2024). This explains hunching posture, decreased movements, loss of appetite, and laboured breathing observed in our NSG mice. Moreover, the study has observed that Pan could cause systemic toxicity, haematological effects, cardiac toxicity, gastrointestinal toxicity and liver toxicity in mice when used $\geq$ 20 mg/kg. In addition to general physical distress, thrombocytopenia and neutropenia could compromise the mice's immune system (Ali et al., 2021; Van Veggel, Westerman, & Hamberg, 2018).

Lawson *et al.* (2015) were the first to investigate the effect of Mel on DMCs in C57BL/KaLwRijHsd (BKAL) mice and observed that DMCs could not be targeted with Mel monotherapy. This is similar to our findings; DMCs could not be targeted with Btz alone. They

also found that DMCs can interact with the BMME around them, like OB and OC (Khoo et al., 2015; Lawson et al., 2015). A study by Adomako *et al.* (2015) treated quiescent U266 *in vitro* and *in vivo* and illustrated that Btz have delayed disease recurrence; cells have stayed in a dormant state for a long time (Adomako et al., 2015). Our study could not target DMCs with Btz, which could be explained by the presence of OB in BM, which maintained DMCs in a dormant state and resisted treatment. Our findings are consistent with the study conducted by Accardi *et al.* (2015). Their study demonstrated the role of Btz in bone remodelling and its ability to regulate bone formation, increase bone mineral density, and potentially contribute to a decline in OC (Accardi et al., 2015). Unfortunately, Pan and the combination of Btz with Pan treatments were stopped early in the project because their toxicity caused some side effects observed in mice.

Recent clinical studies have indicated that the combination of drugs for eradicating tumour cells shows promise in achieving a higher survival rate, particularly when using the Btz and Pan combination (Laubach et al., 2020; Richardson et al., 2013; Kikuchi et al., 2010; Ocio et al., 2010). These studies focused on proliferating myeloma cells. As a result, we aimed to target DMCs in both *in vitro* and *in vivo* settings. Chapter 4 specifically investigated the impact of combining Btz and Pan on DMCs *in vitro*. A PI, such as Btz, can prevent protein breakdown and promote aggresome formation. In addition, Btz can suppress adhesion molecule expression and inhibit angiogenesis. Also, it can inhibit the NFκβ canonical pathway in haematological malignancies (Wang et al., 2020; Suvannasankha & Chirgwin, 2014). On the other hand, a HDACi, like Pan, has the ability to hinder histone-DNA binding and reduce vascular proliferation, limiting the oxygen supply and nutrients to the myeloma cells. The rationale for using these inhibitors together is the different mechanisms of action, which can modulate multiple pathways like cell survival, proliferation, and dormancy by affecting protein stability and gene expression (Laubach et al., 2015; Moreau et al., 2012; Hideshima, Richardson, & Anderson, 2011). Also, this could explain why we had a significant reduction in DMCs *in vitro*.

Tracking dormancy with DID label was discussed previously in Chapter 3, as Yumoto *et al.* (2014), Lawson *et al.* (2015), and Wang *et al.* (2015) used DID dye to track dormancy in live cells *in vitro* and *in vivo* (Lawson et al., 2015; Wang et al., 2015; Yumoto et al., 2014). Based on these studies, this research used DID, a fluorescent lipophilic dye, to label non-dividing

cells. Then, Ki67, a proliferation marker, was used to detect the presence of nuclear antigens associated with cell division. $Ki67^-$ indicates quiescence or dormant cells, while $Ki67^+$ means that these cells are active and have the ability to proliferate. AXL is a tyrosine kinase ligand over-expressed on dormant cell surfaces and associated with dormancy in various cancers (Khoo et al., 2019). Finally, to ensure the absence of apoptotic cell death, Annexin V was employed, confirming the viability of the dormant cell population. This multi-marker strategy strengthens the confidence in our investigation. Our approach was similar to the method used by Wang *et al.* (2015) for tracking dormant prostate cells by labelling the cells with DID and Ki67. Also, Lawson *et al.* (2015) used DID and Ki67 for dormancy and confirmed that DMCs are in the G0 phase of the cell cycle and CMDiL labelling to determine the location of the DMCs. In contrast, Yu (2016) used a different method by labelling AML cells with PKH26 red fluorescent dye to track AML dormant cells. The PKH26 dye is similar to the DID dye but has some limitations. While it is used for cell proliferation studies and labelling exosomes and extracellular vesicles, PKH26 could produce false positive results. Therefore, DID labelling is considered a more potent dye with fewer limitations (Yu, 2016; Lawson et al., 2015; Wang et al., 2015).

Looking at the flow cytometry data this showed that Btz and Pan are used individually and in combination. At the early stage of the disease (day 7), our data showed no clear effect on the DMCs with all treatments, which could be explained by the fact that most DMCs have not been homed to BM yet. This finding supports the notion proposed by Lawson *et al.* (2015) that myeloma cells have the ability to recirculate for several days before settling in the BM (Lawson et al., 2015). Therefore, the cessation of the Pan and the combination of Btz and Pan were due to its hurtful effect on mice. Consequently, the study progressed with the Btz treatment until the end. Regrettably, at the end stage of the disease, the Btz treatment could not target DMCs, with no difference between the vehicle and the treated group therefore, more studies could be done to confirm if these cells were truly in a dormant state or slow proliferating cells. These were similar to the findings of Lawson *et al.* (2015), which showed that DMCs were resistant to Mel (Lawson et al., 2015). This could be due to the increase of OB that kept the DMCs in their dormant state; therefore, they resist the Btz treatment. This confirms the concept by Lawson *et al.* (2015) that the state of dormancy is reversible and can be switched “on” and

"off" by the BMME. Moreover, the 1q21 chromosomal region, often mutated in JJN3 cells, carries genes for proteasome components. Overexpression of these components can increase proteasome activity, reducing JJN3 cell sensitivity to Btz. JJN3's Btz resistance is likely multifactorial, involving microenvironment changes like OB and OC and gene mutation (Marianna D'Anca, 2016; An et al., 2013). One more explanation of DMCs resistance to Btz is that overexpressed AXL on the DMC cell surface allows these cells to interact with the BMME. This interaction activates the GAS6/AXL pathway, which halts cell proliferation, and increases survival, consequently increasing Btz resistance. AXL also plays a role in supporting and maintaining the supportive niche within the BM for myeloma cells (Yeo et al., 2023; Zhai et al., 2023; Yan et al., 2019; Zhu, Wei, & Wei, 2019).

Therefore, further research exploring various drug combinations to target different myeloma cell vulnerabilities is crucial for achieving complete remission in MM.

5.4.1 Conclusion

An *in vivo* myeloma model, using NSG female mice inoculated with JJN3-GFP-DID cells, then treated with Btz or Pan monotherapy and in combination, was used to study drug efficacy on DMCs. Mice treated with Btz monotherapy showed reduced total tumour growth and improved bone health, whilst Pan monotherapy and combination therapy with Btz resulted in adverse effects, which led to these groups of mice being discontinued in the study early. This suggests a lower dosage of Pan should be used for future studies. Regardless of that, the DMCs were not eliminated by Btz alone, potentially due to the increased OB numbers, which may have caused the DMCs to stay dormant and resist Btz treatment. So, this adds to the knowledge that the BMME plays a pivotal role in myeloma cell dormancy, and the Btz works to manipulate the BMME and could be used to keep DMCs in a dormant state.

Chapter 6 General Discussion

6.1 General Discussion

MM is a haematological malignancy that is characterised by the overproduction of plasma cells within the BM. This malignancy, over time, will replace the BM cells and disrupt normal bone homeostasis, which will lead to skeletal, haematological, and organ complications called the CRAB criteria, including hypercalcemia, renal failure, anaemia, and bone lytic lesions with fractures. Whilst current therapies reduce remission, disease relapse remains a significant challenge. Recent research suggests that BMME plays a pivotal role in this process. DMCs that resist current treatments are believed to be the main cause of the relapse. These cells are known to interact with the surrounding cells of the BMME, such as stromal cells, cytokines, bone cells, and extracellular matrix. This interaction will allow the DMCs to be turned "on" and "off" for a specific period (Dadzie & Green, 2022; Khoo et al., 2019; Lawson et al., 2015). Understanding the specific mechanism of the DMCs homing BM and how they could be targeted is crucial for developing an effective therapeutic strategy to eradicate them. Different treatments with various mechanisms of action are used to eradicate myeloma proliferating cells, but there is limited research on studying the effect of these drugs on DMCs. The interaction of dormancy with the microenvironment, homing to the BM and the potential impact of SoC treatments on the viability of DMCs were detailed in Chapter 1. This potential impact underscores the need for further research. Thus, this PhD thesis aims to assess the efficacy of SoC treatments on DMCs inside their BM niche for the first time. There are two important considerations: First, to find the effect of SoC drugs on DMCs *in vitro*, and second, to find the effect of the SoC drugs *in vivo*.

The study began with determining the optimum cell density (2500 or 5000 cells/wells), which was then used in subsequent assessments to monitor dormancy over 21 days and in drug assays. Then, to track the presence of DMCs *in vitro* in monoculture in four myeloma cell lines (5TGM1, JJN3, OPM2, and U266), DID, a lipophilic membrane fluorescence dye, was used to identify DMCs, slow-dividing, and dividing cells. The DMCs retained the dye whilst the dividing cells diluted it over time. The latter study used flow cytometry and fluorescence imaging for assessment. After optimising the DID dye concentration and time of incubation, the study showed that cells tended to lose the DID labelling by half after days 7 and 10, and the small number of cells retained the DID on days 17 and 21 were the DMCs. The murine

5TGM1 and human JJN3 cell lines were fast-growing cells, so their DID^{high}-labelled cells were sorted on day seven. The human OPM2 and U266 cells were slow-growing, so they were DID^{high} isolated on day 10. Subsequently, it was suggested to sort and isolate DID^{high}-labelled cells at their exponential/ log phase before entering the plateau phase or before all cells had lost their DID^{high} labelling, then apply the treatments to the sorted cells (chapter 3). Our research findings were consistent with other studies, such as Lawson *et al.* (2015), Chen *et al.* (2019), and Khoo *et al.* (2019). We used flow cytometry and fluorescent imaging to evaluate DMCs over time using DID dye. Lawson *et al.* (2015) and Chen *et al.* (2019) found that lipophilic dyes like DID and PKH were transferred to daughter cells in myeloma cells, becoming diluted and eventually lost as the cells proliferated. The cells retaining the dye were identified as DMCs (Chen et al., 2019; Lawson et al., 2015). In Wang *et al.* (2015), a similar methodology to ours was used to track dormant PC3 prostate cancer cells using DID (Wang et al., 2015).

In this thesis, four different SoC drugs were chosen, each with a different mechanism of action. Btz disrupts protein recycling, Mel is an alkylating agent, Pom is a second-generation IMiDs with antiproliferative properties, and Pan is an HDACi being developed to treat tumours. The concept of combining different SoC agents is to target DMCs with various pathways through multiple mechanisms of action, reduce resistance to single drug, enhance the efficacy of drugs, targeting cancer cells cycle different phases, and overall to improve patients' outcomes.

Initially, the IC_{50} values of each drug on each MM cell line were determined using AlamarBlue to assess cell viability. The study has used low cell densities of 2500 and 5000 cells/ well in a 96-well plate to provide even drug distribution and nutrients for the myeloma cells. A wide range of drug concentrations was used for each drug (Btz 0.5, 1, 1.5, 2, 2.5, 5, 10, 20, and 30 nM, Mel 1, 5, 10, 20, 50, and 100 µM, Pom 0.1, 0.01, 0.001, 1, 10, and 100 µM, and Pan 5, 10, 15, 20, 50, and 100 nM). MM cell lines showed sensitivity to Btz with IC_{50} values ranging from 6.18 to 40.25 nM for both cell densities. Also, the myeloma cells were susceptible to Mel, and the IC_{50} ranged from 6.76 to 94.08 µM. Only the OPM2 showed sensitivity to Pom after 5 days of treatment with a range of 0.30 and 0.06 µM. Lastly, Pan's IC_{50} values ranged between 15.67 to 26.70 nM for all four MM cell lines (Table 4.1).

Following this, the study focused on OPM2 and JJN3 to determine the most effective drug combination on DID^{high}-sorted cells *in vitro*. The OPM2 DID^{high} exhibited a response and sensitivity to single drugs as well as the combination of Btz with Mel, compared to Btz alone, Btz with Pan compared to Btz, and Mel with Pan compared to Mel. Conversely, the JJN3 DID^{high} exhibited sensitivity to single treatments and the combination of Btz and Pan compared to Btz alone. The observed variations may be attributed to the cells' behaviour and the cell culture conditions, such as seeding density or the number of isolated cells. It is crucial to consider these factors when interpreting the experiment's outcomes, as the sorting process is known to have an impact on the cell's viability through different factors such as shear stress, temperature, buffer solution, nozzle size and pressure, and collection process, these factors could increasing stress on cells that could cause them to become fragile and decrease cell viability (Cheetham et al., 2024).

Previous papers have indicated that the combination of Pan and Btz is remarkably potent (Laubach et al., 2015). As shown in our study, OPM2 DID^{high} and JJN3 DID^{high} cells (potential DMCs) were sensitive to the combination of Pan and Btz, supporting the findings of Laubach *et al.* (2015) on proliferating cells. However, while Laubach *et al.* (2015) mentioned the synergy between Pan and Btz, they did not address DMCs. While most studies have emphasised the efficacy of individual treatments with SoC agents on proliferating cells, our findings suggest that combination therapy could be a promising opportunity to explore. This is particularly interesting given the lack of studies focusing on DMCs in this research area (Ramakrishnan et al., 2014; Ocio et al., 2010; Horton et al., 2006). Khoo *et al.* (2019) identified a gene signature for dormancy. Thus, to enhance our study, we could emphasise the dormancy status by examining the expression of dormancy genes in the myeloma cell lines and treating the cells with single or combined SoC agents (chapter 4).

Limited studies have focused on DMC characterisation, interaction with surrounding areas and targeting them with therapy (Dadzie & Green, 2022a; Chen et al., 2019; Khoo et al., 2019; Lawson et al., 2015). Furthermore, Lawson *et al.* (2015) were one of the first studies investigating targeting DMCs and found that they were Mel resistant, but Btz could target cells in their slow proliferative state. It has been thought that Btz could promote apoptosis in quiescent myeloma cells by activating pro-apoptotic pathways (Lawson et al., 2015).

Therefore, based on our results in chapter four, we focused on using the JJN3 cell line to treat it with the combination of Btz and Pan to find their effect on DMCs in subsequent *in vivo* studies.

Thus, chapter 5 investigated the effect of Btz and Pan single and combined. An *in vivo* model of myeloma growth in bone was used by injecting the JJN3-GFP-Luc-DID human myeloma cell line into female NSG mice aged six to eight weeks. The goal was to mimic human disease and assess the effect of combining Btz and Pan treatments on DMCs. For longer life span, most studies used 6 to 8 weeks old female mice to avoid unstructured variances (Smarr & Kriegsfeld, 2022; Liu et al., 2022; Lawson et al., 2015; Lawson et al., 2015b). 57 female mice were used in the study. Five groups of mice were assigned; each group contained 13 mice (vehicle, Btz, Pan, or a combination of Btz with Pan groups). The naïve group had 5 mice, as a baseline control for healthy mice. The sample size was determined based on Lawson *et al.* (2015) study and GPower 3.1 software. The Data was extracted from Lawson *et al.* (2015) paper to be used to calculate our study sample size, which examined the impact of Mel on 5TGM1 DMCs in the C57BL/6 mice model (Lawson et al., 2015). The study was designed for a period of 21 days as the JJN3 cells are known to result in an aggressive myeloma model (3 weeks duration) that has a fast progression to bone in NSG mice. Our model developed myeloma in bone as previously described by Lawson *et al.* (2015b) using JJN3 cells in NSG mice (Lawson et al., 2015b). The tumour burden increased aggressively in the vehicle group, while the Btz-treated group had a lower tumour burden. However, the Pan-treated group and the combination of Btz with Pan stopped early due to Pan's toxicity, with no changes in bone observed at that time point.

Our study also showed an obvious increase in bone lesions and a reduction in % BV/TV and Tb.Th in the vehicle group compared to non-tumour controls. This was similar to previous studies that used NSG mice with human JJN3, U266, OPM2 cells, and C57BL/6 mice with murine 5TGM1 cells to investigate a murine model for myeloma bone disease when treated with anti-myeloma drugs (Paton-Hough et al., 2019; Lawson et al., 2015b; Paton-Hough, Chantry, & Lawson, 2015; Miyakawa et al., 2004). The thesis showed that the Btz-treated group had lower numbers of bone lesions and improved BV/TV and Tb.Th, with increased numbers of OB compared to the vehicle-treated group. Our findings were consistent with other studies that have shown that Btz affects the microenvironment of myeloma cells and positively

impacts bones by promoting bone formation through the stimulation of OB. In contrast, Pan can decrease bone lesions too, yet can reduce trabecular thickness density (Wang et al., 2020; Accardi et al., 2015; Ocio et al., 2010). Sadly, at the early stage of the disease (day 7), due to the observed toxicity of Pan in mice resulted in a halt to the procedure with Pan and the combination of Btz and Pan treatments. No signs of bone alteration were observed at the early stage of the disease.

The histological analysis in our study showed a significant reduction in tumour cells with Btz treatment compared to the vehicle group at the end stage of the disease (day 19), and the Pan alone and Btz combined with Pan had a negative impact on the BM, causing most cells to appear atrophic in the early stage of the disease (day 7), potentially due to toxicity. Moreno *et al.* (2022) and Homan *et al.* (2021) prevent using a dosage of Pan that could have harmful side effects on mice (Moreno et al., 2022; Homan et al., 2021; Hennika et al., 2017).

DMCs' resistance to Btz in our study was similar to Lawson *et al.'s* (2015), who found that DMCs were resistant to Mel. They also observed that the BMME plays an essential role in controlling the DMC's viability when interacting with OBs and OCs (Lawson et al., 2015). The OB plays a role in bone remodelling, regulating bone formation, increasing bone mineral density, and could halt OC from bone destruction in different ways, as OB can bind to RANKL instead of OC through the secretion of Osteoprotegerin. Also, there is a direct interaction between OB and OC that induces inhibition or differentiation of the OCs. Plus, OB can promote activation and inhibition of OC through WNT signalling (Kim et al., 2020). On the other hand, OBs can affect DMC by keeping them in a dormant state and halting them from dividing and forming tumours. This could explain why DMCs resist Btz treatment in this thesis (Lawson et al., 2015). Furthermore, the JJN3 gene mutation, like the 1q21 chromosomal region, which is correlated to increased expression of proteasome subunits, can lead to higher proteasome activity, making JJN3 resistant to Btz (Marianna D'Anca, 2016; An et al., 2013).

Therefore, using a combination of drugs could potentially overcome the DMC resistance to single drugs. Studies have suggested that combined treatments can achieve higher survival rates, such as combining Btz and Pan (Laubach et al., 2020; Richardson et al., 2013; Kikuchi et al., 2010; Ocio et al., 2010). Although assessing efficacy on proliferating myeloma cells was the main focus of these studies. Accordingly, we targeted DMCs in both *in vitro* and *in vivo*

settings, specifically studying the effect of combining Btz and Pan on DMCs *in vitro*. A PI, such as Btz, can stop protein breakdown and promote aggresome formation. In addition, Btz can suppress adhesion molecule expression and inhibit angiogenesis. It can inhibit the NFκβ canonical pathway in haematological malignancies (Wang et al., 2020; Suvannasankha & Chirgwin, 2014). Oppositely, a HDACi, like Pan, can delay histone-DNA binding and lower vascular proliferation, reducing the oxygen supply and nutrients to the myeloma cells. Using these drugs together can be a powerful treatment approach for targeting multiple pathways and increasing the destruction of DMCs (Laubach et al., 2015; Moreau et al., 2012; Hideshima, Richardson, & Anderson, 2011). A study by Wirries *et al.* (2018) has illustrated that Pan has the ability to reduce OBs. Wirries *et al.* (2018) have found that Pan potently treats osteosarcoma with an obvious decrease in OBs (Wirries et al., 2018). Btz has an anabolic effect on bone maintenance by stimulating OB growth, while Pan has the ability to reduce OBs. There is evidence to suggest that the combination of Btz with Pan can lead to an increase in OC and help defeat DMCs' resistance to Btz.

The drug dosages used in this thesis were based on previous literature (Robinson et al., 2022; Savvidou et al., 2022; Imai et al., 2016; Lawson et al., 2015; Sanchez et al., 2013; Ocio et al., 2010; Wipt et al., 2010). Btz was given at 0.5 mg/kg twice a week via the IP route, Pan was given at 20 mg/kg five times per week via the IP route, and the Btz and Pan combined were given as a mix of both. However, the procedure was stopped early due to the harmful effects observed in mice, such as hunching, lack of locomotion, loss of appetite, ruffled fur, and atrophic cells in the BM. Moreno *et al.* (2022) treated NSG mice with a lower dose of 5 mg/kg of Pan, and Homan *et al.* (2021) used a 15 mg/kg IV dose; in both studies, no side effects were reported (Moreno et al., 2022; Homan et al., 2021). Therefore, using a lower dosage of Pan or changing the administration route to oral instead of IP could help overcome this issue in the future.

Our study used a multi-marker strategy approach to strengthen the detection of DMCs. It used the lipophilic dye DID to track dormancy over time, as the dye tends to be diluted over time through proliferation (chapter 3). Our *in vivo* study used DID to track the presence of DMC inside the NSG mice' BM niche. Many studies used DID as a dormancy marker to track dormant cells *in vitro* and *in vivo* (Lawson et al., 2015; Wang et al., 2015; Yumoto et al., 2014).

Besides, a proliferation marker, Ki67, was applied to detect the presence of nuclear antigens correlated to cell division; therefore, DMCs will be negative to the Ki67 marker as they are not proliferating. Then, AXL, a tyrosine kinase ligand associated with dormancy, is usually overproduced in DMCs (Khoo et al., 2019). Lastly, Annexin V was used to confirm the absence of apoptotic cell death. Our methodology closely resembled the approach implemented by Wang *et al.* (2015) in tracking dormant prostate cells through the utilisation of DID and Ki67 labelling (Wang et al., 2015). Similarly, Lawson *et al.* (2015) employed DID and Ki67 in dormancy tracking and affirmed the placement of DMCs in the G0 phase of the cell cycle. Furthermore, CMDiL labelling was used to ascertain the location of the DMCs when 5TGM1-DID cells were isolated and re-injected into recipient BKAL mice (Lawson et al., 2015). Similarly, Yu (2016) adopted an alternative method by utilising PKH26 red fluorescent dye to track dormant AML cells (Yu, 2016). The PKH26 dye was discovered and named after Paul Karl Horan; it has an excitation wavelength of 551 nm and an emission wavelength of 567 nm. It is mainly used for proliferation and cell-tracking studies and is basically equivalent to the DID dye series. Flow cytometry could also assess it, which is parallel to the DID method, as they both work on cell membrane binding to the lipid bilayer, the DID method explained in (section 2.2.4) (Quayle et al., 2018; Fischer & Mackensen, 2003). Moreover, labelling with PKH demands a suspension of cells in an isosmotic mannitol-based medium, while the DID dye can be applied directly to a culture medium. Despite its application in cell proliferation studies, exosome, and extracellular vesicle labelling, PKH26 has the potential to yield false positive results, like binding to non-specific cell debris or other particles (Dehghani et al., 2020; Quayle et al., 2018; Yu, 2016; Fischer & Mackensen, 2003). Additionally, DID is more potent and stable. It is important to use appropriate controls, optimise labelling conditions, and ensure proper sample handling.

In this thesis, Btz and Pan were used in monotherapy and combination therapy to determine their effect on JJN3-DMCs. Two stages of the *in vivo* experiment were studied; flow cytometry data indicated that the treatments had no effect on the DMCs observed in the early stage of the disease (day 7). In addition, we observed resistance of JJN3-DMCs to Btz monotherapy at the late stage of the disease (day 19). This aligns with the finding by Lawson *et al.* (2015), who found that the DMCs recirculate for several days before homing in the BM endosteal niche by

using real-time intravital two-photon microscopy. Plus, 5TGM1-DMCs were resistant to Mel monotherapy, while the Btz could reduce tumour burden and target both dividing and non-dividing cells, but the reduction in the 5TGM1-DMCs appears to be complex (Lawson et al., 2015). As highlighted by Lawson *et al.* (2015), the BMME can exert a deep influence on the dormancy state of DMCs. OBs and OCs within the BMME can interact with DMCs, potentially maintaining their dormant state or reactivating them under specific conditions. This dynamic interplay between DMCs and the BMME may explain the observed resistance to Btz monotherapy and the potential for DMC reactivation even after significant tumour reduction (Lawson et al., 2015). In the context of the observed Btz resistance in DMCs, one more contributing factor that may play a role in BMME interaction with DMCs is the overexpression of AXL on the DMC surface. This highlighted AXL expression facilitates interaction with the BMME, leading to activation of the GAS6/AXL pathway. This pathway activation appears to promote cell survival while simultaneously suppressing proliferation, ultimately contributing to the observed drug resistance in dormant cells. Furthermore, AXL's role extends to the maintenance of a supportive niche within the BM, further shielding myeloma cells from therapeutic interventions (Yeo et al., 2023; Zhai et al., 2023; Yan et al., 2019; Zhu, Wei, & Wei, 2019).

The findings of our study, in conjunction with those of Lawson *et al.* (2015), underscore the importance of targeting both the tumour cells and the microenvironment in the treatment of myeloma. Strategies that disrupt the effects of the BMME on DMCs may be essential for achieving durable disease control and preventing relapse

6.1.1 Conclusions

This study has used a method to target DMCs *in vitro* and *in vivo* with SoC drugs. The *in vitro* investigation was initiated by labelling DMCs with DID dye in monoculture in four myeloma cell lines: 5TGM1, JJN3, OPM2, and U266 to track the presence of DMCs. Then the thesis aimed to investigate the impact of SoC agents such as Btz, Mel, Pan, and Pom on DMCs on JJN3, OPM2, and U266 due to insufficient research on the effect of SoCs on DMCs. Therefore, the study focused on OPM2 and JJN3 cell lines to isolate their DID^{high}-labelled cells and employed the combined treatment to assess the effect on DMCs. It was observed that OPM2

DID^{high} cells were more sensitive to single and combined agents, like the combination of Btz with Mel compared to Btz, Btz with Pan compared to Btz, and Mel with Pan compared to Mel, than JJN3 DID^{high} cells. The JJN3 DID^{high} cells were only sensitive to the combination of Btz and Pan.

Finally, an *in vivo* study was conducted on NSG mice injected with JJN3-GFP-DID cells and then treated with Btz, Pan, and a combination of both. Due to Pan's toxicity, the experiment ended the Pan treatment and followed up with Btz. The early stage of the disease (day 7) showed no change in bone health or tumour burden with all treatments. While the late stage of the disease (day 19) observed BM replacement with myeloma cells in vehicle mice, compared to Btz treatment, The Btz has lowered tumour burden with reduced bone destruction. Also, the Btz has halted OC from bone destruction. The survival and Btz resistance of DMCs were significantly influenced by a complex of BMME factors, including OB, OC, and AXL. This interaction appears to have fostered a dormant state and conferred resistance to Btz.

Despite the promising *in vitro* findings, the *in vivo* study was unable to fully validate our hypothesis due to the premature termination of the Pan treatment. This limitation significantly impacted our ability to assess the effectiveness of drug combinations in targeting DMCs.

6.1.2 Future Work

Regarding time limitations, further research is needed to develop targeted therapies for DMCs, including testing a broader range of SoC drugs or combining SoC agents with novel treatments such as oncolytic viruses (OVs). For example, Stewart *et al.* (2021) suggested combining OVs with SoC agents to stop relapse (Stewart et al., 2021). Also, co-culture myeloma cells with osteoblast-like (MG63 and MC3T3) or human foetal osteoblast cells (hFOb) should increase DMCs to have a high number of DMCs, then apply combined drugs. Many studies have tested newly diagnosed myeloma patient samples. Thus, it is suggested that more similar studies could be conducted on primary myeloma patient DMCs CD138 sorted cells could be labelled with a lipophilic dye like DID and co-cultured with osteoblast-like cells to induce dormancy to investigate the anti-myeloma drug sensitivity (Chen et al., 2019; Lawson et al., 2015).

AXL has been suggested as a poor prognostic marker, while TRIM44 is still under investigation, but some studies have suggested high expression of TRIM44 leads to poor

outcomes(Chen et al., 2019; Khoo et al., 2019; Zhu, Wei, & Wei, 2019). Moreover, studies focused on targeting AXL as it is over-expressed on DMCs; therefore, reducing AXL will cause the reactivation of dormant cells, and then they will be rendered to be targeted by chemotherapy. This has been suggested as a potential therapeutic strategy to eliminate dormant cells (Yeo et al., 2023; De Veirman et al., 2019; Shiozawa et al., 2010; Yan et al., 2019; Zhu et al., 2019). On the other hand, this method could be a risky strategy as it could reactivate many types of dormant cells in many niches of the body, such as the liver, lung, brain, and perivascular niche (Mukherjee & Bravo-Cordero, 2023).

Despite significant improvements in MM treatment, relapse remains a major hurdle. DMCs residing in the BMME are believed to be a key contributor to relapse. While our research had identified potential mechanisms of resistance to Btz in a mouse model of myeloma, it is crucial to gain a more comprehensive understanding of these elusive cells. Therefore, further research is warranted, employing both *in vivo, ex vivo* studies and patients' peripheral blood before validating clinical trials. Our data highlights the complex interplay between the tumour and BMME, AXL, and drug resistance, suggesting that targeting these pathways may hold promise for future therapeutic strategies. Furthermore, the presence of trisomy 21 within myeloma cells has been linked to worse overall survival in MM in individuals with trisomy 21, also known as Down syndrome. The relationship between trisomy 21 within myeloma cells and the mechanisms controlling dormancy, potentially involving genes like AXL and Trim44, requires further investigation to determine if trisomy 21 status could offer a specific prognostic understanding of this particular state of myeloma.

Lastly, regarding time limitation we could not investigate the presence of DMCs inside their BM endosteal niche, which could be illustrated under a fluorescence microscope, will allow us to illustrate the presence of DMCs inside the BM niche, bone samples could be embedded into a gelatine medium in order to avoid DID labelling elimination during calcium removal and tissue processing procedure. By combining these approaches, we can gain a deeper understanding of DMCs and develop more effective therapies to eradicate them, ultimately improving patient outcomes.

References

Abduh, M. S. (2024). An Overview of Multiple Myeloma: A Monoclonal Plasma Cell Malignancy's Diagnosis, Management, and Treatment Modalities. *Saudi Journal of Biological Sciences*, 31(2), 103920. Retrieved July 20, 2024, from https://linkinghub.elsevier.com/retrieve/pii/S1319562X23003650

Accardi, F., Toscani, D., Bolzoni, M., Dalla Palma, B., Aversa, F. & Giuliani, N. (2015). Mechanism of Action of Bortezomib and the New Proteasome Inhibitors on Myeloma Cells and the Bone Microenvironment: Impact on Myeloma-Induced Alterations of Bone Remodeling. *BioMed Research International*, 2015, 1–13. Retrieved from http://www.hindawi.com/journals/bmri/2015/172458/

Adams, J., Palombella, V. J., Sausville, E. A., Johnson, J., Destree, A., Lazarus, D. D., Maas, J., Pien, C. S., Prakash, S. & Elliott, P. J. (1999). Proteasome Inhibitors: A Novel Class of Potent and Effective Antitumor Agents. *Cancer research*, 59(11), 2615–22. Retrieved from http://www.ncbi.nlm.nih.gov/pubmed/10363983

Adomako, A., Calvo, V., Biran, N., Osman, K., Chari, A., Paton, J. C., Paton, A. W., Moore, K., Schewe, D. M. & Aguirre-Ghiso, J. A. (2015). Identification of Markers That Functionally Define a Quiescent Multiple Myeloma Cell Sub-Population Surviving Bortezomib Treatment. *BMC Cancer*, 15(1), 444.

Aguirre-Ghiso, J. A. (2006). The Problem of Cancer Dormancy: Understanding the Basic Mechanisms and Identifying Therapeutic Opportunities. *Cell Cycle*, 5(16), 1740–1743.

Aguirre-Ghiso, J. A. (2007). Models, Mechanisms and Clinical Evidence for Cancer Dormancy. *Nature Reviews Cancer*, 7(11), 834–846. Retrieved from https://doi.org/10.1038/nrc2256

Ahmed Al-Anazi, K. (2023). Multiple Myeloma in the Era of Novel Agents and Stem Cell Therapies, in: *Recent Updates on Multiple Myeloma*. IntechOpen. Retrieved from https://www.intechopen.com/chapters/85536

Al-Amer, O. (2015). Homing of Myeloma Cells into Calvarial Bone Using Myeloma Murine Models. *International Journal of Health Sciences and Research*, 5(7), 357–363.

Ali, A. I., Wang, M., von Scheidt, B., Dominguez, P. M., Harrison, A. J., Tantalo, D. G. M., Kang, J., Oliver, A. J., Chan, J. D., Du, X., Bai, Y., Lee, B., Johnstone, R. W., Darcy, P. K., Kershaw, M. H. & Slaney, C. Y. (2021). A Histone Deacetylase Inhibitor, Panobinostat, Enhances Chimeric Antigen Receptor T-Cell Antitumor Effect Against Pancreatic Cancer. *Clinical Cancer Research*, 27(22), 6222–6234. Retrieved from https://aacrjournals.org/clincancerres/article/27/22/6222/671763/A-Histone-Deacetylase-Inhibitor-Panobinostat

Al-Nasiry, S., Geusens, N., Hanssens, M., Luyten, C. & Pijnenborg, R. (2007). The Use of Alamar Blue Assay for Quantitative Analysis of Viability, Migration and Invasion of Choriocarcinoma Cells. *Human Reproduction*, 22(5), 1304–1309. Retrieved from http://academic.oup.com/humrep/article/22/5/1304/2914638/The-use-of-Alamar-Blue-assay-for-quantitative

Althwaiqeb, S. A. & Bruno, B. (2024). Histology, B Cell Lymphocyte, in: Treasure Island (FL): StatPearls Publishing. Retrieved from https://www.ncbi.nlm.nih.gov/books/NBK560905/?report=printable

Altogen labs. (2024). OPM2 Xenograft Model. Retrieved July 10, 2024, from https://altogenlabs.com/xenograft-models/lymphoma-xenograft/opm2-xenograft-model/

An, G., Xu, Y., Deng, S., Zou, D., Sui, W., Shi, L., Zhan, F. & Qiu, L. (2013). Chromosome 1q21 Gains Confer Inferior Outcomes in Multiple Myeloma Treated with Bortezomib but Copy Number Variation and Percentage Of Plasma Cells Involved Have No Additional Prognostic Value. *Blood*, 122(21), 1992–1992.

Arber, D. A., Orazi, A., Hasserjian, R., Thiele, J., Borowitz, M. J., Le Beau, M. M., Bloomfield, C. D., Cazzola, M. & Vardiman, J. W. (2016). The 2016 Revision to the World Health Organization (WHO) Classification of Myeloid Neoplasms and Acute Leukemia. *Blood*, 127(20), blood-2016-03-643544. Retrieved from http://www.ncbi.nlm.nih.gov/pubmed/27069254

Atadja, P. (2009). Development of the Pan-DAC Inhibitor Panobinostat (LBH589): Successes and Challenges. *Cancer Letters*, 280(2), 233–241. Retrieved from http://dx.doi.org/10.1016/j.canlet.2009.02.019

Attal, Michel, Lauwers-Cances, Valerie, Hulin, Cyrille, Leleu, Xavier, Caillot, Denis, Escoffre, Martine, Arnulf, Bertrand, Macro, Margaret, Belhadj, Karim, Garderet, Laurent, Roussel, Murielle, Payen, Catherine, Payen, Catherine, Mathiot, Claire, Fermand, Jean P., Meuleman, Nathalie, Rollet, Sandrine, Maglio, Michelle E., Zeytoonjian, Andrea A., Weller, Edie A., Munshi, Nikhil, Anderson, Kenneth C., Richardson, Paul G., Facon, Thierry, Avet-Loiseau, Hervé, Harousseau, Jean-Luc, Moreau, Philippe (2017). Lenalidomide, Bortezomib, and Dexamethasone with Transplantation for Myeloma. *New England Journal of Medicine*, 376(14), 1311–1320.

Barwick, B. G., Gupta, V. A., Vertino, P. M. & Boise, L. H. (2019). Cell of Origin and Genetic Alterations in the Pathogenesis of Multiple Myeloma. *Frontiers in Immunology*, 10.

Benoit Tessoulin, Agnes Moreau-Aubry, Alban Gaignard, Martine Amiot & Catherine Pellat-Deceunynck. (2017). Human Myeloma Cell Lines Mutation Landscape: Toward a Rationale Use of Cell Lines to Assess Drug Efficacy Prediction in Myeloma. *Blood*, 130, 1770. Retrieved May 15, 2024,

Brookens, S. K., Cho, S. H., Paik, Y., Meyer, K., Raybuck, A. L., Park, C., Greenwood, D. L., Rathmell, J. C. & Boothby, M. R. (2024). Plasma Cell Differentiation, Antibody Quality, and Initial Germinal Center B Cell Population Depend on Glucose Influx Rate. *The Journal of Immunology*, 212(1), 43–56. Retrieved from https://journals.aai.org/jimmunol/article/212/1/43/266442/Plasma-Cell-Differentiation-Antibody-Quality-and

Carrasco, D. D. R. D. D. E., Sukhdeo, K., Protopopova, M., Sinha, R., Enos, M., Carrasco, D. D. R. D. D. E., Zheng, M., Mani, M., Henderson, J., Pinkus, G. S., Munshi, N., Horner, J., Ivanova, E. V., Protopopov, A., Anderson, K. C., Tonon, G. & DePinho, R. A. (2007). The Differentiation and Stress Response Factor XBP-1 Drives Multiple Myeloma Pathogenesis. *Cancer Cell*, 11(4), 349–360. Retrieved December 16, 2020, from https://linkinghub.elsevier.com/retrieve/pii/S153561080700061X

Catley, L., Weisberg, E., Kiziltepe, T., Tai, Y. T., Hideshima, T., Neri, P., Tassone, P., Atadja, P., Chauhan, D., Munshi, N. C. & Anderson, K. C. (2006). Aggresome Induction by Proteasome Inhibitor Bortezomib and α-Tubulin Hyperacetylation by Tubulin

Deacetylase (TDAC) Inhibitor LBH589 Are Synergistic in Myeloma Cells. *Blood*, 108(10), 3441–3449.

Chai, R. C., McDonald, M. M., Terry, R. L., Kovačić, N., Down, J. M., Pettitt, J. A., Mohanty, S. T., Shah, S., Haffari, G., Xu, J., Gillespie, M. T., Rogers, M. J., Price, J. T., Croucher, P. I. & Quinn, J. M. W. (2017). Melphalan Modifies the Bone Microenvironment by Enhancing Osteoclast Formation. *Oncotarget*, 8(40), 68047–68058. Retrieved January 28, 2022, from https://www.oncotarget.com/lookup/doi/10.18632/oncotarget.19152

Chakraborty, R. & Majhail, N. S. (2020). Treatment and Disease-related Complications in Multiple Myeloma: Implications for Survivorship. *American Journal of Hematology*, 95(6), 672–690. Retrieved from https://onlinelibrary.wiley.com/doi/abs/10.1002/ajh.25764

Chanan-Khan, A. A., Swaika, A., Paulus, A., Kumar, S. K., Mikhael, J. R., Rajkumar, S. V, Dispenzieri, A. & Lacy, M. Q. (2013). Pomalidomide: The New Immunomodulatory Agent for the Treatment of Multiple Myeloma. *Blood Cancer Journal*, 3(9), e143–e143. Retrieved from https://www.nature.com/articles/bcj201338

Chauhan, D., Ray, A., Viktorsson, K., Spira, J., Paba-Prada, C., Munshi, N., Richardson, P., Lewensohn, R. & Anderson, K. C. (2013). In Vitro and In Vivo Antitumor Activity of a Novel Alkylating Agent, Melphalan-Flufenamide, against Multiple Myeloma Cells. *Clinical Cancer Research*, 19(11), 3019–3031. Retrieved January 27, 2022, from /pmc/articles/PMC4098702/

Cheetham, M., Davies, D., Hall, C., Petersen, C. C., Schulte, R. & Walker, R. (2024a). Practicalities of Cell Sorting, in: (pp. 125–143).

Chen, J., Garssen, J. & Redegeld, F. (2021). The Efficacy of Bortezomib in Human Multiple Myeloma Cells Is Enhanced by Combination with Omega-3 Fatty Acids DHA and EPA: Timing Is Essential. *Clinical Nutrition*, 40(4), 1942–1953. Retrieved from https://linkinghub.elsevier.com/retrieve/pii/S0261561420304659

Chen, Z., Lin, T.-C., Bi, X., Lu, G., Dawson, B. C., Miranda, R., Medeiros, L. J., McNiece, I. & McCarty, N. (2019). TRIM44 Promotes Quiescent Multiple Myeloma Cell Occupancy

and Survival in the Osteoblastic Niche via HIF-1α Stabilization. *Leukemia*, 33(2), 469–486. Retrieved from https://doi.org/10.1038/s41375-018-0222-x

Chng, W. J., Glebov, O., Bergsagel, P. L. & Kuehl, W. M. (2007). Genetic Events in the Pathogenesis of Multiple Myeloma. *Best Practice & Research Clinical Haematology*, 20(4), 571–596. Retrieved from http://www.sciencedirect.com

Chretien, Marie-Lorraine, Corre, Jill, Lauwers-Cances, Valerie, Magrangeas, Florence, Cleynen, Alice, Yon, Edwige, Hulin, Cyrille, Leleu, Xavier, Orsini-Piocelle, Frederique, Blade, Jean-Sebastien, Sohn, Claudine, Karlin, Lionel, Delbrel, Xavier, Hebraud, Benjamin, Roussel, Murielle, Marit, Gerald, Garderet, Laurent, Mohty, Mohamad, Rodon, Philippe, Voillat, Laurent, Royer, Bruno, Jaccard, Arnaud, Belhadj, Karim, Fontan, Jean, Caillot, Denis, Stoppa, Anne-Marie, Attal, Michel, Facon, Thierry, Moreau, Philippe, Minvielle, Stephane, Avet-Loiseau, Hervé (2015). Understanding the Role of Hyperdiploidy in Myeloma Prognosis: Which Trisomies Really Matter? *Blood*, 126(25), 2713–2719. Retrieved from https://doi.org/10.1182/blood-2015-06-650242

Cruz, J., Alsina, M., Craig, F., Yoneda, T., Anderson, J. & Dallas, M. (2001). Ibandronate Decreases Bone Disease Development and Osteoclast Stimulatory Activity in an in Vivo Model of Human Myeloma. *Exp Hematol*, 29(4). Retrieved December 16, 2020,

Cruz, M. P. (2016). Lenalidomide (Revlimid): A Thalidomide Analogue in Combination With Dexamethasone For the Treatment of All Patients With Multiple Myeloma. *P & T : a peer-reviewed journal for formulary management*, 41(5), 308–13. Retrieved from http://www.ncbi.nlm.nih.gov/pubmed/27162471

Dadzie, T. G., Green, A. C. (2022). The Role of the Bone Microenvironment in Regulating Myeloma Residual Disease and Treatment. *Frontiers in Oncology*, 12. Retrieved from https://www.frontiersin.org/articles/10.3389/fonc.2022.999939/full

Damen, M. P. F., van Rheenen, J. & Scheele, C. L. G. J. (2020). Targeting Dormant Tumor Cells to Prevent Cancer Recurrence. *The FEBS Journal*, n/a(n/a). Retrieved from https://febs.onlinelibrary.wiley.com/doi/abs/10.1111/febs.15626

Dehghani, M., Gulvin, S. M., Flax, J. & Gaborski, T. R. (2020). Systematic Evaluation of PKH Labelling on Extracellular Vesicle Size by Nanoparticle Tracking Analysis. *Scientific Reports*, 10(1), 9533.

Dias, I. B., Bouma, H. R. & Henning, R. H. (2021). Unraveling the Big Sleep: Molecular Aspects of Stem Cell Dormancy and Hibernation. *Frontiers in Physiology*, 12.

Dispenzieri, A., Kyle, R. A. (2005). Multiple Myeloma: Clinical Features and Indications for Therapy. *Best Practice and Research: Clinical Haematology*, 18(4 SPEC. ISS.), 553–568.

van de Donk, N. W. C. J., Pawlyn, C. & Yong, K. L. (2021). Multiple Myeloma. *The Lancet*, 397(10272), 410–427.

Durie, B. G. M., Hoering, A., Abidi, M. H., Rajkumar, S. V., Epstein, J., Kahanic, S. P., Thakuri, M., Reu, F., Reynolds, C. M., Sexton, R., Orlowski, R. Z., Barlogie, B. & Dispenzieri, A. (2017). Bortezomib with Lenalidomide and Dexamethasone versus Lenalidomide and Dexamethasone Alone in Patients with Newly Diagnosed Myeloma without Intent for Immediate Autologous Stem-Cell Transplant (SWOG S0777): A Randomised, Open-Label, Phase 3 Trial. *Lancet (London, England)*, 389(10068), 519–527. Retrieved January 9, 2024, from https://pubmed.ncbi.nlm.nih.gov/28017406/

Edwards, C. M., Zhuang, J. & Mundy, G. R. (2008). The Pathogenesis of the Bone Disease of Multiple Myeloma. *Bone*, 42(6), 1007–1013. Retrieved April 9, 2022, from https://www.sciencedirect.com/science/article/pii/S8756328208000719?via%3Dihub#bib1

Eleutherakis-Papaiakovou, E., Kanellias, N., Kastritis, E., Gavriatopoulou, M., Terpos, E. & Dimopoulos, M. A. (2020). Efficacy of Panobinostat for the Treatment of Multiple Myeloma. *Journal of Oncology*, 2020.

Fischer, K. & Mackensen, A. (2003). The Flow Cytometric PKH-26 Assay for the Determination of T-Cell Mediated Cytotoxic Activity. *Methods*, 31(2), 135–142.

Flanagan, K., Majumder, M. M., Kumari, R., Miettinen, J., Slipicevic, A., Holstein, S. A., Varney, M. L., Suvela, M., Lehmann, F., Nupponen, N. N. & Heckman, C. A. (2019). In Vitro and InVivo Activity of Melflufen in Amyloidosis. *Blood*, 134(Supplement_1),

3100–3100. Retrieved from https://ashpublications.org/blood/article/134/Supplement_1/3100/423613/In-Vitro-and-inVivo-Activity-of-Melflufen-in

Fuhler, G. M., Brooks, R., Toms, B., Iyer, S., Gengo, E. A., Park, M. Y., Gumbleton, M., Viernes, D. R., Chisholm, J. D. & Kerr, W. G. (2012). Therapeutic Potential of SH2 Domain-Containing Inositol-5′-Phosphatase 1 (SHIP1) and SHIP2 Inhibition in Cancer. *Molecular Medicine*, 18(1), 65–75. Retrieved December 16, 2020,

Galustian, C., Meyer, B., Labarthe, M. C., Dredge, K., Klaschka, D., Henry, J., Todryk, S., Chen, R., Muller, G., Stirling, D., Schafer, P., Bartlett, J. B. & Dalgleish, A. G. (2009). The Anti-Cancer Agents Lenalidomide and Pomalidomide Inhibit the Proliferation and Function of T Regulatory Cells. *Cancer Immunology, Immunotherapy*, 58(7), 1033–1045. Retrieved April 15, 2022, from https://link.springer.com/article/10.1007/s00262-008-0620-4

Garrett, I. R., Dallas, S., Radl, J. & Mundy, G. R. (1997). A Murine Model of Human Myeloma Bone Disease. *Bone*, 20(6), 515–520.

Gay, F., Mina, R., Troia, R. & Bringhen, S. (2013). Pharmacokinetic Evaluation of Pomalidomide for the Treatment of Myeloma. *Expert Opinion on Drug Metabolism & Toxicology*, 9(11), 1517–1527. Retrieved from http://www.tandfonline.com/doi/full/10.1517/17425255.2013.827169

Ghiaur, G., Matsui, W., Alonso, S. & -, -. (2015). Bone Marrow Niche - Multiple Myeloma Cross-Talk Generates Bortezomib Resistance. *Blood*, 126. Retrieved from https://discovery.researcher.life/article/bone-marrow-niche-multiple-myeloma-cross-talk-generates-bortezomib-resistance/27e3187d40e037c7917f6ec06d9441e5

Giliberto, M., Santana, L. M., Holien, T., Misund, K., Nakken, S., Vodak, D., Hovig, E., Meza-Zepeda, L. A., Coward, E., Waage, A., Taskén, K. & Skånland, S. S. (2022). Mutational Analysis and Protein Profiling Predict Drug Sensitivity in Multiple Myeloma Cell Lines. *Frontiers in Oncology*, 12, 1040730. Retrieved May 15, 2024, from https://cellmass.cytobank.org/cytobank/

Gkotzamanidou, M., Terpos, E., Dimopoulos, M. A. & Souliotis, V. L. (2022). The Combination of Panobinostat and Melphalan for the Treatment of Patients with Multiple Myeloma. *International Journal of Molecular Sciences*, 23(24), 15671. Retrieved March 19, 2023, from https://www.mdpi.com/1422-0067/23/24/15671

González, D., van der Burg, M., García-Sanz, R., Fenton, J. A., Langerak, A. W., González, M., van Dongen, J. J. M., San Miguel, J. F. & Morgan, G. J. (2007). Immunoglobulin Gene Rearrangements and the Pathogenesis of Multiple Myeloma. *Blood*, 110(9), 3112–3121. Retrieved from https://doi.org/10.1182/blood-2007-02-069625

Growney, J. D., Atadja, P., Shao, W., Wang, Y., Pu, M., Firestone, B., Cheng, J., Kowal, C., Miller, C., Eckman, J., Yao, Y.-M., Fawell, S., Spencer, A., Miguel, J. F. S. & Anderson, K. C. (2007). Efficacy of Panobinostat (LBH589) in Multiple Myeloma Cell Lines and In Vivo Mouse Model: Tumor-Specific Cytotoxicity and Protection of Bone Integrity in Multiple Myeloma. *Blood*, 110(11), 1510–1510. Retrieved from http://dx.doi.org/10.1182/blood.V110.11.1510.1510

Gu, C., Peng, H., Lu, Y., Yang, H., Tian, Z., Yin, G., Zhang, W., Lu, S., Zhang, Y. & Yang, Y. (2017). BTK Suppresses Myeloma Cellular Senescence through Activating AKT/P27/Rb Signaling. *Oncotarget*, 8(34), 56858–56867. Retrieved from https://pubmed.ncbi.nlm.nih.gov/28915637

Guglielmelli, T., Giugliano, E., Brunetto, V., Rapa, I., Cappia, S., Giorcelli, J., Rrodhe, S., Papotti, M. & Saglio, G. (2015). MTOR Pathway Activation in Multiple Myeloma Cell Lines and Primary Tumour Cells: Pomalidomide Enhances Cytoplasmic-Nuclear Shuttling of MTOR Protein. *Oncoscience*, 2(4). Retrieved February 5, 2024, from www.impactjournals.com/oncoscience

Hanahan, D. (2022). Hallmarks of Cancer: New Dimensions. *Cancer Discovery*, 12(1), 31–46.

Hanahan, D. & Weinberg, R. A. (2000). The Hallmarks of Cancer. *Cell*, 100(1), 57–70.

Heider, M., Nickel, K., Högner, M. & Bassermann, F. (2021). Multiple Myeloma: Molecular Pathogenesis and Disease Evolution. *Oncology Research and Treatment*, 44(12), 672–681.

Hennika, T., Hu, G., Olaciregui, N. G., Barton, K. L., Ehteda, A., Chitranjan, A., Chang, C., Gifford, A. J., Tsoli, M., Ziegler, D. S., Carcaboso, A. M. & Becher, O. J. (2017). Pre-Clinical Study of Panobinostat in Xenograft and Genetically Engineered Murine Diffuse Intrinsic Pontine Glioma Models. *PLOS ONE*, 12(1), e0169485.

Hideshima, T., Richardson, P. G. & Anderson, K. C. (2011). Mechanism of Action of Proteasome Inhibitors and Deacetylase Inhibitors and the Biological Basis of Synergy in Multiple Myeloma. *Molecular Cancer Therapeutics*, 10(11), 2034–2042. Retrieved from https://aacrjournals.org/mct/article/10/11/2034/91057/Mechanism-of-Action-of-Proteasome-Inhibitors-and

Holien, T., Misund, K., Olsen, O. E., Baranowska, K. A., Buene, G., Børset, M., Waage, A. & Sundan, A. (2015). MYC Amplifications in Myeloma Cell Lines: Correlation with MYC-Inhibitor Efficacy. *Oncotarget*, 6(26), 22698–22705.

Homan, M. J., Franson, A., Ravi, K., Roberts, H., Pai, M. P., Liu, C., He, M., Matvekas, A., Koschmann, C. & Marini, B. L. (2021). Panobinostat Penetrates the Blood–Brain Barrier and Achieves Effective Brain Concentrations in a Murine Model. *Cancer Chemotherapy and Pharmacology*, 88(3), 555–562.

Horton, T. M., Gannavarapu, A., Blaney, S. M., D'Argenio, D. Z., Plon, S. E. & Berg, S. L. (2006). Bortezomib Interactions with Chemotherapy Agents in Acute Leukemia in Vitro. *Cancer Chemotherapy and Pharmacology*, 58(1), 13–23. Retrieved from http://link.springer.com/10.1007/s00280-005-0135-z

Huang, Y., Wang, C., Wang, H., Liu, H. & Zhou, L. (2024). Rediscovering Hemostasis Abnormalities in Multiple Myeloma: The New Era. *Heliyon*, 10(13), e34111.

Hurchla, M. A. M., Garcia-Gomez, A., Hornick, M. C., Ocio, E. M., Li, A., Blanco, J. F., Collins, L., Kirk, C. J., Piwnica-Worms, D., Vij, R., Tomasson, M. H., Pandiella, A., San Miguel, J. F., Garayoa, M. & Weilbaecher, K. N. (2013). The Epoxyketone-Based Proteasome Inhibitors Carfilzomib and Orally Bioavailable Oprozomib Have Anti-Resorptive and Bone-Anabolic Activity in Addition to Anti-Myeloma Effects. *Leukemia*, 27(2), 430–440. Retrieved December 16, 2020,

Imai, Y., Ohta, E., Takeda, S., Sunamura, S., Ishibashi, M., Tamura, H., Wang, Y. hua, Deguchi, A., Tanaka, J., Maru, Y. & Motoji, T. (2016). Histone Deacetylase Inhibitor Panobinostat Induces Calcineurin Degradation in Multiple Myeloma. *JCI Insight*, 1(5), 85061. Retrieved April 18, 2022, from /pmc/articles/PMC5033869/

Imane, T., Meryem, K. & Moncef, A. (2024). *Morphological Aspects of Plasma Cells in Multiple Myeloma*. Morocco.

Iwakoshi, N. N., Lee, A. H., Vallabhajosyula, P., Otipoby, K. L., Rajewsky, K. & Glimcher, L. H. (2003). Plasma Cell Differentiation and the Unfolded Protein Response Intersect at the Transcription Factor XBP-I. *Nature Immunology*, 4(4), 321–329.

Jalil, A. T., Suleiman, A. A., Abdul-Hussein, A. H., Ismaeel, G. L., Qasim, H. M., Abed, N. K. & Dilfy, S. H. (2023). Therapeutic Targeting of Dormant Cancer Stem Cells in Solid Tumors. *Gene Reports*, 30. Retrieved from https://discovery.researcher.life/article/therapeutic-targeting-of-dormant-cancer-stem-cells-in-solid-tumors/19a23506fc19341f8715a8368500699a

Kane, S. F. (2020). Bone Tumors: Multiple Myeloma. *FP essentials*, 493, 30—35. Retrieved from http://europepmc.org/abstract/MED/32573185

Kapoor, P. & Gonsalves, W. I. (2022). Melflufen for Multiple Myeloma: A Promise Unfulfilled? *The Lancet Haematology*, 9(2), e82–e84. Retrieved from https://linkinghub.elsevier.com/retrieve/pii/S2352302622000023

Kapoor, P., Ramakrishnan, V. & Rajkumar, S. V. (2012). Bortezomib Combination Therapy in Multiple Myeloma. *Seminars in hematology*, 49(3), 228. Retrieved January 13, 2022, from /pmc/articles/PMC3597231/

Katoh, M. (2017). Canonical and Non-Canonical WNT Signaling in Cancer Stem Cells and Their Niches: Cellular Heterogeneity, Omics Reprogramming, Targeted Therapy and Tumor Plasticity (Review). *International Journal of Oncology*, 51(5), 1357–1369. Retrieved from https://www.spandidos-publications.com/10.3892/ijo.2017.4129

Katz, M., Bjorklund, C. C., Thakurta, A. & Serbina, N. (2018). Mechanistic Insights of Pomalidomide Activity in Combination with Bortezomib and Dexamethasone in Multiple Myeloma and Immune Cells. *Blood*, 132(Supplement 1), 1934–1934.

Khamyath, M., Melhem, H., Balabanian, K. & Espéli, M. (2024). New Insights into the Mechanisms Regulating Plasma Cell Survival and Longevity. *Current Opinion in Immunology*, 88, 102442. Retrieved from https://linkinghub.elsevier.com/retrieve/pii/S0952791524000323

Khoo, W. (2018). Single Cell Transcript Profiling of Dormant Myeloma Cells Identifies Therapeutic and Prognostic Targets. Retrieved from https://doi.org/10.26190/unsworks/20778

Khoo, W. H., Ledergor, G., Weiner, A., Roden, D. L., Terry, R. L., McDonald, M. M., Chai, R. C., De Veirman, K., Owen, K. L., Opperman, K. S., Vandyke, K., Clark, J. R., Seckinger, A., Kovacic, N., Nguyen, A., Mohanty, S. T., Pettitt, J. A., Xiao, Y., Corr, A. P., Seeliger, C., Novotny, M., Lasken, R. S., Nguyen, T. V., Oyajobi, B. O., Aftab, D., Swarbrick, A., Parker, B., Hewett, D. R., Hose, D., Vanderkerken, K., Zannettino, Andrew C.W., et al. (2019). A Niche-Dependent Myeloid Transcriptome Signature Defines Dormant Myeloma Cells. *Blood*, 134(1), 30–43.

Kikuchi, J., Koyama, D., Mukai, H. Y. & Furukawa, Y. (2014). Suitable Drug Combination with Bortezomib for Multiple Myeloma under Stroma-Free Conditions and in Contact with Fibronectin or Bone Marrow Stromal Cells. *International Journal of Hematology*, 99(6), 726–736. Retrieved February 14, 2022, from https://link.springer.com/article/10.1007/s12185-014-1573-3

Kikuchi, J., Wada, T., Shimizu, R., Izumi, T., Akutsu, M., Mitsunaga, K., Noborio-Hatano, K., Nobuyoshi, M., Ozawa, K., Kano, Y. & Furukawa, Y. (2010). Histone Deacetylases Are Critical Targets of Bortezomib-Induced Cytotoxicity in Multiple Myeloma. *Blood*, 116(3), 406–417. Retrieved from https://ashpublications.org/blood/article/116/3/406/27607/Histone-deacetylases-are-critical-targets-of

Kim, J.-M., Lin, C., Stavre, Z., Greenblatt, M. B. & Shim, J.-H. (2020). Osteoblast-Osteoclast Communication and Bone Homeostasis. *Cells*, 9(9), 2073.

Kleffel, S. & Schatton, T. (2013). Tumor Dormancy and Cancer Stem Cells: Two Sides of the Same Coin?, in: Enderling, H., Almog, N., and Hlatky, L. (Eds.), *Systems Biology of Tumor Dormancy*, (pp. 145–179). New York, NY: Springer New York. Retrieved from https://doi.org/10.1007/978-1-4614-1445-2_8

Komarova, N. L. & Wodarz, D. (2007). Effect of Cellular Quiescence on the Success of Targeted CML Therapy. *PLOS ONE*, 2(10), 1–9. Retrieved from https://doi.org/10.1371/journal.pone.0000990

Kozalak, G., Bütün, İ., Toyran, E., & Koşar, A. (2023). Review on Bortezomib Resistance in Multiple Myeloma and Potential Role of Emerging Technologies. Pharmaceuticals, 16(1), 111. Retrieved from https://doi.org/10.3390/ph16010111

Kumar, S. K., Rajkumar, V., Kyle, R. A., Van Duin, M., Sonneveld, P., Mateos, M. V., Gay, F. & Anderson, K. C. (2017). Multiple Myeloma. *Nature Reviews Disease Primers*, 3, 1–20. Retrieved from http://dx.doi.org/10.1038/nrdp.2017.46

Lacy, M. Q. & McCurdy, A. R. (2013). Pomalidomide. *Blood*, 122(14), 2305–2309. Retrieved from https://www.sciencedirect.com/science/article/pii/S0006497120499458

Landgren, O., Kyle, R. A., Pfeiffer, R. M., Katzmann, J. A., Caporaso, N. E., Hayes, R. B., Dispenzieri, A., Kumar, S., Clark, R. J., Baris, D., Hoover, R. & Rajkumar, S. V. (2009). Monoclonal Gammopathy of Undetermined Significance (MGUS) Consistently Precedes Multiple Myeloma: A Prospective Study. *Blood*, 113(22), 5412–5417.

Laubach, J. P., Schjesvold, F., Mariz, M., Dimopoulos, M., Lech-Marańda, E., Spicka, I., Hungria, V., Shelekhova, T., Abdo, A., Jacobasch, L., Polprasert, C., Hajek, R., Illes, A., Wróbel, T., Sureda Balari, A., Beksac, M., Goncalves, I., Bladé Creixenti, J., Rajkumar, S. V., Chari, A., Lonial, S., Spencer, A., Maison-Blanche, P., Moreau, P., Richardson, P., San-Miguel, J. (2020). Efficacy and Safety of the Panobinostat-Bortezomib-

Dexamethasone Combination in Relapsed or Relapsed/Refractory Multiple Myeloma: Results from the Randomized Panorama 3 Study. *Blood*, 136(Supplement 1), 4–6.

Laubach, J. P., Moreau, P., San-Miguel, J. F. & Richardson, P. G. (2015). Panobinostat for the Treatment of Multiple Myeloma. *Clinical Cancer Research*, 21(21), 4767–4773.

Lawson, M., Paton-Hough, J., Evans, H., Walker, R., Harris, W., Ratnabalan, D., Snowden, J., Chantry, A. (2015). Osteoclasts Control Reactivation of Dormant Myeloma Cells by Remodelling the Endosteal Niche. *Nature Communications*, 6(1), 8983. Retrieved May 5, 2023, from https://doi.org/10.1038/ncomms9983

Lawson, M. A., Paton-Hough, J. M., Evans, H. R., Walker, R. E., Harris, W., Ratnabalan, D., Snowden, J. A. & Chantry, A. D. (2015). NOD/SCID-GAMMA Mice Are an Ideal Strain to Assess the Efficacy of Therapeutic Agents Used in the Treatment of Myeloma Bone Disease. *PLoS ONE*, 10(3), e0119546. Retrieved September 28, 2021, from https://journals.plos.org/plosone/article?id=10.1371/journal.pone.0119546

Lawson, M., Les, C., Frank, E., Karin, V. & Peter, C. (2008). Geranylgeranyl Transferase Type II Inhibition Prevents Myeloma Bone Disease | Elsevier Enhanced Reader. *Biochemical and Biophysical Research Communications*, 377, 453–457. Retrieved December 16, 2020, from https://reader.elsevier.com/reader/sd/pii/S0006291X0801944X?token=19B8AD98E699C7B8E3506E8B0B1C90027C9764E282180053A2F1195804078C11CB9AE7294ED4655B7B96BFB1EFB8ECFE

Lemaire, M., Fristedt, C., Agarwal, P., Menu, E., Van Valckenborgh, E., De Bruyne, E., Österborg, A., Atadja, P., Larsson, O., Axelson, M., Van Camp, B., Jernberg-Wiklund, H. & Vanderkerken, K. (2012). The HDAC Inhibitor LBH589 Enhances the AntimyelomaEffects of the IGF-1RTK Inhibitor Picropodophyllin. *Clinical Cancer Research*, 18(8), 2230–2239. Retrieved February 17, 2022, from https://aacrjournals.org/clincancerres/article/18/8/2230/77806/The-HDAC-Inhibitor-LBH589-Enhances-the-Antimyeloma

Di Lernia, G., Leone, P., Solimando, A. G., Buonavoglia, A., Saltarella, I., Ria, R., Ditonno, P., Silvestris, N., Crudele, L., Vacca, A. & Racanelli, V. (2020). Bortezomib Treatment Modulates Autophagy in Multiple Myeloma. *Journal of Clinical Medicine*, 9(2), 552.

Li, B., Huang, Y., Ming, H., Nice, E. C., Xuan, R. & Huang, C. (2021). Redox Control of the Dormant Cancer Cell Life Cycle. *Cells*, 10(10). Retrieved April 19, 2022, from /pmc/articles/PMC8535080/

Liu, J., Zhang, Z., Xu, W., Jia, M.-Y., Wu, C. & Hua, Y. (2023). Targeting RBM39-MEK5 Axis Synergizes with Bortezomib to Inhibit Multiple Myeloma Malignancy. *Blood*, 142(Supplement 1), 4674–4674. Retrieved from https://ashpublications.org/blood/article/142/Supplement%201/4674/499381/Targeting-RBM39-MEK5-Axis-Synergizes-with

Liu, X., Feng, X., Huang, H., Huang, K., Xu, Y., Ye, S., Tseng, Y.-T., Wei, P., Wang, L. & Wang, F. (2022). Male and Female Mice Display Consistent Lifelong Ability to Address Potential Life-Threatening Cues Using Different Post-Threat Coping Strategies. *BMC Biology*, 20(1), 281.

Lonial, S. (2010). Relapsed Multiple Myeloma. *Hematology*, 2010(1), 303–309. Retrieved April 18, 2022, from https://ashpublications.org/hematology/article/2010/1/303/96365/Relapsed-Multiple-Myeloma

Mahindra, A. & Ng, A. K. (2016). Multiple Myeloma and Other Plasma Cell Neoplasms, in: *Clinical Radiation Oncology*, (pp. 1547-1555.e2). Elsevier. Retrieved from https://linkinghub.elsevier.com/retrieve/pii/B9780323240987000782

Maiso, P., Carvajal-Vergara, X., Ocio, E. M., López-Pérez, R., Mateo, G., Gutiérrez, N., Atadja, P., Pandiella, A. & San Miguel, J. F. (2006). The Histone Deacetylase Inhibitor LBH589 Is a Potent Antimyeloma Agent That Overcomes Drug Resistance. *Cancer Research*, 66(11), 5781 LP – 5789. Retrieved from http://cancerres.aacrjournals.org/content/66/11/5781.abstract

Manier, S., Salem, K. Z., Park, J., Landau, D. A., Getz, G. & Ghobrial, I. M. (2017). Genomic Complexity of Multiple Myeloma and Its Clinical Implications. *Nature Reviews Clinical Oncology*, 14(2), 100–113.

Marianna D'Anca. (2016). Identification and Validation of Critical 1Q21 Achilles Heel' Vulnerabilities of Multiple Myeloma, Università Degli Studi Di Milano. Retrieved from https://dx.doi.org/10.13130/m-d-anca_phd2016-02-18.

Di Marzo, L., Desantis, V., Solimando, A. G., Ruggieri, S., Annese, T., Nico, B., Fumarulo, R., Vacca, A. & Frassanito, M. A. (2016). Microenvironment Drug Resistance in Multiple Myeloma: Emerging New Players. *Oncotarget*, 7(37), 60698–60711.

Matyskiela, M. E., Zhang, W., Man, H.-W., Muller, G., Khambatta, G., Baculi, F., Hickman, M., LeBrun, L., Pagarigan, B., Carmel, G., Lu, C.-C., Lu, G., Riley, M., Satoh, Y., Schafer, P., Daniel, T. O., Carmichael, J., Cathers, B. E. & Chamberlain, P. P. (2018). A Cereblon Modulator (CC-220) with Improved Degradation of Ikaros and Aiolos. *Journal of Medicinal Chemistry*, 61(2), 535–542. Retrieved from https://pubs.acs.org/doi/10.1021/acs.jmedchem.6b01921

Mayo Clinic. (2020). Hypercalcemia - Symptoms and Causes - Mayo Clinic. *Mayo Clinic*, 1. Retrieved February 16, 2021, from https://www.mayoclinic.org/diseases-conditions/hypercalcemia/symptoms-causes/syc-20355523

Mehdi, S. H., Nafees, S., Mehdi, S. J., Morris, C. A., Mashouri, L. & Yoon, D. (2021). Animal Models of Multiple Myeloma Bone Disease. *Frontiers in Genetics*, 12(June), 1–12.

Miller, I., Min, M., Yang, C., Tian, C., Gookin, S., Carter, D. & Spencer, S. L. (2018). Ki67 Is a Graded Rather than a Binary Marker of Proliferation versus Quiescence. *Cell Reports*, 24(5), 1105-1112.e5. Retrieved from http://www.sciencedirect.com/science/article/pii/S2211124718310520

Minges Wols, H. A., Ippolito, J. A., Yu, Z., Palmer, J. L., White, F. A., Le, P. T. & Witte, P. L. (2007). The Effects of Microenvironment and Internal Programming on Plasma Cell Survival. *International Immunology*, 19(7), 837–846.

Mitra, A. K., Mukherjee, U. K., Harding, T., Jang, J. S., Stessman, H., Li, Y., Abyzov, A., Jen, J., Kumar, S., Rajkumar, V. & Van Ness, B. (2015). Single-Cell Analysis of Targeted Transcriptome Predicts Drug Sensitivity of Single Cells within Human Myeloma Tumors. *Leukemia 2016 30:5*, 30(5), 1094–1102. Retrieved May 15, 2024, from https://www.nature.com/articles/leu2015361

Miyakawa, Y., Ohnishi, Y., Tomisawa, M., Monnai, M., Kohmura, K., Ueyama, Y., Ito, M., Ikeda, Y., Kizaki, M. & Nakamura, M. (2004). Establishment of a New Model of Human Multiple Myeloma Using NOD/SCID/$γ$cnull (NOG) Mice. *Biochemical and Biophysical Research Communications*, 313(2), 258–262. Retrieved December 16, 2020, from https://linkinghub.elsevier.com/retrieve/pii/S0006291X03025129

Moreau, P., Richardson, P. G., Cavo, M., Orlowski, R. Z., San Miguel, J. F., Palumbo, A. & Harousseau, J.-L. (2012). Proteasome Inhibitors in Multiple Myeloma: 10 Years Later. *Blood*, 120(5), 947–959. Retrieved from https://ashpublications.org/blood/article/120/5/947/30255/Proteasome-inhibitors-in-multiple-myeloma-10-years

Moreno, D. A., Junior, H. L. R., Laranjeira, A. B. A., Cruzeiro, G. A. V., Borges, K. S., Salomão, K. B., Ramalho, F. S., Yunes, J. A., Silva, C. L. A., Rego, E. M., Scrideli, C. A. & Tone, L. G. (2022). Panobinostat (LBH589) Increase Survival in Adult Xenografic Model of Acute Lymphoblastic Leukemia with t(4;11) but Promotes Antagonistic Effects in Combination with MTX and 6MP. *Medical Oncology*, 39(12), 216. Retrieved from https://link.springer.com/10.1007/s12032-022-01813-w

Morgan, G. J., Walker, B. A. & Davies, F. E. (2012). The Genetic Architecture of Multiple Myeloma. *Nature Reviews Cancer*, 12(5), 335–348. Retrieved from https://doi.org/10.1038/nrc3257

Moser, K., Tokoyoda, K., Radbruch, A., MacLennan, I. & Manz, R. A. (2006). Stromal Niches, Plasma Cell Differentiation and Survival. *Current Opinion in Immunology*, 18(3), 265–270. Retrieved from http://www.sciencedirect.com/science/article/pii/S0952791506000525

Mukherjee, A. & Bravo-Cordero, J. J. (2023). Regulation of Dormancy during Tumor Dissemination: The Role of the ECM. *Cancer and Metastasis Reviews*, 42(1), 99–112.

Mura, M., Feillet, C., Bertolusso, R., Delaunay, F. & Kimmel, M. (2019). Mathematical Modelling Reveals Unexpected Inheritance and Variability Patterns of Cell Cycle Parameters in Mammalian Cells. *PLoS Computational Biology*, 15(6), 1–26.

Nanni, C., Fanti, S. & Zanoni, L. (2019). *Molecular Imaging in Multiple Myeloma*.

Nau, K. C. & LeWis, W. (2008). *Multiple Myeloma: Diagnosis and Treatment*. Retrieved January 17, 2021, from www.aafp.org/afp.

Ocio, E. M., Vilanova, D., Atadja, P., Maiso, P., Crusoe, E., Fernandez-Lazaro, D., Garayoa, M., San-Segundo, L., Hernandez-Iglesias, T., de Alava, E., Shao, W., Yao, Y. M., Pandiella, A. & San-Miguel, J. F. (2010). In Vitro and in Vivo Rationale for the Triple Combination of Panobinostat (LBH589) and Dexamethasone with Either Bortezomib or Lenalidomide in Multiple Myeloma. *Haematologica*, 95(5), 794–803. Retrieved April 18, 2022, from http://www.haematologica.org/cgi/doi/10.3324/haematol.2009.015495

Offidani, M., Corvatta, L., Caraffa, P., Leoni, P., Pautasso, C., Larocca, A. & Palumbo, A. (2014). Pomalidomide for the Treatment of Relapsed-Refractory Multiple Myeloma: A Review of Biological and Clinical Data. *Expert review of anticancer therapy*, 14(5), 499–510. Retrieved April 11, 2022, from http://www.tandfonline.com/doi/full/10.1586/14737140.2014.906904

Ookura, M., Fujii, T., Yagi, H., Ogawa, T., Kishi, S., Hosono, N., Shigemi, H., Yamauchi, T., Ueda, T. & Yoshida, A. (2017). YM155 Exerts Potent Cytotoxic Activity against Quiescent (G0/G1) Multiple Myeloma and Bortezomib Resistant Cells via Inhibition of Survivin and Mcl-1. *Oncotarget*, 8(67), 111535–111550.

Oracki, S. A., Walker, J. A., Hibbs, M. L., Corcoran, L. M. & Tarlinton, D. M. (2010). Plasma Cell Development and Survival. *Immunol Rev*, 237(1), 140–159.

Owen, Katie L., Gearing, Linden J, Zanker, Damien J, Brockwell, Natasha K, Khoo, Weng Hua, Roden, Daniel L, Cmero, Marek, Mangiola, Stefano, Hong, Matthew K, Spurling, Alex J, McDonald, Michelle, Chan, Chia-Ling, Pasam, Anupama , Lyons, Ruth J ,

Duivenvoorden, Hendrika M , Ryan, Andrew, Butler, Lisa M, Mariadason, John M, Giang Phan, Tri, Hayes, Vanessa M, Sandhu, Shahneen, Swarbrick, Alexander, Corcoran, Niall M, Hertzog, Paul J, Croucher, Peter I, Hovens, Chris, Parker, Belinda S (2020). Prostate Cancer Cell-intrinsic Interferon Signaling Regulates Dormancy and Metastatic Outgrowth in Bone. *EMBO reports*, 21(6). Retrieved from https://www.embopress.org/doi/10.15252/embr.202050162

Panga, S., Podila, N. K. & Ciddi, V. (2018). Design, Synthesis, Characterization, and In Vitro Evaluation of Isatin-Pomalidomide Hybrids for Cytotoxicity against Multiple Myeloma Cell Lines. *Journal of Heterocyclic Chemistry*, 55(12), 2919–2928.

Paton-Hough, J., Chantry, A. D., Lawson, M. A. (2015). A Review of Current Murine Models of Multiple Myeloma Used to Assess the Efficacy of Therapeutic Agents on Tumour Growth and Bone Disease. *Bone*, 77, 57–68. Retrieved from http://dx.doi.org/10.1016/j.bone.2015.04.004

Paton-Hough, J., Tazzyman, S., Evans, H., Lath, D., Down, J. M., Green, A. C., Snowden, J. A., Chantry, A. D. & Lawson, M. A. (2019). Preventing and Repairing Myeloma Bone Disease by Combining Conventional Antiresorptive Treatment with a Bone Anabolic Agent in Murine Models. *Journal of Bone and Mineral Research*, 34(5), 783–796. Retrieved from https://academic.oup.com/jbmr/article/34/5/783-796/7605955

Perfectionalis, M. (2018). *Multiple Myeloma | A Malignancy of Plasma Cells! - YouTube*. Retrieved January 14, 2021, from https://www.youtube.com/watch?v=SVlV68XVQLg

Phan, T. G., Croucher, P. I. (2020). The Dormant Cancer Cell Life Cycle. *Nature Reviews Cancer*, 20(7), 398–411. Retrieved from http://dx.doi.org/10.1038/s41568-020-0263-0

Pick, A. M. (2014). Multiple Myeloma : An Overview of the Disease and Treatment Options. *hematology*, 39(1), 7–11. Retrieved April 8, 2022, from https://www.uspharmacist.com/article/multiple-myeloma-an-overview-of-the-disease-and-treatment-options

Pinto, V., Bergantim, R., Caires, H. R., Seca, H., Guimarães, J. E. & Vasconcelos, M. H. (2020). Multiple Myeloma: Available Therapies and Causes of Drug Resistance. *Cancers*, 12(2), 407.

Pitcher, D. S., de Mattos-Shipley, K., Tzortzis, K., Auner, H. W., Karadimitris, A. & Kleijnen, M. F. (2015). Bortezomib Amplifies Effect on Intracellular Proteasomes by Changing Proteasome Structure. *EBioMedicine*, 2(7), 642–648. Retrieved from http://dx.doi.org/10.1016/j.ebiom.2015.05.016

Poczta, A., Krzeczyński, P., Tobiasz, J., Rogalska, A., Gajek, A. & Marczak, A. (2022). Synthesis and In Vitro Activity of Novel Melphalan Analogs in Hematological Malignancy Cells. *International Journal of Molecular Sciences*, 23(3), 1760. Retrieved from https://www.mdpi.com/1422-0067/23/3/1760

Poczta, A., Rogalska, A. & Marczak, A. (2021). Treatment of Multiple Myeloma and the Role of Melphalan in the Era of Modern Therapies—Current Research and Clinical Approaches. *Journal of Clinical Medicine*, 10(9), 1841. Retrieved from https://www.mdpi.com/2077-0383/10/9/1841

Pranzini, E., Raugei, G. & Taddei, M. L. (2022). Metabolic Features of Tumor Dormancy: Possible Therapeutic Strategies. *Cancers*, 14(3), 547. Retrieved April 28, 2022, from /pmc/articles/PMC8833651/

Pratt, G., Bowcock, S., Chantry, A., Cook, G., Jackson, G., Lai, M., Low, E., Mulholland, N., Owen, R., Rabin, N., Ramasamy, K., Snowden, J. A., Streetly, M., Wechalekar, A., Yong, K. & Bird, J. (2015). Time to Redefine Myeloma. *British Journal of Haematology*, 171(1), 1–10. Retrieved January 15, 2021, from http://doi.wiley.com/10.1111/bjh.13620

Quayle, L. A., Ottewell, P. D. & Holen, I. (2018). Chemotherapy Resistance and Stemness in Mitotically Quiescent Human Breast Cancer Cells Identified by Fluorescent Dye Retention. *Clinical and Experimental Metastasis*, 35(8), 831–846.

Ramakrishnan, V., Kimlinger, T., Timm, M., Haug, J., Rajkumar, S. V. & Kumar, S. (2014). Multiple Mechanisms Contribute to the Synergistic Anti-Myeloma Activity of the Pan-Histone Deacetylase Inhibitor LBH589 and the Rapalog RAD001. *Leukemia Research*,

38(11), 1358–1366. Retrieved from https://linkinghub.elsevier.com/retrieve/pii/S0145212614002690

Ren, Q., Khoo, W. H., Corr, A. P., Phan, T. G., Croucher, P. I. & Stewart, S. A. (2022). Gene Expression Predicts Dormant Metastatic Breast Cancer Cell Phenotype. *Breast Cancer Research*, 24(1), 1–16. Retrieved from https://doi.org/10.1186/s13058-022-01503-5

Richardson, P. G., Mark, T. M. & Lacy, M. Q. (2013). Pomalidomide: New Immunomodulatory Agent with Potent Antiproliferative Effects. *Critical Reviews in Oncology/Hematology*, 88(SUPPL.1). Retrieved April 11, 2022,

Robinson, R. M., Basar, A. P., Reyes, L., Duncan, R. M., Li, H. & Dolloff, N. G. (2022). PDI Inhibitor LTI6426 Enhances Panobinostat Efficacy in Preclinical Models of Multiple Myeloma. *Cancer Chemotherapy and Pharmacology 2022*, 1–11. Retrieved April 18, 2022, from https://link.springer.com/article/10.1007/s00280-022-04425-3

Rudge, E. U., Cutler, A. J., Pritchard, N. R. & Smith, K. G. C. (2002). Interleukin 4 Reduces Expression of Inhibitory Receptors on B Cells and Abolishes CD22 and FcγRII-Mediated B Cell Suppression . *Journal of Experimental Medicine*, 195(8), 1079–1085. Retrieved from https://doi.org/10.1084/jem.20011435

Saito, N., Shirai, Y., Uwagawa, T., Horiuchi, T., Sugano, H., Haruki, K., Shiba, H., Ohashi, T. & Yanaga, K. (2018). Pomalidomide Enhanced Gemcitabine and Nab-Paclitaxel on Pancreatic Cancer Both in Vitro and in Vivo. *Oncotarget*, 9(21), 15780–15791. Retrieved April 11, 2022, from /pmc/articles/PMC5884664/

Sanchez, W. Y., McGee, S. L., Connor, T., Mottram, B., Wilkinson, A., Whitehead, J. P., Vuckovic, S. & Catley, L. (2013). Dichloroacetate Inhibits Aerobic Glycolysis in Multiple Myeloma Cells and Increases Sensitivity to Bortezomib. *British Journal of Cancer*, 108(8), 1624–1633.

Savvidou, I., Khong, T., Whish, S., Carmichael, I., Sepehrizadeh, T., Mithraprabhu, S., Horrigan, S. K., de Veer, M. & Spencer, A. (2022). Combination of Histone Deacetylase Inhibitor Panobinostat (LBH589) with β-Catenin Inhibitor Tegavivint (BC2059) Exerts

Significant Anti-Myeloma Activity Both In Vitro and In Vivo. *Cancers*, 14(3). Retrieved April 18, 2022, from /pmc/articles/PMC8834319/

Schey, S. & Ramasamy, K. (2011). Pomalidomide Therapy for Myeloma. *Expert Opinion on Investigational Drugs*, 20(5), 691–700. Retrieved from http://www.tandfonline.com/doi/full/10.1517/13543784.2011.567265

Schueler, J., Wider, D., Klingner, K., Siegers, G. M., May, A. M., Wäsch, R., Fiebig, H. H. & Engelhardt, M. (2013). Intratibial Injection of Human Multiple Myeloma Cells in NOD/SCID IL-2Rγ(Null) Mice Mimics Human Myeloma and Serves as a Valuable Tool for the Development of Anticancer Strategies. *PLoS ONE*, 8(11). Retrieved December 16, 2020,

Shiozawa, Y., Pedersen, E. A., Patel, L. R., Ziegler, A. M., Havens, A. M., Jung, Y., Wang, J., Zalucha, S., Loberg, R. D., Pienta, K. J. & Taichman, R. S. (2010). GAS6/AXL Axis Regulates Prostate Cancer Invasion, Proliferation, and Survival in the Bone Marrow Niche. *Neoplasia*, 12(2), 116-IN4. Retrieved from https://www.sciencedirect.com/science/article/pii/S1476558610800910

Smarr, B. & Kriegsfeld, L. J. (2022). Female Mice Exhibit Less Overall Variance, with a Higher Proportion of Structured Variance, than Males at Multiple Timescales of Continuous Body Temperature and Locomotive Activity Records. *Biology of Sex Differences*, 13(1), 41.

Smith, J. & Chai, R. C. (2024). Bone Niches in the Regulation of Tumour Cell Dormancy. *Journal of Bone Oncology*, 100621. Retrieved from https://linkinghub.elsevier.com/retrieve/pii/S2212137424001015

Sodickson, A., Baeyens, P. F., Andriole, K. P., Prevedello, L. M., Nawfel, R. D., Hanson, R. & Khorasani, R. (2009). Recurrent CT, Cumulative Radiation Exposure, and Associated Radiation-Induced Cancer Risks from CT of Adults. *Radiology*, 251(1), 175–184. Retrieved September 28, 2021, from https://pubs.rsna.org/doi/abs/10.1148/radiol.2511081296

Srour, Samer A., Bashir, Qaiser, Milton, Denái R., Nieto, Yago, Mehta, Rohtesh S., Saini, Neeraj, Delgado, Ruby, Rondon, Gabriela, Ciurea, Stefan O., Popat, Uday R., Khouri, Issa F., Kebriaei, Partow, Manasanch, Elisabet E., Hosing, Chitra, Patel, Krina K., Lee, Hans C., Shpall, Elizabeth J., Orlowski, Robert Z., Champlin, Richard E., Qazilbash, Muzaffar H. (2020). Long-Term Survival for Myeloma after Autologous Stem Cell Transplantation. *Blood*, 136(Supplement 1), 23–24. Retrieved from https://ashpublications.org/blood/article/136/Supplement%201/23/472082/Long-Term-Survival-for-Myeloma-after-Autologous

Stewart, G., Chantry, A. & Lawson, M. (2021). The Use of Oncolytic Viruses in the Treatment of Multiple Myeloma. *Cancers*, 13(22), 5687.

Suominen, M. I., Fagerlund, K. M., Alhoniemi, E., Rissanen, J. P., Halleen, J. M. & Aftab, D. T. (2015). Abstract 786: Effects of Combination Treatment with Cabozantinib and Bortezomib in the 5TGM1 Murine Multiple Myeloma Model. *Cancer Research*, 75(15_Supplement), 786–786. Retrieved from https://aacrjournals.org/cancerres/article/75/15_Supplement/786/604946/Abstract-786-Effects-of-combination-treatment-with

Suvannasankha, A. & Chirgwin, J. M. (2014). Role of Bone-Anabolic Agents in the Treatment of Breast Cancer Bone Metastases. *Breast Cancer Research*, 16(6), 484.

Tagoug, A. & Safra, I. (2023). The Impact of Panobinostat on Cell Death in Combination with S63845 in Multiple Myeloma Cells. *Indian Journal of Hematology and Blood Transfusion*, 39, 245–257. Retrieved March 5, 2024, from https://doi.org/10.1007/s12288-022-01584-4

Tarlinton, D., Radbruch, A., Hiepe, F. & Dörner, T. (2008). Plasma Cell Differentiation and Survival. *Current Opinion in Immunology*, 20(2), 162–169. Retrieved January 22, 2021,

Thurley K, Gerecht D, Friedmann E, HöferT (2015) Three-Dimensional Gradients of CytokineSignaling between T Cells. PLoS Comput Biol 11(4):e1004206. doi:10.1371/journal.pcbi.1004206

vailable from:https://www.researchgate.net/publication/275660606_Three-

Dimensional_Gradients_of_Cytokine_Signaling_between_T_Cells#fullTextFileContent [accessed Apr 11 2025].

Ueda, T., Fujii, T., Ookura, M., Hosono, N., Shigemi, H., Yoshida, A., Yamauchi, T. & Kishi, S. (2015). YM155 Exerts Potent Cytotoxic Activity Against Quiescent (G0/G1) Multiple Myeloma and Bortezomib Resistant Cells Via Inhibition of Mcl-1 and Survivin. *Blood*, 126. Retrieved from https://discovery.researcher.life/article/ym155-exerts-potent-cytotoxic-activity-against-quiescent-g0-g1-multiple-myeloma-and-bortezomib-resistant-cells-via-inhibition-of-mcl-1-and-survivin/62dc9975ff003d2ba54c878df3aecf3c

Ullah, T. R. (2019). The Role of CXCR4 in Multiple Myeloma: Cells' Journey from Bone Marrow to beyond. *Journal of Bone Oncology*, 17, 100253. Retrieved March 3, 2021,

Vallet, S. & Raje, N. (2011). Bone Anabolic Agents for the Treatment of Multiple Myeloma. *Cancer Microenvironment*, 4(3), 339–349.

Van Veggel, M., Westerman, E. & Hamberg, P. (2018). Clinical Pharmacokinetics and Pharmacodynamics of Panobinostat. *Clinical Pharmacokinetics*, 57(1), 21–29. Retrieved from http://link.springer.com/10.1007/s40262-017-0565-x

De Veirman, K., Yan, S., Maes, K., De Beule, N., Faict, S., De Bruyne, E., Menu, E. & Vanderkerken, K. (2019). Receptor Tyrosine Kinase AXL: A Potential Strategy to Counter Immune Suppression and Dormancy in Multiple Myeloma. *Blood*, 134(Supplement_1), 4335–4335.

Vichai, V. & Kirtikara, K. (2006). Sulforhodamine B Colorimetric Assay for Cytotoxicity Screening. *Nature Protocols*, 1(3), 1112–1116. Retrieved from https://www.nature.com/articles/nprot.2006.179

Wang, H., Zhang, H., Srinivasan, V., Tao, J., Sun, W., Lin, X., Wu, T., Boyce, B. F., Ebetino, F. H., Boeckman, R. K. & Xing, L. (2020). Targeting Bortezomib to Bone Increases Its Bone Anabolic Activity and Reduces Systemic Adverse Effects in Mice. *Journal of Bone and Mineral Research*, 35(2), 343–356. Retrieved from https://academic.oup.com/jbmr/article/35/2/343/7516336

Wang, N., Docherty, F., Brown, H. K., Reeves, K., Fowles, A., Lawson, M., Ottewell, P. D., Holen, I., Croucher, P. I. & Eaton, C. L. (2015). Mitotic Quiescence, but Not Unique 'Stemness,' Marks the Phenotype of Bone Metastasis-Initiating Cells in Prostate Cancer. *FASEB journal : official publication of the Federation of American Societies for Experimental Biology*, 29(8), 3141–50. Retrieved from http://www.ncbi.nlm.nih.gov/pubmed/25888599

Wang, Y., Mi, T., Li, Y., Kan, W., Xu, G., Li, Jingya, Zhou, Y., Li, Jia & Jiang, X. (2021). Design, Synthesis and Biological Evaluation of Thioether-Containing Lenalidomide and Pomalidomide Derivatives with Anti-Multiple Myeloma Activity. *European Journal of Medicinal Chemistry*, 209, 112912. Retrieved from https://doi.org/10.1016/j.ejmech.2020.112912

Weston, W. A. & Barr, A. R. (2023). A Cell Cycle Centric View of Tumour Dormancy. *British Journal of Cancer*, 129(10), 1535–1545.

Wiedmeier-Nutor, J. E. & Bergsagel, P. L. (2022). Review of Multiple Myeloma Genetics Including Effects on Prognosis, Response to Treatment, and Diagnostic Workup. *Life*, 12(6), 812.

Wirries, A., Jabari, S., Jansen, E. P., Roth, S., Figueroa-Juárez, E., Wissniowski, T. T., Neureiter, D., Klieser, E., Lechler, P., Ruchholtz, S., Bartsch, D. K., Boese, C. K. & Di Fazio, P. (2018). Panobinostat Mediated Cell Death: A Novel Therapeutic Approach for Osteosarcoma. *Oncotarget*, 9(68), 32997–33010.

Xiong, T., Wei, H., Chen, X. , Xiao, H. (2015). PJ34, a Poly (ADP-Ribose) Polymerase (PARP) Inhibitor, Reverses Melphalan-Resistance and Inhibits Repair of DNA Double-Strand Breaks by Targeting the FA/BRCA Pathway in Multidrug Resistant Multiple Myeloma Cell Line RPMI8226/R. *International Journal of Oncology*, 46(1), 223–232. Retrieved from https://www.spandidos-publications.com/10.3892/ijo.2014.2726

Yadav, P., Cook, M. & Cockwell, P. (2016). Current Trends of Renal Impairment in Multiple Myeloma. *Kidney diseases*, 1(4), 241–257.

Yan, S., Vandewalle, N., De Beule, N., Faict, S., Maes, K., De Bruyne, E., Menu, E., Vanderkerken, K. & De Veirman, K. (2019). AXL Receptor Tyrosine Kinase as a Therapeutic Target in Hematological Malignancies: Focus on Multiple Myeloma. *Cancers*, 11(11). Retrieved from https://www.mdpi.com/2072-6694/11/11/1727

Yang, J., Cheng, D., Zhou, S., Zhu, B., Hu, T. & Yang, Q. (2015). Overexpression of X-Box Binding Protein 1 (XBP1) Correlates to Poor Prognosis and Up-Regulation of PI3K/MTOR in Human Osteosarcoma. *International journal of molecular sciences*, 16(12), 28635–28646. Retrieved from https://pubmed.ncbi.nlm.nih.gov/26633383

Young, T.-H., Hung, S.-H. & Hsu, J.-P. (2004). Analysis of Cell Aggregation in the Culturing of Cerebellar Granule Neurons. *Chemical Engineering Science*, 59(24), 5931–5936. Retrieved January 23, 2024, from https://linkinghub.elsevier.com/retrieve/pii/S0009250904004634

Yu, N. (2016). Identifying and Targeting Dormant Cells in Acute Myeloid Leukaemia. *phd thesis*, (July).

Yumoto, K., Berry, J. E., Taichman, R. S. & Shiozawa, Y. (2014). A Novel Method for Monitoring Tumor Proliferation in Vivo Using Fluorescent Dye DiD. *Cytometry Part A*, 85(6), 548–555. Retrieved from https://onlinelibrary.wiley.com/doi/10.1002/cyto.a.22434

Yumoto, K., Eber, M. R., Wang, J., Cackowski, F. C., Decker, A. M., Lee, E., Nobre, A. R., Aguirre-Ghiso, J. A., Jung, Y. & Taichman, R. S. (2016). Axl Is Required for TGF-B2-Induced Dormancy of Prostate Cancer Cells in the Bone Marrow. *Scientific Reports*, 6.

Zhou, Y., Liu, X., Xue, J., Liu, L., Liang, T., Li, W., Yang, X., Hou, X. & Fang, H. (2020). Discovery of Peptide Boronate Derivatives as Histone Deacetylase and Proteasome Dual Inhibitors for Overcoming Bortezomib Resistance of Multiple Myeloma. *Journal of Medicinal Chemistry*, 63(9), 4701–4715.

Zhu, C., Wei, Y. & Wei, X. (2019). AXL Receptor Tyrosine Kinase as a Promising Anti-Cancer Approach: Functions, Molecular Mechanisms and Clinical Applications. *Molecular Cancer*, 18(1).